In Vivo Assessment of the Performance of Strain-Encoded MRI (DENSE) in Healthy Subjects and Patients with Myocardial Infarction

Christie McComb

MSci (Hons), MSc

Submitted in fulfilment of the requirements for the degree of

Doctor of Philosophy

Department of Clinical Physics

College of Medical, Veterinary and Life Sciences

University of Glasgow

April 2014

Abstract

Introduction: In patients with myocardial infarction (MI), regional left ventricular contractile function has important prognostic value. Displacement ENcoding with Stimulated Echoes (DENSE) is an MRI technique which has been developed to allow quantitative assessment of myocardial strain. To date, much of the research performed with DENSE has been methods development, and its application in a routine clinical setting has been incompletely investigated. The purpose of the research presented within this thesis was to investigate variations in strain within the healthy heart, and then to assess the in vivo performance of DENSE strain imaging in acute and chronic myocardial infarction (MI).

Methods: 80 healthy subjects (M:F = 40:40, age 43 ± 17 years) were recruited from the community. 50 male patients (age 56 ± 10 years) were recruited from the clinical service and scanned within 7 days of myocardial infarction ("acute MI"), and invited to return for a follow-up scan after 6 months ("chronic MI").

MR imaging was performed on a 1.5T Siemens Avanto scanner, using an imaging protocol which included DENSE, cine, late gadolinium enhancement (LGE, patients only) and T2-weighted imaging acquired from left ventricular (LV) short-axis slices in both basal and mid-ventricular positions, which were divided into 6 segments for analysis. The percentage of LGE and T2 hyperenhancement within each segment were calculated, and the area at risk (acute MI) and myocardial salvage index (chronic MI) were determined. DENSE images were analysed to obtain values for strain parameters relating to circumferential strain (Ecc).

Strain measurements obtained from healthy subjects were used to investigate the variations in Ecc with age, gender, slice position and myocardial segment.

Strain measurements obtained from MI patients were used to investigate the relationships between Ecc and the extent of myocardial infarction, area at risk and/or salvage, and to determine whether DENSE strain measurements are informative in acute and chronic MI.

Results: Comparison of DENSE strain measurements in healthy subjects revealed statistically significant differences between males and females, and between

measurements obtained from basal and mid-ventricular short-axis slice positions. These differences must be taken into account to allow appropriate analysis of DENSE data in patients.

DENSE was found to be informative in both acute and chronic MI. At both time points, strain measurements can be used to distinguish between myocardial segments with 0%, <50% and >50% infarction. There is the potential for the development of reference ranges which could be applied to strain measurements from future MI patients to allow assessment of the extent of infarction.

In acute MI, four additional applications were identified: i) comparison with references ranges, established from strain measurements in healthy subjects, can be used to identify the presence of infarction with high specificity and moderate to high sensitivity, ii) peak Ecc can be used to distinguish between segments categorised as remote and adjacent, iii) strain measurements in the acute setting may provide prognostic information relating to the potential progression or recovery of contractile abnormalities in the chronic setting, iv) peak Ecc may allow a preliminary assessment of LV ejection fraction. Sensitivity for the detection of injured but non-infarcted segments was low.

In chronic MI, two additional applications were identified: i) strain recovery can be detected in infarcted myocardial segments, and also in non-infarcted segments which are located adjacent to infarcted segments, which could improve identification of changes in contractile function compared to conventional qualitative analysis of cine imaging, ii) strain measurements can be used to distinguish between segments in which the extent of infarction has increased and those in which it has decreased. The relationships with myocardial salvage index were not found to be informative.

Conclusions: DENSE images were successfully acquired and analysed from both healthy subjects and patients with myocardial infarction, which indicates that the technique is feasible in different clinical settings. DENSE strain measurements were found to be informative in both acute and chronic MI, and can provide insight into the presence and extent of infarction and the progression or recovery of contractile abnormalities.

In memory of my dad, John McComb

1951 - 2012

Contents

List of Figures

List of Tables

Abbreviations

AV	Atrioventricular
BMI	Body Mass Index
CMR	Cardiac Magnetic Resonance
DENSE	Displacement ENcoding via Stimulated Echoes
EPI	Echo Planar Imaging
FLASH	Fast Low Angle SHot
LAD	Left Anterior Descending (Artery)
LCA	Left Coronary Artery
LCX	Left Circumflex
LGE	Late Gadolinium Enhancement
LV	Left Ventricle
LVEF	Left Ventricular Ejection Fraction
LVEDV	Left Ventricular End-Diastolic Volume
LVESV	Left Ventricular End-Systolic Volume
LVOT	Left Ventricular Outflow Tract
MI	Myocardial Infarction
MRI	Magnetic Resonance Imaging
NMV	Net Magnetisation Vector
NSTEMI	Non-ST Elevation Myocardial Infarction
RCA	Right Coronary Artery
ROI	Region of Interest
SAR	Specific Absorption Rate
SD	Standard Deviation
SSFP	Steady State Free Precession
STE	Stimulated Echo
STEAM	STimulated Echo Acquisition Mode
STEMI	ST Elevation Myocardial Infarction
TE	Echo Time
TI	Inversion Time
TR	Repetition Time

Relevant Conference Abstracts

McComb C, Carrick D, Woodward R, McClure J, Radjenovic A, Berry C, Foster J. Assessment of Contractile Function using DENSE in Patients with Myocardial Infarction. International Society for Magnetic Resonance in Medicine (ISMRM) 22nd Annual Meeting, Milan, Italy, May 2014

McComb C, Carrick D, Woodward R, McClure J, Radjenovic A, Foster J, Berry C. Assessment of Longitudinal Changes in Strain Using DENSE in Patients with Myocardial Infarction. Society for Cardiovascular Magnetic Resonance (SCMR) 17th Annual Scientific Sessions, New Orleans, USA, January 2014

McComb C, Carrick D, Woodward R, McClure J, Radjenovic A, Foster J, Berry C. In-vivo Assessment of the Diagnostic Performance of DENSE in Patients with Myocardial Infarction. Society for Cardiovascular Magnetic Resonance (SCMR) 17th Annual Scientific Sessions, New Orleans, USA, January 2014

McComb C, Payne A, Barrett R, McClure J, Foster J, Berry C. Measurement of Left Ventricular Strain with Strain-encoded MRI (DENSE) is Feasible and Informative in Patients with Acute Myocardial Infarction. Scottish Society for Experimental Medicine Autumn Meeting, Glasgow, UK, November 2011.

McComb C, Payne A, Barrett R, Smith C, Casey M, McClure J, Oldroyd K, Wen H, Foster J, Berry C. Measurement of Left Ventricular Strain with Strain Encoded MRI (DENSE) is Feasible and Informative in Patients with Recent or Chronic Myocardial Infarction. European Society of Cardiology (ESC) Congress, Paris, France, August 2011.

McComb C, Payne A, Smith C, Foster J, McClure J, Oldroyd K, Wen H, Berry C. Correlation between Left Ventricular Strain as Measured by DENSE and Transmural Extent of Infarct Scar. British Society of Cardiovascular Magnetic Resonance (BSCMR) Annual Meeting, Leicester, UK, March 2011.

Acknowledgements

The research presented within this thesis would not have been possible without the help and support of many people. I am incredibly grateful to each and every one of them, but would like to specifically mention a number of people whose contributions have been particularly appreciated.

Firstly, thank you to my supervisors, Dr John Foster (Clinical Physics) and Professor Colin Berry (Cardiology), for their guidance over the years. I would also like to thank Dr Aleksandra Radjenovic for her input and advice in the final months of the study.

Cardiology research fellows, Dr Alexander Payne and Dr David Carrick, provided training for the analysis of all cardiac MR images other than DENSE. Dr Payne was involved in the "preliminary evaluation" study, and all further assistance was provided by Dr Carrick. I am very grateful to them both, and in particular I would like to thank Dr Carrick for regularly going above and beyond the call of duty to help me.

Assistance with the assessment of DENSE repeatability was provided by Rachael Barrett, Cardiology BMedSci student, who kindly assumed the role of “operator 2”.

Thank you to Dr Han Wen at NIH and to Siemens Healthcare for allowing me to have access to their DENSE pulse sequences and analysis software. In particular, thanks to Peter Weale, cardiac applications specialist at Siemens, for all of his assistance.

Statistical advice was provided by Dr John McClure at the University of Glasgow, and I am very grateful for his help.

This research would not have been possible without the patients and volunteers who participated in the studies. I cannot thank them enough for their time and enthusiasm.

Thank you to the radiographers at the Golden Jubilee National Hospital and the BHF Glasgow Cardiovascular Research Centre. Without them, there would be no images and no study. I would particularly like to thank the GCRC radiographers – Tracey

Steedman, Kirsten Lanaghan, Rosie Woodward, Heather Boylan, Evonne Mclennan and Alison Frood, and our Healthcare Assistant, Margaret Hay. In addition to producing wonderful images, they have provided me with an endless supply of tea, cake and good advice, and I truly could not have made it through this without them.

Last but not least, a huge thank you to my amazing parents, partner and friends, who have encouraged and supported me through all the ups and downs.

Author's Declaration

I declare, except where explicit reference is made to the contribution of others, that this thesis is the result of my own work and has not been submitted for any other degree at the University of Glasgow or any other institution.

The STEMI patient data used in Chapters 4, 7 and 8 were obtained as part of larger clinical studies carried out at the Golden Jubilee National Hospital. Recruitment of STEMI patients was performed by Cardiology research fellows, Dr Alexander Payne and Dr David Carrick. The author does not claim ownership of these studies.

C. McComb

April 2014

Chapter 1

Introduction

1.1 Motivation

In patients with myocardial infarction (MI), regional left ventricular contractile function has important prognostic value. Contractile function can be assessed using various imaging modalities, including magnetic resonance imaging (MRI). Many cardiac MRI techniques involve qualitative analysis, such as cine imaging of left ventricular displacement, and there is growing interest in alternative methods which enable quantitative measurements and which have the potential to improve diagnostic sensitivity and specificity [1].

In routine clinical practice, quantitative assessments of contractile function are often made by measuring the change in wall thickness between diastole and systole [2, 3]. However, this technique is dependent on accurate delineation of endo- and epi-cardial surfaces, and while motion of the surfaces provides information on the radial components of wall motion, it is not possible to assess circumferential components or measure the transmural distribution of motion within the myocardium [4]. A more informative picture of contractile function can be obtained by quantifying myocardial strain, which has been shown to be more sensitive for the detection and assessment of injury due to ischaemic heart disease than wall thickening [1, 5].

Several MRI techniques have been developed to allow measurement of myocardial strain, and one such method, named DENSE, has recently become available at our institution. To date, much of the research performed with DENSE has been methods development, and its application in a routine clinical setting has been incompletely investigated. The purpose of the research presented within this thesis is to investigate variations in strain within the healthy heart, and then to assess the in vivo performance of DENSE strain imaging in acute and chronic myocardial infarction.

1.2 Key Aims of Thesis

The investigations described within this thesis aimed to test the following hypotheses relating to the implementation of DENSE available at our institution:

1. There is no difference in myocardial strain as measured by DENSE and myocardial strain as measured by other techniques.
2. There is a strong relationship between DENSE strain parameters and the extent of myocardial infarction.
3. DENSE strain parameters can be used to distinguish between varying extents of infarction.
4. DENSE strain parameters can be used to distinguish between remote and infarcted tissue.
5. DENSE strain parameters have high sensitivity and specificity for the detection of contractile abnormalities associated with myocardial infarction and injury.
6. Longitudinal measurements of strain with DENSE can provide information relating to the changes in contractile abnormalities over time following infarction.

Positive outcomes for the above would enable the technique to be developed further as a diagnostic tool.

1.3 Outline of Thesis

Chapter 2 begins with a review of the relevant anatomy, followed by a discussion on the current MRI techniques which can be used to assess myocardial strain, and their application in healthy volunteers and patients with myocardial infarction. A detailed description of the development of the DENSE pulse sequence is then provided.

Chapter 3 contains details of the image acquisition and analysis protocols that are used throughout the thesis.

Chapter 4 describes a preliminary clinical assessment which was carried out to evaluate the two versions of the DENSE pulse sequence which were available, and to

determine whether DENSE showed potential for providing useful clinical information.

Chapter 5 contains a more thorough evaluation of the DENSE pulse sequence, in which the repeatability of image acquisition and analysis is assessed, and a comparison is performed of the strain measurements obtained using DENSE with those obtained using myocardial tagging, which is an established MRI method for strain measurement.

Chapter 6 involves the application of DENSE in healthy volunteers, and investigates whether strain as measured by DENSE varies with gender, age, myocardial segment and slice position. This information is then used to establish reference ranges for each strain parameter. In addition, the effect of magnetic field strength on DENSE results is assessed using images acquired at both 1.5T and 3T.

Chapter 7 investigates the clinical application of DENSE in patients with acute myocardial infarction, and assesses the relationships between strain parameters and contractile abnormalities associated with both the extent of infarction and area at risk.

Chapter 8 follows up on the results from Chapter 7 by measuring strain in the same group of patients at 6 months after myocardial infarction. The relationships between strain parameters and contractile abnormalities associated with both the final extent of infarction and salvage are investigated.

Chapter 9 provides a summary of the main findings of the thesis, and identifies potential future investigations involving DENSE.

Chapter 2

Imaging of Myocardial Function and Injury

2.1 Introduction

Magnetic Resonance Imaging (MRI) is a modality which can produce images with high resolution and excellent soft tissue contrast, and which does not involve the use of ionising radiation. Although the potential of MRI as a tool for the non-invasive diagnosis of heart disease has long been recognised, the application of the technique was initially complicated by the movement of the heart during the cardiac cycle, and the movement of the chest during respiration. However, improvements in ECG gating in the MR environment and the development of fast image acquisition techniques have allowed these issues to be overcome. Cardiac MR (CMR) is becoming increasingly popular for the assessment of myocardial morphology, perfusion and function, and can provide useful clinical information in a variety of conditions.

The purpose of this chapter is firstly to give a brief introduction to the anatomy of the heart, and then to describe the MRI techniques currently used in the assessment of myocardial function and injury, specifically in myocardial infarction (MI). Finally, the MRI techniques which are currently available for the quantitative assessment of myocardial strain will be discussed.

2.2 The Human Heart

2.2.1 Anatomy

The heart is a muscular organ which is located near the anterior chest wall, directly posterior to the sternum, and whose purpose is to provide a continuous circulation of blood throughout the body. A diagram of the anatomy of the heart is shown in Figure 2-1 [6].

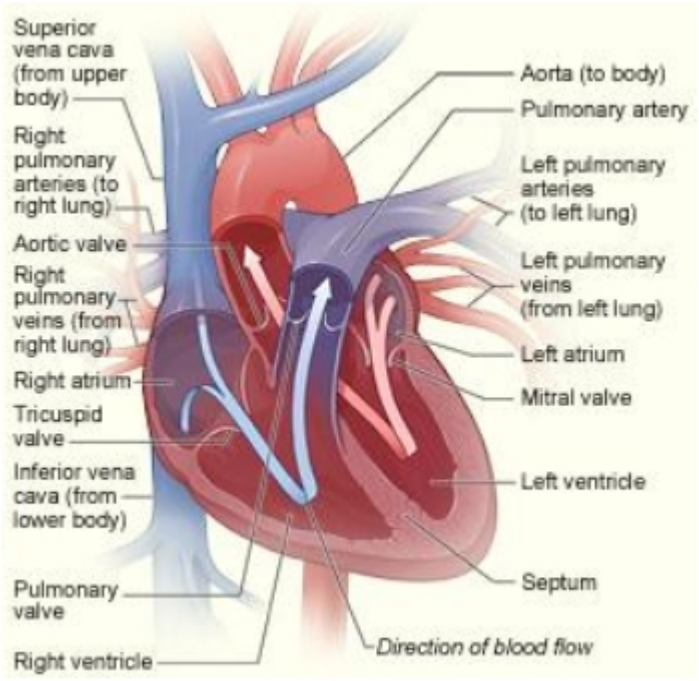

Figure 2-1: The human heart

Blood is carried around the body by a network of blood vessels that extend between the heart and the peripheral tissues. The blood vessels can be divided into two circuits – the pulmonary circuit, which carries blood to and from the lungs, and the systemic system, which carried blood to and from the rest of the body. The heart contains four chambers – right atrium, right ventricle, left atrium and left ventricle – and the two chambers on the right are associated with the pulmonary circuit, while the two chambers of the left are associated with the systemic circuit.

Blood returning from the body enters the right atrium via the superior and inferior vena cava, which deliver blood from the upper body (head, neck, upper limbs and chest) and lower body (remainder of trunk, viscera and lower limbs) respectively. The right atrium and right ventricle are separated by the right atrioventricular (AV) valve, which is also known as the tricuspid valve. This valve opens when the right atrium contracts to allow blood to pass into the right ventricle, then closes during ventricular contraction to prevent the backflow of blood. When the right ventricle contracts, blood flows through the pulmonary valve into the pulmonary trunk, which is the start of the pulmonary circuit. Similarly to the AV valve, the pulmonary valve opens during ventricular contraction then closes to prevent backflow of blood. The pulmonary trunk divides into the left and right pulmonary arteries, which travel to the

left and right lungs, and then subdivide repeatedly within the lungs until the blood reaches the capillaries where gas exchange takes place. The capillaries then form into small veins that eventually unite to form the pulmonary veins, which carry blood back towards the heart.

Blood returning from the lungs enters the left ventricle via the pulmonary veins. The left atrium and left ventricle are separated by the left AV valve, which is also known as the bicuspid or mitral valve. The left ventricle has thicker walls than the right ventricle since it must pump blood throughout the entire body, whereas the right ventricle only needs to pump blood to the lungs. When the left ventricle contracts, blood flows through the aortic valve into the ascending aorta, through the aortic arch and into the descending aorta, from where it travels to tissues throughout the body to provide oxygen. De-oxygenated blood returns to the right atrium of the heart via the vena cava, and the cycle begins again.

At the beginning of the cardiac cycle, the left ventricle is fully relaxed, and this state is known as end-diastole (ED). When the left ventricle is in a state of maximum contraction, this is known as end-systole (ES).

In order to pump blood around the body, the muscles of the heart themselves require a blood supply, which is provided by the coronary circulation, as illustrated in Figure 2-2 [7]. The left and right coronary arteries originate at the base of the ascending aorta. The right coronary artery (RCA) supplies blood to the right atrium and portions of both ventricles. The left coronary artery (LCA) splits into the circumflex artery (LCX) and the left anterior descending (LAD) artery, and supplies blood to the left atrium, left ventricle and intra-ventricular septum.

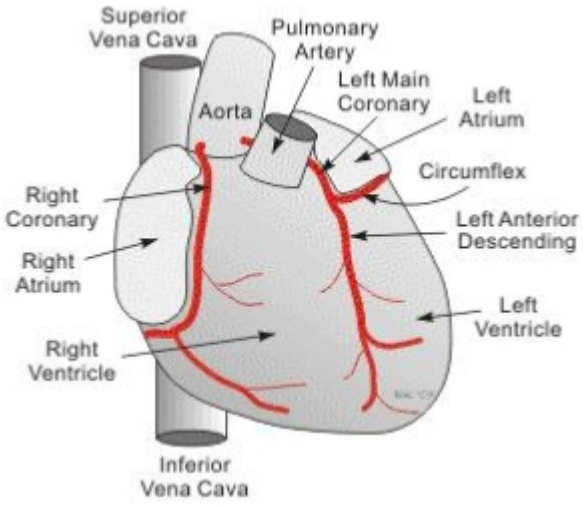

Figure 2-2: The coronary arteries

The heart walls consist of three distinct layers – an outer layer called the epicardium, a middle layer called the myocardium and an inner layer called the endocardium. The epi- and endo-cardium are membranes which cover the outer and inner surfaces of the heart, while the myocardium consists of concentric layers of contractile muscle tissue [8].

2.2.2 Ischaemia and Infarction

The average healthy human heart weights 300 – 350g, which is ~0.5% of the total body mass, yet the oxygen demand of the heart accounts for 7% of the resting body oxygen consumption and 5% of the cardiac output.

Myocardial ischaemia is defined as the situation where myocardial tissue oxygen demand is greater than supply, and is caused by transient or incomplete occlusion of one or more of the coronary arteries. Occlusion most commonly occurs due to thrombosis caused by fissure or rupture of atherosclerotic plaques. During short-term ischaemic episodes, the heart responds to the imbalance in oxygen supply by down-regulating contractile function and by increasing the rate of anaerobic energy production, or glycolysis. Following prompt reperfusion, myocardial tissue can usually be described as “normal” or “stunned”. In the stunned myocardium, impairment of myocardial function occurs due to reperfusion injury caused by the presence of oxygen radicals and changes in intracellular calcium levels, but is acute and completely reversible. If the decrease in oxygen supply is sustained for a

prolonged period, it is possible for the myocardium to enter a state known as "hibernation". Hibernation is a chronic hypocontractile state, and full recovery of function may only occur after revascularisation.

As an ischaemic episode becomes more prolonged due to sustained coronary occlusion, the heart becomes unable to produce a sufficient amount of energy via glycolysis, and cellular necrosis begins. This state is known as myocardial infarction, and no recovery of contractile function occurs. The most vulnerable layer of the heart is the sub-endocardium, as it has a relatively greater metabolic demand compared to the mid and epicardial layers due to higher systolic wall stress. Myocardial infarcts spread from the sub-endocardium to the sub-epicardium in a period of 3 - 4 hours [9].

Shortly after the onset of myocardial infarction, an inflammatory reaction occurs, and circulating neutrophils and macrophages begin to break down the necrotic cells. The extracellular collagen matrix also begins to degrade as a result of enzymes released by neutrophils. This inflammatory response peaks at 1 – 2 weeks, and disappears within 3 – 4 weeks post-MI.

Following the initial phase of collagen degradation, lost tissue begins to be replaced by fibrosis. The remaining viable myocytes in the region of injury are realigned and attached in a dense collagen matrix, which forms scar tissue. In patients with extensive MI, fibrosis may also develop in non-infarcted myocardium [10, 11, 12].

In the early phase of ischaemic injury, the balance of ions within myocytes is disrupted, which causes an increase in intracellular osmotic pressure and results in a net inflow of water. In addition, water is released from proteins due to lactate-induced acidosis, which increases the amount of unbound water in the intracellular space. The combined effect of these processes causes the myocytes to swell, and is known as intracellular oedema.

Prolonged ischaemia of more than 60 – 90 minutes results in damage to capillary membranes, and causes leakage of water from the intravascular space into the interstitial space. This is known as interstitial oedema. Following reperfusion, an

inflammatory reaction takes place that promotes an additional increase in interstitial oedema [13, 14].

There are two diagnostic forms of myocardial infarction – ST elevation myocardial infarction (STEMI) and non-ST elevation myocardial infarction (NSTEMI). STEMI occurs when the artery is completely occluded and often results in transmural infarction, and is usually treated using reperfusion therapy, such as percutaneous coronary intervention (PCI) or thrombolysis. Elevation of the ST segment in the ECG recording occurs due to changes in transmembrane action potentials in ischaemic tissue, which result in a voltage gradient, and hence an "injury current", between ischaemic and non-ischaemic tissue [15]. In NSTEMI, the artery is only partially or transiently occluded, and usually results in a smaller area of infarction which can often be treated medically.

2.2.3 The AHA Model

There are several imaging techniques which can be used to assess cardiac anatomy and function, e.g. echocardiography, computed tomography (CT) and single photon emission computer tomography (SPECT), and each of these modalities has independently evolved to use different definitions for cardiac imaging planes, myocardial segments etc. In order to facilitate cross-modality cardiac imaging for clinical and research purposes, the American Heart Association (AHA) produced recommendations for the names of the cardiac planes, the number of myocardial segments, and the nomenclature and location of segments [16].

Traditionally, modalities such as MRI and CT oriented and displayed images of the body using planes which were parallel or perpendicular to the long axis of the body. However, this did not provide an optimal view of the ventricles or atria. Echocardiography and SPECT, on the other hand, define the orientation of the heart for display as perpendicular to the long axis of the left ventricle that transects the centre of the apex and mitral valve plane. This approach maintains the integrity of the cardiac chambers, and is recommended by the AHA. The definitions of the three main imaging planes of the heart – short axis, vertical long axis (two chamber) and horizontal long axis (four chamber) – are illustrated in Figure 2-3.

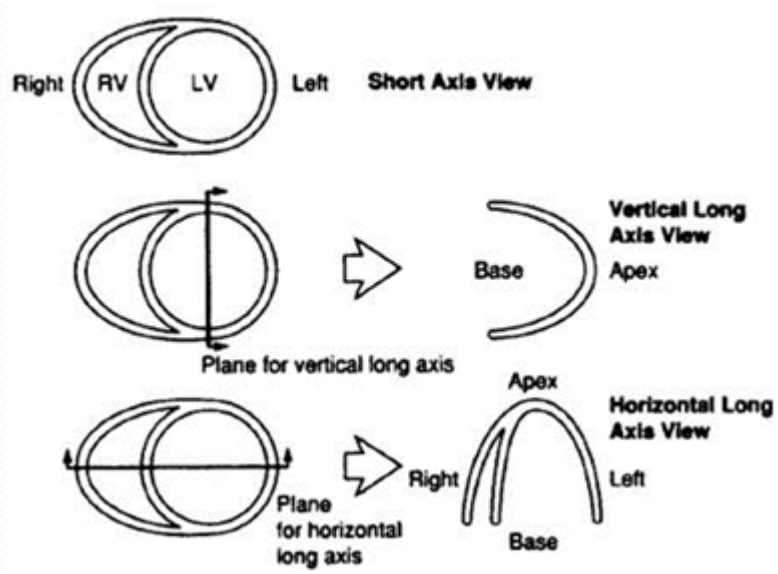

Figure 2-3: Cardiac imaging planes

For regional assessment of left ventricular function, the ventricle should be divided into equal thirds perpendicular to the long axis of the heart, resulting in basal, mid-ventricular and apical short-axis slices. These slices can be further divided into segments for analysis purposes. The AHA model contains 17 segments, which were defined using precise data on the mass and size of the myocardium from autopsy studies, resulting in a distribution of 35%, 35% and 30% for the basal, mid-ventricular and apical sections of the heart. The numbering and nomenclature for the segments are shown in Figure 2-4 [17].

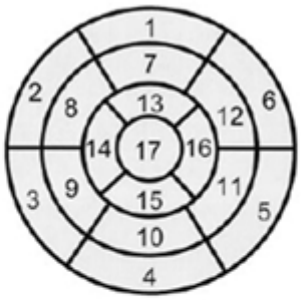

1. basal anterior
2. basal anteroseptal
3. basal inferoseptal
4. basal inferior
5. basal inferolateral
6. basal anterolateral
7. mid-anterior
8. mid-anteroseptal
9. mid-inferoseptal
10. mid-inferior
11. mid-inferolateral
12. mid-anterolateral
13. apical anterior
14. apical septal
15. apical inferior
16. lateral
17. apex

Figure 2-4: AHA 17 segment model

2.3 MRI Techniques for Imaging of Myocardial Function and Injury

2.3.1 Contractility - Cine Imaging

Cine imaging provides a dynamic visualisation of the beating heart throughout the cardiac cycle, and is used in the assessment of cardiac function. Images are acquired with ECG-gating and breath-holding to eliminate artefacts from cardiac and respiratory motion, and a balanced steady state free precession (b-SSFP) pulse sequence is used, as illustrated in Figure 2-5 [18].

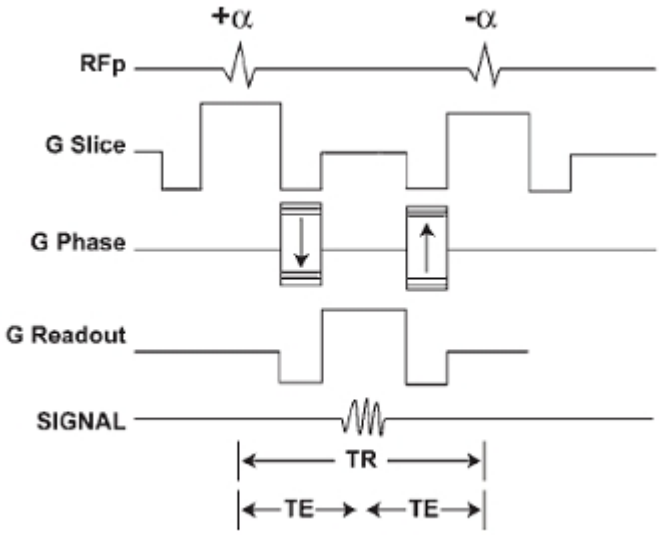

Figure 2-5: Balanced SSFP pulse sequence for cine imaging**.**

In a b-SSFP pulse sequence, a series of RF pulses with equal amplitude, flip angle and spacing are applied in order to maintain a steady state of both longitudinal and transverse magnetisation. In general, several TR periods are required before the steady state is reached. However, for a b-SSFP sequence with a flip angle α, an initial RF pulse of $\alpha/2$ at time TR/2 before the first application of the pulse sequence will immediately force the magnetisation into a steady state. Magnetic field gradients are applied between the RF pulses, and must be completely balanced in all directions to ensure that the net phase accumulation during the TR is zero. Additionally, the TR must be short to prevent the accumulation of phase errors due to magnetic field inhomogeneities, which can result in banding artefacts. Banding artefacts can also be reduced by alternating the phase of the RF pulse by 180^{o} in subsequent RF periods,

which is equivalent to alternating the sign of the flip angle i.e. $+\alpha, -\alpha, +\alpha$ etc. The intrinsic contrast of a b-SSFP sequence is determined by the T_2/T_1 ratio of the tissue, which results in excellent contrast between blood and the myocardium, and makes this type of pulse sequence particularly useful for cardiac cine imaging [18, 19].

The acquisition technique used in cine imaging involves k-space segmentation. Following a single ECG "R" wave trigger, multiple lines of k-space are acquired for each cardiac phase. This reduces the number of heartbeats required to completely fill k-space, and allows images to be acquired during a feasible breath hold [20].

In a typical cardiac MRI examination, cine images are obtained in the vertical long axis, horizontal short axis and a stack of short axis slices covering the extent of the left ventricle.

Cine images can be used to measure myocardial thickening, and hence to assess if wall motion abnormalities are present. Thickening is defined as the difference between the measured myocardial thicknesses at ES and ED, and is typically expressed as a percentage increase relative to the thickness at ED. As mentioned in Chapter 1, the motion of the endo- and epi-cardial surfaces between ED and ES provides information on the radial components of wall motion, but it is not possible to assess circumferential components or measure the transmural distribution of motion within the myocardium.

Several studies have investigated wall thickening in the healthy myocardium, and a range of values have been found e.g. a mean value of 59% was reported in volunteers aged 53 ± 7 years [21], 80 ± 23% in volunteers aged 22 – 65 years and 89 ± 22% in volunteers aged 65 – 91 years [22], 48 ± 28% in volunteers aged 21 – 37 years [23] and a range of 18 – 100% in volunteers aged 25 – 34 years [24]. Differences in thickening were observed between the myocardial segments, but these were not found to be statistically significant [23].

The full stack of short axis cine images can be used to quantify the volume of the left ventricular cavity at end-diastole (LVEDV) and end-systole (LVESV). LVEDV and

LVESV are calculated by outlining the endocardial border at end-diastole and end-systole respectively in each slice and multiplying by the slice separaration, then summing the results for all slices in the stack. Left ventricular ejection fraction (LVEF) can then be calculated using Equation 2-1 [25].

$$LVEF(\%) = \frac{LVEDV - LVESV}{LVEDV} \times 100 \qquad \textbf{(Equation 2-1)}$$

Examples of short axis images obtained at ED and ES in both a healthy subject and a patient with MI are shown in Figure 2-6. The red arrow indicates a region of hypocontractility.

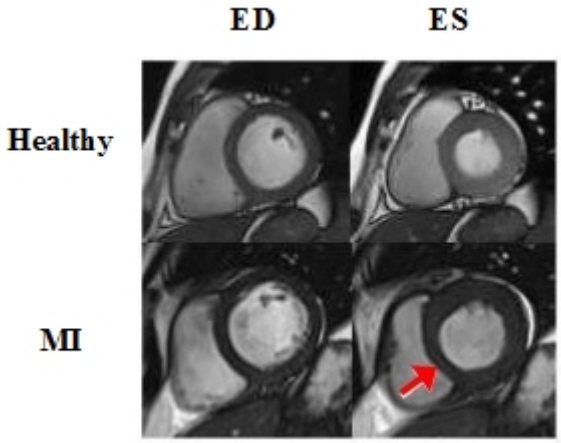

Figure 2-6: Cine images at ED and ES for healthy subject and patient with MI

2.3.2 Infarction – Late Gadolinium Enhancement Imaging

Late gadolinium enhancement (LGE) imaging, also known as delayed contrast enhancement imaging, is used for the assessment of myocardial viability. A gadolinium (Gd) chelate contrast agent is used, which has paramagnetic properties and acts to shorten the T_1 of adjacent tissues. Gd is administered intravenously and distributes rapidly into both the intravascular and interstitial spaces, and is then gradually washed out by subsequent blood flow. The degradation of cells in a region of myocardial infarction results in an increase in the interstitial space, and hence an increased volume for the accumulation of Gd. The washout of Gd from infarcted tissue occurs more slowly than in healthy myocardium, and consequently infarcted

regions appear brighter on T_1-weighted images [26]. Imaging takes place 10 minutes after administration of Gd [27].

Images are acquired with ECG-gating and breath-holding, and a phase sensitive inversion recovery (PSIR) turbo FLASH pulse sequence is used [28]. A non-selective 180^o inversion pulse is applied following the detection of the "R" wave trigger, and the turbo FLASH imaging component of the sequence occurs after a time delay, or inversion time (TI). The TI is chosen such that the signal from normal myocardium is nulled, thus giving the best contrast between infarcted and non-infarcted tissue. A frequency scout is run before the PSIR sequence to determine the optimal value of TI for a particular patient, with typical values being ~280 - 320ms.

Fast Low Angle SHot (FLASH) is an gradient-spoiled gradient echo sequence. Small flip angles, e.g. 20^o, are used which means that a large proportion of the longitudinal magnetisation is unaffected, and is therefore available for immediate subsequent excitations. Following each RF pulse, a magnetic field gradient is applied to disperse any remaining transverse magnetisation before the application of the next pulse [29].

Initial validation of LGE was performed in animals [30, 31], and quantification of the region of LGE was performed by setting a threshold of 2 or 3 standard deviations (SD) above the mean signal intensity in remote myocardium. However, imaging was performed ex vivo with a resolution of $0.5 \times 0.5 \times 0.5$mm. In an in vivo clinical setting, the voxels are much larger and imaging is complicated by cardiac motion, and consequently partial volume effects are much more of an issue, resulting in "intermediate" voxels which contain a mixture of both infarcted and non-infarcted tissue. In this situation, a 2SD threshold may overestimate the size of the infarct, and a threshold of 5SD may be more appropriate [32].

Some studies have suggested that LGE occurs not only in regions of cellular necrosis, but also in a border zone of injured but viable myocardium. The enhancement of the border zone may be related to the presence of sufficient residual flow to the periphery of the infarct via collateral vessels [33, 34]. This would occur in the acute setting only, and so the infarct size would appear to have decreased in the chronic setting. However, a study conducted in a canine model which compared the spatial extent of

LGE to the spatial extent of myocyte necrosis revealed by histology and found that the two were identical, which indicates that there is no hyperenhancing border zone. The authors concluded that LGE does not occur in reversibly injured regions, and that temporal changes in the spatial extent of hyperenhancement could be explained by infarct shrinkage during the transition from necrosis to collagen scar formation [35].

An example of an LGE image obtained from a patient with acute MI is shown in Figure 2-7. The red arrow indicates the region of enhancement defined using a threshold of 5SD above the mean signal intensity in remote myocardium.

Figure 2-7: LGE image in acute MI

2.3.3 Oedema – T_2 Mapping

As described in Section 2.2.2, oedema occurs following acute injury to the myocardium. The extent of oedema is indicative of the area at risk, i.e. the area of myocardium which could potentially be saved but is likely to become infarcted in the absence of reperfusion. Visualisation of the area at risk can be achieved using T_2 maps, which are generated using a T_2-prepared single-shot SSFP pulse sequence [36, 37] applied with ECG-gating and breath-holding.

T_2-preparation was achieved using a Carr-Purcell Malcom-Levitt (MLEV) sequence consisting of an initial 90^o pulse, followed by a train of 180^o pulses which refocus the transverse magnetisation and invert any longitudinal magnetisation, with a final 90^0 pulse to return the magnetisation to the longitudinal plane [38]. The pulse sequence is applied after every 4^{th} RR interval to allow sufficient time for T_1 recovery, which ensures maximal T_2 weighting. Three applications of the sequence allows three images to be acquired, each at the same diastolic phase but with a different T_2

preparation time (TE_{T2P} = 0, 25, 55ms), the values of which were chosen to cover the expected range of T_2 values in the myocardium. A non-rigid registration algorithm is applied to compensate for in-plane motion between the images, then a T_2 map is generated by fitting the two-parameter equation shown in Equation 2-2 to corresponding pixels from each of the three images:

$$S(x,y) = M_0(x,y)\exp\left(\frac{-TE_{T2P}}{T_2(x,y)}\right) \qquad \textbf{(Equation 2-2)}$$

where $S(x,y)$ is the signal intensity in the pixel located at position (x,y) and M_0 is the equilibrium magnetisation.

The area at risk can be defined by setting a threshold of 2SD above the mean value in remote myocardium [39]. Myocardial salvage is measured in the chronic setting, and is defined as the difference between the area at risk ($\%T_2$) and the final area of infarction ($\%LGE$) [40, 41]. Myocardial salvage index (MSI) is defined using Equation 2-3 [41]:

$$MSI = \frac{\%T_2 - \%LGE}{\%T_2} \qquad \textbf{(Equation 2-3)}$$

Examples of T_2 maps from a healthy volunteer and a patient with acute MI are shown in Figure 2-8. The red arrow indicates a region of T_2 hyperenhancement.

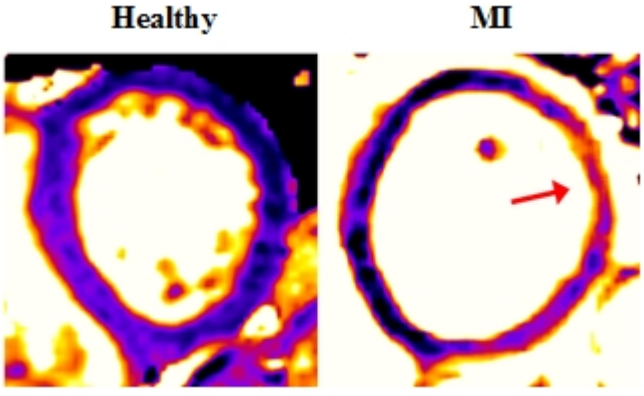

Figure 2-8: T_2 Maps for healthy subject and acute MI

In 2012, a review paper was published which questioned the validity of using T_2-weighted imaging to define the area at risk [42]. Three pre-clinical studies [43 - 45] are widely considered as proof that hyperintense regions in T_2 images represent the

area at risk. However, the review paper pointed out the small sample sizes in each of the studies, and also a number of limitations such as incomplete histopathology and low spatial resolution. The authors were of the opinion that many of the conclusions from these studies were based on size comparisons of abnormal regions defined by different MR imaging techniques, and none of the studies showed any images or data which allowed a direct comparison between the shape and contour of the T_2-weighted abnormalities with the shape and contour of the area at risk as defined by an appropriate pathology reference standard.

Many other studies have also suggested that T_2-weighted imaging can be used to depict the area at risk, but rather than providing a comparison between the MR images and a pathology reference, the authors have based their conclusions on the fact that the T_2 hyperintense region is larger than the infarct size as determined by LGE imaging. The authors of the review paper noted that many studies define a threshold of 2 standard deviations above the mean value in remote tissue for delineating hyperintense T_2 regions, and a threshold of 5 standard deviations above the mean for delineating the region of infarction in LGE images. They were of the opinion that using a lower threshold for T_2 images increases the likelihood that the region of oedema will be substantially greater than infarct size simply because of partial volume effects.

There are also a number of questions about the physiological basis for the observed T_2 findings. For example, the evidence from several studies indicates that substantial oedema occurs within regions of irreversible injury, i.e. infarction, with minimal or no oedema within regions of reversible injury. A homogenously bright area at risk on a T_2-weighted image is incompatible with this, and signal differences between infarcted and reversibly injured tissue should be far greater than those between reversibly injured and unaffected tissue.

The authors of the review paper acknowledge that there a number of potential applications for T_2-weighted imaging, for example differentiation between acute and chronic MI and identification of acute myocarditis, but based on the currently available data, the technique may not be appropriate for the delineation of area at risk in ischaemic myocardial injury.

2.4 MRI Techniques for the Assessment of Myocardial Strain

2.4.1 Myocardial Strain

Strain is a measure of deformation, and is defined in the Lagrangian frame of reference as the fractional change in length of an object relative to its original length, as shown in Equation 2-4:

$$E(t) = \frac{L(t) - L(0)}{L(0)} \qquad \textbf{(Equation 2-4)}$$

where *L(t)* is the length of the object at time *t*, and *L(0)* is the original length of the object, which remains constant over time.

Myocardial strain is a 3D tensor which takes into account both the fractional change in length and the direction of that change in length. In the Radial-Circumferential-Longitudinal (RCL) coordinate system, the 3D myocardial strain tensor is defined as shown in Equation 2-5:

$$E = \begin{pmatrix} E_{RR} & E_{RC} & E_{RL} \\ E_{CR} & E_{CC} & E_{CL} \\ E_{LR} & E_{LC} & E_{LL} \end{pmatrix} \qquad \textbf{(Equation 2-5)}$$

The diagonal components, known as "normal" strains, describe strains in the orthogonal directions which define the system, while off-diagonal components represent shear strain in the plane defined by the two indices. In each case, positive values of strain represent lengthening and negative values represent shortening [46].

The directions of the normal strains are illustrated in Figure 2-9 [47]. Radial strain (E_{RR}) occurs perpendicular to the long axis and the epicardium and represents myocardial thickening and thinning in the short axis. Circumferential strain (E_{CC}) represents the change in radius of the short axis, and longitudinal strain (E_{LL}) represents motion from the base to the apex.

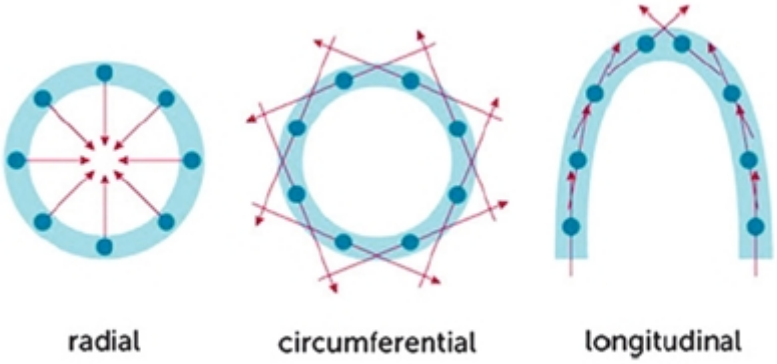

Figure 2-9: Directions of normal strains in the RCL coordinate system

2.4.2 Tagging

The first MRI method which allowed myocardial motion and deformation to be visualised and quantified was myocardial tagging. The basic principle of tagging, which involves perturbing the magnetisation to create visible tags which can then be tracked, was first introduced in 1988 [48]. Slice-selective RF pulses are applied perpendicular to the imaging plane to perturb the longitudinal magnetisation along parallel lines within the plane, while the remainder of the magnetisation is undisturbed. The imaging sequence is then applied, and since the magnetisation in the "tagged" lines is already saturated, these regions have low signal intensity in the resulting image compared to the non-tagged tissues. Magnetisation is an intrinsic property of the tissue, and hence the tags follow the motion of the tissue during the cardiac cycle. In the original implementation of the technique, the slice-selective RF pulses were applied at end-diastole following the detection of the R-wave of the electrocardiogram, and imaging occurred at end-systole to allow the maximum contraction of the myocardium to be assessed.

While it was possible to use the early tagging pulse sequence to follow myocardial motion, the technique had several limitations. During the time delay between the application of the tags and imaging, the longitudinal relaxation of the tagged tissues recovered at an exponential rate depending on the time constant T_1 of the tissue. This meant that as the time delay between tagging and imaging increased, for example in patients with low heart rates, the contrast between tagged and non-tagged tissues decreased. A separate RF pulse was required for each tag line, which resulted in long time delays to allow the tags to be applied and a high specific absorption rate (SAR)

for the patient, which subsequently limited the number of tags which could practically be produced, and hence limited the tagging resolution which could be achieved [49].

The second implementation of a tagging pulse sequence was developed in 1989, and named "SPAtial Modulation of Magnetisation" or SPAMM [50]. An example of a typical SPAMM pulse sequence diagram is shown in Figure 2-10 [49].

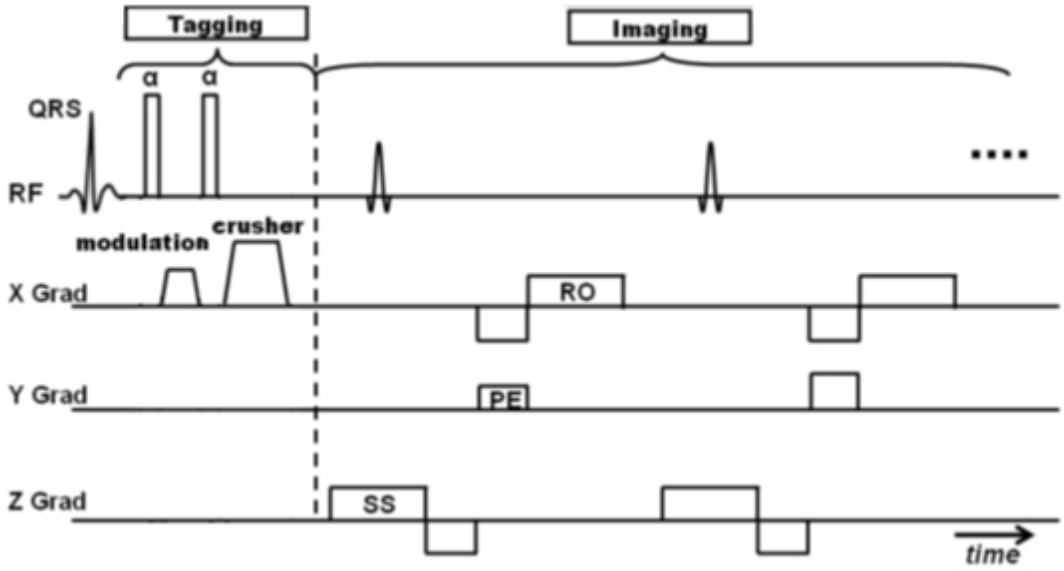

Figure 2-10: Basic SPAMM pulse sequence diagram

The basic pulse sequence consists of a "tagging" component and an "imaging" component. The tagging component consists of two non-selective RF pulses, the first of which tips the magnetisation into the transverse plane, with all of the spins initially in phase. 90^{o} RF pulses can be used to modulate the entire magnetisation, or a smaller flip angle can be used for partial modulation, which leaves part of the longitudinal magnetisation intact and allows the pulse sequence to be repeated with a shorter TR. A modulation or tagging gradient is then applied in the required tagging direction, which induces a range of phases and has the effect of "wrapping" the transverse magnetisation in a sinusoidal manner along the gradient direction. The second RF pulse then returns the modulated magnetisation to the longitudinal plane, and a crusher gradient is applied to eliminate any remaining transverse magnetisation before the imaging component begins. The modulated longitudinal magnetisation results in a corresponding intensity modulation in the final image, which appears as regularly

spaced parallel lines in a direction perpendicular to that of the modulating gradient. The spacing, *S*, between the stripes is determined by the amplitude and duration of the tagging gradient *G*, as shown in Equation 2-6:

$$S = \frac{1}{\gamma \int G dt} \qquad \textbf{(Equation 2-6)}$$

where γ is the gyromagnetic ratio. The imaging component in the original paper consisted of a "conventional cardiac gated imaging sequence", the details of which were not specified.

As for the original implementation of tagging, the phase of the tissue magnetisation is an intrinsic property of the tissue. In the time between the application of the tagging and imaging components of the pulse sequence, myocardial motion occurs, and the deformation of the tags in the resulting images reflects this. In this implementation of tagging, the R wave of the ECG was used to trigger the tagging component, and different time delays before the application of the imaging component were used to acquire a series of images at different points in the cardiac cycle.

Two-dimensional tagging grids are achieved by applying a second tagging component immediately following the first, with the tagging gradient applied in an orthogonal direction. To avoid producing artefacts from stimulated echo formation, the phase of the RF pulse is shifted by 90^{o} between the two tagging components [51]. Examples of myocardial tagging images acquired during diastole and systole with 7mm tag spacing are shown in Figure 2-11.

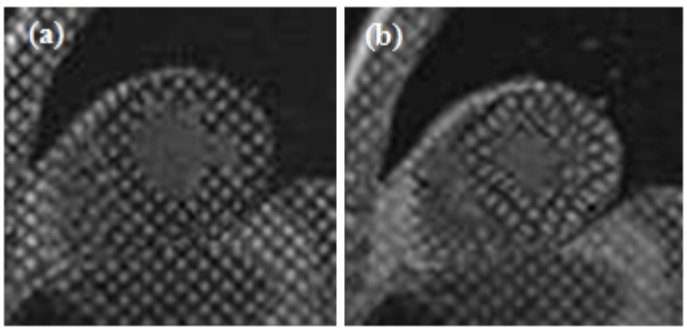

Figure 2-11: Myocardial tagging examples at a) diastole and b) systole

An alternative to the SPAMM tagging technique is Delay Alternating with Nutation for Tailored Excitation (DANTE) [52]. The tagging component of the DANTE pulse sequence consists of a series of short, high power RF pulses with flip angle $<90^{o}$ and equal spacing τ between, and with a continuous frequency-encoding gradient applied throughout instead of the SPAMM approach of applying separate gradients between the RF pulses. If the width of the RF pulses is less than τ, then the pulse sequence is approximately equivalent to the superposition of a number of RF signals with frequencies spaced $1/\tau$ Hz apart, which can be regarded as "sidebands" around the applied RF frequency. Selective excitation occurs at the applied and sideband frequencies, resulting in a series of bands parallel to the gradient direction in the final image [53]. The tagging process can be repeated in an orthogonal direction to produce a grid of tags.

The distance between the tag lines is determined by the magnitude of the applied gradient and the delay between the RF pulses – increasing the magnitude or lengthening the delay will produce tags which are closer together. Tag thickness is inversely proportional to the total length of the RF pulse train. The flexibility of adjusting the tag spacing and thickness is an advantage of the DANTE tagging technique, but the long duration of the tagging component is a disadvantage.

In 1992, myocardial tagging was developed further with the integration of a tagging component with a cine imaging component, which allowed visualisation of myocardial deformation throughout the cardiac cycle in a single breath-hold [54]. The tagging component used was a hybrid DANTE/SPAMM sequence, in which a gradient was applied throughout the RF pulse train, and reduced to a non-zero value during the application of the RF pulses. This reduced the bandwidth required to tag the myocardium, and decreased the duration of the tagging component. Cine imaging was achieved using a gradient-recalled acquisition in the steady state (GRASS) pulse sequence with segmented k-space acquisition, which produced cine images of the heart with 24ms temporal resolution in 4 – 16 heartbeats.

A major limitation of both the SPAMM and DANTE tagging techniques is the fading of the tag contrast during the cardiac cycle, which prevents the analysis of end-

diastolic motion. A modified version of SPAMM, called Complementary SPAtial Modulation of Magnetisation (CSPAMM) was developed to compensate for this limitation [55].

The reduction in contrast during the cardiac cycle is caused by two processes: i) longitudinal (T_1) relaxation which reduces the magnitude of the tagging grid and ii) longitudinal relaxation in tissue which contains no tagging information. The aim of CSPAMM was to enhance the fading tagging grid, and to eliminate the non-tagged magnetisation. The component of the magnetisation with the tagging information was separated from the relaxed components by performing two measurements – one with a positive tagging grid and one with a negative tagging grid. The positive grid was produced using a conventional 2D SPAMM sequence, and the negative grid was produced by applying the same 2D SPAMM sequence but with one of the four RF pulses inverted. Subtracting the two measurements resulted in an image containing the tagging information, but with no contribution from the relaxed component of the magnetisation. One limitation of CSPAMM is that it doubles the scan time compared to SPAMM.

A number of analysis techniques have been developed to allow quantitative assessment of myocardial strain from tagged images, including active contour analysis using snakes or spline curves and Harmonic Phase (HARP) analysis in which Fourier-based spatial frequency and phase information is used to track horizontal and vertical tag lines. The disadvantages of these techniques include complicated analysis, long processing times and substantial user interaction [49].

A recently developed analysis technique, which is faster and requires less user interaction, is sine-wave modelling, or SinMod [56]. SinMod maps displacement by analysing a series of images, in which the image intensity in the environment of each pixel is modelled as a summation of sine wavefronts with local frequency and amplitude, which move with the myocardial tissue. For each wave, the component of displacement perpendicular to the wavefront is estimated in each pixel to create a map of this component. 2D motion can be measured by combining the maps for different wave directions.

Validation of tagging techniques has been performed using phantoms, canine models, in which comparison was made with sonomicrometry measurements, and healthy human volunteers [57-60]. The results of these studies showed that tagging techniques allow highly accurate and precise measurements of myocardial strain, with higher precision observed for measurements of circumferential strain than for radial strain.

While tagging techniques are straightforward to implement and visualise, they have a disadvantage since the deliberate suppression of myocardial signal limits the resolution, which means that it is difficult to measure transmural variations in motion [61].

Strain ENCoded (SENC) imaging [62] is similar to tagging, and was developed to allow a more accurate assessment of longitudinal strain, which can be restricted by the small number of long axis images that can be acquired in addition to a full short axis stack during a typical patient scan. Instead of orienting the tag planes perpendicular to the imaging plane, the SENC tag planes are initially oriented parallel to the imaging plane. SENC measures through-plane strain, and hence longitudinal strain is measured using a short axis image and circumferential strain is measured using a long axis image. It is not possible to measure radial strain using this technique.

2.4.3 Phase Contrast Imaging

Another category of technique which can be used to assess myocardial motion is phase contrast imaging [46, 63, 64]. This type of technique involves the application of a bipolar magnetic field gradient which is used to encode velocity directly into the phase of the signal. An initial gradient G is applied with a duration τ which will induce a phase change along the direction of the gradient in all spins, as shown in Equation 2-7.

$$\varphi = \gamma G \tau \qquad \textbf{(Equation 2-7)}$$

where γ is the gyromagnetic ratio. After a time delay of Δt**,** a second gradient with equal magnitude and duration but opposite polarity to the first gradient is applied. For stationary spins, the net phase change will be zero, but for spins which are moving

with velocity v, and have therefore moved through a distance $\Delta x = v\Delta t$ in time Δt, the net phase change is given by Equation 2-8:

$$\varphi_{moving} = \gamma G \tau v \Delta t = \gamma G \tau \Delta x \qquad \textbf{(Equation 2-8)}$$

The phase change is directly proportional to the velocity, and hence the displacement, of the spins in the direction of the encoding gradient, however velocities that result in phase shifts greater than $\pm \pi$ will result in aliasing. The encoding velocity, v_{enc}, is the largest velocity which can be measured without aliasing, and is controlled by varying the amplitude and duration of the encoding gradients. For myocardial phase contrast imaging, the required v_{enc} is typically 15 – 25cm/s, and relatively high amplitude gradients are required [46].

Validation of phase contrast imaging techniques has been performed using phantoms and canine models with tantalum markers [65, 66].

Since there is no suppression of myocardial signal in phase contrast imaging techniques, higher spatial resolution can be achieved than with tagging techniques, and analysis of the resulting images is relatively straightforward. However, phase contrast imaging techniques are susceptible to artefactual phase shifts due to eddy currents which can be difficult to correct for, and signal decay means that the time delay Δt between the application of the bipolar gradients must be short, and hence myocardial motion can only be recorded over a limited period of time.

2.4.4 DENSE

Displacement ENcoding with Stimulated Echoes (DENSE) is a technique which was developed to overcome the limitations of tagging and phase-contrast imaging methods for the assessment of myocardial strain. In order to encode displacement over a time comparable to T_1 of the myocardium, it is necessary to store the magnetisation vector along the direction of the static magnetic field, i.e. in the longitudinal plane, to avoid signal decay due to T_2*. This is accomplished in the DENSE pulse sequence through the use of stimulated echoes.

2.4.4.1. Stimulated Echo Formation

In a pulse sequence which uses three or more unequally spaced RF pulses, both spin echoes (SE) and stimulated echoes (STE) will be generated [67, 68, 69], as illustrated in Figure 2-12 [67].

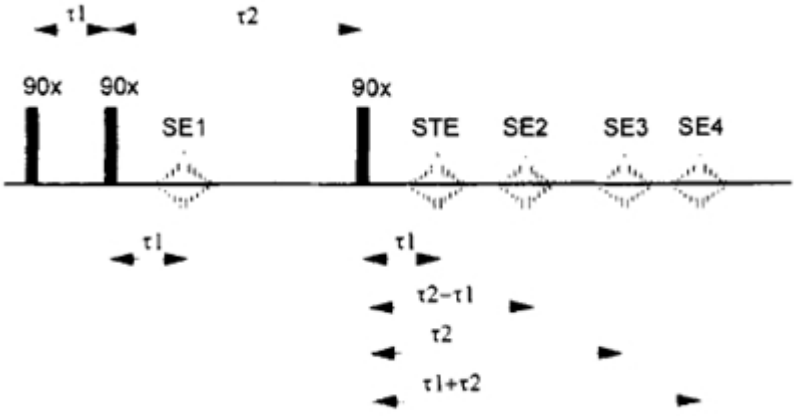

Figure 2-12: Formation of stimulated echoes

Following the application of the first RF pulse, there is a time delay of *τ1* during which some dephasing of spins occurs. When the second RF pulse is applied, the fan of spins is rotated through 90°, leaving some components in the transverse plane which refocus to form the first spin echo (SE1) after a further time *τ1*. Other components are moved into the longitudinal plane where they relax with T_1 only until the third RF pulse is applied after a time delay of *τ2*, which is also known as the mixing time (TM). These components are rotated into the transverse plane again, where they refocus to produce an STE. The second spin echo (SE2) occurs due to dephasing of the spins following the formation of SE1 and the subsequent rephasing by the third RF pulse, and is formed at a time *τ2- τ1* after the pulse. If there were any spins present in the transverse plane following the application of the second RF pulse, which is dependent on relaxation effects, or any spins present in the transverse plane after the first RF pulse which were not refocused by the second RF pulse, then these could be refocused by the third RF pulse to create SE3 and SE4 respectively.

In a STimulated Echo Acquisition Mode (STEAM) pulse sequence, three RF pulses are used, and the timing parameters and gradients are applied such that the STE is the only signal which is refocused during the acquisition period

2.4.4.2. Development of the DENSE Pulse Sequence

The first application of a pulse sequence which utilised stimulated echoes to spatially encode the internal displacement of tissues was for the detection of breast cancer [70]. Measurement of tissue displacement allows assessment of elastic properties, such as Young's elastic moduli, which are known to be altered by tumours. In soft tissue, a shear wave caused by an oscillating deformation force travels at a speed of 1–20ms^{-1}, and hence will require tens of milliseconds to travel through an object which is ~100mm in size. However, reflected waves can take longer than this to dampen, and hence any measurements which attempt to encode displacement during shear wave propagation may be confounded by interference from reflected or standing shear waves. To overcome this, a method which measures internal displacement between two or more deformations while the object is in mechanical equilibrium for each measurement was used, and this was achieved using a stimulated echo pulse sequence, with bipolar displacement encoding gradient pulses. A diagram of the pulse sequence used is shown in Figure 2-13 [70].

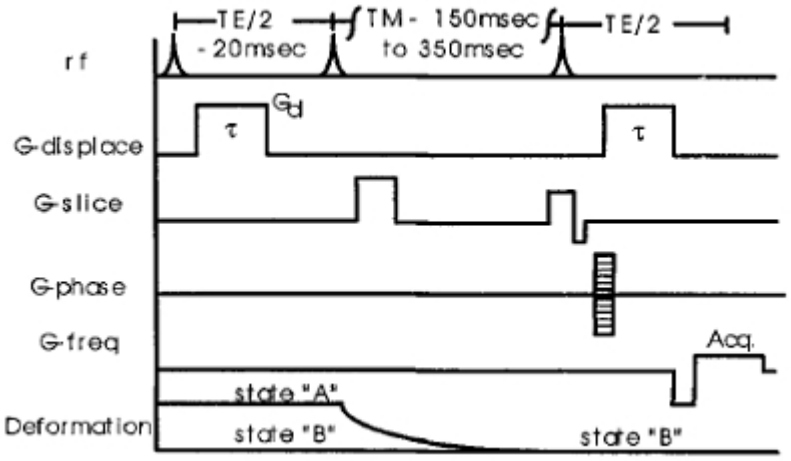

Figure 2-13: Displacement encoding of shear wave propagation pulse sequence

The first gradient is applied while the tissue is in state "A", and induces a range of phase shifts. Mechanical transition from state "A" to state "B" occurs during the stimulated echo mixing time, TM, which is relatively long and allows long-lived elastic vibrations to dampen before spatial encoding occurs. The second magnetic field gradient is applied when the tissue is in state "B", and the net phase shifts at this time are directly related to the tissue displacements between states "A" and "B", as shown for the phase contrast imaging techniques in Section 2.4.3 (Equation 2-8).

In addition, a phase reference dataset is acquired to allow removal of any pre-existing phase shifts that are unrelated to displacement. Reference data are acquired with the same pulse sequence shown in Figure 2-13, but with the tissue maintained in state "B" throughout. Local displacement is calculated directly from the local phase of the corrected dataset.

The first implementation of a DENSE pulse sequence [61] was based on the same principles. A diagram of the basic pulse sequence is shown in Figure 2-14 [61].

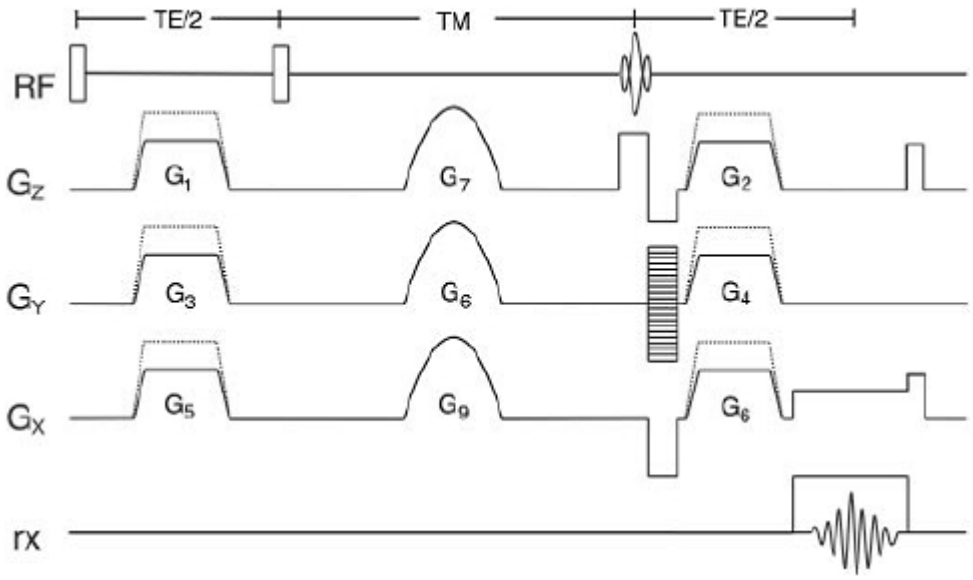

Figure 2-14: Basic DENSE pulse sequence

After an initial 90° RF excitation which rotates the net magnetisation vector (NMV) into the transverse plane, a magnetic field gradient (G_1, G_3, G_5) is applied in the desired direction, with amplitude G and duration τ, to introduce phase dispersion. A second 90° RF pulse is then applied to rotate the NMV back into the longitudinal plane. Displacement of the tissue occurs during the long mixing period TM (~100ms) which follows, in which crusher gradients (G_7, G_8, G_9) are applied to suppress signal not pertaining to the stimulated echo experiment, and then a third 90° RF pulse returns the NMV into the transverse plane. A second magnetic field gradient of equal magnitude to the first (G_2, G_4, G_6) is applied to rewind the phase dispersion. For stationary spins the phase rewinding is complete, but for spins that have moved a distance Δx during TM, a net phase is accumulated, as shown for the phase contrast

imaging techniques in Section 2.4.3 (Equation 2-8). *TM* is gated to occur over the 105ms before end-systole to allow measurement of systolic displacement.

Imaging is performed with slice selection during the third RF pulse followed by sequential k-space sampling with one line per excitation.

In order to obtain displacement encoded short axis data from a mid-ventricular slice of the heart, DENSE acquisitions are repeated a total of three times – the first repetition serves as a reference scan (with G_1, G_3, $G_5 = G_2$, G_4, $G_6 = 0$), and each of the remaining two repetitions is carried out with a modified amplitude of magnetic field gradient along a specific direction. The difference between the gradient pulses of the reference scan and each of the remaining datasets is set to provide a displacement encoding of 2.3mm/π, and the difference phase maps between each dataset and the reference scan provides information about the displacement of the myocardium along a given direction.

The original implementation of DENSE was used to acquire in vivo displacement data from the canine heart on a 4T MRI scanner, with a voxel size of $0.9\text{mm} \times 1.9\text{mm} \times 7.0\text{mm}$. However, the long acquisition time of 4.3 minutes per image was prohibitive for clinical imaging.

Single shot imaging of the heart using a STEAM pulse sequence had been demonstrated as far back as 1991 [71]. The sequence was similar to that shown in Figure 2-14, except that instead of using three 90^o RF pulses, the third pulse was replaced by a series of low flip angle pulses, each of which acquired a different phase-encoded stimulated echo. The sequence was successfully used to acquire in vivo images of the human heart with imaging times of 127 – 254ms, but was SNR-limited due to inadequate RF and gradient coil performance at the time. As MR systems developed, the faster and stronger gradients which became available were utilised to combine high-speed STEAM imaging with DENSE encoding in a sequence called Fast-DENSE [72]. A diagram of the Fast-DENSE pulse sequence is shown in Figure 2-15 [72].

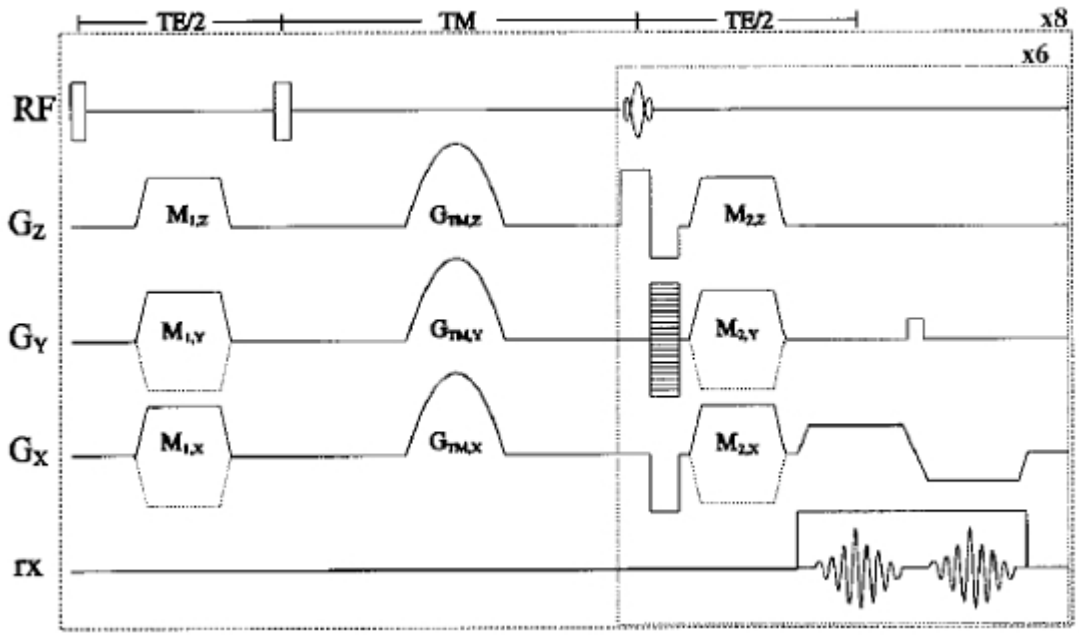

Figure 2-15: Fast-DENSE pulse sequence

In the Fast-DENSE pulse sequence, the final RF pulse is replaced by a train of small flip angle RF pulses, i.e. an EPI readout, which allow several lines of k-space to be acquired from a single STEAM preparation. For each of the RF pulses, two gradient echoes are formed and acquired. In this implementation of Fast-DENSE, six 30^{o} RF pulses are used, allowing 12 lines of k-space to be acquired for each application of the sequence. Each image is acquired in eight segments, with one segment being acquired per heartbeat with ECG triggering. The three images which are required (x-encoded, y-encoded, reference) can therefore be acquired in 24 heartbeats, which is feasible within a single breath-hold. As with the original implementation of DENSE, displacement encoding takes place over the 100ms prior to end-systole, and imaging is performed at end-systole.

The voxel size used in Fast-DENSE is $2.5\text{mm} \times 2.5\text{mm} \times 7.0\text{mm}$. The slice thickness of 7mm was determined experimentally, and it was found that thicker slices resulted in signal loss due to intravoxel dephasing, while thinner slices reduced the SNR.

To verify the calibration of the Fast-DENSE pulse sequence and the post-processing software (see Section 2.4.4.4), data were acquired from a cylindrical agar phantom rotating at 34.3 revolutions per minute, and the computed average rotation and strain

were compared with the known rate of rotation. Due to the high rotational velocity of the phantom, motion artefacts occurred which would not be present in human acquisitions. This was compensated for by collecting data in 48 segments instead of 8, but since the acquisition parameters were different to those which would be used for human imaging, no further comparisons could be made.

The implementations of DENSE described so far were limited to imaging a single cardiac phase at end-systole. The next step in the evolution of the sequence was the development of a cine DENSE pulse sequence, which produced 2D displacement-encoded images at multiple phases of the cardiac cycle. A fast gradient echo EPI pulse sequence was used, and six cine datasets were acquired - a reference dataset and two complementary acquisitions for artefact suppression (see Section 2.4.4.3) in each of two orthogonal directions, which was feasible within a single breath-hold [73].

Two versions of cine DENSE were made available at the institution where the research presented in this thesis took place – Sequence 1 was developed at the National Institutes of Health (NIH) National Heart, Lung and Blood Institute (NHLBI) (Bethesda, MD, USA), and Sequence 2 was developed by Siemens Healthcare (Erlangen, Germany). The pulse sequence parameters for both versions of DENSE can be found in Chapter 3.

2.4.4.3. Elimination of Image Artefacts

Three distinct echoes are produced by the DENSE pulse sequence: 1) the displacement-encoded stimulated echo, 2) the complex conjugate echo, which is also referred to as the simulated anti-echo, and 3) a gradient echo due to T_1 relaxation. The complex conjugate echo and the T_1 relaxation echo give rise to artefacts in the DENSE images, which result in errors in the measurement of displacement [74, 75].

At the start of the mixing period TM, the longitudinal magnetisation is given by Equation 2-9.

$$M_z(x) = M\cos(k_{enc}x) \qquad \textbf{(Equation 2-9)}$$

where M is the value of M_z just prior to the application of the second RF pulse, k_{enc} is the displacement encoding value due to the displacement encoding gradient and x is

the tissue position at the time of displacement encoding. Over a time period t, T_1 relaxation occurs and the longitudinal magnetisation will vary according to the Bloch Equations [76], as shown in Equation 2-10.

$$\begin{aligned} M_z(x,t) &= M_z(0)\exp(-t/T_1) + M_0(1-\exp(-t/T_1)) \\ &= M\cos(k_{enc}x)\exp(-t/T_1) + M_0(1-\exp(-t/T_1)) \\ &= (M\cos(k_{enc}x) - M_0)\exp(-t/T_1) + M_0 \\ &= \left(\frac{M}{2}(\exp(-jk_{enc}x) + \exp(jk_{enc}x)) - M_0\right)\exp(-t/T_1) + M_0 \end{aligned}$$

(Equation 2-10)

At the end of TM, an RF pulse with flip angle α is applied, along with a second gradient, and the tissue has been displaced by a distance $\Delta x = x - x_i$. The resulting transverse magnetisation is given by Equation 2-11.

$$\begin{aligned} M_{xy}(x,t) = &\left[\left(\frac{M}{2}(\exp(-jk_{enc}x) + \exp(jk_{enc}x)) - M_0\right)\exp(-t/T_1) + M_0\right] \\ &\times \exp(-jk_{enc}(x+\Delta x))\sin(\alpha) \end{aligned}$$

(Equation 2-11)

Equation 2-11 can be rearranged to represent the transverse magnetisation as a sum of three terms, as shown in Equation 2-12.

$$\begin{aligned} M_{xy}(x,t) = &\frac{M}{2}\exp(-t/T_1)\exp(-jk_{enc}\Delta x)\sin(\alpha) \\ &+ \frac{M}{2}\exp(-t/T_1)\exp(-jk_{enc}(\Delta x + 2x))\sin(\alpha) \\ &+ M_0(1-\exp(-t/T_1))\exp(-jk_{enc}(\Delta x + x))\sin(\alpha) \end{aligned}$$

(Equation 2-12)

The first term in Equation 2-12 describes the displacement encoded echo, the second term describes the complex conjugate echo, whose phase is additionally modulated by a factor of $2k_{enc}x$, and the third term describes the T_1 relaxation echo, whose phase is additionally modulated by a factor of $k_{enc}x$ [74].

If all three echoes, with the corresponding three different phases, are present during the imaging component of DENSE, this will result in cosine-modulated magnitude-reconstructed images, which appears as banding artefacts. The contribution from the complex conjugate echo can be eliminated by setting k_{enc} such that this echo is encoded with a frequency which is higher than the frequencies detected during data acquisition. However, this method cannot be used to eliminate the T_1 relaxation echo, as a further increase in k_{enc} causes substantial signal loss due to intravoxel dephasing [73].

For the single cardiac phase implementations of DENSE, the T_1 relaxation echo can be suppressed by applying a 180^o inversion recovery pulse during TM, with timing parameters set such that the longitudinal magnetisation of the unwanted magnetisation is zero at the time when the second RF pulse is applied. Different tissues within the body have different T_1 values so it is not possible to completely eliminate all banding artefacts with a single inversion pulse. Multiple inversion pulses could be used, but since this would increase the SAR, a single pulse is generally used to eliminate artefacts occurring within the myocardium [77].

While the inversion recovery approach was successful when imaging a single cardiac phase, it did not sufficiently suppress the T_1 relaxation echo at multiple time points as required for a cine acquisition. Instead, a CSPAMM technique (see Section 2.4.2) was used, in which two datasets are acquired with the flip angle of the second RF pulse set to $+90^o$ in the first dataset and -90^o in the second dataset [73]. The transverse magnetisations for the two datasets are given by Equations 2-13a and 2-13b respectively, and the final magnetisation obtained by subtracting the two datasets is given by Equation 2-14.

$$M^{1}{}_{xy}(x,t) = \frac{M}{2}\exp(-t/T_1)\exp(-jk_{enc}\Delta x)\sin(\alpha) + M_0(1-\exp(-t/T_1))\exp(-jk_{enc}(\Delta x + x))\sin(\alpha)$$

(Equation 2-13a)

$$M^{2}{}_{xy}(x,t) = -\frac{M}{2}\exp(-t/T_1)\exp(-jk_{enc}\Delta x)\sin(\alpha) + M_0(1-\exp(-t/T_1))\exp(-jk_{enc}(\Delta x + x))\sin(\alpha)$$

(Equation 2-13b)

$$M^{C}{}_{xy}(x,t) = M^{1}{}_{xy}(x,t) - M^{2}{}_{xy}(x,t) = M\exp(-t/T_1)\exp(-jk_{enc}\Delta x)\sin\alpha$$

(Equation 2-14)

Application of this technique found that incomplete suppression of the T_1 relaxation echo occurred when the heart rate was variable. Improved artefact suppression was obtained by combining the technique with through-plane dephasing [75]. At the same time as the DENSE frequency encoding gradient k_{enc} is applied, a second gradient k_d is applied in the through plane (slice select) direction. Equation 2-12 can be modified to take account of the through plane displacement Δz which occurs during time t, as shown in Equation 2-15.

$$M_{xy}(x,z,t) = \frac{M}{2}\exp(-t/T_1)\exp(-jk_{enc}\Delta x)\exp(-jk_d\Delta z)\sin(\alpha) + \frac{M}{2}\exp(-t/T_1)\exp(-jk_{enc}(\Delta x + 2x))\exp(-jk_d(\Delta z + 2z))\sin(\alpha) + M_0(1-\exp(-t/T_1))\exp(-jk_{enc}(\Delta x + x))\exp(-jk_d(\Delta z + z))\sin(\alpha)$$

(Equation 2-15)

From Equation 2-15, it can been seen that the complex conjugate echo and the T_1 relaxation echo, given by the 2nd and 3rd components of the equation, undergo phase shifts of $2k_{enc}$ and k_{enc} respectively due to the frequency encoding gradient, and $2k_d$ and k_d due to the dephasing gradient. The displacement encoded echo is not dephased by the dephasing gradient, but does undergo a phase shift due to Δz. To account for

this, the dephasing gradient is also applied during the reference scan (where k_{enc} is set to zero), and the unwanted phase shift will be removed when the reference dataset is subtracted from the displacement encoded dataset.

2.4.4.4. DENSE Image Processing and Analysis

Each of the two DENSE pulse sequences has associated offline image analysis software. For Sequence 1, the analysis software is named "DENSEView" and was developed at NIH. For Sequence 2, the analysis software is named "CIM_DENSE2D" and was developed at the University of Auckland in conjunction with Siemens.

The underlying principles of the analysis are the same for both DENSEView and CIM_DENSE2D, and consist of the following steps: reconstruction of magnitude and phase images, segmentation, phase unwrapping, displacement extraction and strain calculation [73, 78, 79].

The process of reconstructing the magnitude and phase images begins with the subtraction of the complementary datasets in each encoding direction to eliminate the contribution from the T_1 relaxation echo, followed by inverse Fourier transform to generate a complex subtraction image. Complex reference images are also generated by applying an inverse Fourier transform to the reference datasets for each encoding direction, and these are used to phase correct the subtracted images. Magnitude images are formed using Equation 2-16, and phase images are formed using Equation 2-17, where Re and Im are the real and imaginary component of the complex signal respectively.

$$Magnitude = \sqrt{\mathrm{Re}^2 + \mathrm{Im}^2} \qquad \textbf{(Equation 2-16)}$$

$$Phase = \tan^{-1}\left(\frac{\mathrm{Im}}{\mathrm{Re}}\right) \qquad \textbf{(Equation 2-17)}$$

All of the displacement information is contained within the phase images, while the magnitude images are purely anatomical. Examples of magnitude and phase images obtained from a healthy volunteer at ED and ES are shown in Figure 2-16.

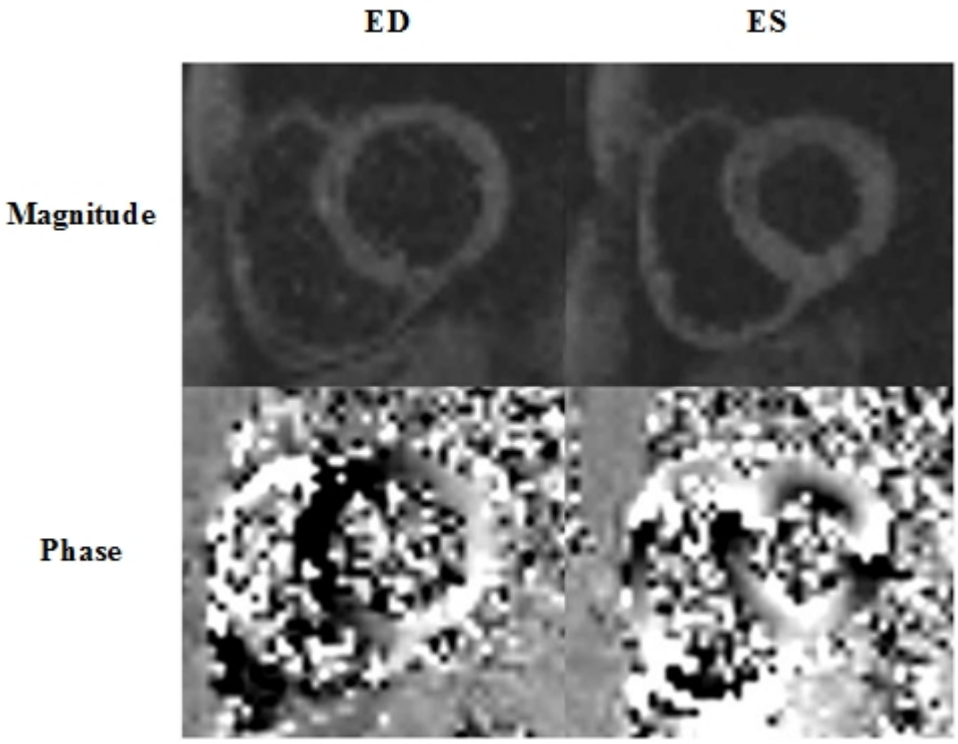

Figure 2-16: DENSE magnitude and phase images at ED and ES

Segmentation involves manual delineation of the epicardial and endocardial borders during diastole using the magnitude images, and identification of the insertion points of the right ventricle to allow the myocardium to be divided into segments according to the AHA model (see Section 2.2.3). This is facilitated by the black-blood contrast of DENSE images, which occurs due to intravoxel dephasing and subsequent signal loss caused by the incoherent motion of blood during the long TM period [72].

Phase unwrapping is required because the phase of MR signals is inherently confined to the range $-\pi < \phi < \pi$ radians. Large displacements may result in net phase changes outwith this range, and the true phase will then be wrapped to lie within the allowed range. This can be seen in the mid-septal and mid-lateral walls in the ES phase image in Figure 2-16. In CIM_DENSE2D, phase unwrapping is performed by using Poisson's equation with Neumann boundary conditions to generate a set of simultaneous equations, and a least-squares solution is found using the fast discrete cosine transform [80, 81]. DENSEView uses a region growing phase unwrapping technique, in which a region is incrementally expanded from a seed point on the phase map, and when a phase fringe is encountered, appropriate multiples of 2π are added or

subtracted. The decision on whether to include a pixel within a region is made via comparison with quality maps, which depend on the phase gradient, the signal level, or both [78, 82].

Following phase unwrapping, the pixel phase is converted to 1D displacement using Equation 2-14 (page 34). The 2D displacement of each pixel is then computed by vector addition of the datasets from the two encoding directions.

As shown in Equation 2-5 (page 18), myocardial strain can be represented by a 3D tensor with principal strains E_{RR} (radial), E_{CC} (circumferential) and E_{LL} (longitudinal). If the displacement vector is $\boldsymbol{u}$, then the strain tensor $\boldsymbol{E}$ can be calculated using Equation 2-18, where ∇ is the Gradient matrix operator [83].

$$E = \frac{1}{2}\left((\nabla u) + (\nabla u)^T + (\nabla u)^T (\nabla u)\right) \qquad \textbf{(Equation 2-18)}$$

In DENSEView and CIM_DENSE2D, only the first two principal strains, i.e. radial and circumferential strain, are calculated.

2.4.4.5. Validation of DENSE

Validation of cine DENSE has been carried out through comparison with myocardial tagging. In one study, DENSE and tagging were acquired from 12 healthy volunteers. Good correlation was found between the results from DENSE and tagging, with a correlation coefficient of 0.87 when comparing peak circumferential strain [73]. Another study compared DENSE and tagging in 11 healthy volunteers, and obtained a correlation coefficient of 0.92 [84].

A further study compared circumferential and radial strains measured by DENSE and tagging in 12 healthy subjects, and found that the mean differences in the results obtained between the two techniques was $-1 \pm 9\%$ for circumferential strain and $1 \pm 29\%$ for radial strain. The authors state that possible explanations for the larger variability in measurement of radial strain include large transmural strain gradients and widely varying systolic wall thickening [85]. Another possible explanation is the

effects of through-plane motion on the tracking process, which has more of an effect on radial strain than circumferential strain [86].

A recent (2013) paper investigated the performance of DENSE circumferential and radial strain for the identification of contractile abnormalities in myocardial segments with late gadolinium enhancement, and compared this with the performance achieved by systolic wall thickening. Receiver Operator Characteristic (ROC) analysis was performed, and the area under the curve was found to be 0.87, 0.92 and 0.83 for radial strain, circumferential strain and wall thickening respectively [87].

2.4.4.6. Further Developments of DENSE

The implementations of DENSE described so far, and which will be used in this thesis, apply displacement encoding to a single 2D slice, and take no account of through-plane motion or strain along the longitudinal axis of the heart.

A pulse sequence which allowed multi-slice imaging with 3D displacement encoding was developed using a murine model [88]. On detection of the ECG "R" wave at end-diastole, non-selective displacement encoding was applied. At end-systole, a slice-selective RF pulse followed by a gradient echo readout with a DENSE unencoding gradient were used to sample the displacement-encoded stimulated echo of a basal slice. At end-systole of the next two cardiac cycles, the displacement-encoded stimulated echoes of a mid-ventricular and an apical slice were sampled. Three slices can be imaged after a single displacement-encoding module due to the short R-R interval in mice (~120ms). Slice thickness was 1mm, and the slices were separated by 0.5mm. For in-plane imaging, displacement encoding was applied in the frequency encoding direction, and displacement encoding in two orthogonal directions was achieved by rotating the frequency encoding direction through 90^{o}. For through-plane imaging, displacement encoding was applied in the slice select direction. Reference data with no phase encoding were also acquired. The time taken to acquire a complete DENSE dataset was 45 - 50 minutes.

DENSE images were processed in a similar way to that described in Section 2.4.4.4. In addition to radial and circumferential strain, twist angles and normalised torsion were calculated for each slice. Twist angles were calculated for each pixel using the

epicardial centre of mass and calculating the angle subtended by the local displacement vector, and the overall twist angle for the slice was calculated as the mean of the individual pixel values. Normalised torsion was calculated by linear regression of the twist angle as a function of longitudinal position. The 3D displacement encoding pulse sequence was used to acquire images from the mouse heart pre- and post-infarction, and the results were found to be in good agreement with previous tagging studies.

A method which allowed 3D measurement of strain in a single slice of the human heart was developed by combining DENSE and SENC [89]. Cine DENSE images were acquired from two adjacent 8mm thick slices, and cine SENC was acquired from a 16mm thick slice which encompassed the two cine DENSE slices. The images were acquired during five breath-holds – four for DENSE (an *X*-encoded and a *Y*-encoded images for each of the two planes) and one for SENC (a *Z*-encoded image). In-plane displacements were calculated from the DENSE data and through-plane displacements were calculated from the SENC data, and from this the deformation gradient tensor was formed, which is the 3D equivalent of the 2D displacement vector $\boldsymbol{u}$ in Equation 2-18. This technique was validated in six healthy volunteers, and the results were found to be in agreement with values reported in the literature obtained using a 3D tagging technique.

An alternative method for 3D DENSE utilised a slice-following technique, which removed the requirement to acquire in-plane DENSE images in two adjacent slices [90]. In slice-following techniques, spatial encoding is applied to a thin slice, and the imaged slice is then chosen to be large enough to accommodate the motion of the encoded tissue. A CSPAMM approach is then used, and subtraction of the two images cancels out the signal from unencoded tissue, and leaves only the signal from the slice-selectively encoded tissue [91].

The techniques described so far in this section allow the calculation of 3D strain relating to a single imaging slice. 3D DENSE was developed further to allow volumetric coverage of the entire LV [92]. This involved a free-breathing, navigator-gated acquisition method, with an interleaved stack-of-spirals trajectory to sample the 3D k-space during readout. Post-processing was performed to obtain the

displacement-encoded phase images in the *x*, *y* and *z* directions at each cardiac phase for each of a number of 3D partitions. When evaluating the technique in healthy volunteers, 14 3D partitions were acquired, and this was zero-filled to 28 partitions during image reconstruction. An entire dataset was collected during 532 navigator-accepted heartbeats. The tissue tracking algorithms used for 2D DENSE were extended to 3D, and from this the circumferential, radial and longitudinal strains, as well as twist and torsion, were calculated for each partition. The results were found to be in good agreement with values reported in the literature using a 3D tagging technique.

2.5 Assessment of Strain in the Human Myocardium

2.5.1 Healthy Myocardium

A number of studies have been performed to assess strain in the healthy myocardium using MRI techniques, many of which considered circumferential and longitudinal strain rather than radial strain. Investigations have been carried out into variations in strain with myocardial segment, gender and age, and the results are summarised in this section.

Variation with Myocardial Segment:

A summary of the variation in peak strain in each myocardial segment is shown in Table 2-1, where strain is expressed as a percentage (mean ± SD) using data acquired in a mid-ventricular short axis slice, and the method (M.) used to acquire the data is indicated by T (tagging), S (SENC), D (DENSE) or PC (phase contrast).

Ref.	M.	Slice	AS (S)	A (A)	AL (L)	IL	I (I)	IS
Circumferential Strain								
[93]	S	-	-22 ± 3	-24 ± 3	-23 ± 3	-	-20 ± 3	-
[94]	S	-	-22 ± 3	-	-21 ± 3	-	-	-
[93]	T	-	-21 ± 2	-21 ± 2	-21 ± 3	-	-20 ± 3	-
[85]	T	-	-14 ± 3	-13 ± 3	-16 ± 3	-18 ± 3	-18 ± 3	-14 ± 3
[94]	T	-	-23 ± 3	-	-23 ± 4	-	-	-
[95]	T	-23 ± 2	-21 ± 3	-26 ± 3	-20 ± 4	-27 ± 3	-21 ± 4	-23 ± 4
[96]	T	-	-21 ± 6	-25 ± 6	-23 ± 4	-	-20 ± 4	-
[97]	T	-30 ± 7	-34 ± 15	-26 ± 12	-30 ± 10	-	-31 ± 11	-
[98]	T	-	-28 ± 14	-22 ± 13	-27 ± 12	-	-27 ± 8	-
[99]	T	-	-21 ± 2	-23 ± 2	-24 ± 3	-22 ± 3	-18 ± 2	-20 ± 3
[85]	D	-	-18 ± 4	-17 ± 4	-19 ± 4	-20 ± 3	-14 ± 4	-14 ± 4
[100]	D	-	-20 ± 3	-18 ± 2	-22 ± 4	-20 ± 4	-16 ± 3	-18 ± 3
Radial Strain								
[85]	D	-	20 ± 14	17 ± 8	16 ± 9	24 ± 11	18 ± 10	17 ± 10
[85]	T	-	18 ± 13	14 ± 10	13 ± 10	25 ± 17	15 ± 12	21 ± 14
[101]	PC	38 ± 6	40 ± 20	42 ± 24	34 ± 10	43 ± 18	42 ± 16	27 ± 14

Table 2-1: Variation in strain with AHA segment in the healthy myocardium

Variation with Gender:

Differences have been observed in strain values between male and female subjects using tagging. Global circumferential strain was found to be higher in females than in males (-21 ± 2% vs -19 ± 2%, p = 0.025), and a similar result was found for global longitudinal strain (-16 ± 2% vs -14 ± 3%, p = 0.007). No statistically significant difference was found for radial strain [102]. However, another study found no statistically significant differences between peak circumferential strain between males and females using tagging [103] or SENC [93].

Variation with Age:

A comparison of peak circumferential strain obtained using SENC in a group of younger volunteers (age 22 – 25 years) and a group of older volunteers (age 55 – 69 years) found no statistically significant differences [93]. A similar result was obtained in a study which used tagging in a group of younger volunteers (age 19 – 26 years) and a group of older volunteers (age 60 – 74 years), however statistically significant differences were observed for the time taken for circumferential strain to return to 50% of the peak value and the peak rate of change of circumferential strain, with the obtained values being slower in the older group [104].

2.5.2 Infarcted Myocardium

For the assessment of strain in the infarcted myocardium, segments can be classified as infarcted, adjacent (infarcted segment on at least one side) or remote (no infarcted segments on either side) based on the results of late gadolinium enhancement (LGE) imaging. A study of 21 post-MI patients found statistically significant differences between the peak circumferential strain measured by tagging in remote and infarcted segments. Based on the mean (μ) and standard deviation (σ) of the peak circumferential strain in the remote segments, a threshold for detecting dysfunction was defined as $\mu + \sigma$. Dysfunctional segments were identified in 12% of remote, 26% of adjacent and 58% of infarcted segments. For peak radial strain, statistically significant differences were observed between strain in remote segments compared to both adjacent and infarcted segments, and dysfunctional segments were identified in 12% of remote, 32% of adjacent and 50% of infarcted segments [105].

Alternatively, strain can be compared with wall motion abnormalities observed from cine imaging. A study of 38 post-MI patients classified segments as normokinetic, hypokinetic or a/dyskinetic, and compared the circumferential strain values obtained using SENC. Statistically significant differences were observed between peak circumferential strain in normokinetic segments compared to both hypokinetic and a/dyskinetic segments, and also between hypokinetic and a/dyskinetic segments. Receiver Operating Characteristics (ROC) analysis showed that a peak circumferential strain value of -17% was related to hypokinesia with a sensitivity of 85% and a specificity of 86%, and a value of -10% was related to a/dyskinesia with a sensitivity of 95% and a specificity of 92% [106].

A study which investigated the relationships between circumferential strain as measured by tagging and salvage found statistically significant differences between myocardial segments with salvage of 0 – 25% and 26 – 50% compared with segments with salvage of 50 – 100%. The strain within all ischaemic segments showed improvement after 1 year, with the smallest improvement occurring in segments with salvage of 0 – 25% [107].

2.6 Summary

MRI is a valuable tool for the assessment of myocardial function and injury, and techniques such as tagging, SENC and phase contrast imaging have been successfully implemented to allow quantitative assessments of myocardial strain. However, each of these techniques had limitations which could restrict their performance in a clinical evaluation of contractile function. DENSE has the potential to be a more robust method for the measurement of myocardial strain, but as mentioned in Chapter 1, much of the research performed with DENSE to date has been methods development, and its application in a routine clinical setting has been incompletely investigated. The studies contained within this thesis aim to build upon the existing knowledge by further investigating the performance of DENSE in healthy subjects and patients with myocardial infarction.

Chapter 3

Image Acquisition and Analysis Methods

3.1 Introduction

This chapter contains details of the basic image acquisition and analysis protocols which were common to all of the investigations contained within this thesis. Additional analysis was carried out for specific investigations, and details will be provided within the relevant chapters.

3.2 MRI Scanning

All imaging was performed using a 1.5T Siemens Avanto MRI scanner (Siemens, Erlangen, Germany) with a 6-channel cardiac coil (anterior) in conjunction with 2 or 3 elements of an 8-channel spine coil (posterior). In Chapter 6, imaging was also performed using a 3T Siemens Verio MRI scanner, again with a 6-channel cardiac coil in conjunction with an 8-channel spine coil.

Cine, LGE and T_2 images were acquired as a short axis stack extending from the base to the apex of the heart. DENSE images were acquired in three short axis slices – basal (just below the level of the LVOT and aortic valve), mid-ventricular (mid-papillary level) and apical, with each slice corresponding to the position of a slice within the short axis stack of cine, LGE and T_2 images. Two- and four-chamber cine and LGE images were also acquired, and four-chamber T_2 and DENSE images – these were used to assist with analysis, but were not analysed directly.

In all cases, images were acquired during a single breath-hold and with ECG gating.

Image analysis was performed by dividing the short axis images into segments according to the AHA model, as described in Section 2.2.3.

3.3 Cine Image Acquisition and Analysis

The pulse sequence parameters used for cine image acquisitions at both 1.5T and 3T using a b-SSFP pulse sequence are shown in Table 3-1. Retrospective ECG gating was used.

Parameter	1.5T	3T
TR (ms)	3.3	3.4
TE (ms)	1.2	1.5
Flip Angle (deg)	70	50
FoV Read (mm)	340	340
FoV Phase (%)	80	84.4
Slice Thickness (mm)	7	7
Resolution	180×256	256×256
Bandwidth (Hz/pixel)	930	977

Table 3-1: Pulse sequence parameters for cine imaging

Cine images were analysed using Argus software on the Syngo MultiModality Workplace (version VE36A, Siemens, Erlangen, Germany). A qualitative assessment was performed by visually inspecting the images throughout the cardiac cycle and assigning a score for wall motion to each segment using the definitions in Table 3-2. Wall motion scoring was carried out by Cardiology research fellows (AP and DC).

Score	Definition
0	Normal
1	Hypokinetic
2	Severely Hypokinetic
3	Akinetic
4	Dyskinetic
5	Aneurysmal

Table 3-2: Definition of scores for wall motion assessment

A quantitative assessment was performed by measuring systolic thickening for each segment, expressed as a percentage increase compared to the thickness at diastole, as described in Section 2.3.1.

LVESV, LVEDV and LVEF were determined by a Cardiology research fellow (DC). Endo- and epi-cardial borders were defined manually, and papillary muscles were excluded from the calculation.

3.4 LGE Image Acquisition and Analysis

The pulse sequence parameters used for LGE image acquisitions at 1.5T using a PSIR turboFLASH pulse sequence are shown in Table 3-3.

Parameter	1.5T
TR (ms)	26.8
TE (ms)	3.4
Flip Angle (deg)	20
FoV Read (mm)	340
FoV Phase (%)	80
Slice Thickness (mm)	8
Resolution	156×256
Bandwidth (Hz/pixel)	130

Table 3-3: Pulse sequence parameters for LGE imaging

LGE images were acquired 10 minutes after a bolus injection (0.15 mmol/kg) of gadolinium contrast agent (Dotarem - Guerbet, Villepinte, France).

LGE images were analysed using Argus software. A region of interest (ROI) containing at least 100 pixels was drawn in remote myocardium to obtain the mean (μ) and standard deviation (σ) of the image intensity, and the images were windowed using a threshold of $\mu \pm 5\sigma$, as described in Section 2.3.2. Remote myocardium was defined as approximately the central third of the non-enhanced tissue, located on the opposite side of the short axis slice from the region of infarction, as illustrated in

Figure 3-1. A score relating to the transmural extent of infarction, LGE_score, was then assigned using the definitions in Table 3-4 [108, 109].

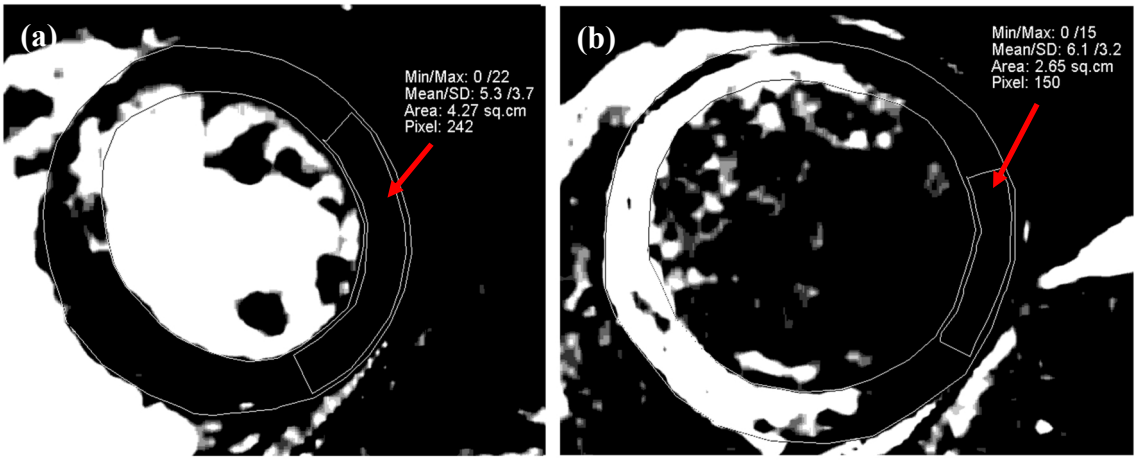

Figure 3-1: Illustration of ROI in remote myocardium for LGE analysis for a) small and b) large infarctions

Score	Definition
0	0%
1	1% - 25%
2	26% - 50%
3	51% - 75%
4	76% - 100%

Table 3-4: Definition of scores for transmural extent of infarction

3.5 T_2 Image Acquisition and Analysis

The pulse sequence parameters used for T_2-map image acquisitions at 1.5T using a T_2-prepared single shot SSFP pulse sequence are shown in Table 3-5.

Parameter	1.5T
TR (ms)	3.9
TE (ms)	1.1
Flip Angle (deg)	70
FoV Read (mm)	340
FoV Phase (%)	75
Slice Thickness (mm)	8
Resolution	116×192
Bandwidth (Hz/pixel)	930

Table 3-5: Pulse sequence parameters for T_2 imaging

T_2 images were analysed using Argus software. An ROI containing at least 100 pixels was drawn in remote myocardium to obtain the mean (μ) and standard deviation (σ) of the image intensity, and the T_2 images were windowed using a threshold of $\mu \pm 2\sigma$, as described in Section 2.3.3. The regions of the T_2 image which exceeded the threshold were manually outlined, and the percentage of T_2 hyperenhancement was calculated.

Area at risk was defined as the percentage of T_2 hyperenhancement, and myocardial salvage index (MSI) was calculated using Equation 2-3 in Section 2.3.3.

3.6 DENSE Image Acquisition and Analysis

The pulse sequence parameters used for DENSE image acquisition at 1.5T (sequence 1 and sequence 2) and 3T (sequence 2 only) are shown in Table 3-6. As described in Section 2.4.4.2, sequence 1 was provided by NIH and sequence 2 was provided by Siemens Healthcare.

Parameter	Seq. 1 (1.5T)	Seq. 2 (1.5T)	Seq. 2 (3T)
TR (ms)	15.0	16.3	13.7
TE (ms)	8	8	6.34
Flip Angle (deg)	6	20	20
FoV Read (mm)	448	360	380
FoV Phase (%)	37.5	75	85.7
Slice Thickness (mm)	8	8	8
Resolution	48×128	84×112	96×112
	$3.5\text{mm} \times 3.5\text{mm}$	$3.2\text{mm} \times 3.2\text{mm}$	$3.4\text{mm} \times 3.4\text{mm}$
Bandwidth (Hz/pixel)	1300	1207	1207
Displacement Encoding Frequency (π/mm)	0.23	0.2	0.2

Table 3-6: Pulse sequence parameters for DENSE imaging

The images obtained using sequence 1 were analysed using DENSEView, and the images obtained using sequence 2 were analysed using CIM_DENSE2D (see Section 2.4.4.4).

The output from DENSEView provides the set of time points and strain values for circumferential (Ecc) and radial (Err) strain, along with values for peak Ecc, peak Err, time to peak Ecc and time to peak Err. The output from CIM_DENSE2D provides only the set of time and strain values for the Ecc and Err curves, so Matlab code was written to extract the peak strain and time to peak strain values (see Appendix A).

Peak Ecc is a negative number, which represents a contraction. The analysis within this thesis will be carried out using the magnitude of the peak Ecc results to avoid potential confusion, for example when evaluating correlations.

Time to peak Ecc and time to peak Err are displayed in ms, so to take into account the varying heart rates, and hence duration of cardiac cycle, between individuals, the times were also expressed as a percentage of the mean RR interval.

3.7 Statistical Analysis

Statistical analyses were performed using Minitab 16 (Minitab Inc, PA, USA) and SPSS 19 (IBM, New York, USA).

Prior to performing any analysis, data were checked for normality using an Anderson-Darling test, and parametric or non-parametric tests were used accordingly. Further information relating to the statistical tests used for data analysis in the investigations contained within this thesis can be found in Appendix B, including the corrections used for multiple comparison tests.

Chapter 4

Preliminary Clinical Assessment of DENSE

4.1 Introduction

Prior to the commencement of this study, the two versions of the DENSE pulse sequence described in Section 2.4.4 had been installed on a 1.5T MRI scanner, and were being used in research protocols involving patients who had suffered a myocardial infarction (MI). This chapter describes a retrospective investigation into the relationships between the strain parameters measured using DENSE and other clinical MRI measures of cardiac function, and a preliminary assessment of the potential clinical utility of DENSE in the post-MI patient group.

4.2 Aims

The aims of the research presented in this chapter are:

- To assess the repeatability of strain measurements using the two versions of the DENSE pulse sequence and corresponding analysis software
- To investigate the relationships between DENSE strain parameters (peak circumferential strain, peak radial strain, time to peak circumferential strain and time to peak radial strain), as measured by two versions of the DENSE pulse sequence, with other MRI measures used for the clinical assessment of cardiac function i.e. transmural extent of MI as shown by late gadolinium enhancement (LGE) imaging and wall motion score

4.3 Methods

4.3.1 STEMI Patients

57 patients with STEMI were scanned within 7 days of infarction, and divided into two groups according to the DENSE pulse sequence which was used. Group 1 contained 31 patients (M:F = 23:8, age 59 ± 11 years), and DENSE images were acquired using sequence 1. Group 2 contained 26 patients (M:F = 19:7, age 57 ± 14 years), and DENSE images were acquired using sequence 2. Ethics approval for the study had been obtained from the West of Scotland Research Ethics Committee, and written consent was obtained from all patients.

4.3.2 Image Acquisition and Analysis

Cine, LGE and DENSE images were acquired in at least one slice position (basal and/or mid-ventricular) and analysed as described in Chapter 3.

4.3.3 Repeatability of Image Analysis

Repeatability was assessed using images from 10 patients for each of the two DENSE pulse sequences, giving a total of 60 segments for analysis in each case.

DENSEView provides values for each strain parameter on a segment-by-segment basis. CIM_DENSE2D also provides this information, but in addition, a value is provided for each strain parameter on a whole slice basis. For both sequences, analysis was performed using segment data, and additional analysis was performed using sequence 2 images and CIM_DENSE2D for whole slice data.

Analysis was performed independently by two operators (CM, RB), and each set of images were analysed four times. Intra-operator repeatability was assessed by calculating coefficients of variation (CoV) for each strain parameter in each patient dataset across the four analyses. Inter-operator repeatability was assessed by calculating RMS coefficients of variation (RMS-CoV) [110], using Levene's test to compare the equality of variance between the results obtained by the two operators, and using a paired t-test or a Wilcoxon signed rank test to compare the obtained values for each parameter.

Further assessment of inter-operator repeatability was performed by calculating the mean difference in the values obtained by the two operators, $\bar{d}$, and the standard deviation (*SD*) of the differences. The limits of agreement were then calculated using Equation 4-1.

$$Limits = \bar{d} \pm 1.96SD \qquad \textbf{(Equation 4-1)}$$

Limits of agreement are a component of the methods described by Bland and Altman for the comparison of two methods, and this will be discussed in more detail in Chapter 5.

4.3.4 Comparison with Clinical Assessment

From the 31 patients scanned using sequence 1 and the 26 patients scanned using sequence 2, a total of 228 and 210 segments respectively were available for analysis.

The assumption was made that DENSE strain parameters are not affected by the segment of the heart in which they are being measured, or by the position of the imaging slice within the heart. A study of DENSE strain values in healthy volunteers will be required to assess the validity of these assumptions.

A statistical assessment of the relationship between each of the DENSE strain parameters and each of the clinical MRI measures of cardiac function was performed using correlation tests and box plots.

4.4 Results – Sequence 1

4.4.1 Repeatability of Image Analysis

The results of the Anderson-Darling test for normality showed that the data for each strain parameter were not normally distributed ($p < 0.05$), and hence Wilcoxon signed rank tests were used to assess inter-operator repeatability. The results of the intra- and inter-operator repeatability assessment for images acquired using DENSE sequence 1 and DENSEView analysis software are shown in Table 4-1. Statistically significant results are highlighted using * ($p < 0.05$) and ** ($p < 0.001$).

	Intra-Operator	Inter-Operator			
Strain Parameter	**Average CoV (%)**	**RMS CoV**	**p-value (Levene)**	**p-value (Wilcoxon)**	**Limits of Agreement**
Peak Ecc	7.0	2.1	0.836	0.012*	(-2.4, 1.7)
Time to Peak Ecc	4.5	2.1	0.829	0.679	(-151.5, 132.4)
Peak Err	5.9	2.4	0.985	<0.001**	(-5.6, 10.1)
Time to Peak Err	2.7	1.5	0.983	0.376	(-64.4, 63.6)

Table 4-1: Intra- and inter-operator repeatability with DENSEView

The results show that intra-operator repeatability is high. The inter-operator RMS-CoV is small and Levene's test showed no statistically significant differences in variances between the two operators. However, the Wilcoxon signed ranks test showed statistically significant differences in the mean values obtained by the two operators for peak Ecc and peak Err.

4.4.2 Relationship between Strain and Late Gadolinium Enhancement

Table 4-2 shows the allocation of LGE scores for the 228 segments which were analysed.

LGE Score	No. of Segments
0	149
1	18
2	21
3	14
4	26

Table 4-2: Allocation of LGE scores for post-MI patient data (1)

The results of the correlation tests between strain parameters and LGE scores are shown in Table 4-3, and are expressed as a Pearson correlation coefficient. Statistically significant results are indicated by * ($p < 0.05$) and ** ($p < 0.001$). The relationships are illustrated using box plots in Figure 4-1.

Strain Parameter	Pearson Coefficient
Peak Ecc	-0.60**
Time to Peak Ecc (ms)	0.17*
Time to Peak Ecc (%RR)	0.17*
Peak Err	-0.35**
Time to Peak Err (ms)	0.19*
Time to Peak Err (%RR)	0.17*

Table 4-3: Analysis of strain vs LGE score in post-MI patients (1)

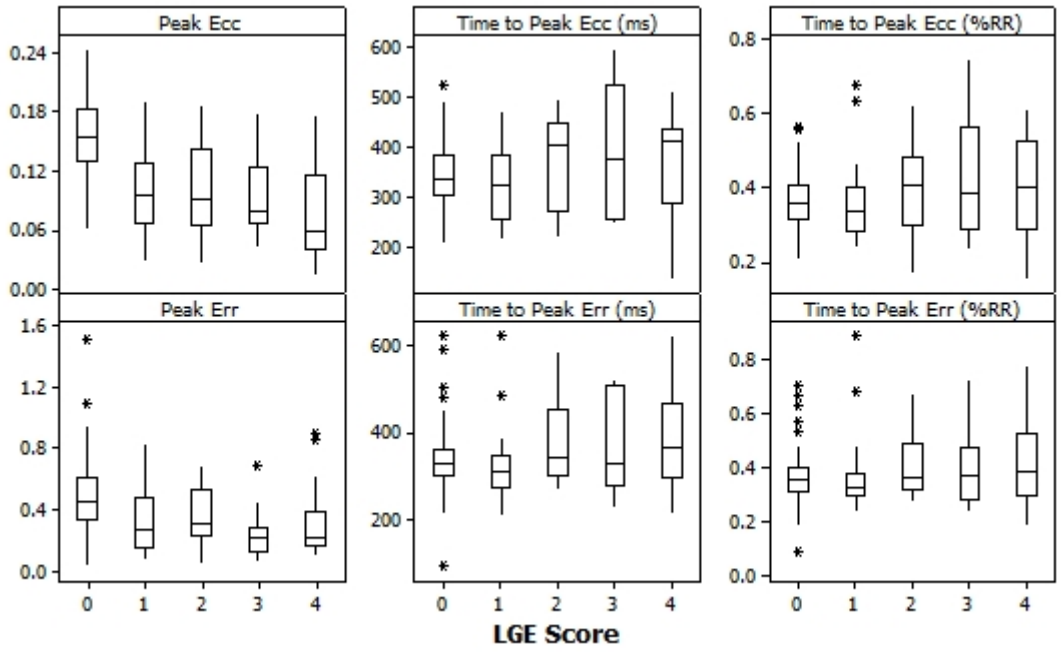

Figure 4-1: Strain parameters vs LGE score in post-MI patients (1)

4.4.3 Relationship between Strain and Wall Motion

Table 4-4 shows the allocation of wall motion scores for the 228 segments which were analysed.

Wall Motion Score	No. of Segments
0	153
1	34
2	22
3	18
4	1

Table 4-4: Allocation of wall motion scores for post-MI patient data (1)

The results of the correlation tests between strain parameters and wall motion abnormalities are shown in Table 4-5, and are expressed as a Pearson correlation coefficient. Statistically significant results are indicated by * ($p < 0.05$) and ** ($p < 0.001$). The relationships are illustrated using box plots in Figure 4-2.

Strain Parameter	Pearson Coefficient
Peak Ecc	-0.68**
Time to Peak Ecc (ms)	0.23**
Time to Peak Err (%RR)	0.28**
Peak Err	-0.49**
Time to Peak Err (ms)	0.39**
Time to Peak Err (%RR)	0.39**

Table 4-5: Analysis of strain vs wall motion score in post-MI patients (1)

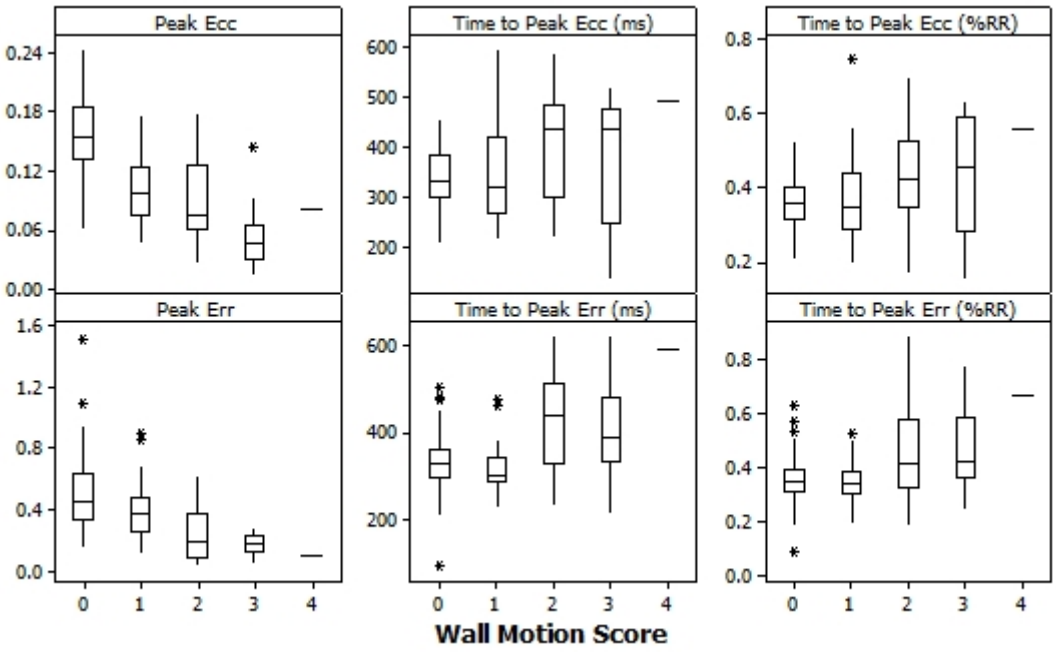

Figure 4-2: Strain parameters vs wall motion score in post-MI patients (1)

4.5 Results – Sequence 2

4.5.1 Repeatability of Image Analysis

The results of the Anderson-Darling test for normality showed that the data for each strain parameter were not normally distributed ($p < 0.05$), and hence Wilcoxon signed rank tests were used to assess inter-operator repeatability. The results of the intra- and inter-operator repeatability assessment for images acquired using DENSE sequence 2 and CIM_DENSE2D analysis software are shown in Table 4-8. Statistically significant results are highlighted using * ($p < 0.05$) and ** ($p < 0.001$).

	Intra-Operator	Inter-Operator			
Strain Parameter	**Average CoV (%)**	**RMS CoV**	**p-value (Levene)**	**p-value (Wilcoxon)**	**Limits of Agreement**
Peak Ecc	10.3	2.8	0.497	0.581	(-2.9, 3.1)
Time to Peak Ecc	7.7	2.4	0.648	0.123	(-157.8, -128.8)
Peak Err	16.5	3.1	0.685	0.039*	(-12.5, 9.6)
Time to Peak Err	14.8	3.2	0.965	0.062	(-155.2, 195.1)

Table 4-6: Intra- and inter-operator repeatability with CIM_DENSE (segments)

	Intra-Operator	Inter-Operator			
Strain Parameter	**Average CoV (%)**	**RMS CoV**	**p-value (Levene)**	**p-value (Wilcoxon)**	**Limits of Agreement**
Peak Ecc	6.1	1.8	0.752	0.415	(-1.5, 1.1)
Time to Peak Ecc	8.0	1.9	0.831	0.345	(-42.5, 55.5)
Peak Err	8.5	8.4	0.964	0.006*	(-2.6, -0.1)
Time to Peak Err	6.8	1.7	0.992	0.893	(-43.5, 43.5)

Table 4-7: Intra- and inter-operator repeatability with CIM_DENSE (whole slice)

The results show that intra-operator repeatability is high. The inter-operator RMS-CoV is small and Levene's test showed no statistically significant differences in

variances between the two operators, for both segment and whole slice data. However, the Wilcoxon signed ranks test showed statistically significant differences in the mean values obtained by the two operators for peak Err.

4.5.2 Relationship between Strain and Late Gadolinium Enhancement

Table 4-8 shows the allocation of LGE scores for the 210 segments which were analysed.

LGE Score	No. of Segments
0	159
1	0
2	7
3	13
4	31

Table 4-8: Allocation of LGE scores for post-MI patient data (2)

The results of the correlation tests between strain parameters and LGE scores are shown in Table 4-9, and are expressed as a Pearson correlation coefficient. Statistically significant results are indicated by * ($p<0.05$) and ** ($p<0.001$). The relationships are illustrated using box plots in Figure 4-3.

Strain Parameter	Pearson Coefficient
Peak Ecc	-0.56**
Time to Peak Ecc (ms)	0.42**
Time to Peak Ecc (%RR)	0.44**
Peak Err	-0.28**
Time to Peak Err (ms)	0.25**
Time to Peak Err (%RR)	0.28**

Table 4-9: Analysis of strain vs LGE score in post-MI patients (2)

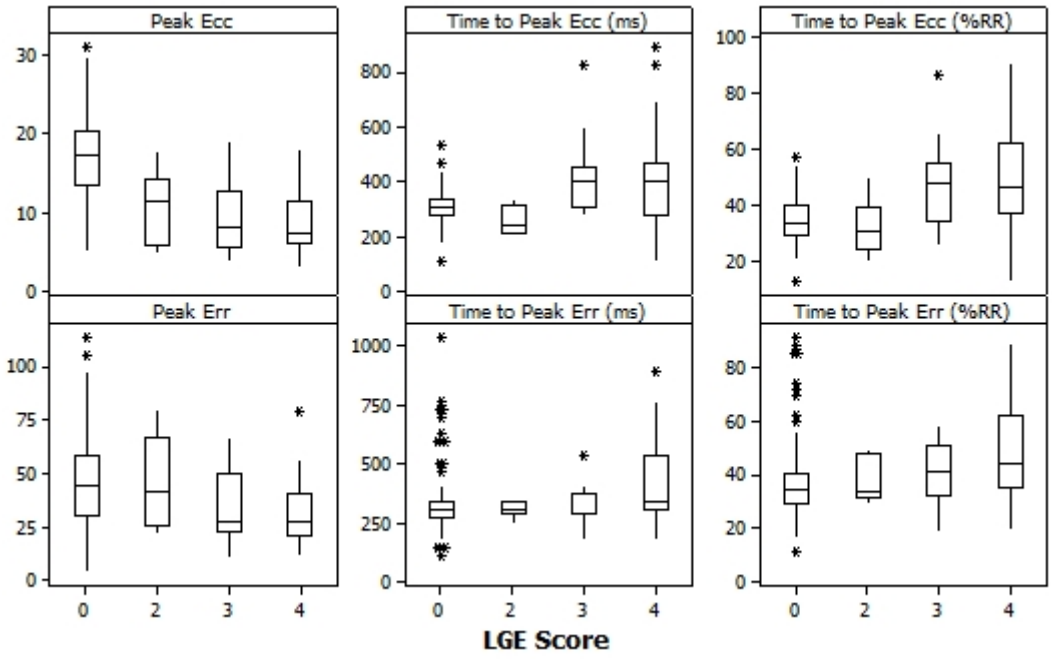

Figure 4-3: Strain parameters vs LGE score in post-MI patients (2)

4.5.3 Relationship between Strain and Wall Motion

Table 4-10 shows the allocation of wall motion scores for the 210 segments which were analysed.

Wall Motion Score	No. of Segments
0	147
1	16
2	19
3	26
4	2

Table 4-10: Allocation of wall motion scores for post-MI patient data (2)

The results of the correlation tests between strain parameters and wall motion abnormalities are shown in Table 4-11, and are expressed as a Pearson correlation coefficient. Statistically significant results are indicated by * ($p<0.05$) and ** ($p<0.001$). The relationships are illustrated using box plots in Figure 4-4.

Strain Parameter	Pearson Coefficient
Peak Ecc	-0.61**
Time to Peak Ecc (ms)	0.48**
Time to Peak Ecc (%RR)	0.46**
Peak Err	-0.39**
Time to Peak Err (ms)	0.38**
Time to Peak Err (%RR)	0.39**

Table 4-11: Analysis of strain vs wall motion score in post-MI patients (2)

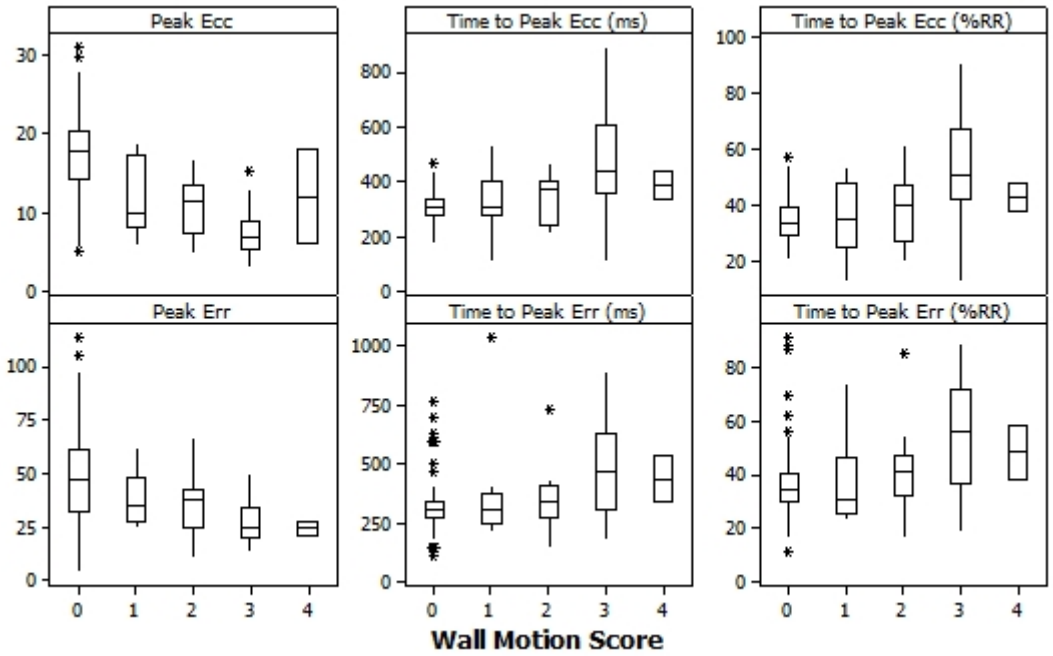

Figure 4-4: Strain parameters vs wall motion score in post-MI patients (2)

4.6 Discussion

The results of the intra- and inter-operator repeatability assessment were favourable for both versions of DENSE, with small coefficients of variation when analysing datasets multiple times, and small RMS coefficients of variation and no statistically significant differences in the variances between two operators. A comparison of the mean values for each strain parameter showed that for sequence 1, operator 2 had a tendency to overestimate peak Ecc and underestimate peak Err compared to operator 1, and for sequence 2, operator 2 had a tendency to overestimate peak Err in both segments and slices compared to operator 1. There may be a systematic error due to the way in which endo- and epi-cardial borders are defined, and this could potentially be resolved with additional training. The limits of agreement for peak Ecc in sequence 1 were (-2.4, 1.7), and differences of this magnitude are unlikely to be of clinical significance. For comparison, the limits of agreement for peak Ecc in sequence 2, which were not found to be statistically significant, were (-2.9, 3.1). The limits of agreement for peak Err in both sequence 1 and sequence 2 showed a wider range, which indicates that DENSE may not be ideally suited for assessing radial strain. The resolution of both DENSE sequences is fairly low, and there may be an insufficient number of pixels across the myocardium to allow accurate quantification of radial strain with the current methods.

While the average CoV values for all strain parameters were small, it was noted that in segments which are contracting very poorly (e.g. peak Ecc < 5%), repeated analysis of the dataset can result in very different values with CoVs as large as 45%. Further investigation of the reliability of DENSE strain values in severely hypokinetic segments will be required.

The results of the correlation tests indicated that there are statistically significant relationships between all DENSE strain parameters (peak Ecc, time to peak Ecc, peak Err and time to peak Err) and both clinical measures of cardiac function (transmural extent of MI and wall motion), with both sequences. However, further consideration is required to determine the clinical significance and the scientific value of the results.

Peak Ecc decreases with increasing transmural extent of MI and increasing wall motion score. The obtained Pearson correlation coefficients were 0.60 and 0.68 (sequence 1) and 0.56 and 0.61 (sequence 2) for transmural extent of MI and wall motion respectively, which implies a moderate relationship. The relationship between peak Ecc and each of the clinical measures is also apparent from the relevant box plots, which show a general decrease in peak Ecc as the score for each clinical measure increases.

Peak Err decreases with increasing transmural extent of MI and increasing wall motion, but in both cases and for both sequences, the correlation results are less strong than for peak Ecc.

Statistically significant relationships were found for time to peak Ecc and time to peak Err with both clinical measures. However, the Pearson correlation coefficients were very low, indicating weak relationships, and no obvious relationship is apparent from visual inspection of the box plots. Slightly higher correlations were observed in the results from sequence 2, particularly for time to peak Ecc, but overall the results for time to peak were unconvincing.

The usefulness of time to peak Ecc and time to peak Err for comparison of different patients is uncertain. The time taken to reach peak contraction of the myocardium will vary depending on the heart rate of the patient, which will be affected by factors such as fitness and whether the patient is taking certain medications e.g. beta blockers, and hence "time to peak" was also considered as a percentage of the R-R interval to determine if this is more informative. Similar correlation coefficients were obtained when considering time to peak in ms and as a percentage of the R-R interval.

In this chapter, strain parameters have been compared with scores representing the transmural extent of MI and wall motion abnormalities. While the overall results are positive, the allocated scores are qualitative, and it may be useful to compare the strain parameters with quantitative measurements. Instead of wall motion score and transmural extent of MI score, myocardial thickening and the percentage of a segment which contains gadolinium respectively could be measured.

Two versions of the DENSE pulse sequence and analysis software are available, one of which is a research sequence from a group at NIH (sequence 1), and the other is a "work in progress" sequence which is currently under development by Siemens (sequence 2). Similar correlation and regression results were obtained using both sequences, indicating that both sequences have the potential to be used in this study. The main consideration is the level of support which is available – there is currently no formal support available for sequence 1, whereas sequence 2 is supported via a research agreement with Siemens. For this reason, the decision was taken to use sequence 2 for the remainder of the study.

4.7 Summary and Conclusions

A preliminary assessment of DENSE at 1.5T has indicated the there is a moderate correlation between strain parameters, particularly peak circumferential strain, with qualitative clinical measures of cardiac function. Analysis of DENSE images has high intra- and inter-operator repeatability. Further investigation with a larger patient group is now required, but the technique has the potential to provide clinically interesting information.

All further research will be performed using the Siemens version of the DENSE pulse sequence and analysis software.

Chapter 5

Evaluation of DENSE

5.1 Introduction

Before any further investigations using DENSE could begin, it was necessary to evaluate the performance of the pulse sequence. Ideally, a purpose-built phantom would have been used which would have allowed the generation of known circumferential and radial strains, but the construction of such a phantom was not considered to be feasible. As discussed in Section 2.4.4.5, validation of DENSE has previously been carried out through comparison with myocardial tagging, and this approach will be taken in this chapter. Prior to this, the repeatability of DENSE image acquisition and analysis will be further assessed. In addition, a comparison will be made with strain values reported for healthy subjects in the literature.

5.2 Aims

The aims of the research presented in this chapter are:

- To assess the repeatability of DENSE image acquisition and analysis when a subject is scanned on two separate occasions
- To compare the repeatability of DENSE image acquisition and analysis for segments with varying degrees of hypokinesis
- To compare the strain results obtained using DENSE and tagging in healthy subjects, and evaluate the extent of agreement
- To compare the strain results obtained using DENSE in healthy subjects with the results reported in the literature

5.3 Methods

5.3.1 Healthy Volunteers

40 volunteers (M:F = 18:22, age 41 ± 13 years) with no history of cardiac disease were recruited from the community, including NHS staff and family members. Approval for the study was obtained from the West of Scotland Research Ethics Committee, and written consent was obtained from all volunteers.

5.3.2 Image Acquisition and Analysis

DENSE images were acquired from basal, mid-ventricular and apical short axis slices and analysed as described in Section 0. Values were obtained for peak circumferential strain (Ecc), time to peak Ecc (%RR), peak radial strain (Err) and time to peak Err (%RR) for each myocardial segment, and also for each slice as a whole. As discussed in Chapter 4, from this point onwards, only DENSE sequence 2 will be used.

Tagging images were acquired in a mid-ventricular short axis slice at the same location as the DENSE mid-ventricular images using the pulse sequence parameters shown in Table 5-1.

Parameter	1.5T
TR (ms)	6.2
TE (ms)	3.9
Flip Angle (deg)	10
FoV Read (mm)	380
FoV Phase (%)	60
Tag Spacing (mm)	5
Slice Thickness (mm)	6
Resolution	1.5×2.2
Bandwidth (Hz/pixel)	184

Table 5-1: Pulse sequence parameters for myocardial tagging

Analysis was performed using InTag software (CREATIS, University of Lyon, France), which utilises the SinMod technique described in Section 2.4.2. InTag produces data relating to peak values and time to peak for circumferential and radial strain on a segment-by-segment basis, and peak values with no corresponding time information for the whole slice.

5.3.3 Repeatability of Image Acquisition and Analysis

The first step in the assessment of repeatability of image acquisition and analysis was carried out during the preliminary clinical assessment of DENSE described in Chapter 4, where intra- and inter-operator repeatability were investigated. To complete the assessment, the repeatability of DENSE image acquisition and analysis between images obtained from the same subject on two occasions was investigated. 10 volunteers completed the scan protocol and were removed from the scanner, then returned to the scanner approximately 15 minutes later. For the second scan, localiser images and 2-chamber, 4-chamber and short axis were obtained, then DENSE images were acquired in basal, mid-ventricular and apical short axis locations, without referring to the previous scan.

The results from scan 1 and scan 2 were compared using paired t-tests or Wilcoxon signed rank tests, and the limits of agreement of the differences were calculated using Equation 4-1 from Chapter 4. Inter-scan RMS-CoV were also calculated. Analysis was performed on both segment and whole slice data.

5.3.4 Variation in Repeatability with Degree of Hypokinesis

As noted in Chapter 4, for segments which are contracting very poorly (e.g. peak Ecc < 5%), there can be considerable variation in the strain values obtained when the same dataset is analysed multiple times. To further investigate the variability, datasets from 15 patients with MI (from Chapter 4) and 5 healthy subjects were analysed 4 times each and for each segment, the CoV was calculated for peak Ecc, time to peak Ecc (%RR), peak Err and time to peak Err (%RR).

Segments were grouped according to the average peak Ecc as normokinetic (peak Ecc > 15%), slightly hypokinetic (10% < peak Ecc < 15%), moderately hypokinetic 5% < peak Ecc < 10%) and severely hypokinetic (peak Ecc < 5%). A one-way ANOVA

with Tukey's post-hoc test or Kruskal-Wallis with individual Mann-Whitney tests was used to compare the mean CoV in the 4 groups for peak Ecc and time to peak Ecc.

A similar analysis was carried out with segments grouped according to the average peak Err as normokinetic (peak Err > 45%), slightly hypokinetic (30% < peak Err < 45%), moderately hypokinetic (15% < peak Err < 30%) and severely hypokinetic (peak Err < 15%), and the mean CoV was compared between the 4 groups for peak Err and time to peak Err.

5.3.5 Comparison with Tagging

An initial assessment of the agreement between the segment strain results obtained using DENSE and tagging was carried out by plotting each pair of results, and superimposing the line $y = x$, which represents perfect agreement between the methods. A quantitative assessment was provided by calculating the Pearson correlation coefficient, in keeping with the studies described in Section 2.4.4.5.

A more thorough assessment was performed using the methods described by Bland and Altman [111, 112]. A Bland-Altman plot of the difference between the results obtained from the two methods against the mean value of the results was produced, which also showed the mean difference (bias) between the results from the two methods, $\bar{d}$, and the estimated limits of agreement, which were calculated using Equation 4-1 from Chapter 4.

Standard errors (*SE*) for the bias and the limits of agreement were calculated using Equations 5-1 and 5-2 respectively, and 95% confidence intervals were calculated using Equations 5-3 and 5-4.

$$SE\left(\bar{d}\right) = \sqrt{\frac{SD^2}{n}} \qquad \textbf{(Equation 5-1)}$$

$$SE\left(Limits\right) \approx \sqrt{\frac{3SD^2}{n}} \qquad \textbf{(Equation 5-2)}$$

$$95\%CI\left(\bar{d}\right) = \bar{d} \pm t\left(5\%, n-1\right) * SE\left(\bar{d}\right) \qquad \textbf{(Equation 5-3)}$$

$$95\%CI\left(Limits\right) = Limits \pm t\left(5\%, n-1\right) * SE\left(Limits\right) \qquad \textbf{(Equation 5-4)}$$

where n is the number of measurements, and $t(5\%, n\text{-}1)$ is the 5% point of a t distribution with n-1 degrees of freedom. Equations 5-1 to 5-4 assume that the data is normally distributed, and this was assessed using Anderson-Darling tests.

Finally, the results obtained using DENSE and tagging were compared using paired t-tests or Wilcoxon signed rank tests.

A comparison of the results obtained using DENSE and tagging for whole slice data was carried out in a similar way to that used for segment data, except that analysis was performed for peak strain only since no information on time to peak was available for tagging.

5.3.6 Comparison with Reported Strain Values

A comparison of the strain values obtained from 40 healthy subjects was made with values from healthy subjects reported in the literature, as shown in Table 2-1 in Section 2.5.1.

5.4 Results

5.4.1 Repeatability of Image Acquisition and Analysis

During the assessment of repeatability, it became apparent that DENSE data acquired from basal and apical slices were problematic. Basal slices were often positioned too close to the left ventricular outflow tract (LVOT), which caused distortion in the strain curves, as illustrated in Figure 5-1(a). The analysis software is restricted to 6-segment analysis which is not appropriate for apical slices, and again sub-optimal positioning often resulted in distorted strain curves, as illustrated in Figure 5-1(b).

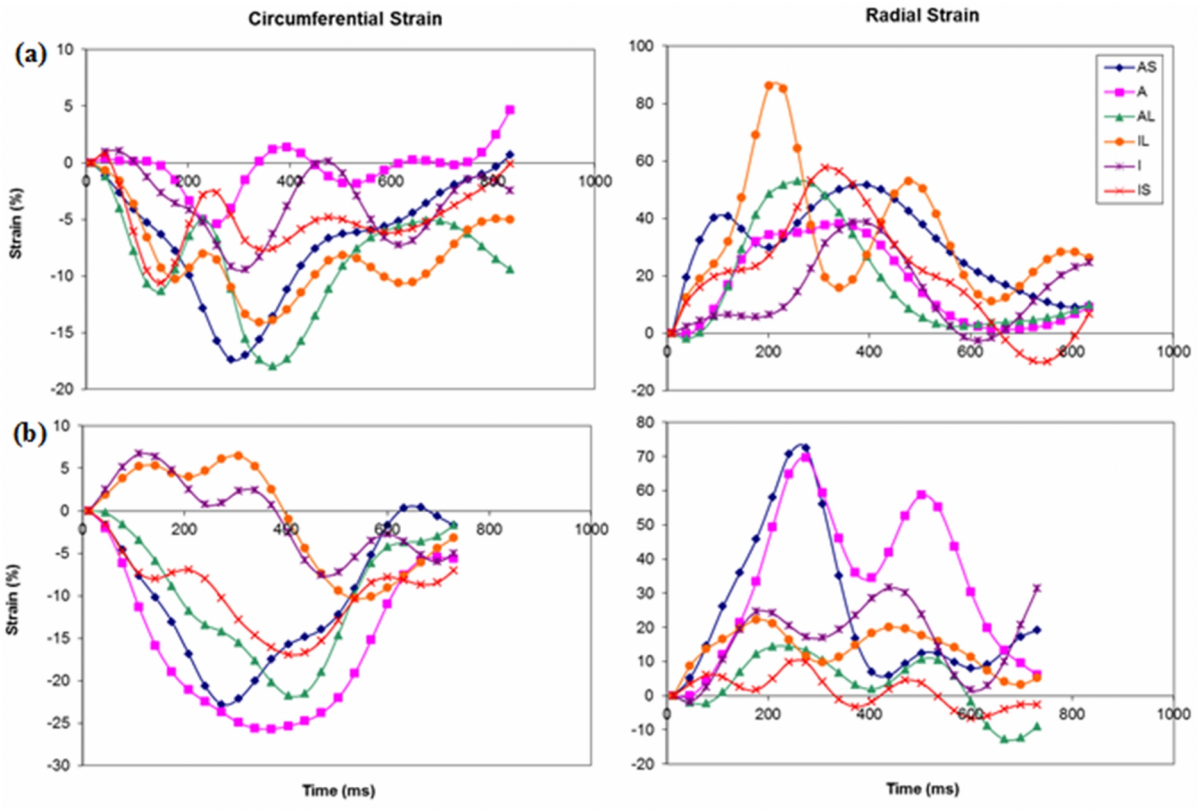

Figure 5-1: Examples of strain curves from a) basal and b) apical locations

Due to the issues encountered with basal and apical slices, the assessment of image acquisition and analysis repeatability was performed on mid-ventricular slices only, and the results are shown in Table 5-2. Statistically significant results are highlighted using * ($p < 0.05$) and ** ($p < 0.001$).

The results of the Anderson-Darling tests showed that peak Ecc was normally distributed, but peak Err, time to peak Ecc and time to peak Err were not. Paired t-tests were used for peak Ecc, and Wilcoxon signed rank tests were used for peak Err, time to peak Ecc and time to peak Err. Wilcoxon signed rank tests were used for all parameters in the whole slice analysis due to the small sample size.

	Segments			Whole Slice		
Strain Parameter	**RMS CoV**	**p**	**Limits of Agreement**	**RMS CoV**	**p**	**Limits of Agreement**
Peak Ecc	2.2	0.706	(-3.0, 3.2)	2.5	0.575	(-3.7, 4.5)
Time to Peak Ecc	3.3	0.534	(-12.6, 12.1)	3.1	0.838	(-11.7, 10.6)
Peak Err	5.4	0.007*	(-37.1, 53.6)	3.6	0.610	(-15.7, 18.7)
Time to Peak Err	4.8	0.868	(-56.9, 48.2)	3.5	0.154	(-11.0, 16.8)

Table 5-2: Repeatability of DENSE acquisition and analysis

The results show that there are statistically significant differences for peak Err when data is analysed on a segment-by-segment basis, but not for any other parameter.

5.4.2 Variation in Repeatability with Degree of Hypokinesis

From the 20 subjects (15 patients with MI and 5 healthy volunteers), there were 120 segments available for analysis. The number of segments/slices allocated to each hypokinesis group is shown in Table 5-3, and the mean CoV values for each strain parameter in each group are shown in Table 5-4. The results are illustrated using box plots in Figure 5-2 and Figure 5-3 for segment and whole slice data respectively.

	Ecc		Err	
Hypokinesis	**Segments**	**Slices**	**Segments**	**Slices**
None	59	6	33	3
Slight	21	7	35	8
Moderate	27	3	44	7
Severe	13	4	8	1

Table 5-3: Allocation of segments to hypokinesis groups

		Degree of Hypokinesis			
Region	**Parameter**	**None**	**Slight**	**Moderate**	**Severe**
Segments	Peak Ecc	6.4	10.1	16.5	58.9
	Time to Peak Ecc	4.6	8.8	9.0	39.6
	Peak Err	14.9	13.6	22.7	17.8
	Time to Peak Err	7.0	9.1	18.4	13.7
Slices	Peak Ecc	3.7	6.3	7.1	4.4
	Time to Peak Ecc	0.8	8.2	2.4	6.9
	Peak Err	8.5	7.8	15.7	-
	Time to Peak Err	3.6	3.2	3.6	-

Table 5-4: Mean CoV in hypokinesis groups

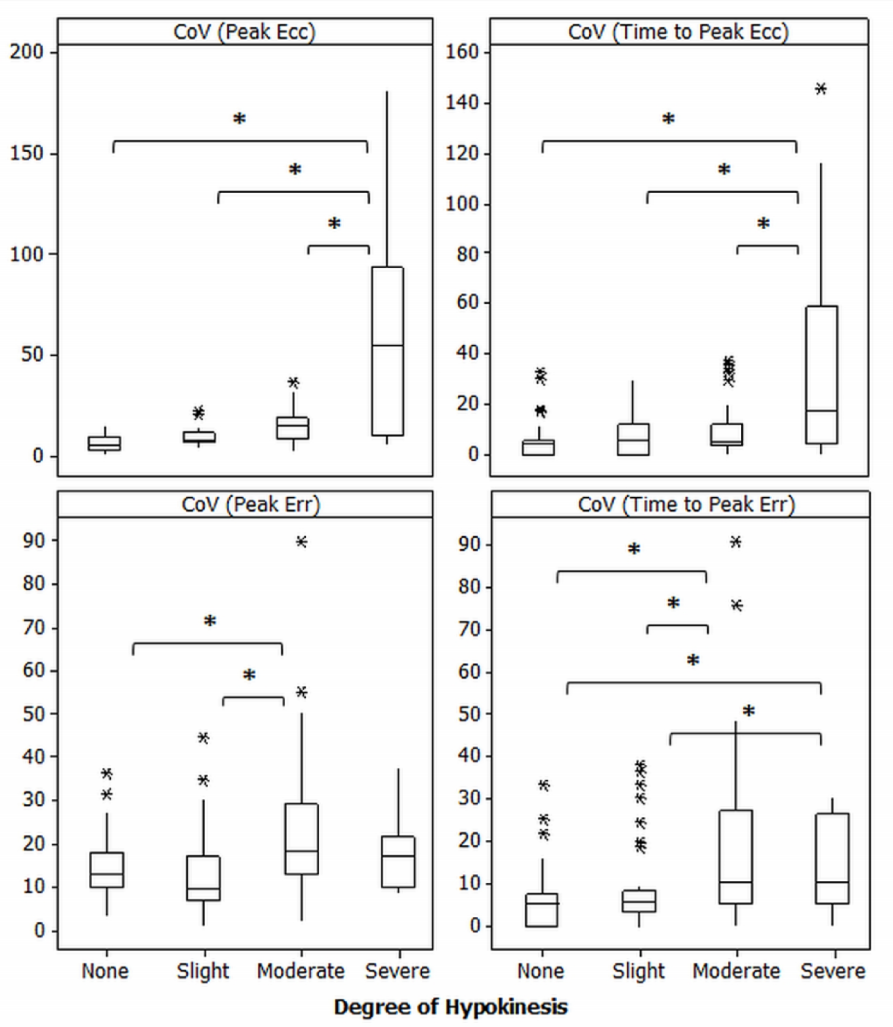

Figure 5-2: Variation in CoV with degree of hypokinesis for segment data

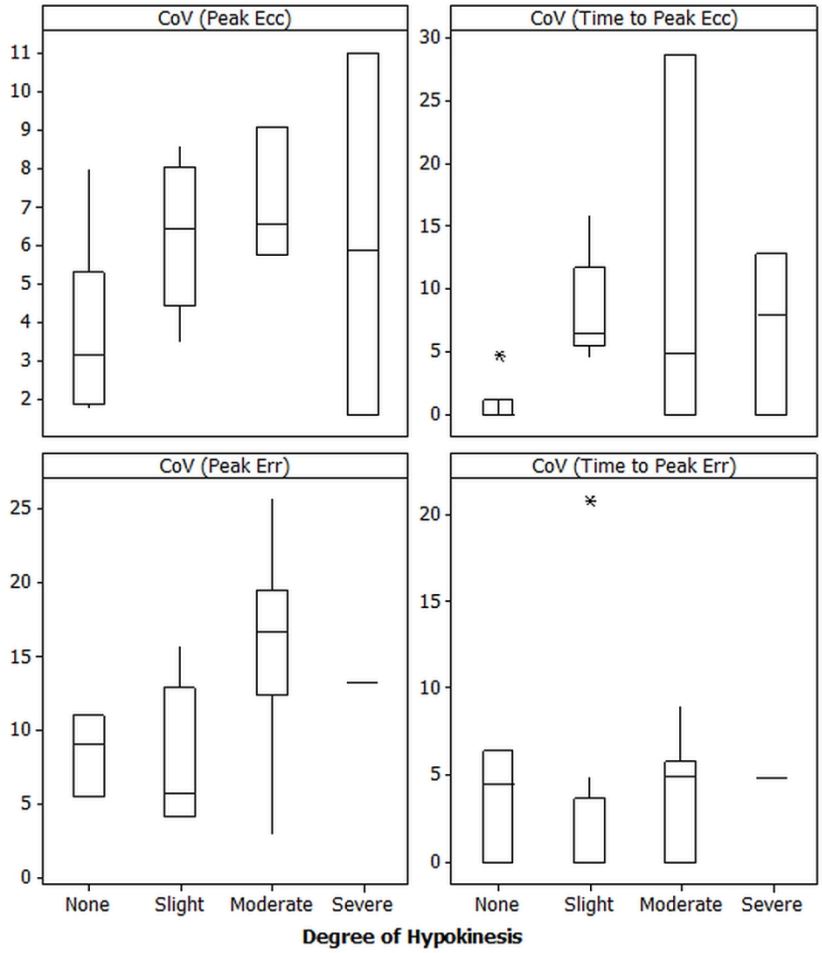

Figure 5-3: Variation in CoV with degree of hypokinesis for whole slice data

The results of the Kruskal-Wallis with individual Mann-Whitney tests for Ecc showed that there were statistically significant differences between the mean CoV obtained for severely hypokinetic segments and the mean CoV for all other segments for peak Ecc and time to peak Ecc. For whole slice data, there were no statistically significant differences in mean CoV between the groups.

The results of the Kruskal-Wallis with individual Mann-Whitney tests for Err showed that there were no statistically significant differences between the mean CoV obtained for normokinetic, slightly hypokinetic and severely hypokinetic segments for peak Err, but there were statistically significant differences between the mean CoV for moderately hypokinetic segments when compared to normokinetic and slightly hypokinetic segments. For time to peak Err, there were no statistically significant differences between normokinetic and slighty hypokinetic segments, or between moderately and severely hypokinetic segments, but there were statistically significant

differences between the two groups. For whole slice data, there were no statistically significant differences in mean CoV between the groups.

The mean CoV values for segments which were severely hypokinetic were considerably larger for peak Ecc and time to peak Ecc than for peak Err and time to peak Err.

5.4.3 Comparison with Tagging

From the 40 healthy subjects, both DENSE and tagging results were obtained for 35 subjects. In 5 subjects, one or both of the DENSE and tagging images were considered non-diagnostic due to excessive breathing artefacts. This resulted in 210 segments available for analysis.

DENSE and tagging results were obtained for both circumferential and radial strain. However, it soon became apparent that the tagging results for radial strain were unreliable, as illustrated in Figure 5-4. As discussed in Section 2.4.2, tagging has a disadvantage due to the fact that deliberate suppression of the myocardial signal limits the resolution, which means that it is difficult to measure transmural variations in motion, and hence the assessment of radial strain can be problematic. The comparisons between DENSE and tagging were therefore performed for circumferential strain only.

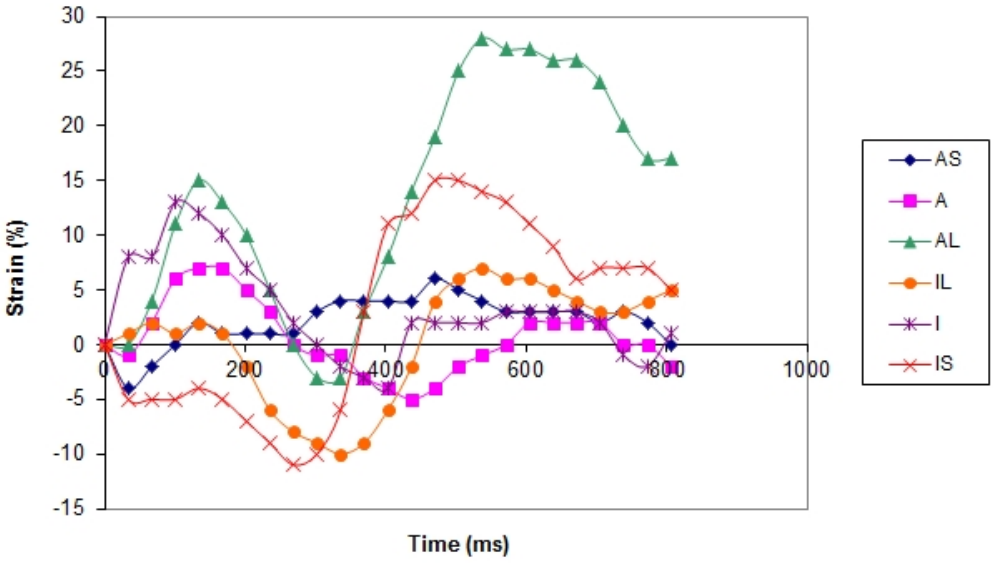

Figure 5-4: Illustration of radial strain curves obtained using tagging

Scatter plots illustrating the agreement between the results obtained with DENSE and tagging are shown in Figure 5-5. The correlation coefficients were found to be 0.24, 0.52 and 0.55 for peak Ecc, time to peak Ecc (%RR) and whole slice peak Ecc respectively.

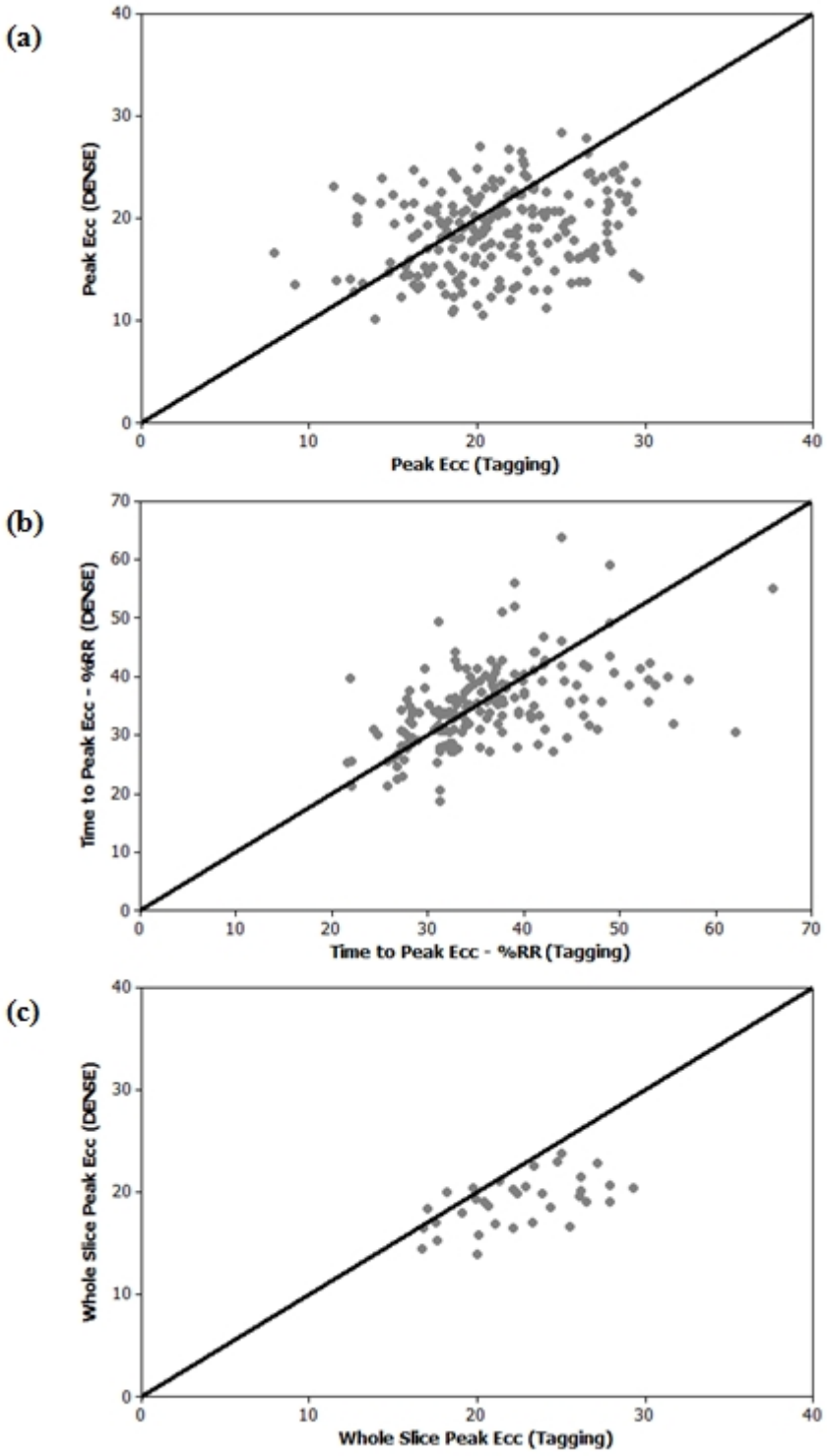

Figure 5-5: DENSE vs tagging for a) peak Ecc, b) time to peak Ecc (%RR) and c) whole slice peak Ecc

Prior to carrying out Bland-Altman analysis, the calculated differences between the results obtained using DENSE and tagging were checked for normality. The resulting histograms are shown in Figure 5-6.

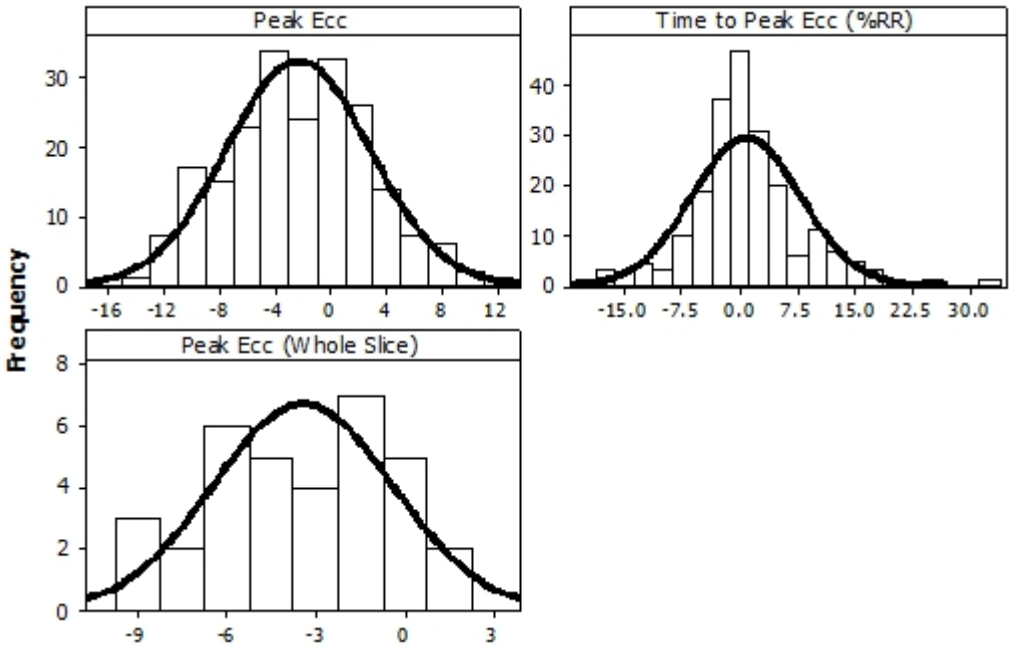

Figure 5-6: Histogram test of data normality

The results of the Anderson-Darling tests confirmed that the data for peak Ecc is normally distributed ($p = 0.130$ for segment data and $p = 0.176$ for whole slice data), however the data for time to peak Ecc (%RR) is not ($p < 0.05$). Bland and Altman stated that non-normality of data may not be as serious in their method of analysis as in other statistical contexts, and that non-normal data is still likely to have 95% within ~2 standard deviations of the mean [112]. In addition, the histogram for time to peak Ecc does not appear to be far removed from a normal distribution, and hence the decision was taken to continue on with the analysis as though the data for all parameters was normally distributed.

Bland-Altman plots are shown in Figure 5-7, and 95% confidence intervals for the bias and limits of agreement are shown in Table 5-5. Values for $t(5\%, n-1)$ were obtained from statistical tables for a two-tailed t distribution for use in the calculations, and were found to be 1.972 and 2.032 for segment and whole slice data respectively. Table 5-5 also shows the mean value of (DENSE + Tagging)/2 for comparison.

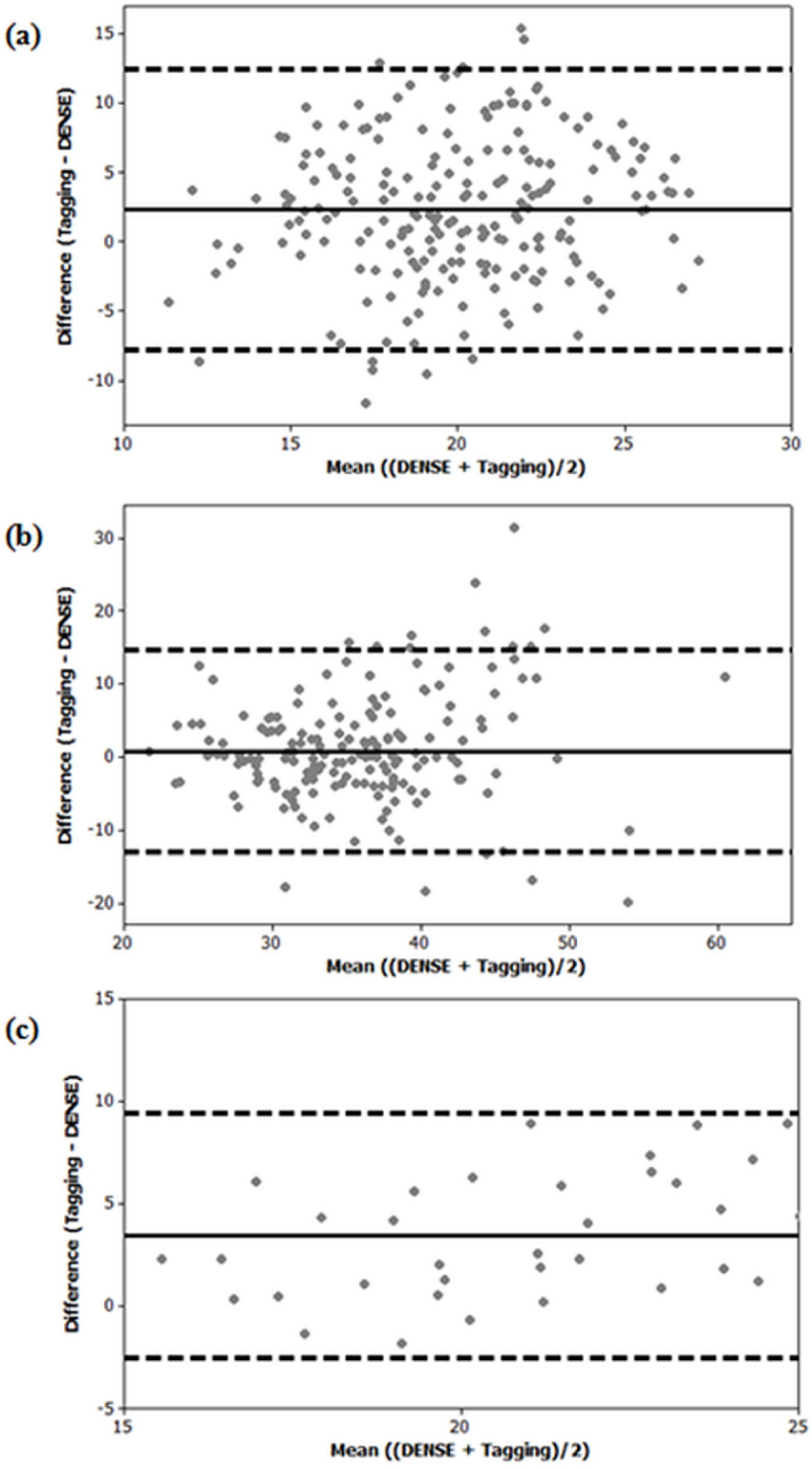

Figure 5-7: Bland-Altman plots for DENSE vs Tagging for a) peak Ecc, b) time to peak (%RR) and c) whole slice peak Ecc

Parameter	Peak Ecc	Time to Peak (%RR)	Whole Slice Peak Ecc
Mean	20.0	35.3	20.7
Bias	(1.6, 3.0)**	(-0.2, 1.8)	(2.4, 4.5)**
Upper Limit	(11.3, 13.7)	(13.0, 16.3)	(6.5, 11.2)
Lower Limit	(-6.6, -9.0)	(-14.7, -11.4)	(-4.3, -0.7)

Table 5-5: 95% confidence intervals for DENSE vs Tagging Bland-Altman analysis

The 95% confidence intervals for the mean difference between the results obtained using tagging and DENSE provided by paired t-tests are the same as the 95% confidence intervals for the bias provided by Bland-Altman analysis. The paired t-tests provided additional information about the statistical significance of the bias, and this is indicated in Table 5-5 by * ($p < 0.05$) and ** ($p < 0.001$).

5.4.4 Comparison with Reported Strain Values

A comparison of the peak Ecc results for each segment obtained in healthy subjects using DENSE with the results reported in the literature, as detailed in Table 2-1, is illustrated in Figure 5-8. The values are shown as mean ± SD. The results are displayed (left → right) in the order that they appear in Table 2-1 (top → bottom), with the final result corresponding to the values obtained in this study.

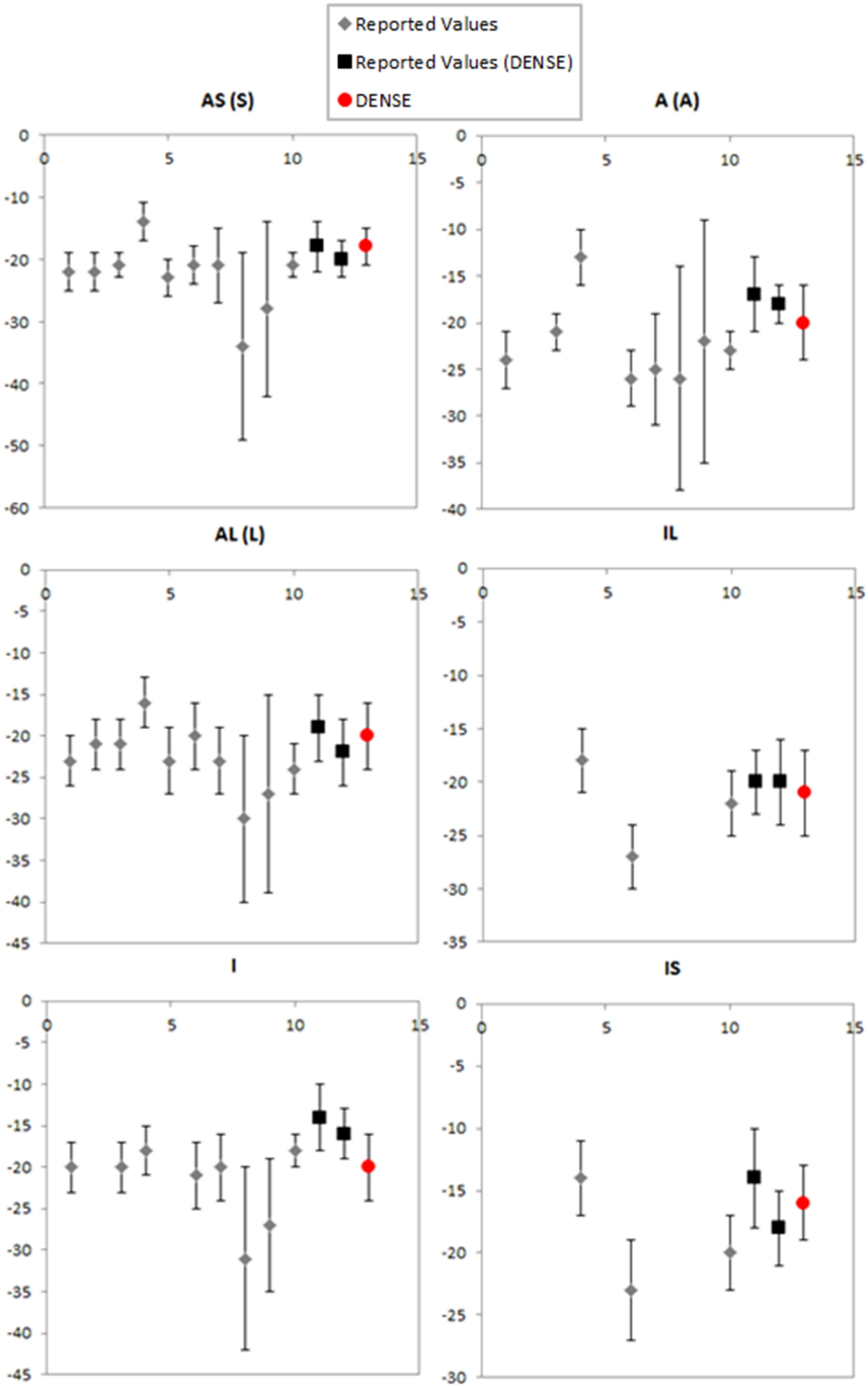

Figure 5-8: Comparison of DENSE results with reported values

5.5 Discussion

A summary of the key results from this chapter is shown in Table 5-6.

Investigation	Results
Repeatability	• No statistically significant difference in the results obtained by two independent operators, except for peak Err • No statistically significant difference in the results from the same subjects on two separate occasions, except for peak Err • Intra-operator CoV and inter-operator RMS-CoV are small for all strain parameters • Inter-scan RMS-CoVs are small for all strain parameters
Repeatability and Hypokinesis	• Statistically significant difference between average CoV for segments with “severe” hypokinesis compared to other segments for both peak Ecc and time to peak Ecc • Statistically significant difference between average CoV for segments with “moderate” hypokinesis compared to other segments for peak Err, and between both “moderate” and “severe” hypokinesis compared to other segments for time to peak Err • Results for whole slice data were not statistically significant • Variation in CoV for segments with peak Ecc < 5% ("severe" hypokinesis) is large and may impact on further analysis, particularly for time to peak Ecc
Tagging	• Results are in reasonable agreement
Reported Values	• Results are in reasonable agreement

Table 5-6: Summary of key results in the evaluation of DENSE

The first finding in the evaluation of DENSE was that the ability to accurately measure strain is highly dependent on slice positioning. Basal slices must be positioned well below the LVOT otherwise distortion of the strain curves will occur. Similarly, careful positioning of apical slices is required to avoid distortion. Additionally, CIM_DENSE2D is currently restricted to 6-segment analysis, and 4-segment analysis of apical slices, as per the AHA model, is not possible. For this reason, only data from mid-ventricular slices was considered for subsequent analysis.

Repeatability of Image Acquisition and Analysis

An assessment of intra- and inter-operator repeatability of image analysis was presented in Chapter 4, which showed small intra-operator CoV and small inter-operator RMS-CoV, and no statistically significant difference in the results obtained by two independent operators for all strain parameters other than peak Err. The final step of this assessment was to scan individuals on two separate occasions and compare the results. Ideally the two scans would have been on two different days rather than 15 minutes apart on the same day, but the volunteers were participating in the healthy volunteer study (see Chapter 6) and as such were already attending for two MRI scans on different days and in different locations, and it was felt that it would be unreasonable to expect them to attend on a third occasion.

Small RMS-CoV values were obtained for peak Ecc and time to peak Ecc. No statistically significant differences were found between the two scans for peak Ecc for both segment and whole slice data, and the limits of agreement were of a magnitude which is unlikely to be clinically significant. No statistically significant differences were found for time to peak Ecc, but the limits of agreement were wider and more likely to be of clinical significance. Analysis of data from a larger sample size is required to assess if the time to peak Ecc information provided by DENSE is clinically useful.

Small RMS-CoV values were obtained for peak Err and time to peak Err. Statistically significant differences were found between the two scans for peak Err, and the limits of agreement were wide, particularly for segment data. As discussed in Chapter 4, the resolution of the pulse sequence is low, and DENSE may not be ideally suited for

measuring radial strain. As for time to peak Ecc, analysis of data from a larger sample size is required to assess if peak Err and time to peak Err are clinically useful.

Variation in Repeatability with Degree of Hypokinesis

The variation in the repeatability of DENSE strain values for segments with different degrees of hypokinesis was assessed by grouping segments as normokinetic, slightly hypokinetic, moderately hypokinetic and severely hypokinetic depending on the value of peak Ecc or Peak Err.

When segments were grouped according to peak Ecc, there were no statistically significant differences between the peak Ecc and time to peak Ecc values obtained for normokinetic, slightly hypokinetic and moderately hypokinetic segments. There were statistically significant differences for severely hypokinetic segments, with mean values which were substantially larger than those found for the other groups, and with a much wider range of individual CoV values. For whole slice data, no statistically significant differences were observed between the groups, however the number of slices in each group was small.

When segments were grouped according to peak Err, there were no statistically significant differences between the peak Err values obtained for normokinetic, slightly hypokinetic and severely hypokinetic segments, but there was a statistically significant difference between these segments and those which were moderately hypokinetic. For time to peak Err, there were statistically significant differences between moderately and severely hypokinetic segments compared to normokinetic and slightly hypokinetic segments. For whole slice data, no statistically significant differences were observed between the groups, but again the number of slices in each group was small.

The variation in CoV for segments with peak Ecc <5% is large, and indicates that measurements obtained from segments which fall into this category could be unreliable. When peak Ecc is very small, repeated measurements can vary by a small amount and yet still result in a large CoV. For example, measurements of 0.9%, 1.9%, 1.8% and 0.1% result in a CoV of 72%, but the variation in the measurements themselves will have no impact on the clinical assessment of this segment – it is

clearly severely hypokinetic in all cases. However, the variation in time to peak Ecc may be more important. For example, measurements obtained for one segment were 92ms, 22ms, 92ms and 12ms, and depending on which value was used for further analysis, very different conclusions on the contractile function of the segment could be drawn. For subsequent analysis within this thesis, all values of peak Ecc will be included, but values of time to peak Ecc corresponding to segments with peak Ecc < 5% will be excluded.

The range in CoV values obtained for peak Err and time to peak Err for segment data are smaller, and although there were statistically significant differences between the groups, the mean CoV values are similar in all groups. Variations in CoV in severely hypokinetic segments are unlikely to have the same impact as for peak Ecc, and so all measurements of peak Err and time to peak Err will be included in subsequent analysis.

Comparison with Tagging

DENSE and tagging images were acquired from healthy subjects, and the results were compared in a similar way to the DENSE validation studies previously reported in the literature. The radial strain results from tagging were found to be unreliable, and hence analysis was performed for circumferential strain only.

A plot of DENSE results against tagging results for segment data showed clustering around the line of perfect agreement ($y = x$), but with a reasonably large spread, for both peak Ecc and time to peak Ecc. This is reflected in the low correlation coefficients of 0.24 and 0.54 respectively. Similar results were obtained for whole slice data (peak Ecc only), but the distribution around $y = x$ was unequal, with larger strain values obtained using tagging than DENSE.

Bland-Altman plots showed no obvious trends, but with a reasonably large spread of values. The 95% CI for the mean differences between the DENSE and tagging results were (1.6, 3.0) for peak Ecc (segments), (-0.2, 1.8) for time to peak Ecc (segments) and (2.5, 4.5) for peak Ecc (whole slice). The 95% CI for time to peak Ecc contains 0, which implies that the two sets of results are in good agreement, but this is not the case for peak Ecc, and the results of paired t-tests comparing the peak Ecc values for

both segments and whole slice data showed statistically significant differences. However, the magnitude of the mean differences in both cases is small compared to the mean values of peak Ecc, and so the difference is unlikely to be clinically significant. The differences are more apparent for the whole slice data than the segment data, but this may be due to the smaller sample size.

Tagging has been treated as the "reference method" in this analysis, as the technique has been well validated and documented in the literature, and previous validation of DENSE has been performed in this way. However, quantitative analysis of tagging is not routinely performed at our institution, and lack of experience may have resulted in a wider range of errors in the tagging results than would normally have been expected. In addition, the tagging analysis software was obtained after the tagging data had been acquired, and the authors of the software recommend that a tag spacing of 7mm is used, rather than the 5mm spacing which was used in this study. Tagging with 5mm spacing results in images which are acceptable for qualitative analysis, but may not be optimal for quantitative analysis. However, in spite of these issues, the results obtained with tagging and DENSE are in reasonable agreement, and as stated above, any differences are unlikely to be of clinical significance.

Both tagging and DENSE were analysed by the same operator, which could potentially have resulted in operator bias. To minimise this, all of the DENSE images were analysed, then all of the tagging images were analysed without referring to the DENSE results.

Comparison with Reported Strain Values

The peak Ecc results obtained using DENSE were visually compared with values reported in the literature by plotting mean ± SD for each segment. Although the number of studies available for comparison was small, the DENSE results were considered to be in reasonable agreement with the published values for all segments.

5.6 Summary and Conclusions

DENSE images can be acquired and analysed in a repeatable manner, on different occasions and by different operators, particularly for peak Ecc. Further work is required to determine if peak Err and time to peak Err can provide information which is clinically useful, as the variation between operators and scans for these parameters is potentially clinically significant.

The variation in repeated measurements of time to peak Ecc for severely hypokinetic segments is large, and could have an impact on further analysis. Any measurements of time to peak Ecc corresponding to values of peak Ecc < 5% will be excluded from further analysis.

The values obtained using DENSE for peak Ecc and time to peak Ecc (%RR) in healthy subjects were found to be comparable with those obtained using tagging, and with values reported in the literature.

Chapter 6

DENSE in Healthy Volunteers

6.1 Introduction

An understanding of how a technique performs in healthy subjects is essential before it can be applied and correctly interpreted in subjects with pathology. There are several potential sources of variability in strain, including age, gender and myocardial location, and each of these will be investigated within this chapter. In addition, a comparison of the strain values obtained using a 1.5T and a 3T MRI scanner will be performed. The majority of the research within this thesis is carried out at 1.5T, but as 3T scanners are becoming more common in both clinical and research settings, any differences in performance must be identified to facilitate further research and clinical applications of DENSE.

6.2 Aims

The aims of the research presented in this chapter are:

- To investigate variations in each of the strain parameters with age
- To investigate variations in each of the strain parameters with gender
- To investigate variations in each of the strain parameters with myocardial segment
- To investigate variations in each of the strain parameters with myocardial slice
- To establish reference ranges for each strain parameter
- To compare the results obtained at 1.5T and 3T

6.3 Methods

6.3.1 Healthy Volunteers

80 volunteers with no history of cardiac disease, connective tissue disease or hypertension were recruited from the community, including NHS staff and family members. All volunteers underwent a 12-lead ECG, and volunteers aged over 45 years underwent LGE imaging with Gd contrast (see Section 3.4) to ensure that there were no undiagnosed cardiac problems. Approval for the study was obtained from the West of Scotland Research Ethics Committee, and written consent was obtained from all volunteers. A copy of the Patient Information Sheet for the study can be found in Appendix C.

6.3.2 Image Acquisition and Analysis

Imaging was performed using a 1.5T Siemens Avanto and a 3T Siemens Verio, with cine and DENSE images acquired and analysed as described in Chapter 3.

For each volunteer, DENSE images were acquired in a basal, mid-ventricular and apical axial slice at both 1.5T and 3T. Images were analysed using CIM_DENSE2D software, and values were obtained for peak circumferential strain (Ecc), time to peak Ecc (%RR), peak radial strain (Err) and time to peak Err (%RR) for each myocardial segment, and also for each slice as a whole. In addition, the average strain rate during the period of active contraction up to end-systole (ES) was calculated for both circumferential and radial strain as the ratio of the peak strain to the time taken to reach the peak. Analysis was only performed on basal and mid-ventricular images due to the current inability of CIM_DENSE2D to consider 4 segments instead of 6, as mentioned in Section 5.4, but the apical images were still acquired for potential use in future studies.

Peak strain values provide a measure of contractile function at a single time point, but the effects of myocardial and injury could alter the way in which contraction occurs throughout the cardiac cycle. In order to assess the overall contractile function, the Matlab code was extended to calculate the area under the strain curves produced by CIM_DENSE2D during the period of active contraction up to ES, and the average area over time.

6.3.3 Investigation of Strain Variation with Age

The relationships between strain parameters and age were initially assessed using correlation tests. The data were then divided into age groups (<30 years, 30 – 60 years, >60 years) and compared using one-way ANOVA with Tukey's post-hoc tests or Kruskal-Wallis with individual Mann-Whitney tests. Analysis was performed on male and female data separately, and used whole slice data to avoid any potential variation in strain in different myocardial segments.

6.3.4 Investigation of Strain Variation with Gender

The variations in strain parameters with gender were assessed using two-sample t-tests or Mann-Whitney tests.

6.3.5 Investigation of Strain Variation in Myocardial Segments

The variations in strain parameters with myocardial segment were assessed using a one-way ANOVA with Tukey's post-hoc test or Kruskal-Wallis with individual Mann-Whitney tests.

6.3.6 Investigation of Strain Variation in Myocardial Slices

The variations in strain parameters between basal and mid-ventricular slices were assessed using paired t-tests or Wilcoxon signed rank tests. Analysis was performed on both segment and whole slice data.

For segment data, the differences in strain between mid-ventricular and basal slices were further investigated by using one-way ANOVA with Tukey's post-hoc tests or Kruskal-Wallis with individual Mann-Whitney tests to compare the differences with data grouped according to segment.

6.3.7 Determination of Reference Ranges

For each strain parameter, reference ranges were determined for segment and whole slice data using Equation 6-1.

$$Range = mean \pm 1.96 * SD \qquad \textbf{(Equation 6-1)}$$

Reference ranges were also determined for each segment (A, AL, AS, I, IL, IS) individually.

6.3.8 Comparison of Strain at 1.5T and 3T

Comparison of strain at 1.5T and 3T was carried out in a similar way to the comparison of DENSE and tagging described in Section 5.3.5.

An initial assessment of agreement was carried out by plotting each pair of results, and superimposing the line $y = x$ which represents perfect agreement. A correlation test was also performed.

A more thorough assessment was carried out using Bland-Altman plots, which showed the mean difference (bias) and the limits of agreement of the two sets of results. The 95% confidence intervals for the bias and the limits of agreement were calculated using Equations 5-1 to 5-4 from Section 5.3.5.

Finally, the results obtained at 1.5T and 3T were compared using paired t-tests or Wilcoxon Signed Rank tests, and inter-scanner RMS-CoV were calculated.

6.4 Results

The clinical characteristics of the 80 volunteers are shown in Table 6-1, where age, body mass index (BMI), LVEF, LVEDV and LVESV are expressed as mean ± SD (range).

Characteristic	Value
Age (years)	43 ± 17 (18 – 89)
M:F	40:40
BMI	26 ± 4 (18 – 35)
Smoker	5 (6%)
Hypercholesterolaemia	5 (6%)
Global LV function by cine MRI:	
LVEF (%)	67 ± 5 (58 – 82)
LVEDV (ml)	150 ± 3 (94 – 222)
LVESV (ml)	51 ± 14 (17 – 81)

Table 6-1: Clinical characteristics of healthy volunteers

Analysis was performed on 72 datasets acquired at 1.5T (M:F = 35:37). For the 8 datasets on which analysis was not performed, 4 DENSE datasets were not acquired, 3 were considered to be non-diagnostic due to excessive breathing artefacts and 1 used the wrong version of DENSE.

From the data acquired at 3T, a further 8 datasets were considered to be non-diagnostic, and one 1 dataset was not acquired, leaving a total of 63 paired datasets (1.5T and 3T) for comparison.

The results of Anderson-Darling tests showed that all strain parameters are normally distributed ($p > 0.05$), and so all statistical analysis was performed using parametric tests.

In Chapter 4 and Chapter 5, it was noted that the limits of agreement for inter-operator and inter-scan repeatability of radial strain were wide, particularly for segment data.

While analysing the healthy volunteer datasets, it was observed that the radial strain curves often appeared distorted. Further investigation revealed that only 15 radial strain curves from 72 volunteers (21%) could be analysed. Examples of radial strain curves which were considered to be acceptable and unacceptable for analysis are shown in Figure 6-1. As mentioned in Sections 2.5.1 and 2.4.4.5, many studies have involved the use of circumferential strain and longitudinal strain rather than radial strain, and large variations in radial strain have been observed when using different measurement techniques. The issues with radial strain in this study are likely to be due to the low resolution of the DENSE images and/or possible errors in post-processing, but without access to the code underlying the analysis software, it is difficult to investigate further at this stage. It seems likely that radial strain in this study is too variable to provide useful clinical information, and all further analysis will be performed on circumferential strain only.

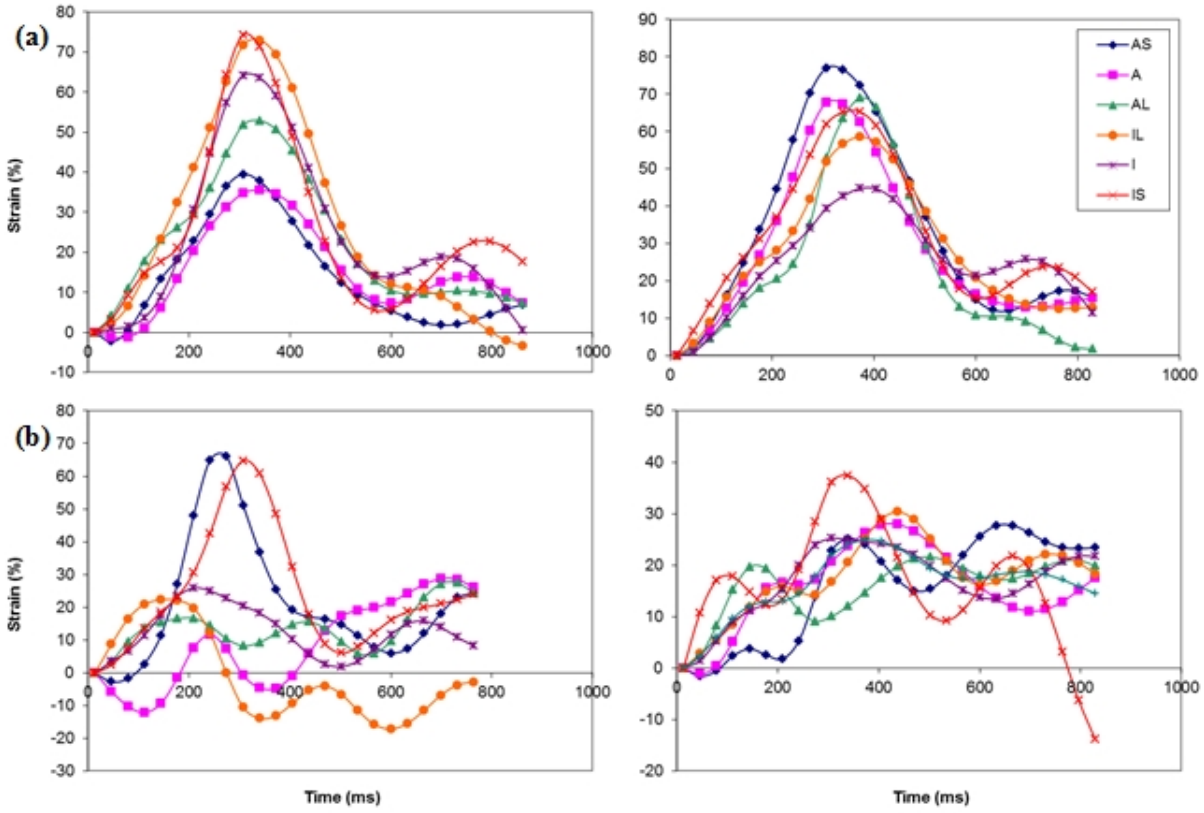

Figure 6-1: Examples of a) acceptable and b) unacceptable radial strain curves

In Section 5.4.1, problems were encountered with strain curves from basal slices, which were often positioned too close to the LVOT. This remained an occasional problem with the data collected from healthy subjects, but more often, over-

compensation occurred and the "basal" slices ended up in a mid-ventricular location. From the basal slices which were positioned correctly, image quality was often lower than that obtained in mid-ventricular slices, resulting in a higher number of non-diagnostic images. One possible explanation for this is the long breath-hold required for DENSE imaging – this could be up to 20 seconds depending on heart rate, and since the basal slice was acquired first, it is likely that volunteers were unprepared for the length of the breath-hold. The long breath-hold is one of the main challenges for the clinical application of DENSE, particularly in acutely ill patients. A further challenge is that radiography staff find it difficult to determine whether DENSE images are of sufficiently high quality due to the low resolution of the images (see Figure 2-16), and problems are often not identified until post-processing is performed.

From the 72 volunteers in whom DENSE was successfully acquired in a mid-ventricular slice, 45 datasets which were considered to be diagnostic were obtained from basal slices. Due to the problems with acquiring data in basal slices, the majority of the subsequent analysis within this thesis will be performed on data from mid-ventricular slices only, however there is a sufficient amount of basal data to allow a comparison of the results obtained in mid-ventricular and basal locations.

6.4.1 Investigation of Strain Variation with Age

The results of the correlation tests are shown in Table 6-2, and are expressed as a Pearson correlation coefficient. Statistically significant results are indicated by * ($p < 0.05$) and ** ($p < 0.001$). The distribution of data with age is illustrated using scatter plots in Figure 6-2.

Strain Parameter	Male	Female
Peak Ecc	0.06	0.16
Time to Peak Ecc (%RR)	0.22	-0.10
Strain Rate	-0.27	0.21
Area	0.32	0.18
Area/Time	0.15	0.26

Table 6-2: Results of variation in strain with age analysis

The number of subjects allocated to each age group is shown in Table 6-3, with the age range for each group expressed as mean ± SD shown in brackets.

Age Group	Male	Female
<30 years	11 (24 ± 3)	12 (24 ± 3)
30 – 60 years	15 (43 ± 10)	17 (45 ± 8)
> 60 years	9 (68 ± 9)	8 (66 ± 5)

Table 6-3: Allocation of healthy subjects to age groups

Box plots illustrating the distribution of data with age groups for male and female subjects are shown in Figure 6-3. The results of the one-way ANOVA with Tukey's post-hoc tests showed no statistically significant differences between the age groups for any strain parameter, for both male and female subjects.

While the lack of variation in strain with age is surprising, it can perhaps be explained by the relatively small number of subjects in each age group, and that fact that the volunteers have no clinically-relevant health problems and are unlikely to be representative of society as a whole. This will be discussed further in Section 6.5 (Discussion), and all subsequent analysis within this chapter will take no account of age.

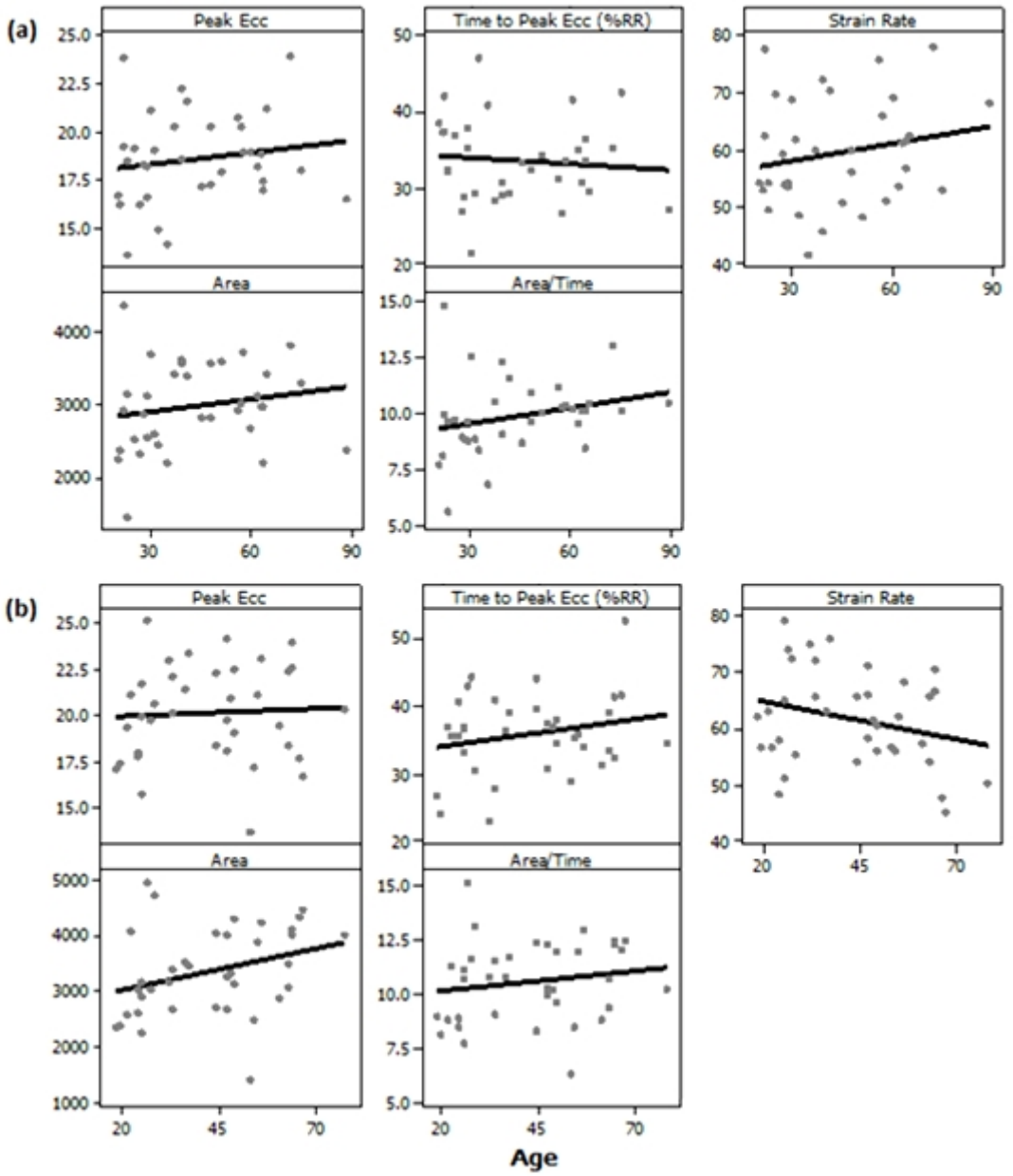

Figure 6-2: Relationships between strain and age for a) male and b) female healthy subjects

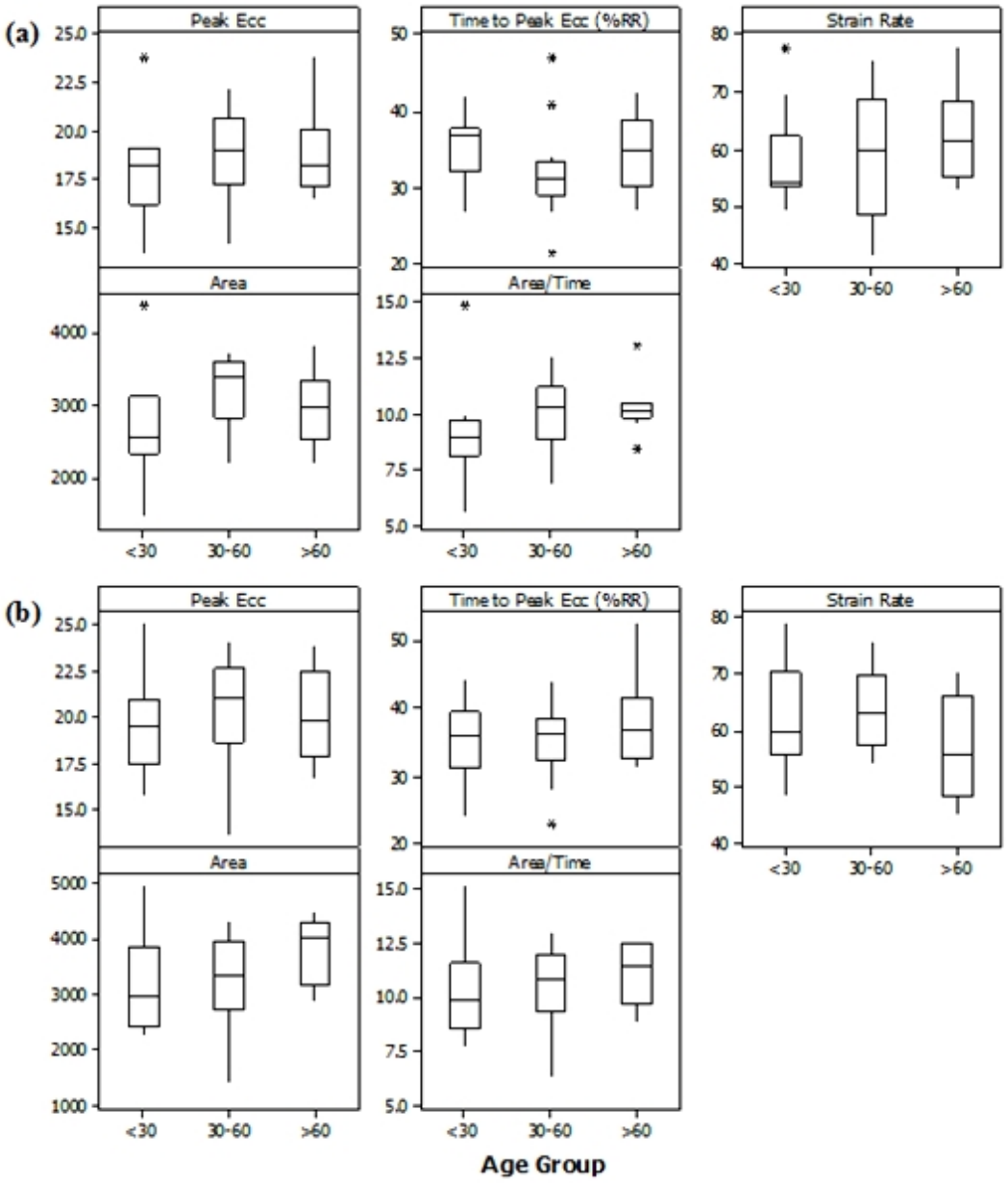

Figure 6-3: Comparison of strain in age groups for a) male and b) female healthy subjects

6.4.2 Investigation of Strain Variation with Gender

Box plots illustrating the distribution of strain parameters with gender are shown in Figure 6-4. Statistically significant results, as determined by two-sample t-tests, are indicated by * ($p < 0.05$) and ** ($p < 0.001$). The age range (mean ± SD) was 44 ± 18 years for male subjects, and 43 ± 17 years for female subjects.

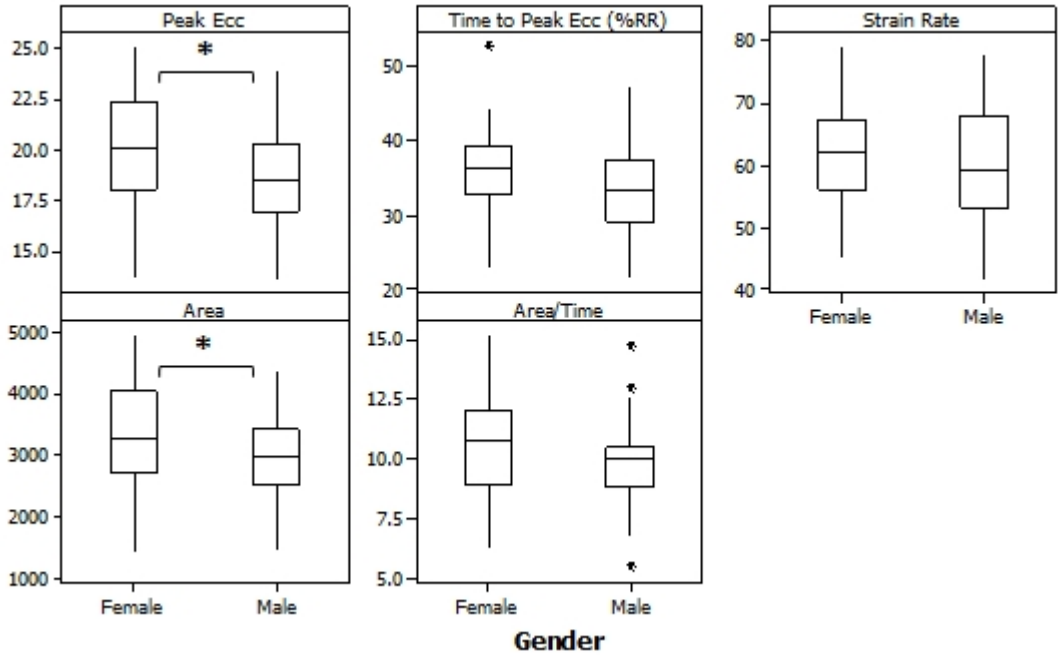

Figure 6-4: Comparison of strain in male and female healthy subjects

Since there are statistically significant differences in peak Ecc and Area, all subsequent analysis within this chapter will consider data from male and female subjects separately.

6.4.3 Investigation of Strain Variation in Myocardial Segments

The strain values obtained for each segment are shown in Table 6-4 and Table 6-5 for male and female subjects respectively, and are expressed as mean ± SD to be consistent with the results from the literature shown in Table 2-1 (Chapter 2).

	Strain Parameter				
Segment	**Peak Ecc**	**Time to Peak Ecc**	**Strain Rate**	**Area**	**Area/Time**
A	20 ± 4	32 ± 5	67 ± 12	3091 ± 819	11 ± 3
AL	20 ± 3	37 ± 7	60 ± 11	3871 ± 967	12 ± 2
AS	18 ± 4	31 ± 5	63 ± 13	2457 ± 834	9 ± 3
I	18 ± 3	35 ± 7	57 ± 13	3192 ± 932	10 ± 2
IL	21 ± 3	38 ± 7	59 ± 9	3902 ± 905	11 ± 2
IS	16 ± 4	31 ± 5	55 ± 14	2221 ± 842	8 ± 3

Table 6-4: Segment strain values for healthy subjects (male)

	Strain Parameter				
Segment	**Peak Ecc**	**Time to Peak Ecc**	**Strain Rate**	**Area**	**Area/Time**
A	21 ± 4	35 ± 6	68 ± 15	3343 ± 897	11 ± 3
AL	22 ± 3	37 ± 7	65 ± 11	3973 ± 1041	12 ± 2
AS	18 ± 3	33 ± 7	61 ± 11	2589 ± 833	9 ± 2
I	21 ± 4	37 ± 7	63 ± 12	3643 ± 1071	11 ± 3
IL	22 ± 4	37 ± 7	66 ± 12	3854 ± 880	12 ± 2
IS	18 ± 3	34 ± 5	58 ± 13	2675 ± 701	9 ± 2

Table 6-5: Segment strain values for healthy subjects (female)

Box plots illustrating the distribution of data with myocardial segment are shown in Figure 6-5. The results of the one-way ANOVA with Tukey's post-hoc tests for both male and female subjects showed statistically significant differences between segments for all strain parameters. For all strain parameters other than strain rate,

higher values were obtained in lateral segments (IL and AL), and lower values were obtained in septal segments (IS and AS).

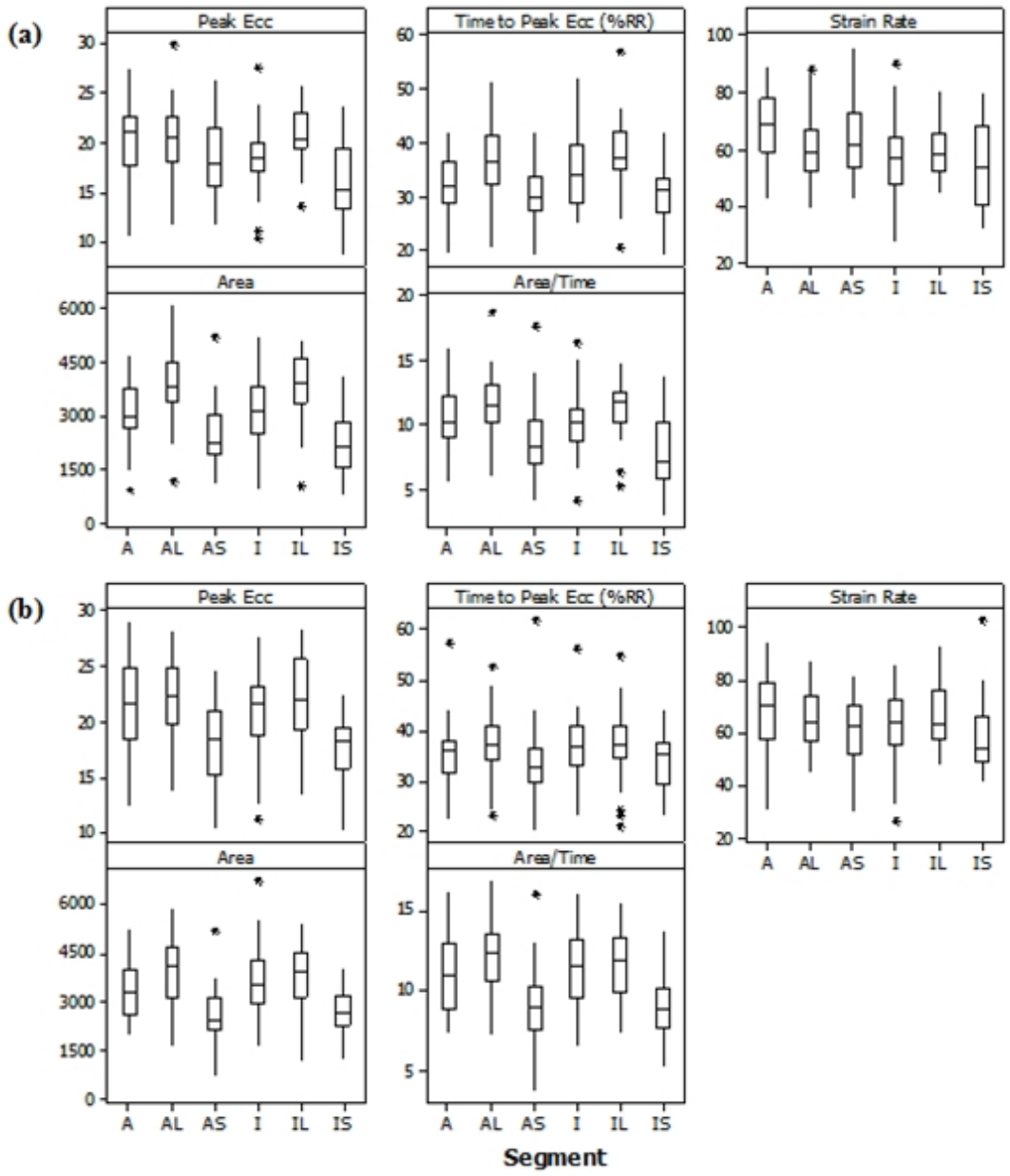

Figure 6-5: Comparison of strain in myocardial segments for a) male and b) female healthy subjects

The variation in strain between myocardial segments has been observed in other studies, as can be seen from Table 2-1. However, these studies made no comment on whether or not the differences were statistically significant, and performed further analysis which took no account of myocardial segment.

6.4.4 Investigation of Strain Variation in Myocardial Slices

The results of the paired t-tests comparing strain in mid-ventricular and basal slices (mid – basal) are shown in Table 6-6, and are expressed as 95% confidence intervals for the mean difference. The mean difference is also shown, and statistically significant results are indicated by * ($p < 0.05$) and ** ($p < 0.001$). The differences between measurements in mid-ventricular and basal slices, along with the mean difference, are illustrated in Figure 6-6.

	Segments		Slices	
Strain Parameter	**Mean**	**95% CI**	**Mean**	**95% CI**
Peak Ecc	2.8	(2.2, 3.3)**	3.0	(2.0, 3.9)**
Time to Peak Ecc (%RR)	-0.8	(-1.5, -0.2)*	-0.4	(-1.5, 0.8)
Strain Rate	8.9	(7.0, 10.8)**	9.3	(6.4, 12.2)**
Area	381	(253, 508)**	414	(184, 644)*
Area/Time	1.4	(1.1, 1.8)**	1.5	(0.9, 2.1)**

Table 6-6: Results of comparison of strain in basal and mid-ventricular slices

The results show that there are statistically significant differences between strain in basal and mid-ventricular slices for all strain parameters, with the exception of time to peak Ecc for whole slice data.

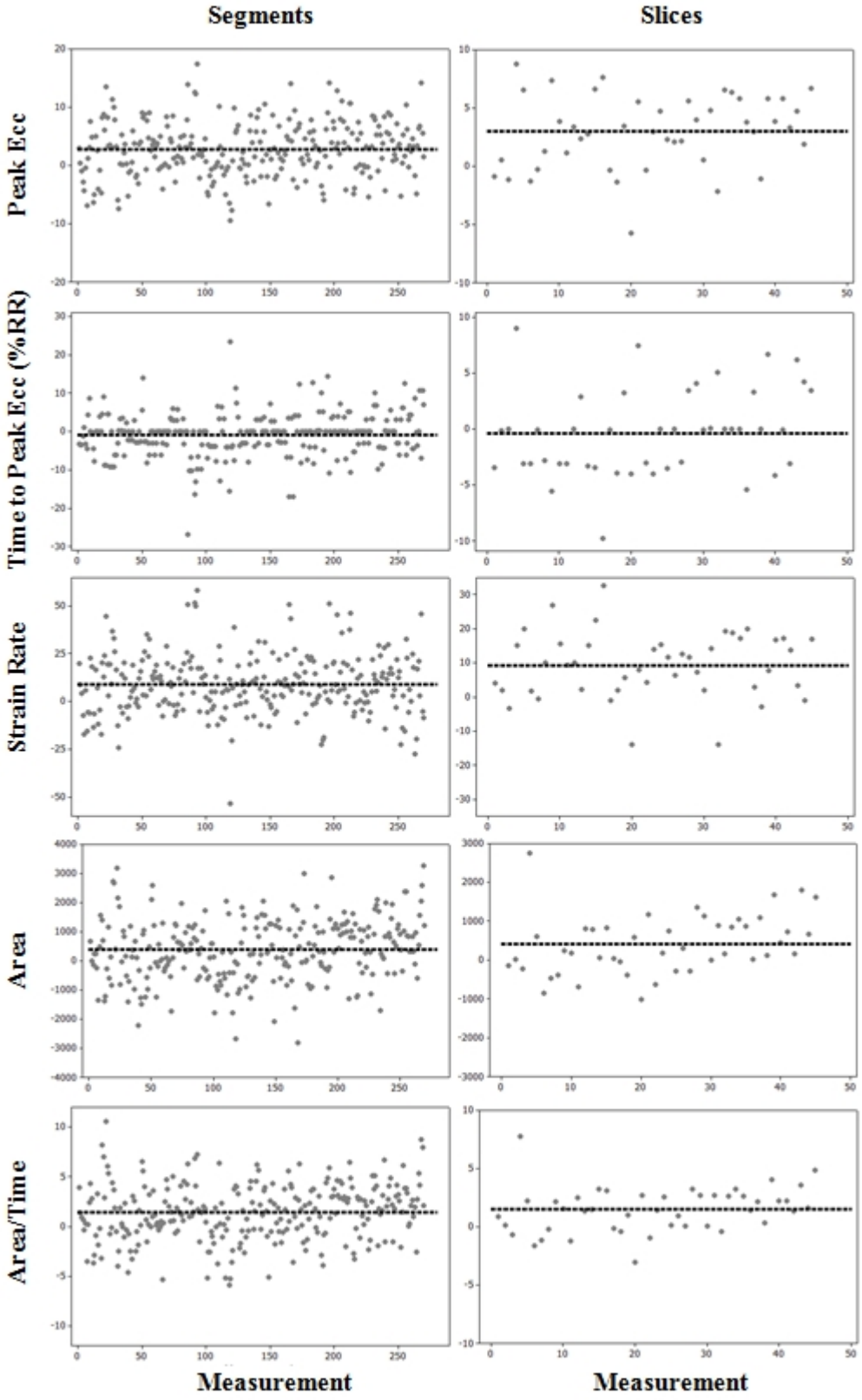

Figure 6-6: Illustration of differences between strain in mid-ventricular and basal slices

The differences in strain with data grouped according to segment are illustrated in Figure 6-7. The results of the one-way ANOVA with Tukey's post-hoc tests showed that there are statistically significant differences between the changes in strain in the segment groups, with a tendency towards larger differences in anterior and lateral segments (A, AL, IL) and smaller differences in inferior and septal segments (I, IS, AS).

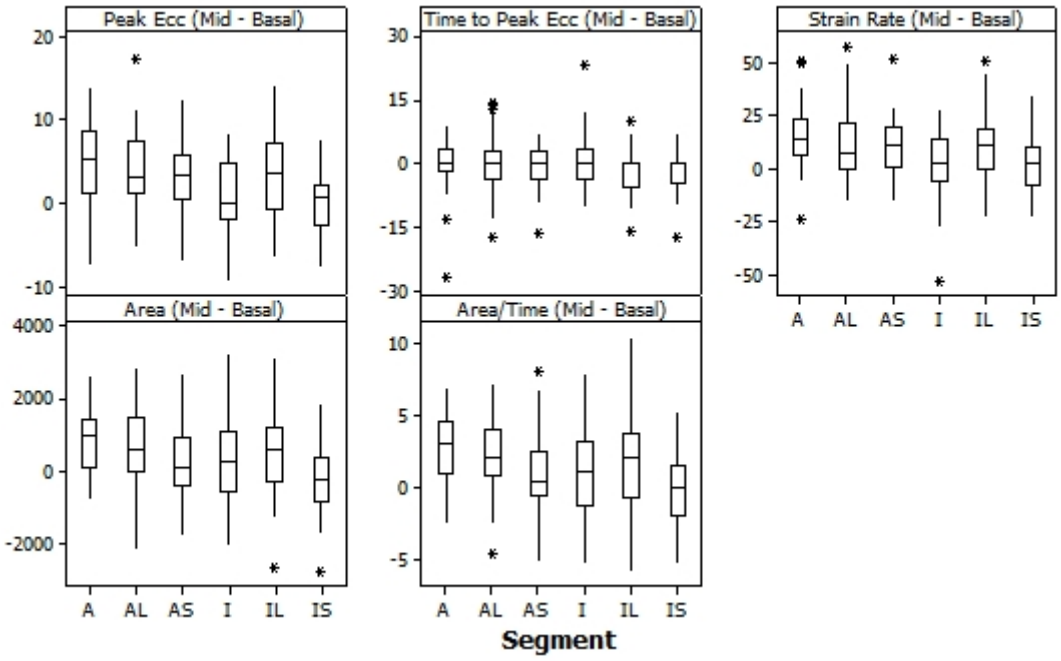

Figure 6-7: Illustration of differences in strain between segment groups

6.4.5 Determination of Reference Ranges

The lower and upper limits of the reference ranges determined for each strain parameter are shown in Table 6-7 and Table 6-8 for male and female subjects respectively. Reference ranges for individual segments are shown in Table 6-9 and Table 6-10.

Strain Parameter	Segments	Slices
Peak Ecc	(11.5, 26.6)	(13.9, 23.3)
Time to Peak Ecc (%RR)	(21.0, 47.0)	(23.1, 44.1)
Strain Rate	(35.7, 84.7)	(41.2, 77.8)
Area	(1011, 5243)	(1820, 4160)
Area/Time	(4.5, 15.5)	(6.5, 13.3)

Table 6-7: Reference ranges for strain parameters (male) in mid-ventricular slices

Strain Parameter	Segments	Slices
Peak Ecc	(12.7, 28.3)	(15.0, 25.2)
Time to Peak Ecc (%RR)	(22.5, 48.8)	(24.4, 47.4)
Strain Rate	(38.2, 89.1)	(45.1, 78.5)
Area	(1282, 5410)	(1819, 4923)
Area/Time	(5.5, 15.7)	(6.9, 14.3)

Table 6-8: Reference ranges for strain parameters (female) in mid-ventricular slices

Segment	Peak Ecc	Time to peak Ecc	Strain Rate	Area	Area/Time
A	(13.2, 27.5)	(22.1, 42.6)	(44.2, 90.6)	(1486, 4696)	(5.7, 15.4)
AL	(13.8, 27.1)	(23.8, 49.6)	(38.5, 81.6)	(1976, 5766)	(6.8, 16.4)
AS	(10.6, 25.7)	(20.5, 41.6)	(36.9, 88.5)	(822, 4092)	(3.4, 14.3)
I	(12.1, 25.0)	(20.6, 49.4)	(32.5, 82.5)	(1365, 5019)	(5.2, 14.9)
IL	(15.3, 26.2)	(24.3, 51.4)	(42.3, 75.6)	(2128, 5676)	(7.1, 15.6)
IS	(8.4, 23.5)	(21.5, 41.2)	(27.4, 82.0)	(571, 3871)	(2.6, 12.9)

Table 6-9: Reference ranges for strain parameters by segment (male) in mid-ventricular slices

Segment	Peak Ecc	Time to peak Ecc	Strain Rate	Area	Area/Time
A	(13.1, 29.9)	(22.1, 47.7)	(38.7, 98.2)	(1585, 5101)	(6.0, 15.9)
AL	(15.9, 28.6)	(24.7, 50.6)	(43.0, 87.8)	(1933, 6013)	(7.4, 16.3)
AS	(11.7, 24.7)	(19.0, 47.5)	(38.3, 83.4)	(956, 4222)	(4.2, 13.6)
I	(13.7, 27.9)	(23.3, 50.0)	(38.9, 87.5)	(1584, 5742)	(6.2, 16.3)
IL	(15.0, 29.9)	(23.8, 50.9)	(43.3, 89.7)	(2129, 5579)	(7.6, 15.8)
IS	(12.3, 23.1)	(23.9, 44.1)	(32.4, 82.9)	(1301, 4049)	(5.0, 12.8)

Table 6-10: Reference ranges for strain parameters by segment (female) in mid-ventricular slices

6.4.6 Comparison of Strain at 1.5T and 3T

Scatter plots illustrating the agreement between the DENSE strain parameters obtained at 1.5T and 3T are shown in Figure 6-8, and the corresponding correlation coefficients are shown in Table 6-11. Statistically significant results are indicated by * ($p < 0.05$) and ** ($p < 0.001$). Since a direct comparison of two sets of measurements (1.5T and 3T) is being made, it is not necessary to perform separate analyses for male and female subjects.

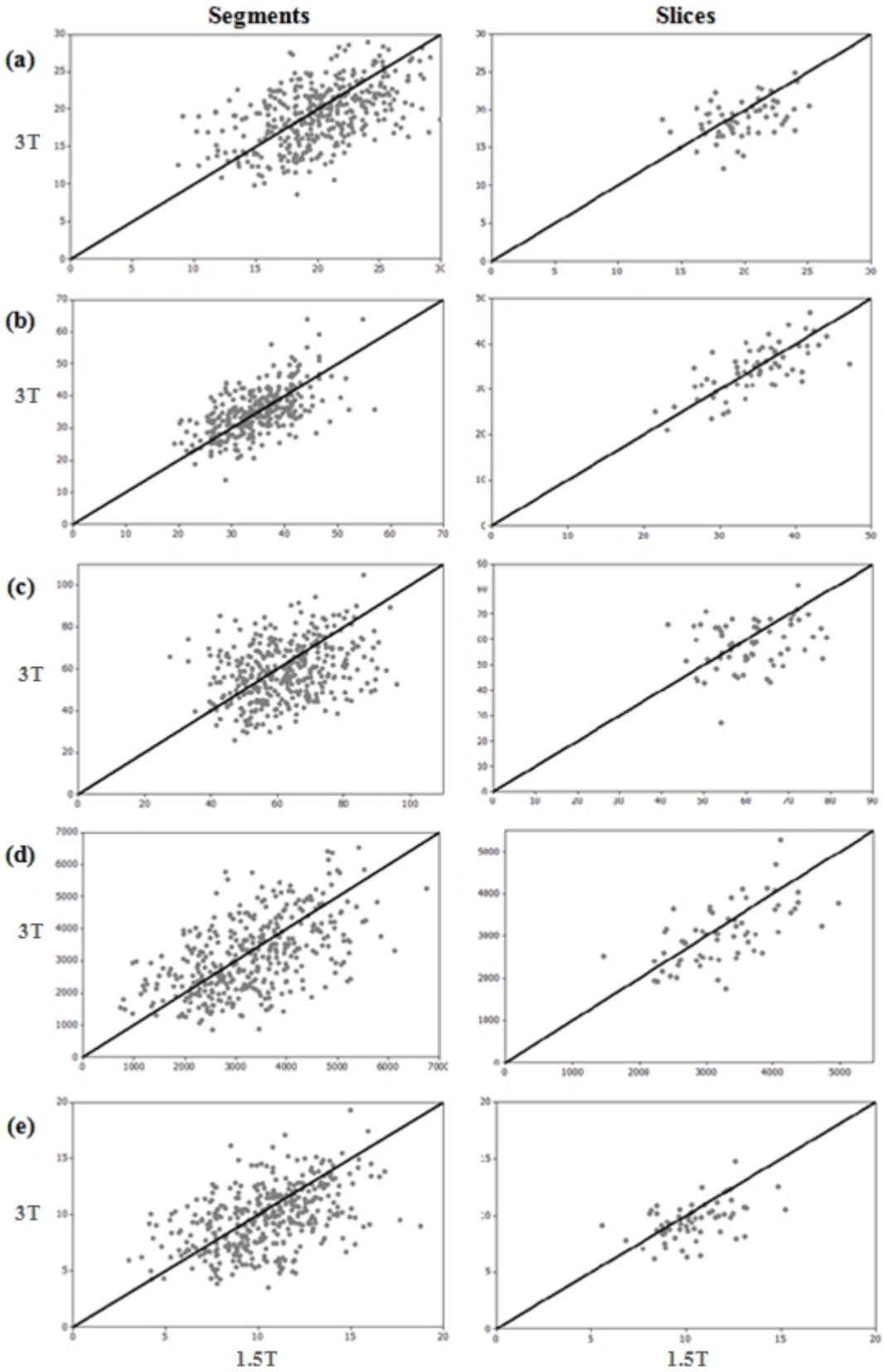

Figure 6-8: Comparison of strain parameters at 1.5T and 3T for a) peak Ecc, b) time to peak Ecc, c) strain rate, d) area, e) area/time

Strain Parameter	Segments	Slices
Peak Ecc	0.49**	0.42**
Time to Peak Ecc (%RR)	0.62**	0.71**
Strain Rate	0.32**	0.26*
Area	0.55**	0.61**
Area/Time	0.46**	0.48**

Table 6-11: Relationships between strain parameters at 1.5T and 3T

Prior to carrying out Bland-Altman analysis, the calculated differences between the results obtained at 1.5T and 3T were checked for normality using Anderson-Darling tests. All parameters were found to be normally distributed ($p > 0.05$).

Bland-Altman plots are shown in Figure 6-9 for segment and whole slice data, and 95% confidence intervals for the bias and limits of agreement are shown in Table 6-12. Values for t(5%, n-1) were obtained from statistical tables for a two-tailed t distribution for use in the calculations, and were found to be 1.967 and 1.999 for segment and whole slice data respectively. Table 6-12 also shows the mean value of (1.5T + 3T)/2 for comparison. The statistical significance of the bias, as determined by paired t-tests, is indicated by * ($p < 0.05$) and ** ($p < 0.001$). The inter-scanner RMS-CoV values are shown in Table 6-13.

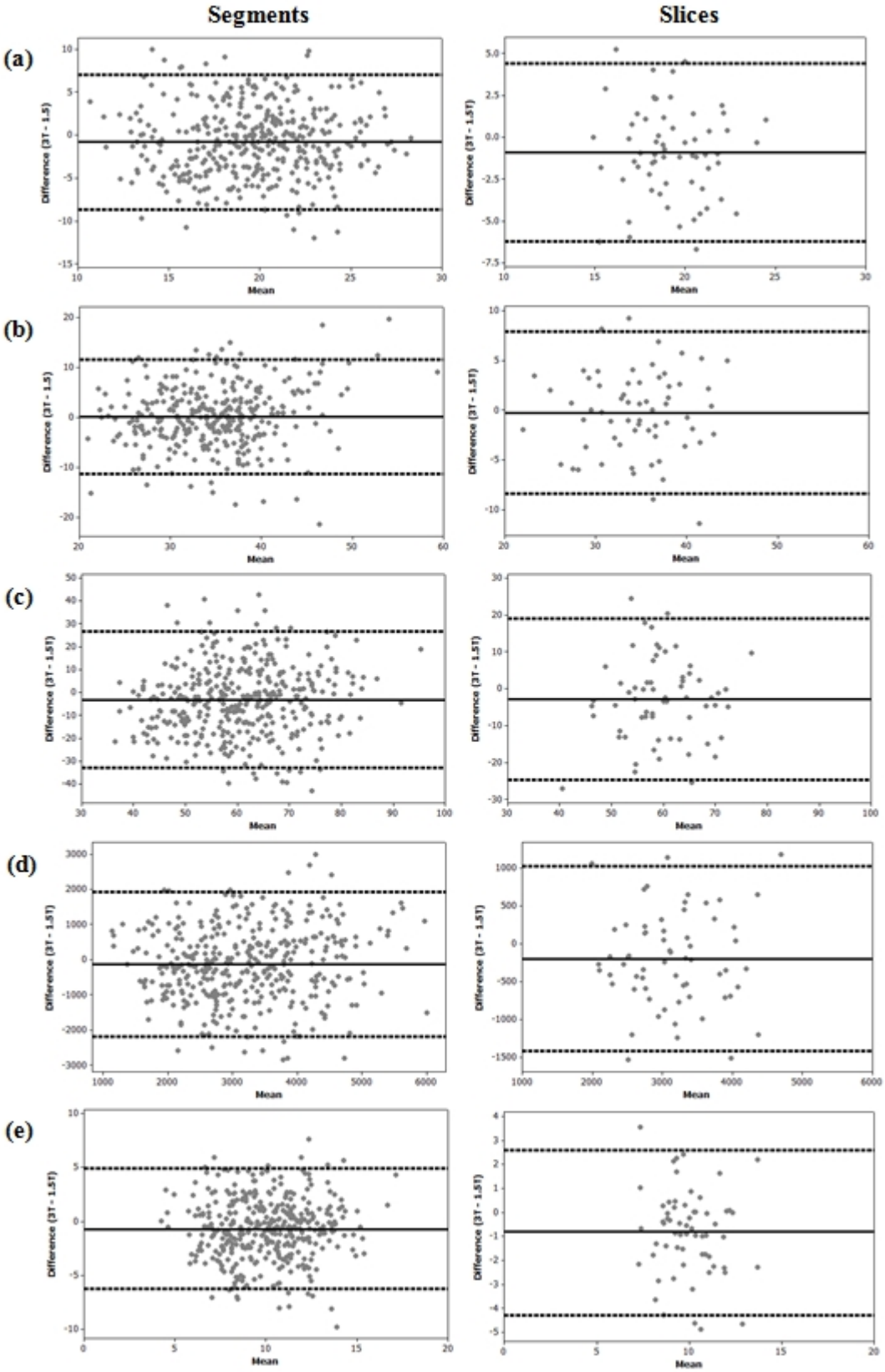

Figure 6-9: Bland-Altman plots of 1.5T vs 3T for a) peak Ecc, b) time to peak Ecc, c) strain rate, d) area, e) area/time

Strain Parameter	Region	Mean	Bias	Upper Limit	Lower Limit
Peak Ecc	Segments	19.6	(-1.2, -0.4)**	(6.3, 7.7)	(-9.4, -8.0)
	Slices	19.2	(-1.6, -0.2)*	(3.2, 5.6)	(-7.4, -5.0)
Time to peak	Segments	34.6	(-0.4, 0.8)	(10.6, 12.7)	(-12.3, -10.3)
Ecc	Slices	34.5	(-1.3, 0.8)	(6.1, 9.7)	(-10.2, -6.6)
Strain Rate	Segments	60.7	(-4.7, -1.6)**	(23.8, 29.1)	(-35.4, -30.1)
	Slices	59.5	(-5.7, -0.1)*	(14.1, 23.8)	(-29.6, -19.9)
Area	Segments	3213	(-232, -20)**	(1745, 2112)	(-2365, -1997)
	Slices	3143	(-358, -45)*	(746, 1228)	(-1691, -1449)
Area/Time	Segments	10.1	(-1.0, -0.4)**	(4.4, 5.4)	(-6.7, -5.7)
	Slices	10.0	(-1.3, -0.4)*	(1.9, 3.4)	(-5.0, -3.5)

Table 6-12: 95% confidence intervals for 1.5T vs 3T Bland-Altman analysis

Strain Parameter	Segments	Slices
Peak Ecc	1.8	2.9
Time to Peak Ecc	0.3	2.6
Strain Rate	2.0	3.3
Area	1.8	3.5
Area/Time	2.2	3.2

Table 6-13: RMS-CoV for inter-scanner (1.5T vs 3T) comparison

The results show that there are statistically significant differences between strain measurements obtained at 1.5T and 3T for all strain parameters other than time to peak Ecc. However, the RMS-CoV values for all strain parameters are small.

6.5 Discussion

A summary of the key results from this chapter is shown in Table 6-14.

Investigation	Results
Variation with Age	• No statistically significant differences were observed with age for male or female subjects
Variation with Gender	• Statistically significant differences between male and female subjects for peak Ecc and area
Variation with Myocardial Segment	• Statistically significant differences between strain in myocardial segments, with higher strain in lateral segments (AL, IL) and lower strain in septal segments (AS, IS)
Variation with Myocardial Slice	• Statistically significant differences between strain in basal and mid-ventricular slices, with higher strain in mid-ventricular slices • Larger differences in strain for anterior and lateral segments (A, AL, IL)
Determination of Reference Ranges	• Two sets of reference ranges were established for segment data – one which used all data, and one which considered each segment group individually • References ranges were established for each strain parameter for whole slice data
Comparison of 1.5T and 3T	• Moderate correlation between strain parameters measured at 1.5T and 3T • Paired t-tests showed statistically significant differences in bias for all strain parameters other than time to peak Ecc • Small RMS-CoV for all strain parameters • Differences are small and are unlikely to be clinically significant

Table 6-14: Summary of key results in healthy volunteers

The first finding in the assessment of DENSE in healthy subjects was that radial strain is unreliable, with strain curves which were considered to be non-diagnostic in 79% of datasets from 72 subjects. The reasons for this are unclear - the pulse sequence parameters may not be optimal, or there may be issues with the post-processing software. This will require further investigation, but without access to the code underlying the analysis software, this will be difficult and is considered beyond the scope of this thesis. Circumferential strain only will be used in all subsequent investigations.

A further observation was that data acquired in basal locations were more likely to be positioned incorrectly, either too close to the LVOT or in a more mid-ventricular location, and were also more likely to be non-diagnostic. The long breath-hold of up to 20 seconds required for DENSE is challenging, even when subjects are asked to breathe in and out twice before breath-holding. This problem did occur in mid-ventricular slices but less frequently, and it is possible that the subjects were unprepared for the length of the breath-hold during the first acquisition, and hence were more likely to breathe through it. Unlike most MR images, it is difficult to perform a qualitative assessment of image quality with DENSE due to the low resolution of the images, and problems are often not identified until post-processing is performed. This issue could potentially be solved if future implementations of the DENSE pulse sequence provided an in-line processing capability, which would allow the strain curves to be reviewed and assessed while the patient was still in the scanner, and the scans could then be repeated if necessary.

Variation with Age

No statistically significant relationships were observed between strain and age for any strain parameter, for both male and female subjects. When subjects were grouped according to age (<30, 30 - 60, >60 years), the results of the one-way ANOVA with Tukey's post-hoc tests showed no statistically significant differences between the groups, which is consistent with the results of previous studies mentioned in Section 2.5.1.

The relationships between age and LV function have been investigated using other imaging modalities e.g. echocardiography. There is convincing evidence of a decline

in diastolic function with increasing age [113 - 115], however the effect of age on measures of systolic function is less clear. Some studies reported statistically significant but weak relationships with age [113, 116], while others observed no statistically significant relationships [117].

The volunteers recruited for this study were mostly members of NHS and their friends and family, medical students and volunteer "patients" at the medical school. They were all fit and healthy and from a similar socioeconomic group, and are therefore unlikely to be representative of society as a whole. It may have been more informative to recruit from the wider community, and this should be considered for future studies.

Variation with Gender

Statistically significant differences were observed between male and female subjects for peak Ecc and area, with higher values occurring in females. This is consistent with the results of a study mentioned in Section 2.5.1.

Variation with Myocardial Segment

When comparing strain in different myocardial segments, the results of one-way ANOVA with Tukey's post-hoc tests showed statistically significant differences in both male and female subjects. For all strain parameters other than strain rate, strain was generally higher in lateral segments (AL and IL) and lower in septal segments (AS and IS). Lateral segments are located in the free wall of the left ventricle, while the septal segments will be affected by the presence and motion of the right ventricle. For strain rate, the difference between segments was less obvious.

The results of strain comparisons between segments from previous studies are shown in Table 2-1 in Section 2.5.1, and differences between segments can be seen. However, no comment was made on whether or not the differences were statistically significant, and further investigations within the cited papers did not consider segment groups individually. Analysis of data by segment group would be time consuming, and would potentially limit the clinical application of this technique. The decision was therefore taken to perform analysis in subsequent chapters with segments considered as a single group.

Variation with Myocardial Slice

A comparison of strain in basal and mid-ventricular slices found statistically significant differences for all strain parameters, with higher values in mid-ventricular slices for all parameters other than time to peak Ecc, which was found to be lower. This is consistent with the results from other studies [85, 93, 98, 99], which showed higher mean strain values in mid-ventricular slices than basal slices, although it was not stated if the differences were statistically significant.

When comparing strain in basal and mid-ventricular slices with data grouped according to segment, statistically significant differences were observed, with a tendency towards larger increases in strain in anterior and lateral segments (A, AL, IL) compared to inferior and septal segments (I, IS, AS). This is similar to the result obtained when investigating the variation in strain with myocardial segment, and again the strain in the septal segments will be affected by the presence and motion of the right ventricle.

Due to the issues with image acquisition in basal slices, all subsequent analysis was performed on mid-ventricular slices only. However, for future investigations, it would be appropriate to consider data from basal and mid-ventricular slices separately, and to establish references ranges which are specific to slice location.

Determination of Reference Ranges

For segment data, reference ranges were determined for male and female subjects separately. As stated in the discussion on Variation with Myocardial Segment, all subsequent analysis will be performed with segments considered as a single group, and hence the reference ranges for each strain parameter were formed using all of the segment data. However, a second set of reference ranges were determined using data which was separated into segment groups, and an investigation into the differences in the detection of pathology which occur when using the two sets of reference ranges will be carried out in subsequent chapters.

Comparison of 1.5T and 3T

A plot of DENSE results obtained at 1.5T against results obtained at 3T showed clustering around the line of perfect agreement ($y = x$) for all strain parameters and for

both segment and whole slice data, but with a reasonably large spread, which is reflected in the moderate correlation coefficients.

Bland-Altman plots showed no obvious trends, but with a reasonably large spread of values. Statistically significant differences were observed between the results obtained at 1.5T and 3T for all strain parameters other than time to peak Ecc, with higher values being obtained at 1.5T than 3T. However, the magnitudes of the differences are small, and are unlikely to be clinically significant. The inter-scanner RMS-CoV values were found to be small for all strain parameters.

The main source of error in this analysis is that the imaging slices at 1.5T and 3T are unlikely to be perfectly co-located. In addition, image quality was generally higher at 1.5T, with only 3 datasets considered to be non-diagnostic in this study, compared to 8 at 3T. The 3T scanner used in this study is a wide-bore scanner (70cm compared to 60cm at 1.5T) and it is more challenging to achieve good homogeneity, which means that there is an increased likelihood of image artefacts, and these are more difficult to detect in DENSE images compared to other cardiac MR imaging due to the lower resolution.

DENSE has been shown to produce similar results using 1.5T and 3T scanners, however further optimisation of the image acquisition protocol may be required before any future studies are carried out at 3T.

Further Discussion

In this chapter, analysis has been performed on five strain parameters calculated from DENSE data – peak Ecc, time to peak Ecc (%RR), strain rate, area and area/time. Peak Ecc, time to peak Ecc and strain rate are inter-related, and performing analysis on all three of these parameters may be excessive. The rate at which strain increases to the peak value is considered to be more informative than the time taken to reach the peak, and so all subsequent analysis will be performed for peak Ecc, strain rate, area and area/time.

6.6 Summary and Conclusions

DENSE has been successfully acquired in a group of 72 healthy subjects aged between 18 and 89 years.

No statistically significant variations in strain parameters were observed with age, which is consistent with the results of previous studies from the literature.

Peak Ecc and the area under the Ecc curve were found to be higher in female subjects than in males, which indicates that strain analysis should be performed on a gender-specific basis.

Strain varies with myocardial segment, with higher strain in lateral segments and lower strain in septal segments. However, the differences are small, and the additional burden of segment-by-segment analysis is likely to impact on the potential for clinical applications of DENSE.

Strain varies with slice position, with higher strain in mid-ventricular slices compared to basal slices. The differences in strain between the two positions are larger for lateral segments compared to septal segments.

Strain results obtained at 1.5T and 3T are in reasonable agreement, although there is a tendency towards lower values at 3T, with statistically significant differences for all strain parameters other than time to peak Ecc. The magnitudes of the differences are small and are unlikely to be clinically significant, however further optimisation of the imaging protocol at 3T is recommended.

Chapter 7

DENSE in Acute Infarction

7.1 Introduction

In patients with myocardial infarction (MI), late gadolinium enhancement imaging is used for the visualisation of infarction. In addition to the extent of infarction, the region of the myocardium which is injured is an important prognostic indicator, and this can be evaluated using T_2-weighted imaging. This chapter describes the application of DENSE in a group of subjects with acute MI, and investigations into the ability of DENSE strain parameters to detect contractile abnormalities associated with both the presence of infarction and the area at risk.

7.2 Aims

The aims of the research presented in this chapter are:

- To investigate the relationships between DENSE strain parameters and the extent of infarction in acute MI
- To investigate whether DENSE can be used to distinguish between differing extents of infarction in acute MI
- To investigate whether DENSE can be used to distinguish between regions with and without infarction in acute MI
- To investigate the relationships between DENSE strain parameters and the area at risk
- To determine the sensitivity and specificity of DENSE for the detection of acute myocardial infarction and injury
- To investigate the relationships between DENSE strain parameters and cardiac function in acute MI

7.3 Methods

7.3.1 STEMI Volunteers

60 male patients underwent CMR within 7 days of STEMI (which is considered to be "acute MI" within this thesis). The study was approved by the West of Scotland Research Ethics Committee, and written consent was obtained from each patient. A copy of the Patient Information Sheet for the study can be found in Appendix D.

7.3.2 Image Acquisition and Analysis

Cine, LGE, T_2-weighted and DENSE images were acquired as described in Chapter 3.

The problems with DENSE in basal and apical slices described in Sections 5.4.1 and 6.4 were also encountered in data acquired from STEMI patients. Since a large amount of data was analysed retrospectively, it was not possible to correct the positioning of the basal and apical slices, and hence the decision was taken not to include this data in the study.

Systolic thickening, LVESV, LVEDV and LVEF were measured from cine images as described in Section 3.3.

LGE images were analysed as described in Section 3.4. In addition to assigning a score for transmural extent of MI (LGE_score), the regions of LGE which exceeded the threshold were manually outlined, and the percentage of LGE (LGE%) present in each segment, and also in each slice, was calculated. A second score, LGE%_score, was assigned using the same definitions as in Table 3-4, but using percentage LGE within the segment instead of transmural extent of MI. Finally, the total percentage LGE in the LV was calculated by outlining the LGE in each acquired slice in the short-axis LV stack. Examples of LGE%, LGE%_score and LGE_score are illustrated in Figure 7-1.

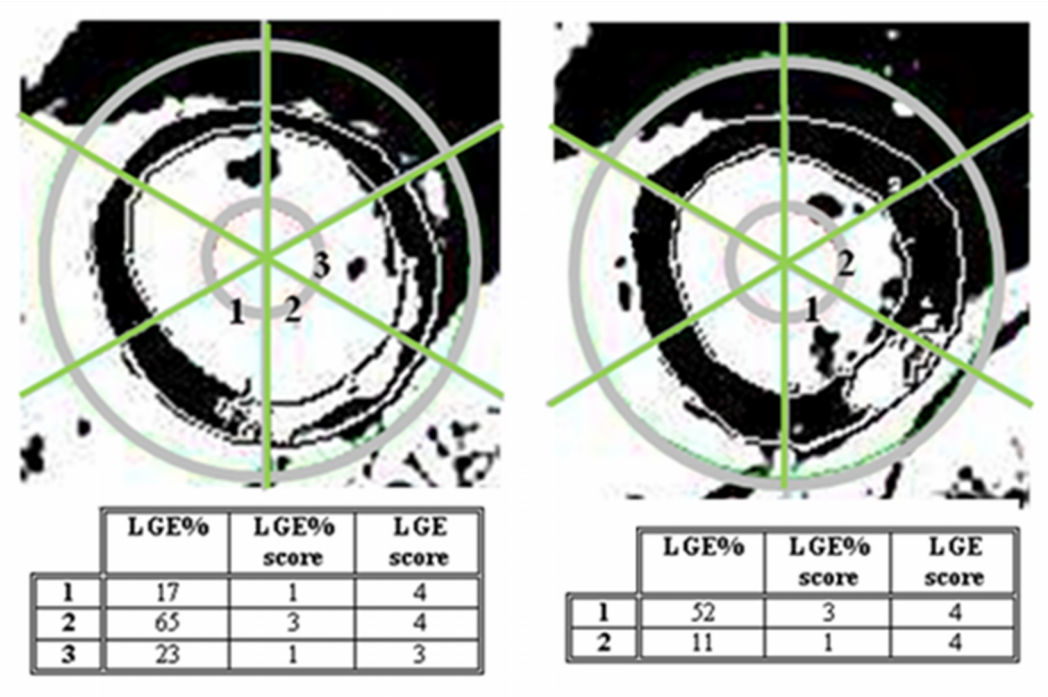

	LGE%	LGE% score	LGE score
1	17	1	4
2	65	3	4
3	23	1	3

	LGE%	LGE% score	LGE score
1	52	3	4
2	11	1	4

Figure 7-1: Examples of LGE%, LGE%_score and LGE_score

A further set of scores, LGE_category and LGE%_category, were assigned to categorise segments as remote, adjacent or infarcted (see Section 2.5.2), as defined in Table 7-1.

Score	Category	Description
0	Remote	No LGE in segment
		No LGE in adjacent segments
1	Adjacent (<50%)	No LGE in segment
		LGE in one or more adjacent segments (<50%)
2	Adjacent (>50%)	No LGE in segment
		LGE in one or more adjacent segments (>50%)
3	Infarcted (<50%)	LGE in segment (<50%)
4	Infarcted (>50%)	LGE in segment (>50%)

Table 7-1: Definitions of LGE categories

T_2-maps were analysed as described in Section 0, and values were obtained for area at risk.

From the 60 patients included in this study, the imaging slice was through the region of infarction for 50 patients, and above or below the region of infarction for 10 patients. In order to compare the DENSE strain parameters with extent of infarction and area at risk, only the 50 patients in whom the imaging slice was through the region of infarction were considered. A separate analysis was performed on the remaining 10 patients to assess whether performing DENSE through a mid-ventricular slice can provide information about infarction elsewhere in the myocardium.

7.3.3 Repeatability of Area under Curve with Degree of Hypokinesis

The results of the investigation into the repeatability of DENSE strain parameters in Chapter 5 showed that high CoV values were obtained for peak Ecc and time to peak Ecc for segments with peak Ecc < 5%, and that the variation in time to peak Ecc for such segments could potentially impact on analysis. The concept of measuring the area under the Ecc curve and the average area over time, and also strain rate, was introduced in Chapter 6, and before any further analysis involving data from MI patients could be carried out, it was necessary to assess the variability of these strain parameters in segments with varying degrees of hypokinesis. Analysis was performed as described in Section 5.3.4, using data from the same 15 patients and 5 healthy subjects.

The mean CoV values for each group were compared for peak Ecc, strain rate, area and area/time.

7.3.4 DENSE and Infarction

7.3.4.1. Relationships with LGE

For segment data, the relationships between each of the DENSE strain parameters with each of the LGE parameters (LGE%, LGE_score, LGE%_score) were assessed using correlation tests. The relationship between each of the LGE parameters and systolic thickening was also assessed.

For whole slice data, the relationships between each of the DENSE strain parameters and LGE% in both the imaging slice (LGE%) and the LV volume (LV LGE%) were assessed using correlation tests.

7.3.4.2. Extent of Infarction

For segment data, the ability of each of the strain parameters to identify the extent of infarction, as defined by each of LGE_score and LGE%_score, was assessed using a one-way ANOVA with Tukey's post-hoc test or Kruskal-Wallis with individual Mann-Whitney tests.

A similar comparison was carried out between non-infarcted (score = 0), <50% infarction (score = 1 or 2) and >50% infarction (score = 3 or 4), where scores are defined as shown in Table 3-4.

7.3.4.3. Proximity to Infarction

For segment data, the ability of each of the strain parameters to identify the proximity of the segment to infarction, as defined by each of LGE_category and LGE%_category, was assessed using a one-way ANOVA with Tukey's post-hoc test or Kruskal-Wallis with individual Mann-Whitney tests.

A similar comparison was carried out between remote (score = 0), adjacent (score = 1 or 2) and infarcted (score = 3 or 4) segments, where scores are defined as shown in Table 7-1.

7.3.4.4. Detection of Infarction

ROC analysis was carried out to evaluate the ability of DENSE to detect the presence of infarction using both segment and whole slice data. For the whole slice analysis, data from all 60 patients was used, with 50 slices through a region of infarction and 10 slices in remote tissue. Strain values were compared with a binary test for the presence/absence of LGE, and ROC curves were produced for each strain parameter. The area under the curve (AUC) was calculated for each strain parameter.

The lower limits of the reference ranges established in Chapter 6 (Table 6-7) were used to define a threshold for each strain parameter, and following comparison with the threshold, a label of "no infarction" or "infarction" was assigned. A comparison with the LGE results was performed, and the number of true positive (TP), false negative (FN), true negative (TN) and false positive (FP) results was recorded. The

sensitivity and specificity of the technique were calculated using Equations 7-1 and 7-2 respectively.

$$Sensitivity = \frac{TP}{TP + FN} \quad \textbf{(Equation 7-1)}$$

$$Specificity = \frac{TN}{TN + FP} \quad \textbf{(Equation 7-2)}$$

Segments were grouped according to LGE_score, and the percentage of segments in each group with LGE_score > 0 which were correctly identified as containing LGE, or wrongly identified as containing LGE for segments with LGE_score = 0, was calculated. This analysis was then repeated with segments grouped according to LGE%_score.

In order to evaluate whether the small differences in strain between segments identified in Section 6.4.3 would have any impact on the ability to detect infarction, the analysis described above was repeated using the reference ranges established for individual segments (Table 6-9).

Each slice was allocated a score based on the percentage of LGE within the slice, in the same manner as for segment data, and the percentage of slices correctly identified as containing LGE for each score was calculated.

7.3.4.5. Assessment of Infarction Using DENSE in a Non-Infarcted Slice

From the 10 patients in whom DENSE had been acquired in a slice which did not contain infarction, there were 60 segments available for analysis. For each segment, the corresponding segments in the four adjacent slices above and four slices below were examined, and if LGE was present then the original segment was allocated a score of 1, otherwise the segment was allocated a score of 0. A two-sample t-test or Mann-Whitney test was performed for each strain parameter to determine whether strain results in a non-infarcted slice gives any information about infarction elsewhere in the myocardium.

7.3.4.6. Comparison of Strain in Remote and Healthy Myocardium

The values obtained for DENSE strain parameters and in remote myocardium were compared to the values obtained from healthy volunteers (see Chapter 6) using 2-sample t-tests or Mann-Whitney tests.

7.3.5 DENSE and Area at Risk

7.3.5.1. Relationships with Area at Risk

For segment data, the relationships between each of the DENSE strain parameters with area at risk were assessed using correlation tests.

For whole slice data, the relationships between each of the DENSE strain parameters and area at risk in both the imaging slice and the LV volume (LV area at risk) were assessed using correlation tests.

7.3.5.2. Detection of Injury

ROC analysis and the calculation of sensitivity and specificity were performed as described in Section 7.3.4.4, with strain values being compared with a binary test for the presence/absence of T_2 hyperenhancement.

7.3.6 DENSE and Cardiac Function

7.3.6.1. Relationships with LVEF and LVESV

For whole slice data, the relationships between each of the DENSE strain parameters and each of LVEF and LVESV were assessed using correlation tests.

7.4 Results

The clinical characteristics of the patients are shown in Table 7-2, where age, BMI, LVEF, LVEDV and LVESV are expressed as mean ± SD (range).

Characteristic	Imaging in Infarct Slice	Imaging in Non-infarct Slice
n	50	10
Age (years)	56 ± 10 (33 – 80)	55 ± 11 (38 – 70)
BMI	28 ± 4 (20 – 38)	27 ± 6 (19 – 39)
Smoker	32 (64%)	6 (60%)
Hypertension	10 (20%)	1 (10%)
Hypercholesterolaemia	8 (16%)	2 (20%)
Prior MI	0	0
Culprit Artery	LAD: 19 (38%)	LAD: 2 (20%)
	LCX: 9 (18%)	LCX: 4 (40%)
	RCA: 22 (44%)	RCA: 4 (40%)
Global LV function by cine MRI:		
LVEF (%)	54 ± 9 (35 – 70)	62 ± 8 (44 – 72)
LVEDV (ml)	153 ± 33 (85 – 230)	139 ± 30 (101 – 195)
LVESV (ml)	72 ± 23 (34 – 119)	53 ± 15 (33 – 77)

Table 7-2: Clinical characteristics of STEMI patients

From the 50 patients in whom the imaging slice was through the region of infarction, there were 300 segments available for analysis.

The results of the Anderson-Darling tests showed that none of the strain parameters were normally distributed, and so non-parametric statistical tests were used.

7.4.1 Repeatability of Area under Curve with Degree of Hypokinesis

The results of the Kruskal-Wallis with individual Mann-Whitney tests for strain rate, area and area/time were similar to those obtained for peak Ecc in Section 5.4.2. Statistically significant differences were observed between the mean CoV in segments with severe hypokinesis and the mean CoV in all other segments. As for peak Ecc, the mean values for severely hypokinetic segments were substantially larger than those found for the other groups, and with a much wider range of individual CoV values.

For whole slice data, there were no statistically significant differences between the groups for any strain parameter.

The mean CoV (%) values for each group for both segments and slices are shown in Table 7-3.

		Degree of Hypokinesis			
Region	**Parameter**	**None**	**Slight**	**Moderate**	**Severe**
Segments	Peak Ecc	6.3	9.8	16.1	58.9
	Strain Rate	8.1	14.0	19.3	62.6
	Area	11.6	22.1	31.7	62.9
	Area/Time	8.4	15.5	28.7	65.4
Slices	Peak Ecc	3.4	6.2	7.1	4.4
	Strain Rate	3.9	10.3	16.6	11.3
	Area	4.6	16.6	19.1	26.9
	Area/Time	3.9	8.7	8.9	26.2

Table 7-3: Mean CoV values for area under curve in hypokinesis groups

The variations which occur with repeated measurements for area are unlikely to change the clinical assessment for a particular segment, but since strain rate and area/time are dependent on measurements of time to peak, all values of strain rate and area/time corresponding to peak Ecc values of <5% will be excluded from subsequent analysis.

7.4.2 DENSE and Infarction

7.4.2.1. Relationships with LGE

For each of LGE_score, LGE%_score, LGE_category and LGE%_category, the number of segments allocated a particular value is shown in Table 7-4.

Score	0	1	2	3	4
LGE_score	170	7	23	16	84
LGE%_score	170	40	38	24	28
LGE_category	71	22	77	30	100
LGE%_category	71	74	25	78	52

Table 7-4: Allocation of LGE scores to segments in acute MI patients

The results of the correlation tests between strain parameters and LGE parameters are shown in Table 7-5, and are expressed as a Pearson correlation coefficient. Statistically significant results are indicated by * ($p<0.05$) and ** ($p<0.001$). The results (magnitude) are illustrated using scatter plots in Figure 7-2. Finally, scatter plots illustrating the distribution of data with LGE% are shown in Figure 7-3.

Strain Parameter	Segment Data			Whole Slice Data	
	LGE%	LGE% score	LGE score	LGE%	LV LGE%
Peak Ecc	-0.62**	-0.64**	-0.63**	-0.54**	-0.51*
Strain Rate	-0.63**	-0.65**	-0.64**	-0.54**	-0.49*
Area	-0.51**	-0.53**	-0.52**	-0.42*	-0.40*
Area/Time	-0.60**	-0.63**	-0.63**	-0.51**	-0.47*
Thickening (%)	-0.42**	-0.44**	-0.44**	-	-

Table 7-5: Results of relationships with LGE analysis in acute MI

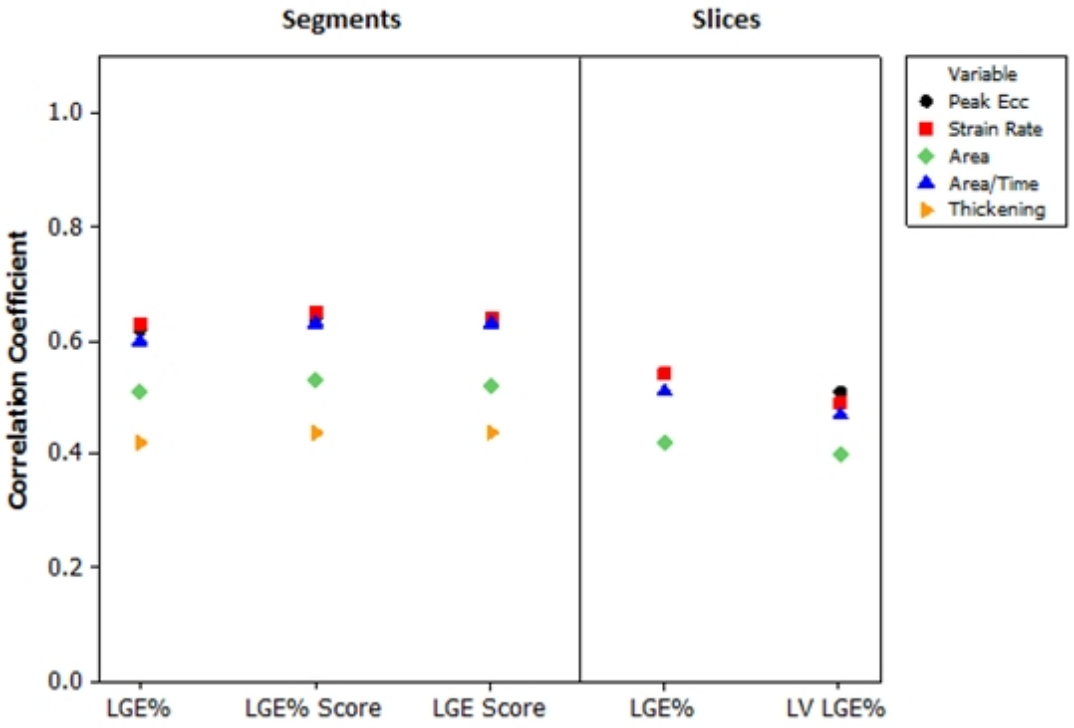

Figure 7-2: Illustration of relationships with LGE results in acute MI

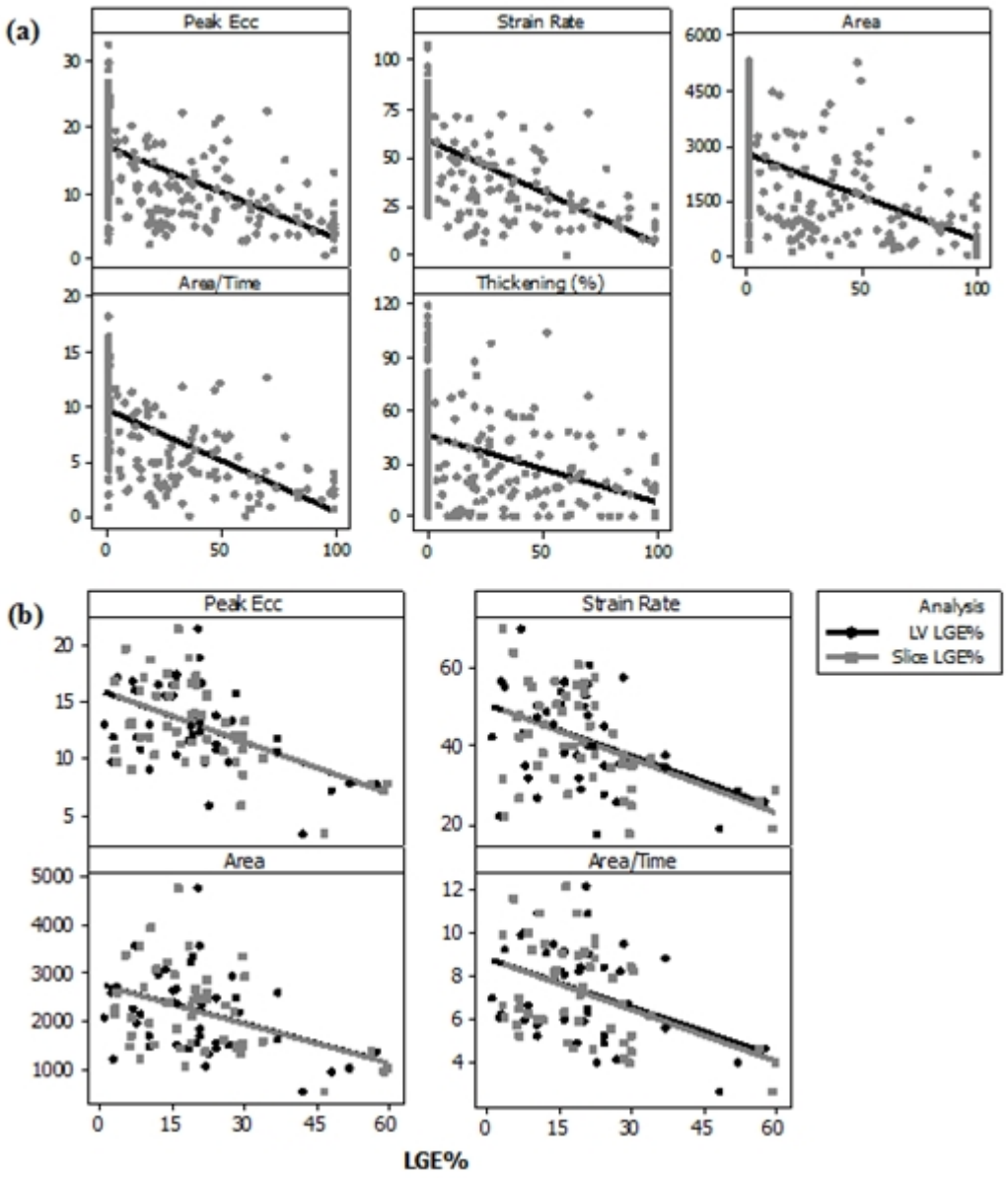

Figure 7-3: Strain parameters vs LGE% in acute MI for a) segment and b) whole slice/LV data

7.4.2.2. Extent of Infarction

Box plots illustrating the distribution of strain values with LGE_score and LGE%_score are shown in Figure 7-4.

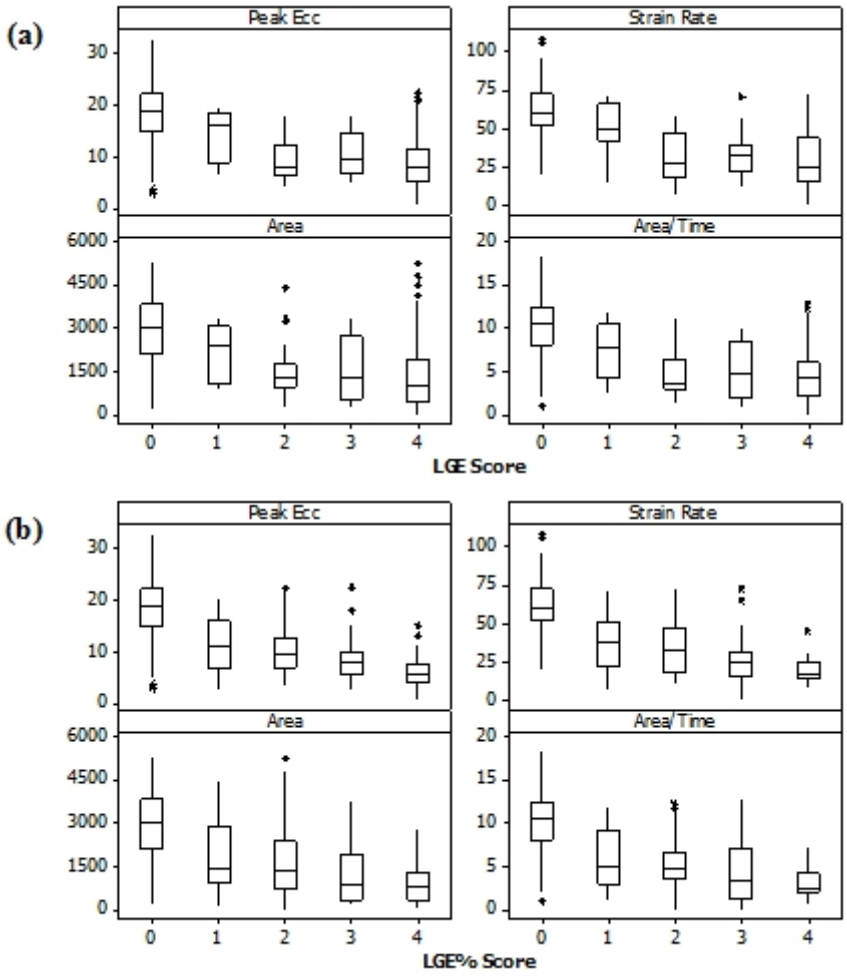

Figure 7-4: a) LGE and b) LGE% scores in acute MI

The results of the Kruskal-Wallis with individual Mann-Whitney tests found no statistically significant difference for any strain parameter between scores 1 and 2 or between scores 3 and 4, for both LGE_score and LGE%_score.

Statistically significant differences were observed for all strain parameters between non-infarcted and <50% infarcted segments, and between non-infarcted and >50% infarcted segments, for both LGE_score and LGE%_score. Statistically significant differences were observed between <50% and >50% infarcted segments for all parameters for LGE%_score, but not for LGE_score.

7.4.2.3. Proximity to Infarction

Box plots illustrating the distribution of strain values with LGE_category and LGE%_category are shown in Figure 7-5.

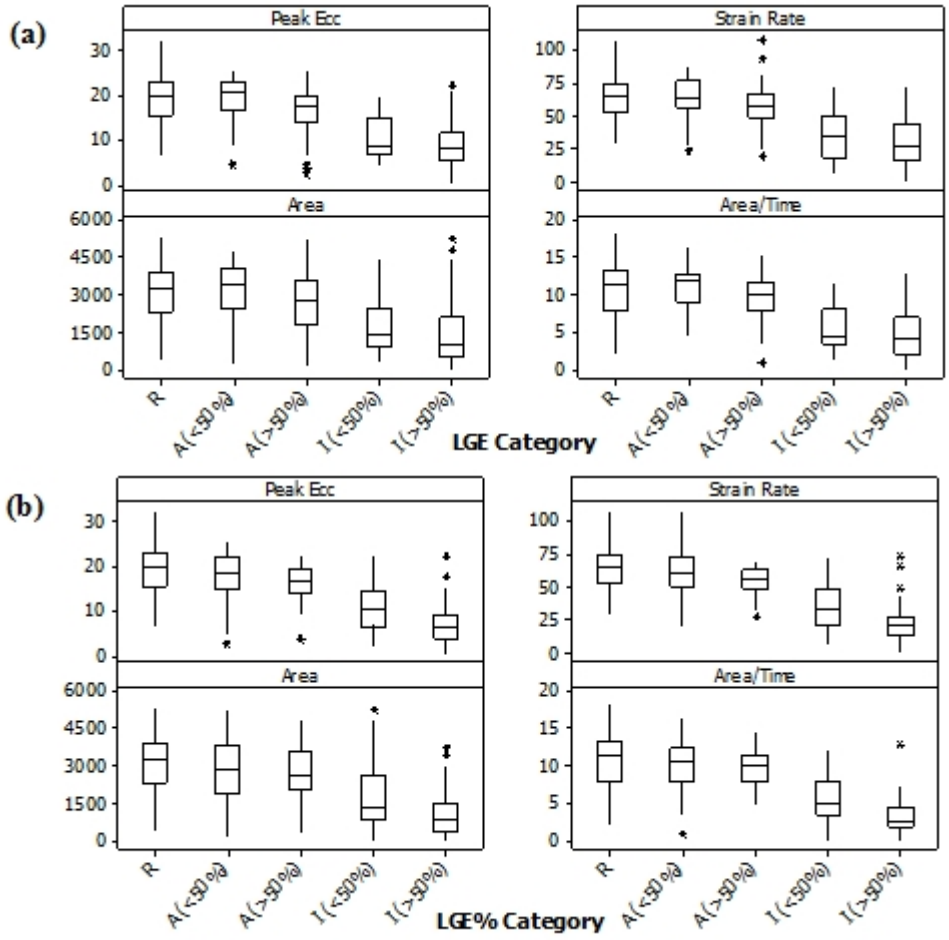

Figure 7-5: a) LGE and b) LGE% categories in acute MI

The results of the Kruskal-Wallis with individual Mann-Whitney tests found no statistically significant difference for any strain parameter between scores 1 and 2 (adjacent <50% and adjacent >50% respectively) for LGE_category and LGE%_category, or between scores 3 and 4 (infarcted <50% and infarcted >50% respectively) for LGE_category. For LGE%_category, a statistically significant difference was found between scores 3 and 4, which is consistent with the results of the Extent of Infarction analysis.

For all strain parameters, statistically significant differences were observed between remote and infarcted segments, and between adjacent and infarcted segments for both

LGE_category and LGE%_category. Statistically significant differences were found between remote and adjacent segments for peak Ecc only, for both LGE_category and LGE%_category.

7.4.2.4. Detection of Infarction

The ROC curves for each strain parameter are shown in Figure 7-6 and Figure 7-7 for segment and whole slice data respectively. The AUC results for segment data are shown in Table 7-6, along with the sensitivity and specificity calculated using the thresholds from both the single reference ranges (Table 6-7) and the segment reference ranges (Table 6-9). The AUC, sensitivity and specificity for whole slice data are shown in Table 7-7.

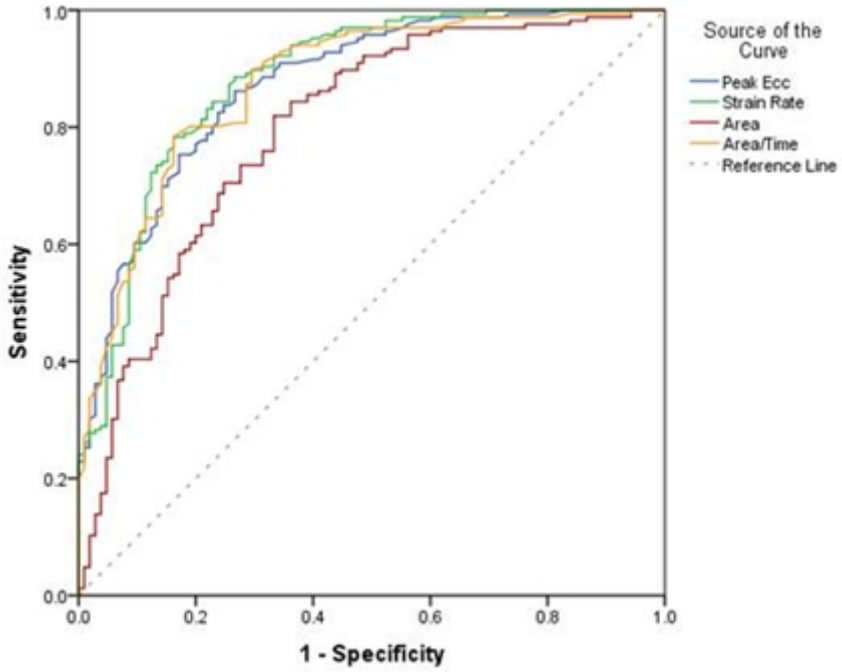

Figure 7-6: ROC curves for detection of infarction in acute MI for segment data

		Single Threshold			Segment Threshold	
Parameter	**AUC**	**Threshold**	**Sensitivity**	**Specificity**	**Sensitivity**	**Specificity**
Peak Ecc	0.88	11.5	0.72	0.88	0.74	0.88
Strain Rate	0.88	35.7	0.64	0.91	0.60	0.92
Area	0.81	1011	0.46	0.95	0.52	0.91
Area/Time	0.87	4.5	0.54	0.94	0.60	0.94

Table 7-6: Results of detection of infarction analysis in acute MI for segment data

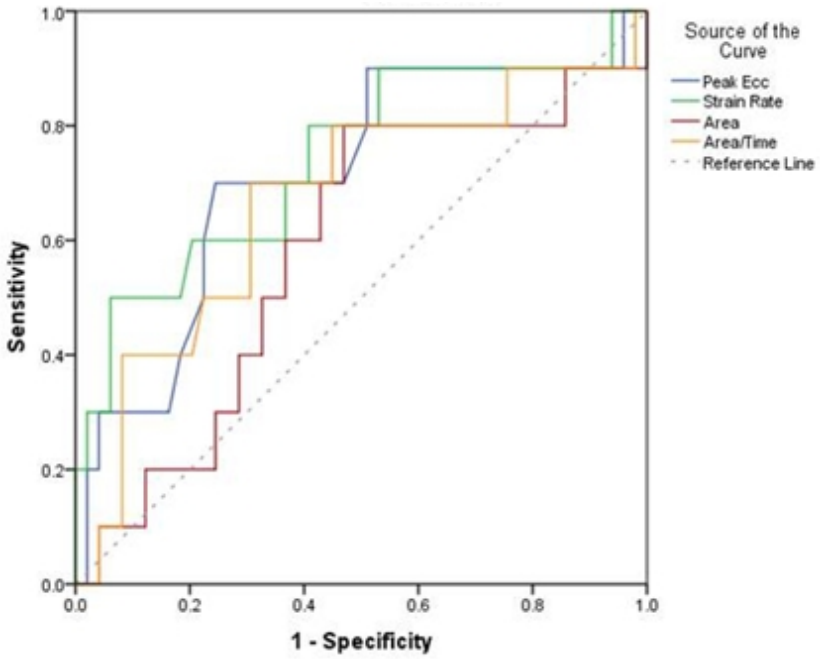

Figure 7-7: ROC curves for detection of infarction in acute MI for slice data

Parameter	AUC	Threshold	Sensitivity	Specificity
Peak Ecc	0.71	13.9	0.66	0.70
Strain Rate	0.74	41.2	0.52	0.80
Area	0.59	1820	0.40	0.80
Area/Time	0.67	6.5	0.42	0.80

Table 7-7: Results of detection of infarction analysis in acute MI for slice data

For non-infarcted segments, the percentage of segments wrongly identified as containing LGE which were adjacent to infarcted segments was calculated, and the results are shown in Table 7-8.

	Single Threshold		Segment Threshold	
Strain Parameter	% Incorrectly Identified	% Adjacent to Infarction	% Incorrectly Identified	% Adjacent to Infarction
Peak Ecc	12	67	12	70
Strain Rate	9	75	8	77
Area	5	78	9	80
Area/Time	6	70	6	82

Table 7-8: Further detection of infarction analysis for non-infarcted segments

For infarcted segments, the percentage of segments which were correctly identified as containing LGE when the segments were grouped according to LGE_score was calculated. The analysis was then repeated with the segments grouped according to LGE%_score. The results obtained using a single threshold and the segment thresholds are shown in Table 7-9 and Table 7-10 respectively.

Strain	% Identified (LGE Score)				% Identified (LGE% Score)			
Parameter	**1**	**2**	**3**	**4**	**1**	**2**	**3**	**4**
Peak Ecc	29	74	56	79	58	71	78	92
Strain Rate	14	63	67	69	46	56	84	94
Area	14	39	44	51	35	37	57	65
Area/Time	29	63	47	56	41	44	68	88

Table 7-9: Further detection of infarction analysis for infarcted segments (single threshold)

Strain	% Identified (LGE Score)				% Identified (LGE% Score)			
Parameter	**1**	**2**	**3**	**4**	**1**	**2**	**3**	**4**
Peak Ecc	29	83	81	74	65	74	74	88
Strain Rate	14	63	60	64	41	56	74	94
Area	0	52	56	56	43	39	65	73
Area/Time	14	74	53	63	49	56	63	88

Table 7-10: Further detection of infarction analysis for infarcted segments (segment threshold)

For whole slice data, the percentage of segments which were correctly identified as containing LGE when grouped according to the percentage of LGE within the slice was calculated, and the results are shown in Table 7-11.

Strain	LGE%_Score % Identified			
Parameter	1	2	3	4
n	35	12	3	0
Peak Ecc	51	100	100	-
Strain Rate	37	91	100	-
Area	26	67	100	-
Area/Time	31	64	100	-

Table 7-11: Further detection of infarction analysis for whole slice data

7.4.2.5. Assessment of Infarction Using DENSE in a Non-Infarcted Slice

From the 60 segments in the 10 non-infarcted slices, 15 segments had LGE in the corresponding segments in slices above or below the measurement slice and were allocated a score of 1, and the remaining 45 segments were allocated a score of 0.

Box plots which illustrate the difference between segments allocated to groups 0 and 1 are shown in Figure 7-8, and statistically significant results are indicated by * ($p<0.05$) and ** ($p<0.001$).

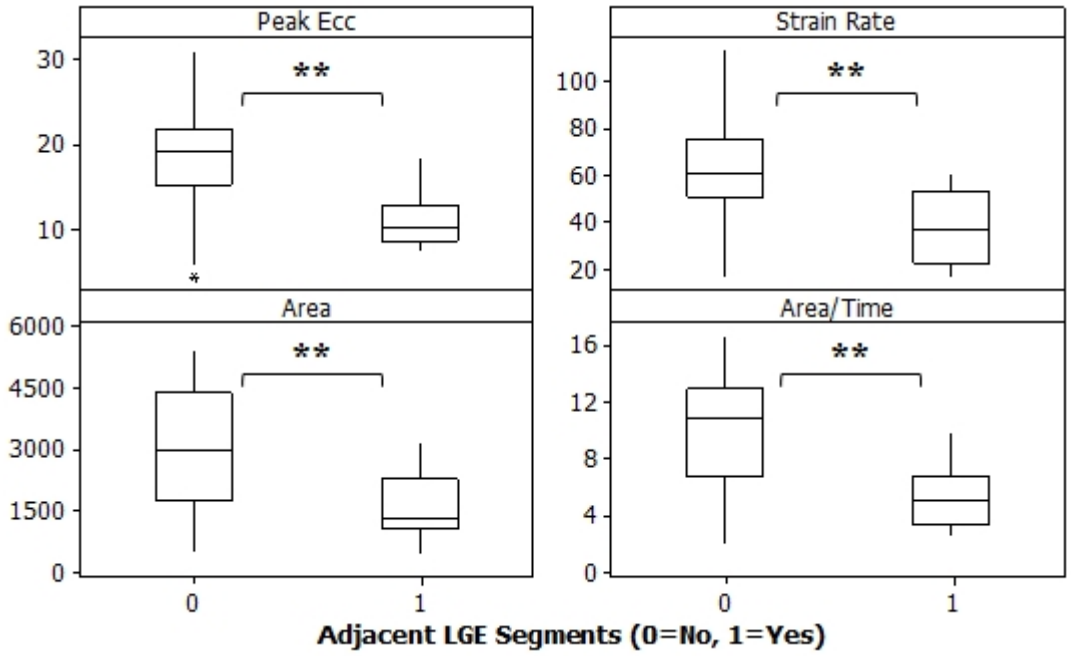

Figure 7-8: Results in non-infarcted slices

7.4.2.6. Comparison of Strain in Remote and Healthy Myocardium

The results of Anderson-Darling tests showed that strain parameters in both healthy and remote myocardium are normally distributed. The results of the two-sample t-tests showed no statistically significant differences between healthy and remote myocardium for any strain parameter, as illustrated in Figure 7-9.

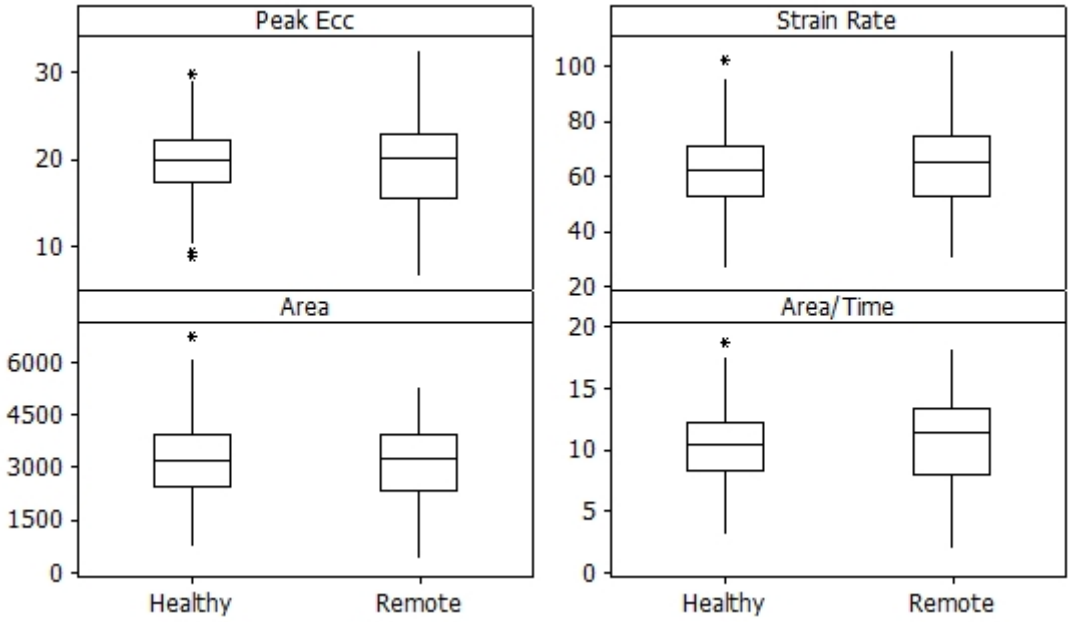

Figure 7-9: Comparison of strain in healthy and remote myocardium in acute MI

7.4.3 DENSE and Area at Risk

7.4.3.1. Relationships with Area at Risk

The results of the correlation tests between each of the strain parameters and area at risk are shown in Table 7-12, for both segment and whole slice data. Results are expressed as Pearson correlation coefficients, and statistically significant results are indicated by * ($p<0.05$) and ** ($p<0.001$). The results are illustrated using scatter plots in Figure 7-10. A scatter plot illustrating the distribution of data with area at risk is shown in Figure 7-11.

	Segments	Whole Slice	
Strain Parameter	**Area at Risk**	**Area at Risk**	**LV Area at Risk**
Peak Ecc	-0.69**	-0.43*	-0.47*
Strain Rate	-0.68**	-0.44*	-0.27
Area	-0.56**	-0.28	-0.39*
Area/Time	-0.65**	-0.36*	-0.29

Table 7-12: Results of area at risk analysis in acute MI

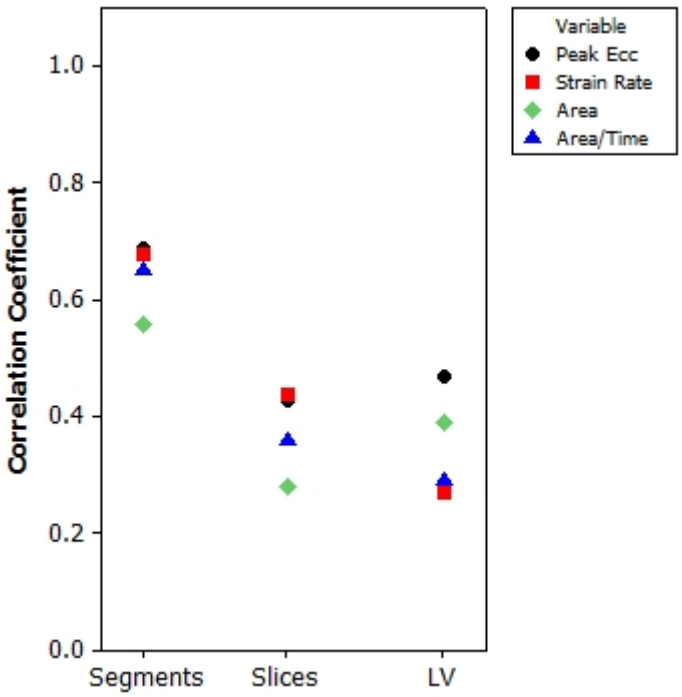

Figure 7-10: Illustration of area at risk analysis in acute MI

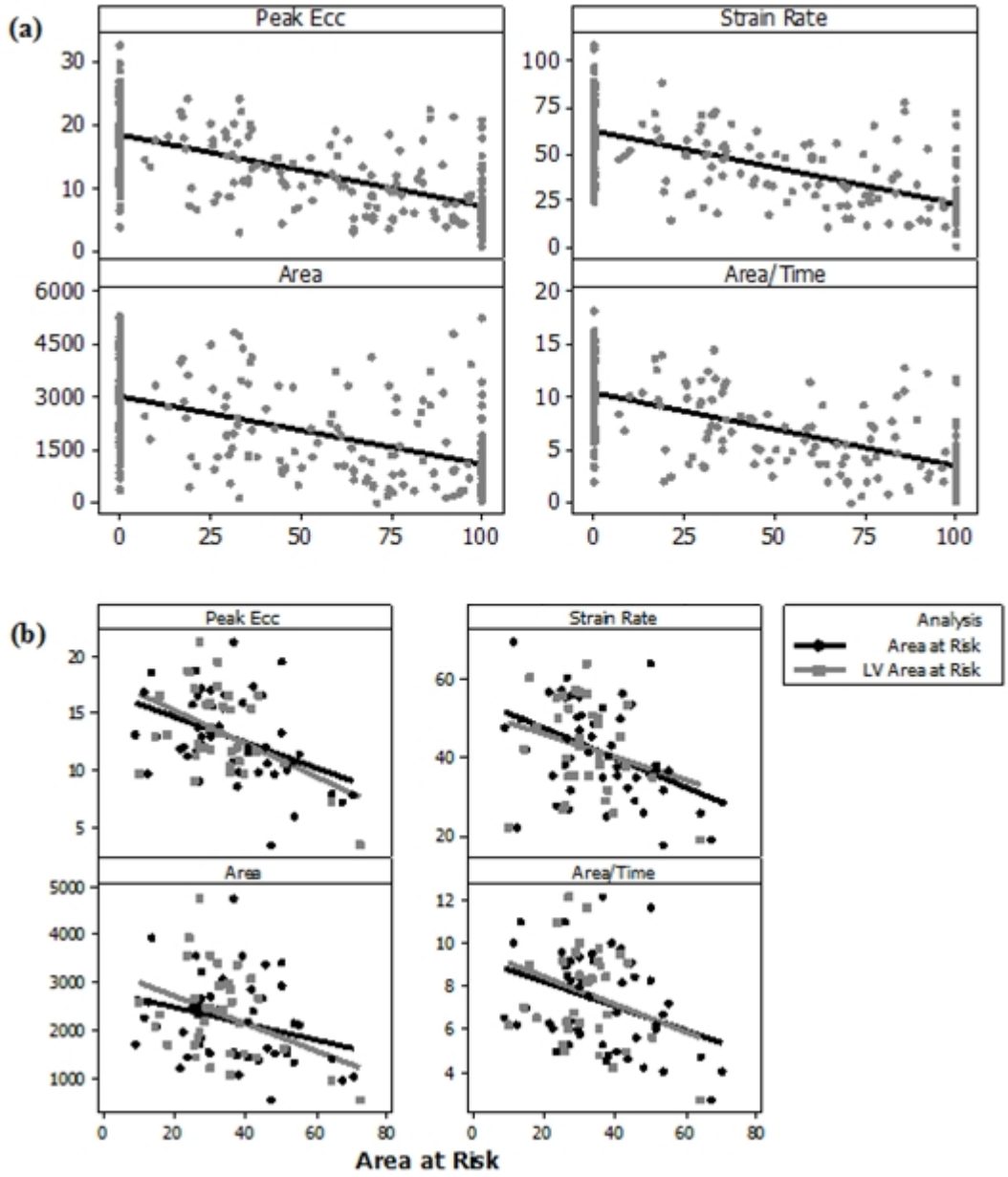

Figure 7-11: Strain parameters vs area at risk for a) segments and b) whole slice/LV data

7.4.3.2. Detection of Injury

The ROC curves for each strain parameter are shown in Figure 7-12 and Figure 7-13 for segment and whole slice data respectively. The AUC results for segment data are shown in Table 7-13, along with the thresholds established using the reference ranges, and the calculated sensitivity and specificity. The corresponding results for whole slice data are shown in Table 7-14.

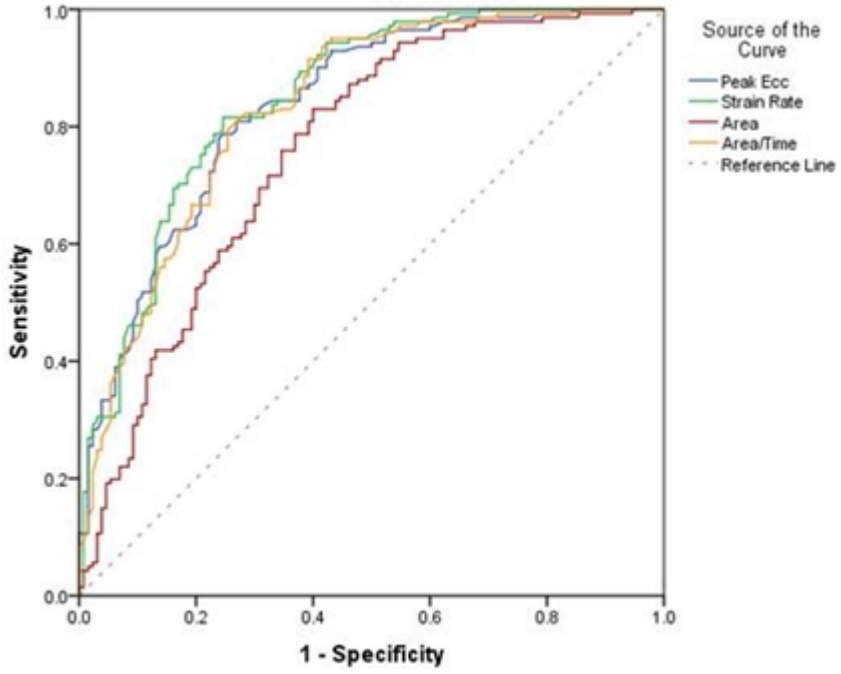

Figure 7-12: ROC curves for detection of injury in acute MI for segment data

		Single Threshold			Segment Threshold	
Parameter	**AUC**	**Threshold**	**Sensitivity**	**Specificity**	**Sensitivity**	**Specificity**
Peak Ecc	0.84	11.5	0.64	0.91	0.64	0.90
Strain Rate	0.85	35.7	0.55	0.94	0.50	0.95
Area	0.76	1011	0.41	0.97	0.46	0.94
Area/Time	0.83	4.5	0.45	0.97	0.49	0.96

Table 7-13: Results of detection of injury analysis in acute MI for segment data

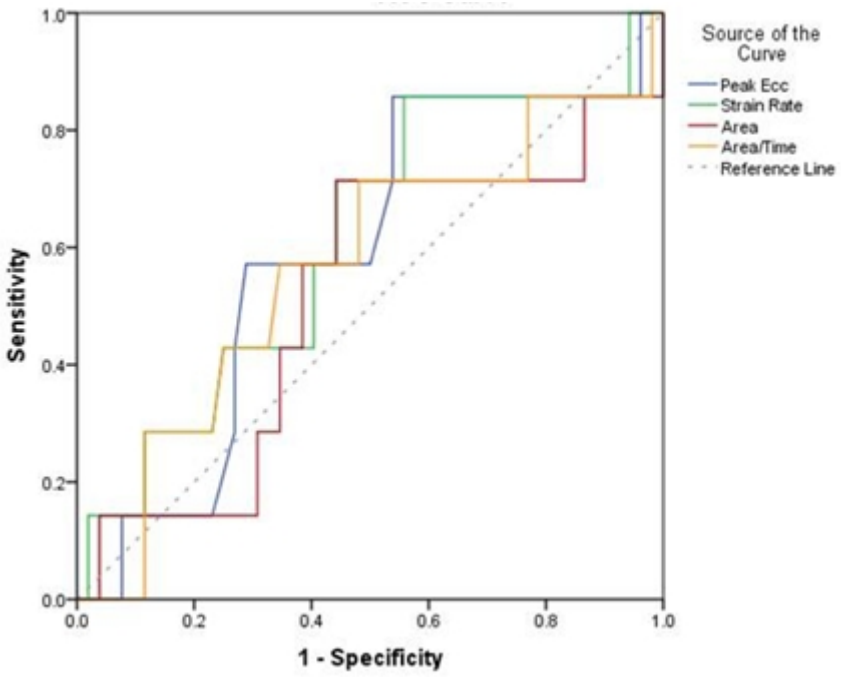

Figure 7-13: ROC curves for detection of injury in acute MI for slice data

Parameter	AUC	Threshold	Sensitivity	Specificity
Peak Ecc	0.59	13.9	0.62	0.57
Strain Rate	0.61	41.2	0.49	0.71
Area	0.52	1820	0.38	0.71
Area/Time	0.57	6.5	0.40	0.71

Table 7-14: Results of detection of injury analysis in acute MI for slice data

Further analysis of segment data was performed by separating the data into two groups: one containing segments with both T_2 hyperenhancement and LGE, and one containing segments with T_2 hyperenhancement only. For each strain parameter, the sensitivity for the detection of injury using the single threshold was calculated for each group, as shown in Table 7-15.

Parameter	All Data	T_2 + LGE	T_2 Only
n	160	130	30
Peak Ecc	0.64	0.72	0.27
Strain Rate	0.55	0.64	0.15
Area	0.41	0.46	0.17
Area/Time	0.45	0.54	0.07

Table 7-15: Sensitivity for detection of injury in segments with and without infarction

7.4.4 DENSE and Cardiac Function

7.4.4.1. Relationships with LVEF and LVESV

The results of the correlation tests between each of the strain parameters and each of the measures of cardiac function are shown in Table 7-16, and are expressed as Pearson correlation coefficients. Statistically significant results are indicated by * ($p<0.05$) and ** ($p<0.001$). The results are illustrated using scatter plots in Figure 7-14. Scatter plots illustrating the distribution of data with LVEF and LVESV are shown in Figure 7-15.

Parameter	LVEF	LVESV
Peak Ecc	0.72**	-0.51**
Strain Rate	0.52**	-0.42*
Area	0.65**	-0.42*
Area/Time	0.65**	-0.43*

Table 7-16: Results of comparison with cardiac function in acute MI

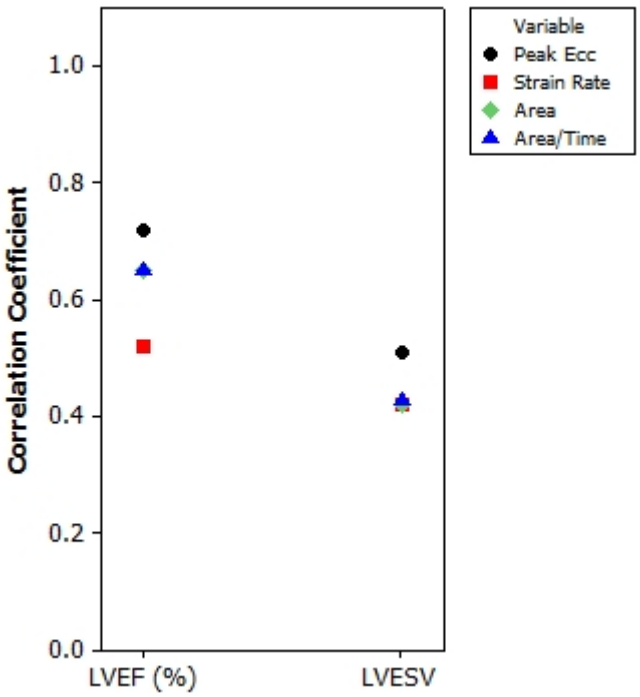

Figure 7-14: Illustration of comparison with cardiac function results in acute MI

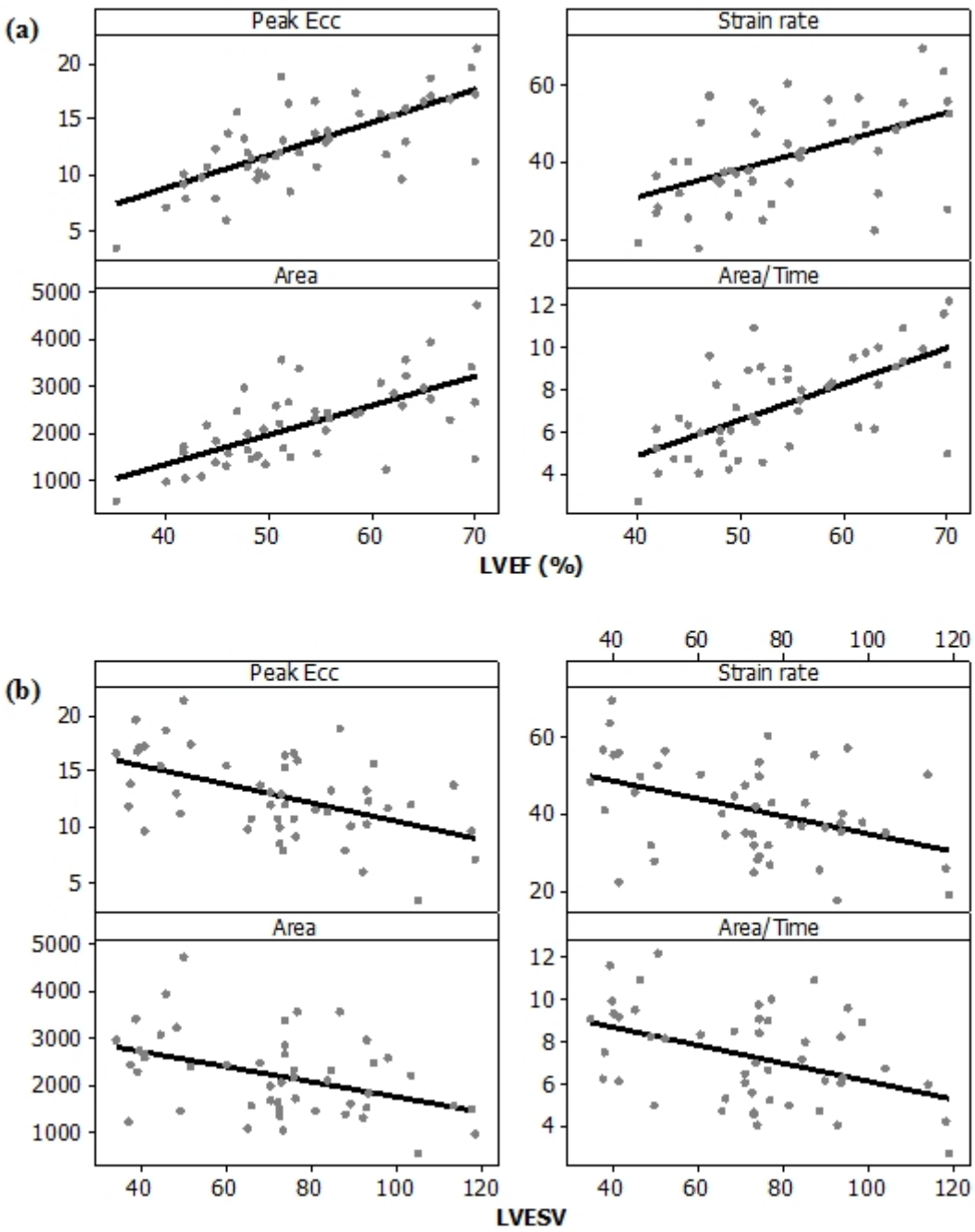

Figure 7-15: Relationships with a) LVEF and b) LVESV in acute MI

7.5 Discussion

A summary of the key results from this chapter is shown in Table 7-17.

Investigation	Results
Repeatability and Hypokinesis	• Statistically significant differences between mean CoV for segments with "severe" hypokinesis compared to other segments for all strain parameters • Measurements of strain rate and area/time corresponding to values of peak Ecc < 5% should be excluded from further analysis
DENSE and Infarction	
Relationships with LGE	**Segment analysis:** • Moderate correlation coefficients (~0.6) • Similar results for peak Ecc, strain rate and area/time, with lower correlation coefficients for area • Similar results for LGE%, LGE%_score and LGE_score • Strain parameters have higher correlations with LGE than thickening **Whole slice analysis (single slice & LV)** • Moderate correlation coefficients (~0.5) • Similar results for peak Ecc, strain rate and area/time, with lower correlation coefficients for area • Similar results for single slice and whole LV analysis
Extent of Infarction	**LGE%_score and LGE_score:** • Can distinguish between non-infarcted and <50% infarction • Can distinguish between non-infarcted and >50% infarction **LGE%_score only:** • Can distinguish between <50% and >50% infarction

Investigation	Results
Proximity to Infarction	**LGE%_score and LGE_score:** • Can distinguish between remote and infarcted segments • Can distinguish between adjacent and infarcted segments • Can distinguish between remote and adjacent segments using peak Ecc
Detection of Infarction	**Segment analysis:** • ROC analysis revealed high AUC for peak Ecc, strain rate and area/time (~0.88) with a slightly lower value for area • High specificity for all parameters • Good sensitivity, with highest value for peak Ecc (~0.7) • ~70% or more of non-infarcted segments which are incorrectly identified as containing LGE are adjacent to segments with LGE • Percentage of infarcted segments correctly identified increases as the extent of infarction increases • Percentage of infarcted segments correctly identified is higher when segments are grouped according to %LGE rather than transmural extent of MI • Similar sensitivity, specificity and identification rates when using single threshold and segment-specific threshold **Whole slice analysis:** • ROC analysis revealed moderate to high AUC for peak Ecc, strain rate and area/time (~0.7) with a slightly lower value for area • Highest sensitivity for peak Ecc (0.66) • Sensitivity is lower than for segment analysis • Moderate specificity for all parameters

Investigation	Results
	• Percentage of slices correctly identified as infarcted increases as %LGE increases
DENSE in Non-Infarcted Slices	• Lower strain in segments with infarction in adjacent slices • Statistically significant differences for all strain parameters
Strain in Remote and Healthy Myocardium	• No statistically significant differences for any strain parameter
DENSE and Area at Risk	
Relationships with Area at Risk	**Segment analysis:** • Moderate to high correlation coefficients (~0.6 - 0.7) • Similar results for peak Ecc, strain rate and area/time, with lower correlation coefficients for area **Whole slice analysis:** • Low correlation coefficients (~0.3 – 0.4) • Similar results for peak Ecc, strain rate and area/time, with lower correlation coefficient for area • Similar results for single slice and whole LV analysis
Detection of Injury	**Segment analysis:** • ROC analysis revealed high AUC for peak Ecc, strain rate and area/time with a slightly lower value for area, and with slightly lower values for all parameters than for detection of infarction • High specificity for all parameters, with similar values to detection of infarction • Moderate sensitivity with highest value for peak Ecc, and lower values for all parameters than for detection of infarction • Similar sensitivity, specificity and identification of injury rates when using single threshold and segment-specific threshold

Investigation	Results
	• With data grouped according to the presence or absence of LGE, sensitivity for segments with LGE was the same as that obtained in the Detection of Infarction analysis, but sensitivity for segments without LGE was considerably lower **Whole slice analysis:** • ROC analysis revealed moderate AUC for all parameters, with lower values than for detection of infarction • Moderate specificity for all parameters, with lower values than for detection of infarction • Low to moderate sensitivity with highest value for peak Ecc, and similar values for all parameters to detection of infarction • Percentage of slices correctly identified as injured is higher for slices with >50% injury than <50% injury
DENSE and Cardiac Function	
Relationships with LVEF and LVESV	**LVEF:** • Moderate to high correlation coefficients (~0.5 – 0.7) • Highest correlations with peak Ecc **LVESV:** • Low to moderate correlation coefficients (~0.4 – 0.5) • Highest correlations with peak Ecc

Table 7-17: Summary of key results in acute MI

Repeatability of Area Under Curve with Degree of Hypokinesis

The results of the assessment of repeatability with degree of hypokinesis were similar to those described in Chapter 5. When segments were grouped according to peak Ecc, there were no statistically significant differences between the strain rate, area and area/time values obtained for normokinetic, slightly hypokinetic and moderately hypokinetic segments. There were statistically significant differences between the results for severely hypokinetic segments and all other segments, with mean values which were substantially larger than those found for the other groups, and with a much wider range of individual CoV values. For whole slice data, no statistically significant differences were observed between the groups, however the number of slices in each group was small.

Measurements of strain rate and area/time corresponding to values of peak Ecc < 5% should be excluded from further analysis.

DENSE and Infarction

Relationships with LGE

For segment data, an investigation into the relationships between strain parameters as measured by DENSE and LGE parameters (LGE%, LGE%_score, LGE_score) revealed moderate correlations in all cases, with similar correlation coefficients for peak Ecc, strain rate and area/time and a lower correlation coefficient for area.

For each strain parameter, similar correlations were observed with LGE%, LGE%_score and LGE_score.

While the correlations between strain parameters and LGE parameters are moderate, they are stronger than the correlations between thickening and LGE parameters. This is consistent with the results from other studies [1, 5, 85], and no further comparisons with thickening will be made.

Visual inspection of the scatter plots of strain parameters and LGE% show a wide range of strain values corresponding to LGE% = 0 for all strain parameters. In this analysis, the segments are considered to be independent, but this assumption is

flawed. If a segment which is not infarcted itself is adjacent to an infarcted segment, or is above or below a slice with infarction in the corresponding segment, then the ability of that segment to contract will be impaired. The impact of this is most clearly seen for LGE% = 0, however the contractile function of all segments will be affected by the status of adjacent segments, and this may account for the spread of results.

When the data were considered on a whole slice basis instead of by segment, moderate correlations were observed between all of the strain parameters and LGE%, with similar correlation coefficients for peak Ecc, strain rate and area/time and a lower correlation coefficient for area. The magnitude of the correlation coefficients were slightly lower than in the segment case, but still highly statistically significant. The correlation between strain parameters and the total LV LGE% was again moderate, and was similar to the correlation with LGE% in the imaging slice.

Extent of Infarction

The ability of DENSE strain parameters to distinguish between non-infarcted (0), <50% infarction (1 – 25% (1) and 26 – 50% (2)) and >50% infarction (51 – 75% (3) and 76 – 100% (4)) segments was assessed, using both the transmural extent of MI (LGE_score) and the percentage of LGE within the segment (LGE%_score) to score each segment. For both LGE_score and LGE%_score, no statistically significant differences were observed between scores 1 and 2 or scores 3 and 4.

The results indicate that all strain parameters can be used to distinguish between non-infarcted and <50% infarcted segments, and between non-infarcted and >50% infarcted segments, when the segments are scored using either LGE_score or LGE%_score. Statistically significant differences were observed between <50% infarcted and >50% infarcted segments for LGE%_score but not for LGE_score, which indicates that strain may be more closely related to the percentage of LGE within the segment, although a larger sample with an increased number of infarcted segments would be required to confirm this.

This analysis was performed using LGE_score, which is based on the transmural extent of MI, and LGE%_score, which is based on the percentage of the segment which is infarcted. It is possible that neither score individually is fully representative

of the injury caused by myocardial infarction, and it may be more informative to consider an additional score which takes into account both the size of the infarction and the transmural extent. Preliminary investigations were carried out into how such a score could be constructed, but validation against DENSE was not considered appropriate, and no tagging data was available for the STEMI group.

Proximity to Infarction

The ability of DENSE strain parameters to distinguish between remote (0), adjacent (<50% (1) and >50% (2)) and infarcted (<50% (3) and >50% (4)) segments was assessed, using both the transmural extent of MI (LGE_category) and the percentage of LGE within the segment (LGE%_category) to categorise each segment. Statistically significant differences were observed for all strain parameters when comparing remote and infarcted segments, and when comparing adjacent and infarcted segments, when the segments are categorised using either LGE_category or LGE%_category. For peak Ecc alone, it was possible to distinguish between remote and adjacent segments, which indicates that this may be the most informative strain parameter.

Detection of Infarction

The ability of DENSE strain parameters for segment data to detect infarction, as indicated by the presence of LGE, was assessed using ROC analysis. For segment data, high AUC values were obtained for peak Ecc, strain rate and area/time with a slightly lower, although still high, value for area. This indicates that DENSE can be used reliably to discriminate between infarcted and non-infarcted tissue.

The lower limits of the reference ranges established in Chapter 6 were set as thresholds, and the corresponding sensitivity and specificity of DENSE for the detection of infarction were calculated for each strain parameter. Two sets of thresholds were used – one set calculated using all data (single threshold) and one set calculated using data for each segment individually (segment-specific threshold). All strain parameters had high specificity (0.88 – 0.95), and moderate to good sensitivity (0.46 – 0.74). Peak Ecc had the highest sensitivity, but the lowest specificity. The results obtained using the single thresholds and the segment-specific thresholds were similar.

Further investigation of the non-infarcted segments which were incorrectly identified as being infarcted showed that 70 – 80% were adjacent to segments which contained LGE. Since segments are not independent, the contractile ability of the non-infarcted segments is likely to have been affected by contractile abnormalities in the adjacent infarcted segments.

With infarcted segments grouped according to the transmural extent of infarction (LGE_score) or the percentage of infarction within the segment (LGE%_score), the percentage of segments which were correctly identified as containing LGE increased as the score increased for all strain parameters. The detection rate for each group was higher when segments were grouped according to LGE%_score than with LGE_score, which is consistent with the results found in the Extent of Infarction investigation. For segments with <50% LGE (scores 1 and 2), peak Ecc had the highest detection rate, and for segments with >50% LGE (scores 3 and 4), peak Ecc and strain rate performed equally well, with a slightly lower detection rate for area/time, and a lower detection rate for area. Again, similar results were obtained using the single thresholds and the segment-specific thresholds. Although there are statistically significant differences between strain values in different myocardial segments, as shown in Section 6.4.3, there does not appear to be any benefit in constructing segment-specific reference ranges.

For whole slice data, ROC analysis revealed moderate to high AUC values for peak Ecc, strain rate and area/time (0.67 - 0.74), with a slightly lower value for area. The sensitivity was found to be low to moderate, with the highest value for peak Ecc (0.66), and specificity for all parameters was moderate. The sensitivity and specificity for the detection of infarction were lower than for segment data, however the number of measurements was smaller, in particular the number of non-infarcted slices, and the results may improve with a larger sample size. When slices were grouped according to the percentage of LGE within the slice, the detection rate increased as the percentage of LGE increased. The highest detection rate was achieved for peak Ecc, which correctly identified 100% of segments with LGE > 25%.

Assessment of Infarction Using DENSE in a Non-Infarcted Slice

In order to determine whether DENSE strain parameters in a non-infarcted imaging slice could provide information about infarction elsewhere in the LV, an investigation was carried out into the differences in strain in segments where infarction was present in the corresponding segments above or below the imaging slice, and in segments where no infarction was present above or below.

Visual inspection of the box plots which compare the two groups of segments show a tendency towards higher values in the segments with no infarction above or below. The results of the Mann-Whitney tests were statistically significant for all strain parameters, which indicates that DENSE strain parameters in a non-infarcted slice may provide information about infarction elsewhere in the LV. However, only 10 slices with 60 segments were used in this analysis, and a larger sample size may be required to confirm the result.

The results of this assessment also emphasise the need to take infarction in adjacent slices into account when analysing DENSE strain data.

Strain in Remote and Healthy Myocardium

No statistically significant differences were observed for any strain parameter between healthy volunteers and remote myocardium in acute MI.

DENSE and Area at Risk

Relationships with Area at Risk

An investigation into the relationships between strain parameters as measured by DENSE and area at risk revealed moderate to high correlations for all strain parameters when analysing data on a segment basis, with similar correlation coefficients for peak Ecc, strain rate and area/time and a lower correlation coefficient for area. The correlations with area at risk were slightly higher than those obtained with extent of infarction for all strain parameters. Visual inspection of the corresponding scatter plots showed a wide range of values for each strain parameter for area at risk = 0 – this is unsurprising, as the previously mentioned issues with non-independent segments will also apply to the area at risk analysis.

The correlations obtained when analysing the data on a whole slice basis were lower than for the segment analysis, and lower than the correlations obtained with whole slice LGE.

As discussed in Section 2.3.3, the use of T_2 hyperenhancement for the definition of the area at risk is not fully validated. However, this does not change the fact that moderate to high correlations were observed with the percentage of T_2 hyperenhancement for segment data, only that the mechanism behind this hyperenhancement is not fully understood.

Detection of Injury

The ability of DENSE strain parameters to detect injury, as indicated by the presence of T_2 hyperenhancement, was assessed using ROC analysis. For segment data, high AUC values were obtained for peak Ecc, strain rate and area/time with a slightly lower value for area. The AUC values for all parameters were slightly lower than the corresponding values obtained for detection of infarction.

All strain parameters had high specificity for the detection of injury, and moderate sensitivity (0.45 – 0.65). The specificity values were similar to those obtained for detection of infarction, but the sensitivity values were lower. Peak Ecc had the highest sensitivity, but the lowest specificity. Similar results were obtained when using the single thresholds and the segment-specific thresholds.

Further analysis was performed with injured segments grouped according to the presence or absence of LGE i.e. one group contained segments with both T_2 hyperenhancement and LGE, and the other group contained segments with T_2 hyperenhancement only. For the group with both T_2 hyperenhancement and LGE, the sensitivity for the detection of injury for each strain parameter was the same as the results obtained in the Detection of Infarction analysis. For segments with T_2 hyperenhancement only, sensitivity for the detection of injury was considerably lower for all strain parameters. The use of reference ranges for the detection of segments which are injured but non-infarcted does not appear to be effective.

For whole slice data, moderate AUC values were obtained for all strain parameters, which were lower than the corresponding values for detection of infarction. Sensitivity was low to moderate with similar values to those obtained in the detection of infarction analysis, while specificity was moderate but with lower values than in detection of infarction. Only 7 slices did not contain T_2 hyperenhancement, so again it is likely that the results have been affected by the small sample size.

Overall, it appears that DENSE is more suited to detecting infarction as revealed by LGE than injury as revealed by T_2 hyperenhancement.

DENSE and Cardiac Function

Relationships with LVEF and LVESV

An investigation into the relationships between strain parameters as measured by DENSE and LVEF revealed moderate to high correlations for all strain parameters. The highest correlation occurred with peak Ecc, and the lowest correlation occurred with strain rate.

For LVESV, the correlations with strain were lower than those obtained for LVEF, but still moderate. Again, the highest correlation occurred with peak Ecc.

Further Discussion

There are a number of limitations in the design of this study which need to be acknowledged.

As mentioned previously in this Discussion, the assumption that the segments are independent is flawed. The status of adjacent segments in the imaging slice, and also segments in adjacent slices, needs to be taken into consideration in order to provide an accurate evaluation of the relationships between strain parameters and myocardial injury. In addition, the fact that repeated measures are made on the same subject, i.e. data for 6 segments are obtained from each person, is not accounted for in the statistical analysis. Complex modelling would be required to take account of these issues, and this was considered to be beyond the scope of this thesis.

Performing analysis on a whole slice basis removes the problems of interactions between adjacent segments and repeated measures on the same subject, although it still does not take adjacent slices into account. In all of the investigations contained within this chapter, lower correlations were obtained for the whole slice data than for the segment data. While analysing data on a whole slice basis may still be informative, it is likely that the effects of smaller infarctions will be harder to detect.

As discussed in Chapter 5, the current implementation of DENSE does not provide informative results for radial strain, and so only circumferential strain has been considered in this chapter, which does not allow a complete assessment of contractile function. At present it is not possible to analyse DENSE images acquired in the longitudinal plane, although this capability may become available in the near future. A further limitation of the current implementation of DENSE is that it takes no account of through-plane motion, which will introduce errors into measurements of strain. The ideal situation would be a 3D version of DENSE which covers the entire LV, but while this is available as a research sequence in other institutions, it is not currently available at our institution.

7.6 Summary and Conclusions

The results of the investigations contained within this chapter showed that DENSE strain measurements are informative in acute MI.

Moderate relationships were observed between strain and the extent of infarction, with similar correlation coefficients for peak Ecc, strain rate and area/time. The relationships with the area under the strain curve were found to be less strong.

All strain parameters can distinguish between non-infarcted and infarcted segments, and depending on the scoring system used, it is possible to distinguish between segments with <50% infarction and >50% infarction. Additionally, all strain parameters can distinguish between remote and infarcted segments, and between adjacent and infarcted segments. Peak Ecc alone can be used to distinguish between remote and adjacent segments.

Slightly stronger relationships were observed between strain parameters and area at risk than with extent of infarction for segment data, but not for whole slice data.

DENSE has high specificity and good sensitivity for the detection of infarction. Peak Ecc has the highest detection rates, particularly in segments with %LGE < 50% or $\%T_2$ < 50%. Although there are statistically significant differences in strain values between different myocardial segments in the healthy heart, there appears to be no benefit in using segment-specific thresholds for the detection of infarction and injury, as similar results can be obtained using a single threshold for all segments.

Strain appears to be more closely correlated with LVEF than LVESV, with the highest correlations in both cases occurring with peak Ecc.

DENSE images can be analysed on a whole slice or segment-by-segment basis, and both approaches provide information on the relationships with LGE and area at risk, and allow detection of infarction with moderate to good sensitivity. Segment analysis produced slightly higher correlations and better sensitivity, and also provided additional information on the extent of infarction within segments and their proximity to infarction. Whole slice analysis additionally provided information on the relationships between strain and cardiac function.

Of the four strain parameters which were measured in this chapter, it appears that peak Ecc may be the most informative.

Only circumferential strain has been considered in this chapter, but a more accurate investigation would require at least longitudinal and radial strain, and ideally a 3D measurement of strain. These techniques are currently under development in other institutions, and there is potential for future work in this area.

Chapter 8

DENSE in Chronic Infarction

8.1 Introduction

In acute MI, the region of tissue which exhibits late gadolinium enhancement consists not only of infarct scar, but also oedema, inflammation and necrotic tissue. In chronic MI, oedema and inflammation has largely resolved, and the infarct region consists mainly of collagen. In addition, remodelling will have taken place within the infarct scar itself, and potentially within remote tissue. Depending on whether reperfusion of injured tissue was achieved, and the timescale over which this occurred, injured tissue may have been salvaged and regained a degree of contractile function, or it may have eventually succumbed to infarction. The purpose of this chapter is to investigate the ability of DENSE strain parameters to detect contractile abnormalities associated with the presence of infarction in the chronic setting, and to determine whether these relationships are different to those obtained in the acute setting.

8.2 Aims

The aims of the research presented in this chapter are:

- To investigate the relationships between DENSE strain parameters and the extent of infarction in chronic MI
- To investigate whether DENSE can be used to distinguish between differing extents of infarction in chronic MI
- To investigate whether DENSE can be used to distinguish between regions with and without infarction in chronic MI
- To investigate the relationships between DENSE strain parameters and myocardial salvage
- To determine the sensitivity and specificity of DENSE for the detection of chronic myocardial infarction

- To investigate the relationships between DENSE strain parameters and cardiac function in acute MI
- To determine if DENSE can provide clinically useful information relating to longitudinal changes in strain

8.3 Methods

8.3.1 STEMI Volunteers

The patients who participated in the study described in Chapter 7 were invited to return for a second scan at 6 months post-MI. From the 50 patients who had imaging at the level of the infarct in the acute scan, 47 returned for a follow-up scan.

8.3.2 Image Acquisition and Analysis

Image acquisition and analysis of cine, DENSE and LGE images were performed as described in Chapter 7.

MSI was calculated using Equation 2-3 from Section 2.3.3, using the extent of infarction measured in chronic MI and the area at risk measured in acute MI. Care must be taken when calculating MSI, since a value of 0 would be allocated to both infarcted segments in which T_2% = LGE%, and in non-infarcted segments where T_2%= LGE% = 0. MSI is only meaningful in injured segments, and so the data relating to non-injured segments was not included in the analysis. To allow all data to be taken into consideration, including non-injured segments, a score, MSI score, was allocated as defined in Table 8-1.

Score	Definition	Category
0	0.0	No Salvage
1	0.01 – 0.25	Limited Salvage
2	0.26 – 0.50	
3	0.51 – 0.75	Extensive Salvage
4	0.76 – 1.00	
5	T_2 = LGE = 0	Uninjured

Table 8-1: Definition of MSI scores

8.3.3 DENSE and Infarction

8.3.3.1. Relationships with LGE

For segment data, the relationships between each of the DENSE strain parameters with each of the LGE parameters (LGE%, LGE_score, LGE%_score) were assessed using correlation tests, and compared to the results from acute MI.

For whole slice data, the relationships between each of the DENSE strain parameters and LGE% in both the imaging slice (LGE%) and the LV volume (LV LGE%) were assessed using correlation tests, and compared to the results from acute MI.

8.3.3.2. Extent of Infarction

For segment data, the ability of each of the strain parameters to distinguish between non-infarcted (score = 0), <50% infarction (transmurally or within segment, score = 1 or 2) and >50% infarction (transmurally or within segment, score = 3 or 4) was assessed using Kruskal-Wallis with individual Mann-Whitney tests.

8.3.3.3. Proximity to Infarction

For segment data, the ability of each of the strain parameters to distinguish between remote, adjacent and infarcted segments was assessed using Kruskal-Wallis with individual Mann-Whitney tests.

8.3.3.4. Detection of Infarction

Analysis was performed as described in Section 7.3.4.4, and the AUC, sensitivity and specificity of the DENSE for the detection of LGE in chronic MI were calculated.

For segment data, the results obtained in acute MI showed no benefit to using segment-specific thresholds, so only the single thresholds were used. A comparison of the detection rates in acute and chronic MI with segments grouped according to LGE%_score was performed.

For whole slice data, no images had been obtained in non-infarcted slices, so calculations were performed for sensitivity only.

8.3.3.5. Assessment of Longitudinal Changes

For the 43 patients who underwent both scans, the acute and chronic results were compared directly in the following ways:

Comparison of Remote, Adjacent and Infarcted Segments: For segments classified as remote, adjacent and infarcted in acute MI, Wilcoxon signed rank tests were used to compare the acute and chronic results for each category separately. A Kruskal-Wallis with individual Mann-Whitney tests was then used to compare the differences in strain between acute and chronic MI between the three categories.

The data were then further categorised according to the change in proximity category between acute and chronic MI e.g. remote (acute) $\rightarrow$ remote (chronic), remote (acute) $\rightarrow$ adjacent (chronic), adjacent (acute) $\rightarrow$ infarcted (chronic) etc. Wilcoxon signed rank tests were used to compare the acute and chronic results for each category.

Segments which were categorised as remote, adjacent and infarcted in the acute setting were then considered separately, and the changes in strain between sub-categories (e.g. remote (acute) $\rightarrow$ remote (chronic) vs remote (acute) $\rightarrow$ adjacent (chronic)) were compared using Kruskal-Wallis with individual Mann-Whitney tests. A similar comparison between sub-categories was performed to assess if strain differences in the acute setting could be detected.

Comparison of Segments with Increased, Unchanged and Decreased LGE Score: For segments with LGE in acute and/or chronic MI, the acute and chronic results for LGE_score were compared to determine whether the score was lower (i.e. decreased extent of LGE), unchanged or higher (i.e. increased extent of LGE) in chronic MI compared to acute. A Kruskal-Wallis with individual Mann-Whitney tests was then used to determine if DENSE strain parameters could distinguish between the three groups. The same analysis was also performed for LGE%_score

Relationship Between Change in Strain and Change in LGE%: The change in each strain parameter between acute and chronic MI was compared with the change in

LGE% using a correlation test. For whole slice data, the change in LGE% in both the imaging slice and the LV volume were used.

8.3.3.6. Comparison of Strain in Remote and Healthy Myocardium

The values obtained for DENSE strain parameters in remote myocardium were compared to the values obtained from healthy volunteers, and also to the values obtained in remote myocardium in acute MI, using a one-way ANOVA with Tukey's post-hoc test.

8.3.4 DENSE and Salvage

8.3.4.1. Relationships with MSI

An assessment of the relationships between each of the DENSE strain parameters and both MSI and MSI score were performed using correlation tests. Analysis was carried out on segment and whole slice data.

8.3.5 DENSE and Cardiac Function

8.3.5.1. Relationships with LVEF and LVESV

For whole slice data, the relationships between each of the DENSE strain parameters and each of LVEF and LVESV were assessed using correlation tests.

8.3.5.2. Assessment of Longitudinal Changes

For whole slice data, the change in each strain parameter between acute and chronic MI and the change in each of LVEF and LVESV were assessed using correlation tests.

8.4 Results

From the 47 patients who attended for a second scan, DENSE images were not acquired for 2 patients, and the DENSE images were considered to be non-diagnostic in a further 2 patients due to excessive breathing artefacts.

From the 43 patients from whom DENSE images were acquired, there were 258 segments available for analysis.

8.4.1 DENSE and Infarction

For each of LGE_score, LGE%_score and LGE_category, the number of segments allocated a particular value is shown in Table 8-2.

Score	0 (Remote)	1 (Adj.)	2	3 (Inf.)	4
LGE_score	161	6	20	27	44
LGE%_score	161	35	36	12	14
LGE_category	75	86	-	97	-

Table 8-2: Allocation of LGE scores to segments in chronic MI

8.4.1.1. Relationships with LGE

The results of the correlation tests between strain parameters and LGE parameters are shown in Table 8-3, and are expressed as a Pearson correlation coefficient. Statistically significant results are indicated by * ($p<0.05$) and ** ($p<0.001$). The results (C) are illustrated using scatter plots in Figure 8-1, along with the results from acute MI (A) for comparison.

Strain Parameter	Segment Data			Whole Slice Data	
	LGE%	LGE% score	LGE score	LGE%	LV LGE%
Peak Ecc	-0.54**	-0.53**	-0.47**	-0.39*	-0.22
Strain Rate	-0.52**	-0.51**	-0.44**	-0.34*	-0.24
Area	-0.36**	-0.36**	-0.32**	-0.31*	-0.18
Area/Time	-0.53**	-0.52**	-0.47**	-0.41*	-0.26

Table 8-3: Results of relationships with LGE analysis in chronic MI

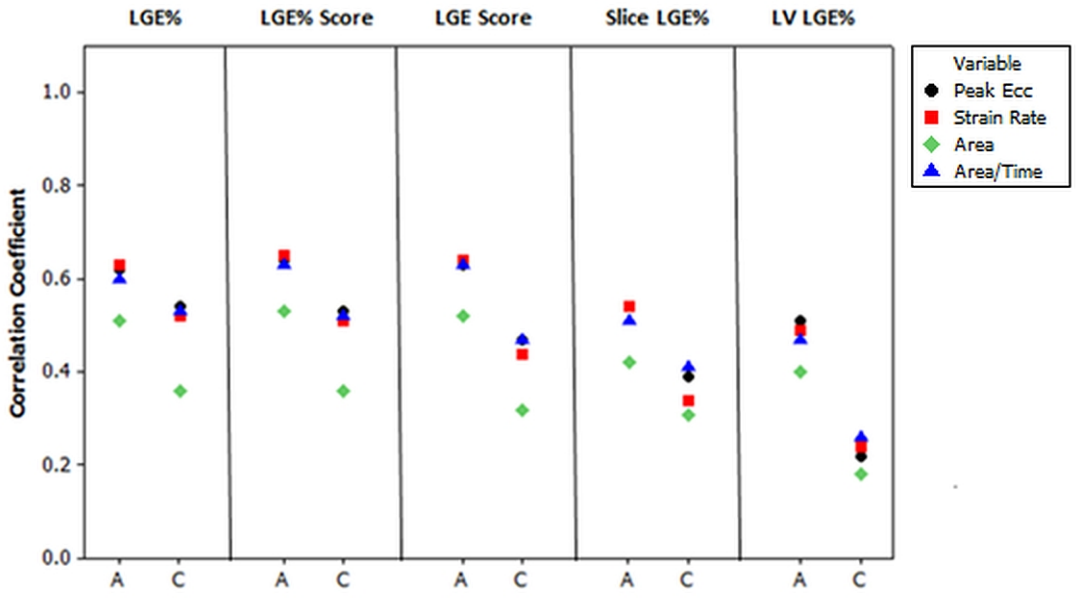

Figure 8-1: Illustration of relationships with LGE results in acute and chronic MI

8.4.1.2. Extent of Infarction

The results of the Kruskal-Wallis with individual Mann-Whitney tests comparing segments with no infarction, <50% infarction and >50% infarction were similar to those obtained in acute MI (see Section 7.4.2.2, Figure 7-4). Statistically significant differences were observed for all strain parameters between non-infarcted and <50% infarcted segments, and between non-infarcted and >50% infarcted segments for LGE_score and LGE%_score. Statistically significant differences were observed between <50% infarcted and >50% infarcted segments for all parameters for LGE%_score, but not for LGE_score.

8.4.1.3. Proximity to Infarction

The results of the Kruskal-Wallis with individual Mann-Whitney tests comparing remote, adjacent and infarcted segments were similar to those obtained in acute MI (see Section 7.4.2.3, Figure 7-5). Statistically significant differences were observed for all strain parameters between remote and infarcted segments, and between adjacent and infarcted segments for both LGE_category and LGE%_category. No statistically significant differences were found between remote and adjacent segments.

8.4.1.4. Detection of Infarction

For segment data, the ROC curves for each strain parameter are shown in Figure 8-2. The AUC results for segment data are shown in Table 8-4, along with the sensitivity and specificity calculated using the thresholds established from the reference ranges. The thresholds established using the reference ranges for whole slice data and the corresponding sensitivity are shown in Table 8-5.

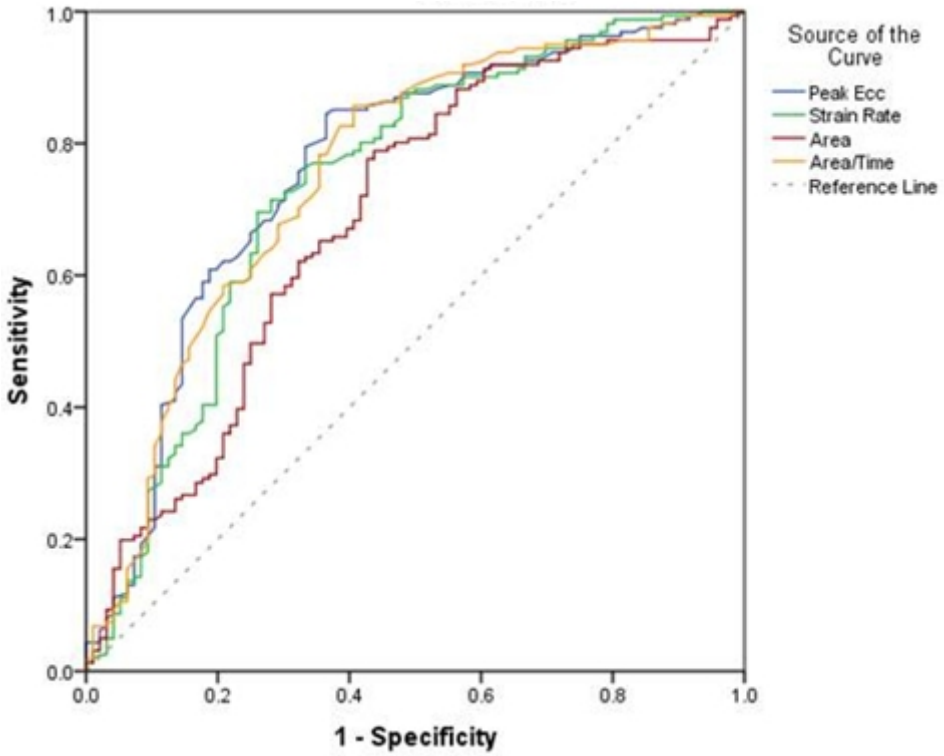

Figure 8-2: ROC curves for detection of chronic MI for segment data

Parameter	AUC	Threshold	Sensitivity	Specificity
Peak Ecc	0.76	11.5	0.28	0.94
Strain Rate	0.74	35.7	0.37	0.91
Area	0.69	1011	0.05	0.98
Area/Time	0.76	4.5	0.16	0.96

Table 8-4: Results of detection of infarction analysis in chronic MI for segment data

Strain Parameter	Threshold	Sensitivity
Peak Ecc	13.9	0.19
Strain Rate	41.2	0.28
Area	1820	0.07
Area/Time	6.5	0.09

Table 8-5: Results of detection of infarction analysis in chronic MI for slice data

For infarcted segments, the differences in detection rates between acute and chronic MI with segments grouped according to LGE%_score are illustrated in Figure 8-3.

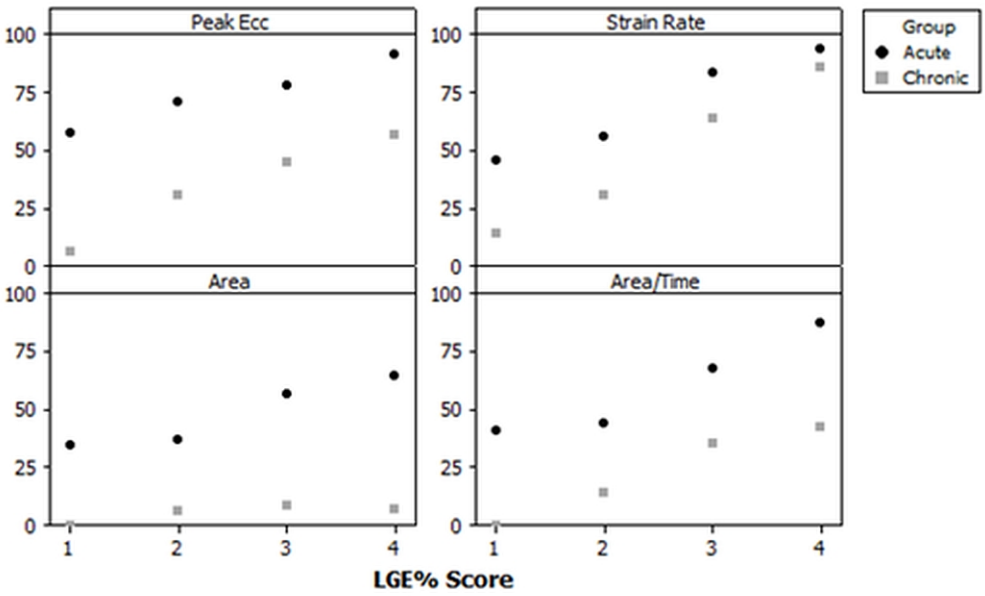

Figure 8-3: Illustration of differences in detection rates with LGE% score between acute and chronic MI

8.4.1.5. Assessment of Longitudinal Changes

For the 43 patients who underwent both scans, 59 segments were classified as remote, 87 as adjacent and 112 as infarcted in acute MI. In chronic MI, 75 segments were classified as remote, 86 as adjacent and 97 as infarcted.

Comparison of Remote, Adjacent and Infarcted Segments:

The results of the Wilcoxon signed rank tests comparing acute and chronic results for remote segments found no statistically significant differences for any strain parameter.

For adjacent segments, statistically significant differences were observed for peak Ecc ($p = 0.005$), area ($p < 0.001$) and area/time ($p = 0.018$), with median differences (chronic – acute) of 1.5, 616 and 0.8 respectively, which indicates a tendency towards an increase in strain. No statistically significant differences were observed for strain rate ($p = 0.576$).

For infarcted segments, statistically significant differences were observed for peak Ecc, strain rate, area and area/time ($p < 0.001$ for all parameters), with median differences of 5.6, 14.1, 1346 and 3.7 respectively, which again indicates a tendency towards an increase in strain.

The results of the Kruskal-Wallis with individual Mann-Whitney tests comparing the changes in strain for the three categories (remote, adjacent, infarcted) found statistically significant differences between remote and infarcted segments ($p < 0.001$ for all strain parameters), and between adjacent and infarcted segments ($p < 0.001$ for all strain parameters). Box plots illustrating the results are shown in Figure 8-4.

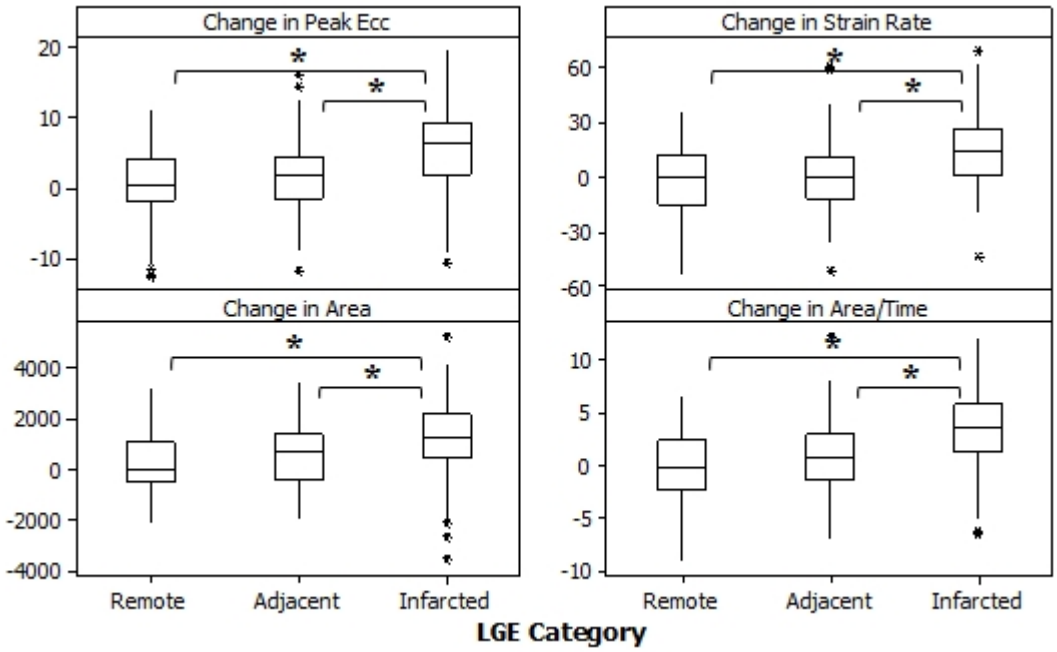

Figure 8-4: Comparison of changes in strain in remote, adjacent and infarcted segments

The results of the Wilcoxon signed rank tests comparing strain in acute and chronic MI with the data sub-categorised according to the change in proximity to infarction are shown in Table 8-6. The results are expressed as p-values, and statistically significant results are highlighted by * ($p < 0.05$) and ** ($p < 0.001$). The proximity to infarction is indicated by R (remote), A (adjacent) and I (infarcted).

Change in Category	n	Peak Ecc	Strain Rate	Area	Area/Time
R → R	51	0.680	0.245	0.431	0.506
R → A	8	0.069	0.093	0.208	0.123
A → R	22	0.783	0.088	0.115	0.709
A → A	55	0.002*	0.900	<0.001**	0.012*
A → I	10	0.241	0.646	0.285	0.445
I → A	25	0.001*	0.003*	<0.001**	0.001*
I → I	87	<0.001**	<0.001**	<0.001**	<0.001**

Table 8-6: Comparison of strain in acute and chronic MI according to change in proximity to infarction

The results of the proximity to infarction sub-category comparisons for both change in strain, and strain in acute MI, are illustrated in Figure 8-5. Statistically significant results are indicated by * ($p < 0.05$) and ** ($p < 0.001$).

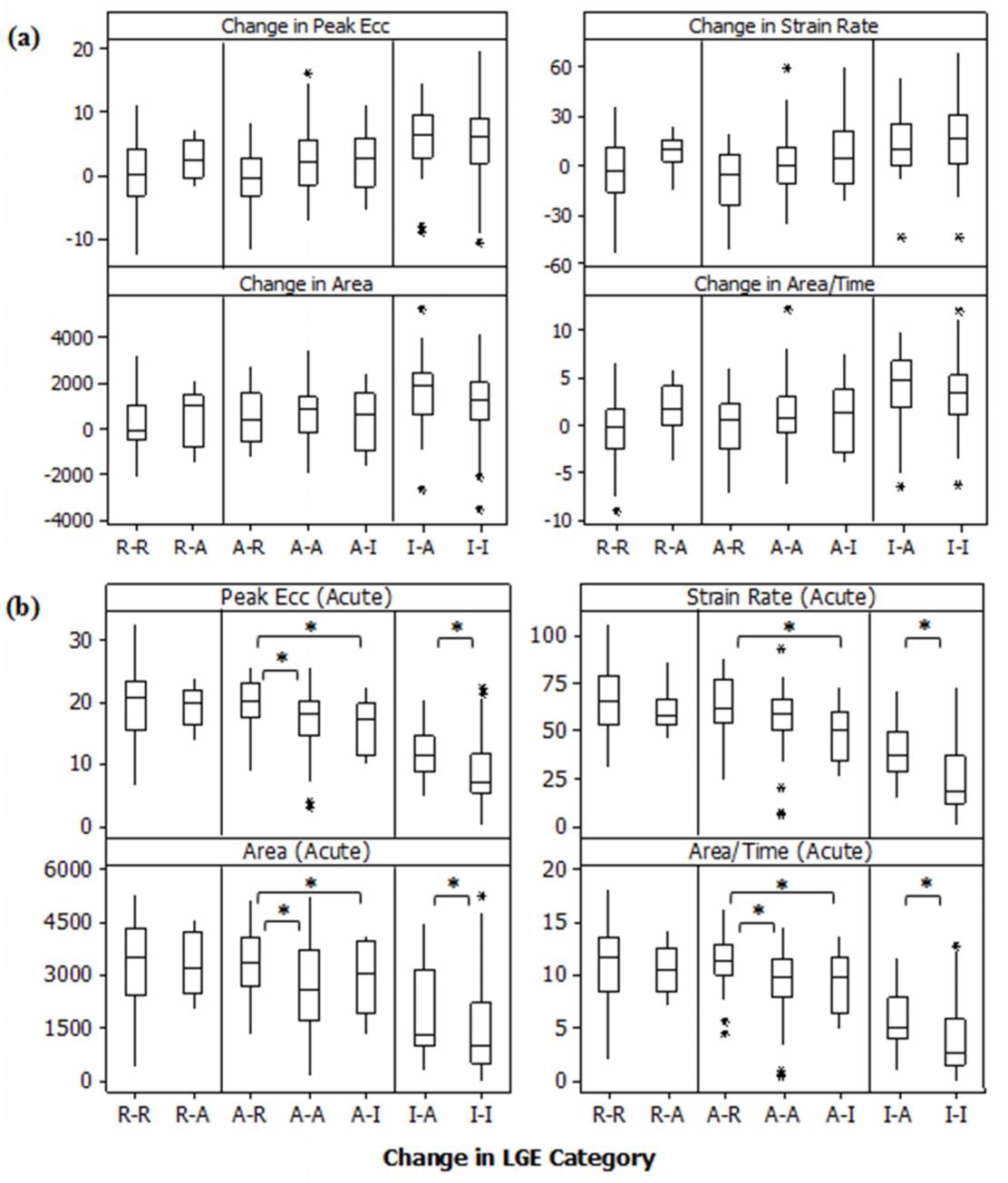

Figure 8-5: Illustration of proximity sub-category comparisons for a) change in strain and b) strain in acute MI

The results of the comparison of strain in acute and chronic infarction with segments sub-categorised according to the change in proximity to infarction are consistent with the previous comparison performed for remote, adjacent and infarcted segments,

which showed statistially significant increases in strain for adjacent and infarcted segments. The sub-category analysis revealed additional information about changes in strain in segments which were categorised as adjacent in acute MI, with statistically significant increases in strain in segments which remained categorised as adjacent, but no statistically significant increase in strain in segments which were subsequently categorised as remote. There was no statistically significant difference in strain in segments which were subsequently categorised as infarcted, however this may be due to the small number of samples in this sub-category.

For each category (remote, adjacent, infarcted), comparisons of the relevant sub-categories showed no statistically significant differences in the changes in strain between acute and chronic MI. However, statistically significant differences between sub-categories were observed for strain measurements obtained in acute MI, for both adjacent and infarcted segments.

Comparison of Segments with Increased, Unchanged and Decreased LGE Score:
For segments with LGE present in acute MI, the number of segments which were allocated a lower, unchanged or higher value for LGE_score and LGE%_score in chronic MI is shown in Table 8-7, and the distribution of strain values for the three groups is illustrated in Figure 8-6.

Change in Score	LGE_Score	LGE%_Score
Lower	56	62
Unchanged	49	32
Higher	17	28

Table 8-7: Changes in LGE_score and LGE%_score between acute and chronic MI

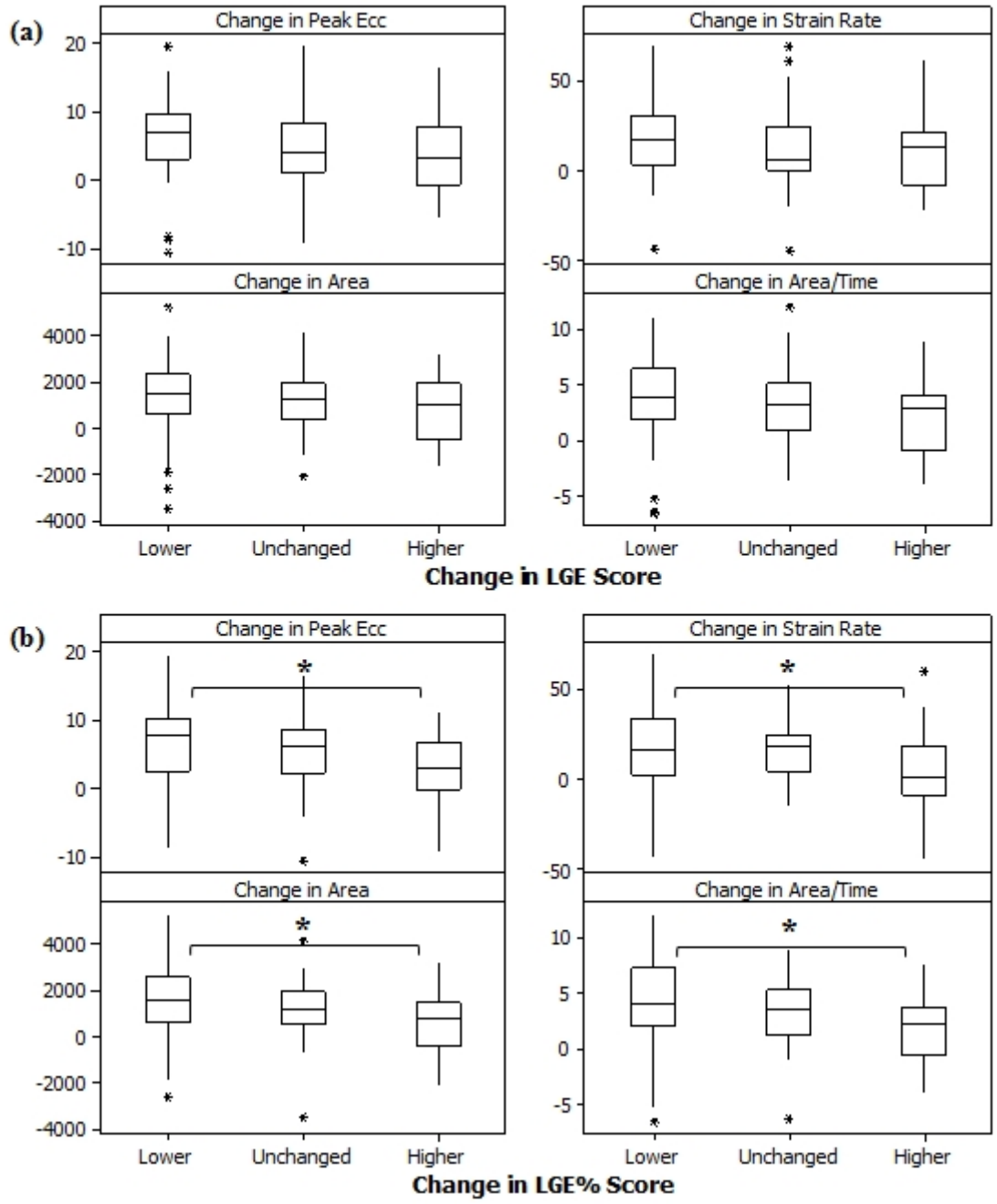

Figure 8-6: Comparison of changes in strain and changes in a) LGE_score and b) LGE%_score

For LGE_score, the results of the Kruskal-Wallis with individual Mann-Whitney tests showed no statistically significant differences between any of the categories, for all strain parameters. For LGE%_score, statistically significant differences were observed between segments with a lower score and those with a higher score for all strain parameters ($p = 0.004, 0.013, 0.048, 0.003$ for peak Ecc, strain rate, area and area/time respectively).

Relationship Between Change in Strain and Change in LGE%:

Scatter plots illustrating the relationships between the change in strain and the change in LGE% between acute and chronic MI, along with a linear regression fit, are shown in Figure 8-7. For segment data, the correlation coefficients obtained for all strain parameters were low (-0.18 – -0.27), but the relationships were found to be statistically significant ($p < 0.05$) for all parameters other than area. For whole slice data, the correlation coefficients were very low (<0.1) and no statistically significant relationships were observed.

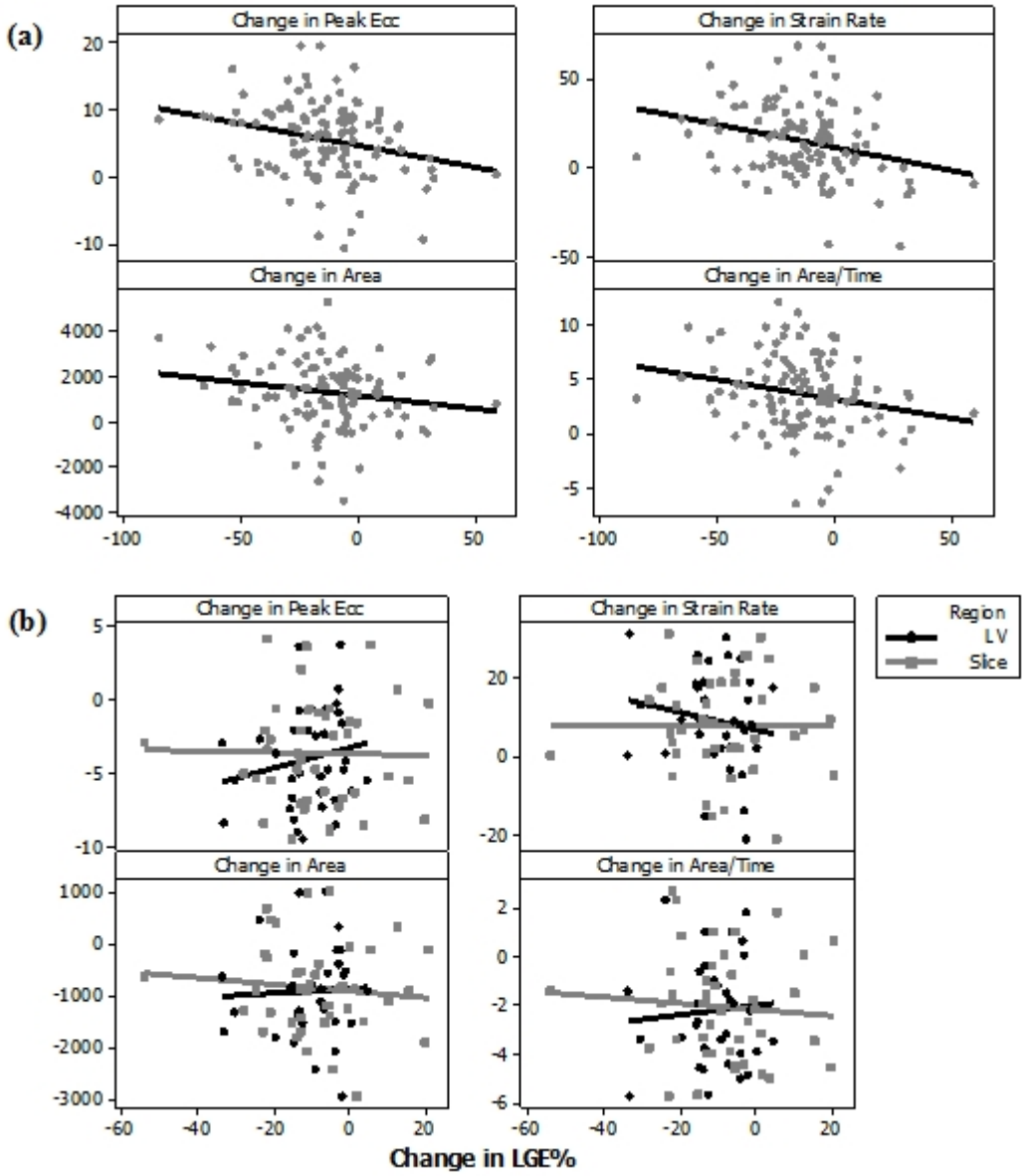

Figure 8-7: Comparison of change in strain and change in LGE% for a) segment and b) whole slice data.

8.4.1.6. Comparison of Strain in Remote and Healthy Myocardium

The results of the one-way ANOVA with Tukey's post-hoc test showed no statistically significant differences between mean strain in healthy myocardium, remote myocardium in acute MI and remote myocardium in chronic MI.

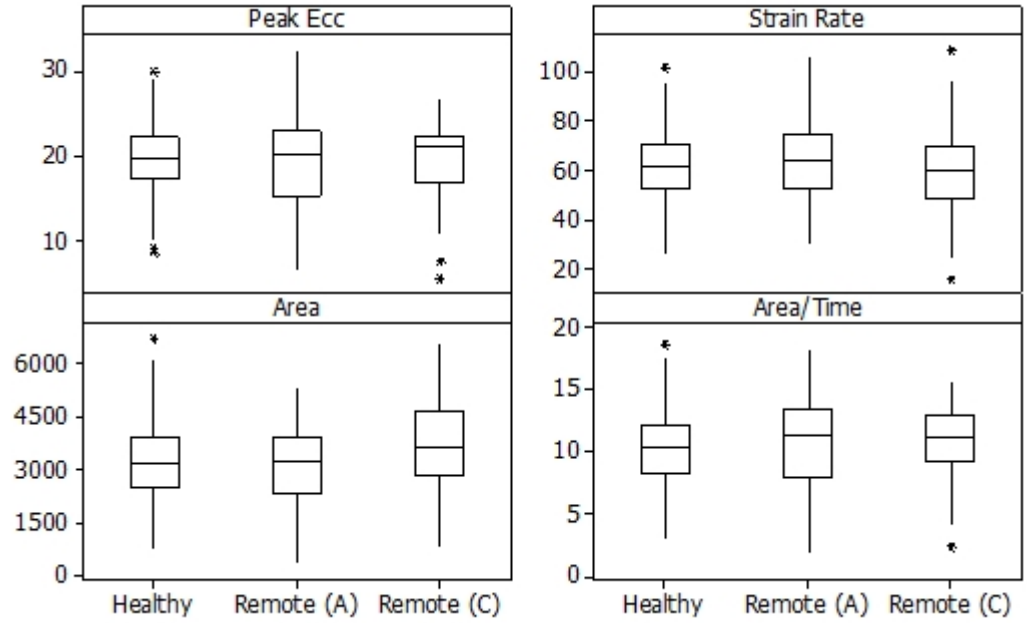

Figure 8-8: Comparison of healthy and remote myocardium in acute and chronic MI

8.4.2 DENSE and Salvage

8.4.2.1. Relationships with MSI

The number of segments allocated to each MSI score is shown in Table 8-8.

Score	Segments
0	9
1	15
2	18
3	34
4	61
5	121

Table 8-8: Allocation of MSI scores in chronic MI

The results of the correlation tests between each of the strain parameters and each of MSI and MSI score are shown in Table 8-9, for both segment and whole slice data. Results are expressed as Pearson correlation coefficients, and statistically significant results are indicated by * ($p<0.05$) and ** ($p<0.001$). The results of both the MSI and MSI score analyses are illustrated using scatter plots in Figure 8-9. Scatter plots illustrating the distribution of data with MSI are shown in Figure 8-10.

	MSI		MSI Score	
Strain Parameter	**Segments**	**Slice**	**Segments**	**Slice**
Peak Ecc	0.40**	0.14	0.49**	0.17
Strain Rate	0.38**	0.08	0.46**	0.13
Area	0.30*	0.24	0.31**	0.23
Area/Time	0.42**	0.24	0.46**	0.26

Table 8-9: Results of MSI and MSI score analysis

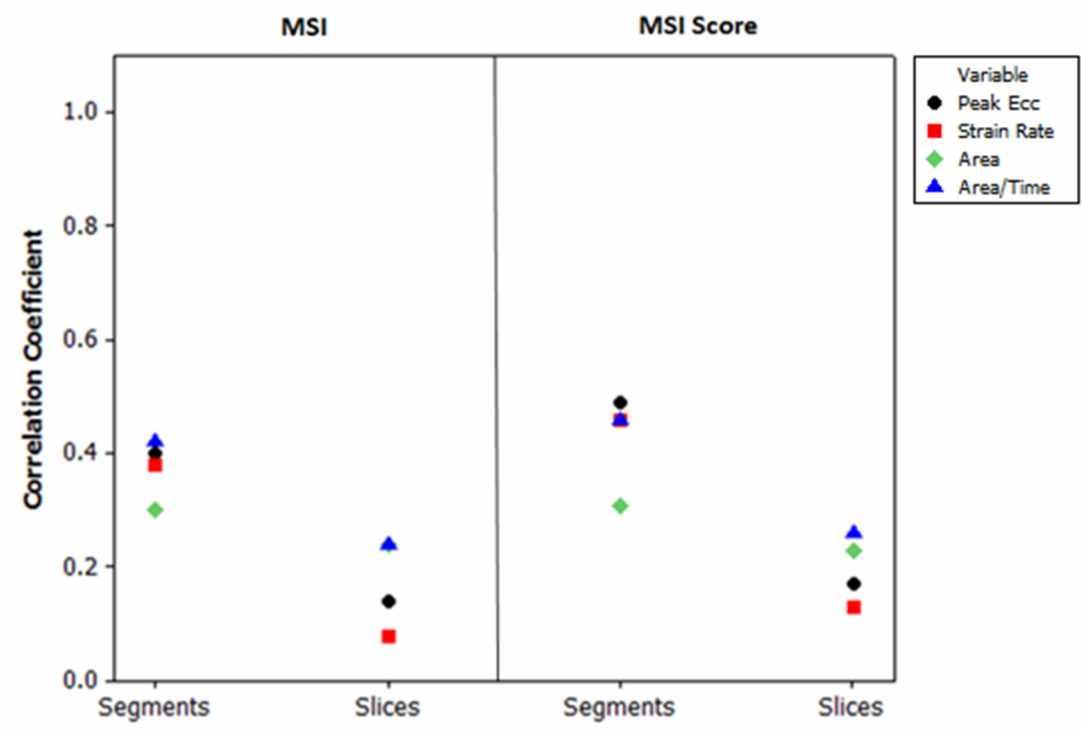

Figure 8-9: Illustration of results for MSI and MSI score

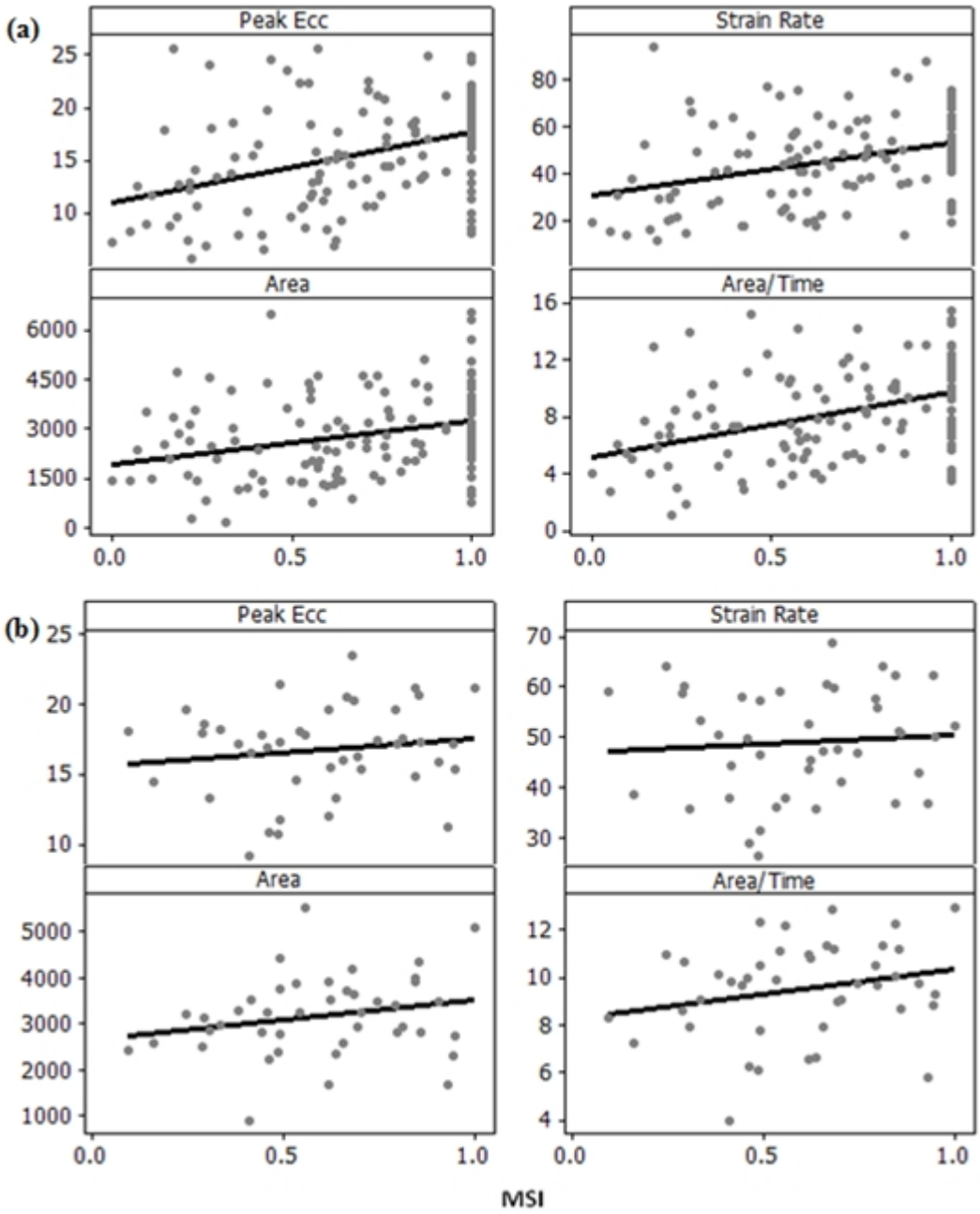

Figure 8-10: Strain parameters vs MSI for a) segment and b) whole slice data

8.4.3 DENSE and Cardiac Function

8.4.3.1. Relationships with LVEF and LVESV

The results of the correlation tests between each of the strain parameters and each of the measures of cardiac function are shown in Table 8-10, and are expressed as Pearson correlation coefficients. Statistically significant results are indicated by * ($p<0.05$) and ** ($p<0.001$). The results are illustrated in scatter plots in Figure 8-11, along with the results from acute MI for comparison.

Parameter	LVEF	LVESV
Peak Ecc	0.45*	-0.37*
Strain Rate	0.38*	-0.30
Area	0.43*	-0.37*
Area/Time	0.50*	-0.41*

Table 8-10: Results of comparison with cardiac function in chronic MI

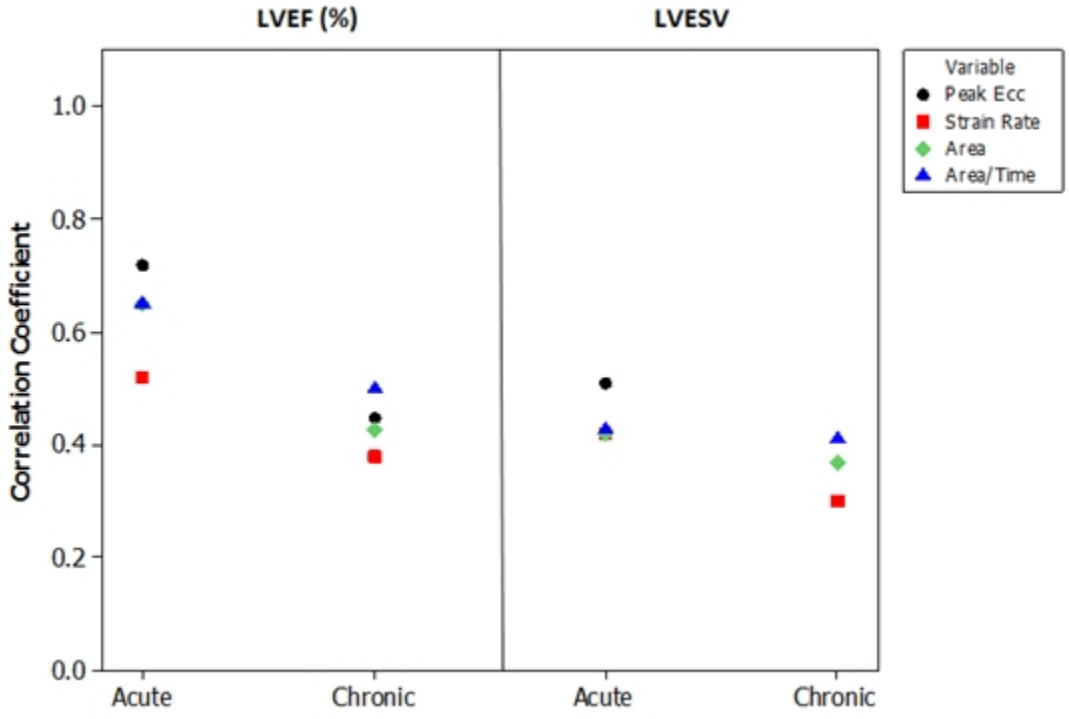

Figure 8-11: Illustration of comparison with cardiac function results in acute and chronic MI

8.4.3.2. Assessment of Longitudinal Changes in Cardiac Function

The results of the correlation tests between the change in each of the strain parameters and the change in each of LVEF and LVESV are shown in Table 8-11, and are expressed as Pearson correlation coefficients. Statistically significant results are indicated by * ($p<0.05$) and ** ($p<0.001$). The results are illustrated in scatter plots in Figure 8-12. Scatter plots illustrating the distribution of data with LVEF and LVESV are shown in Figure 8-13.

Parameter	LVEF	LVESV
Peak Ecc	0.44*	-0.32*
Strain Rate	0.41*	-0.36*
Area	0.36*	-0.27
Area/Time	0.49*	-0.40*

Table 8-11: Results of longitudinal changes in cardiac function analysis

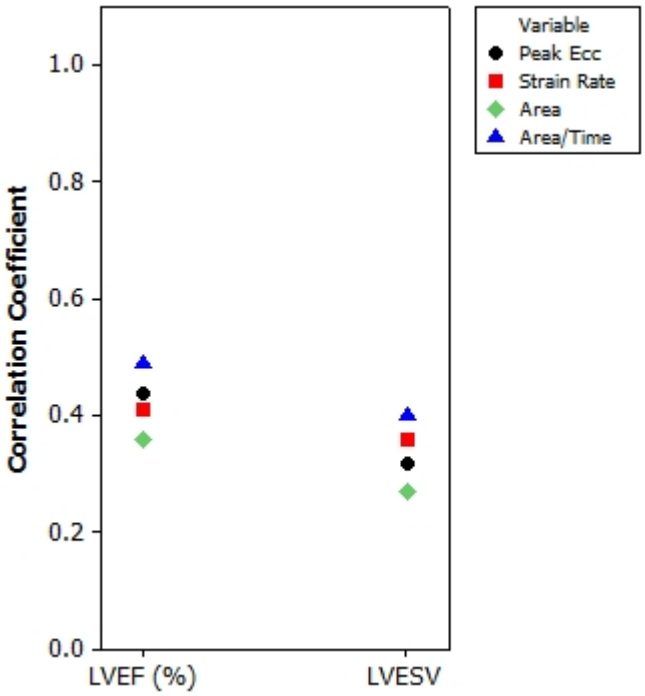

Figure 8-12: Illustration of longitudinal changes in cardiac function results

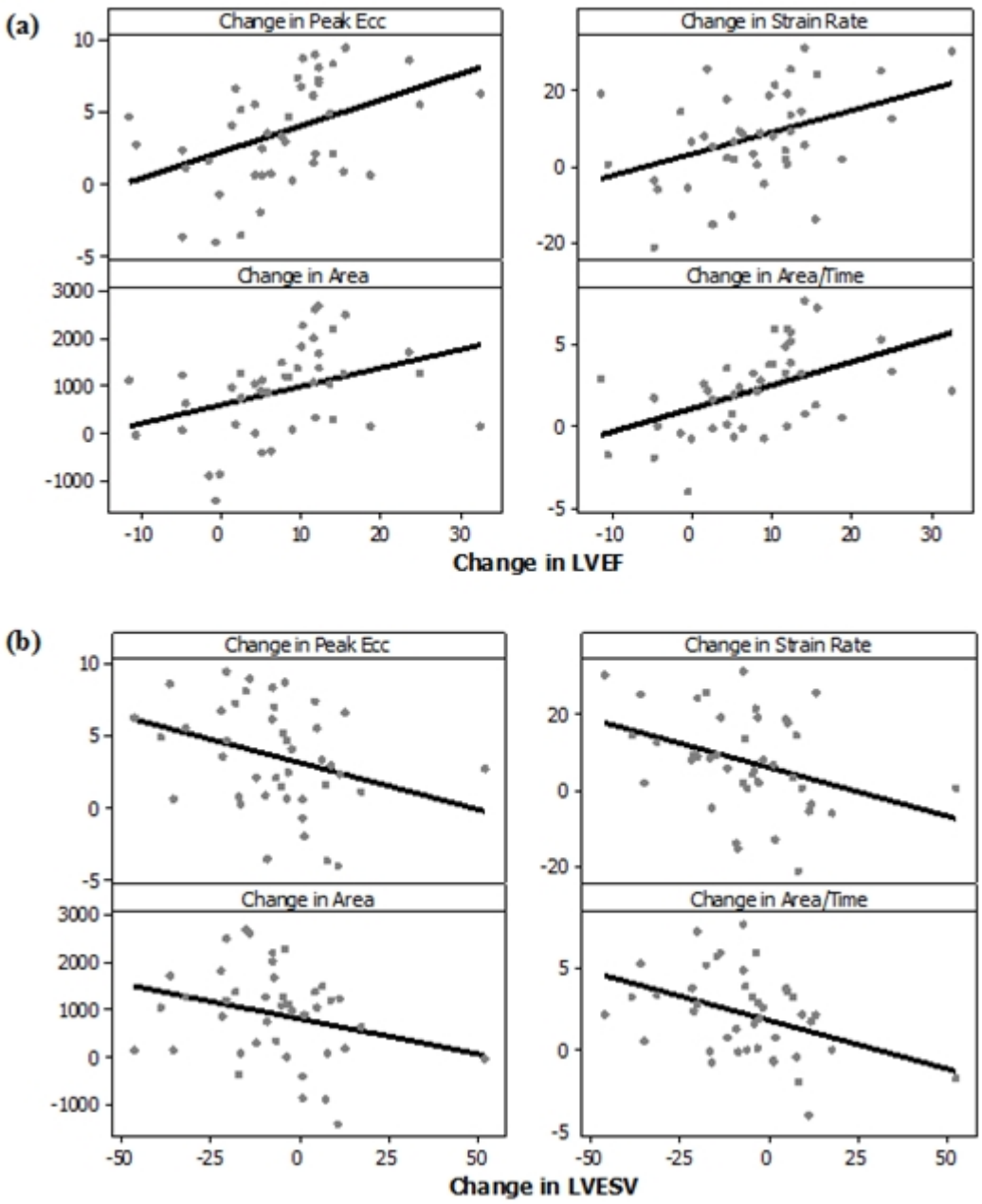

Figure 8-13: Relationships with changes in a) LVEF and b) LVESV

8.5 Discussion

A summary of the key results from this chapter is shown in Table 8-12.

Investigation	Results
DENSE and Infarction	
Relationships with LGE	**Segment analysis:** • Moderate correlation coefficients (~0.5) • Similar results for peak Ecc, strain rate and area/time, with lower correlation coefficients for area • Similar results for LGE% and LGE%_score, with lower correlation coefficients for LGE_score • Lower correlation coefficients than in acute MI **Whole slice analysis (single slice & LV)** • Low correlation coefficients (~0.3 - 0.4) • Similar results for peak Ecc and area/time, with lower correlation coefficients for strain rate and area • Low correlation coefficients (not statistically significant) for whole LV LGE% • Lower correlation coefficients than in acute MI
Extent of Infarction	**LGE%_score and LGE_score:** • Can distinguish between non-infarcted and <50% infarction • Can distinguish between non-infarcted and >50% infarction **LGE%_score only:** • Can distinguish between <50% infarction and >50% infarction
Proximity to Infarction	**LGE%_score and LGE_score:** • Can distinguish between remote and infarcted segments • Can distinguish between adjacent and infarcted segments

Investigation	Results
Detection of Infarction	**Segment analysis:** • ROC analysis revealed moderate AUC values with lower values for area, and lower values than in acute MI • High specificity for all strain parameters • Low sensitivity for all strain parameters • Detection rates increase as %LGE increases • Lower detections rates than in acute MI **Whole slice analysis:** • Low sensitivity for all strain parameters
Assessment of Longitudinal Changes	**Segment analysis:** • Statistically significant increases in strain for both adjacent and remote segments • Statistically significant differences between changes in strain in remote and infarcted segments, and between adjacent and infarcted segments • Statistically significant differences between sub-categories in both adjacent and infarcted segments for strain measurements obtained in acute MI • Statistically significant differences between changes in strain in segments with a decrease in LGE%_score and segments with an increase in LGE%_score • Statistically significant relationships between changes in strain and changes in %LGE, but low correlation coefficients (0.2 – 0.3) **Whole slice analysis:** • No statistically significant relationships between changes in strain and changes in %LGE
Strain in Healthy and Remote Myocardium	• No statistically significant differences between strain in healthy myocardium and remote myocardium in chronic MI, or between remote myocardium in acute and chronic MI

Investigation	Results
DENSE and Salvage	
Relationships with MSI	**Segment analysis:** • Low to moderate correlation coefficients for MSI (~0.4) and MSI score (~0.45 - 0.5) • Similar results for peak Ecc, strain rate and area/time, with lower correlation coefficients for area • Lower correlations in both cases than with area at risk **Whole slice analysis:** • Low correlation coefficients for both MSI and MSI score (~0.1 – 0.3) which are not statistically significant • Lower correlations than with area at risk
DENSE and Cardiac Function	
Relationships with LVEF and LVESV	**LVEF:** • Low to moderate correlation coefficients (~0.4 – 0.5) **LVESV:** • Low correlation coefficients (~0.3 – 0.4)
Assessment of Longitudinal Changes	• Low to moderate correlation coefficients for LVEF (~0.4 - 0.5) • Low correlation coefficients for LVESV (~0.3 - 0.4) • Similar results for peak Ecc, strain rate and area/time, with lower correlation coefficients for area

Table 8-12: Summary of key results in chronic MI

DENSE and Infarction

Relationships with LGE

An investigation into the relationships between strain parameters as measured by DENSE and LGE parameters (LGE%, LGE%_score and LGE_score) in chronic MI revealed statistically significant results when the data were analysed on a segment-by-segment basis and on a whole slice basis (LGE% only). However, the correlations were moderate, and were lower than those obtained in acute MI for all strain parameters. The remodelling process is complex, and this result illustrates that the change in infarct size is not the only factor involved in the recovery of contractile function.

For each LGE parameter, similar correlation coefficients were obtained for peak Ecc, strain rate and area/time, with lower correlation coefficients for area.

For each strain parameter, similar correlation coefficients were obtained with LGE% and LGE%_score, with lower correlation coefficients with LGE_score. This supports the suggestion made in Chapter 7 that strain may be more closely related to the percentage of LGE within the segment than the transmural extent of infarction.

Extent of Infarction

The ability of DENSE strain parameters to distinguish between non-infarcted, <50% infarcted and >50% infarcted segments is similar in chronic MI to the findings in acute MI. Statistically significant differences were found for all strain parameters when comparing non-infarcted and <50% infarcted segments, and non-infarcted and >50% infarcted segments, when the segments are scored using LGE_score or LGE%_score. Statistically significant differences were found between <50% infarcted and >50% infarcted segments for LGE%_score but not for LGE_score.

Proximity to Infarction

The ability of DENSE strain parameters to distinguish between remote, adjacent and infarcted segments is similar in chronic MI to acute MI. Statistically significant differences were found for all strain parameters when comparing remote and infarcted segments, and adjacent and infarcted segments, but while it was possible to

distinguish between remote and adjacent segments using peak Ecc in acute MI, this was not found to be the case in chronic MI.

Detection of Infarction

The ability of DENSE strain parameters for segment data to detect infarction in chronic MI, as indicated by the presence of LGE, was assessed using ROC analysis. For segment data, high AUC values were obtained for peak Ecc, strain rate and area/time with a slightly lower value for area. For all parameters, the AUC values were lower than those obtained in acute MI.

Using the thresholds established in Section 6.4.5, all parameters had high specificity for the detection of infarction, but the sensitivity values were considerably lower (~0.1 – 0.4) than those obtained in acute MI. The sensitivity results obtained for whole slice data were also low. It appears that using strain reference ranges to detect infarction may not be informative in the chronic setting.

When segments were grouped according to LGE%_score, the percentage of infarcted segments which were correctly identified increased as LGE%_score increased. However, the detection rates were lower than in acute MI for all strain parameters.

Assessment of Longitudinal Changes

For segments classified as remote, adjacent and infarcted in acute MI, the strain values in chronic and acute MI were compared using Wilcoxon signed rank tests, and statistically significant differences were observed for both adjacent and infarcted segments. For adjacent segments, the median differences revealed a slight increase in strain for peak Ecc, area and area/time, while larger increases were revealed for all strain parameters in infarcted segments.

The differences between chronic and acute MI for the three categories (remote, adjacent, infarcted) were compared using Kruskal-Wallis with individual Mann-Whitney tests, and the results showed statistically significant differences between the changes in strain in remote and infarcted segments, and between the changes in strain in adjacent and infarcted segments.

Further information was obtained with segments sub-categorised according to the change in proximity to infarction. For segments which were classified as adjacent in acute MI, statistically significant increases in strain were observed in segments which remained classified as adjacent, but no statistically significant differences were observed for segments which were re-classified as remote. Segments which are adjacent to infarction in both acute and chronic MI are more likely to be affected by contractile abnormalities, and by changes in contractile function, in the adjacent infarcted segment, while adjacent segments which are re-categorised as remote appear to behave in a similar way to segments which are categorised as remote in acute MI. No statistically significant differences in strain were observed for adjacent segments which were re-categorised as infarcted, however the number of segments in this sub-category was small, and this may have affected the results.

For each category (remote, adjacent, infarcted), comparisons of the relevant sub-categories showed no statistically significant differences in the changes in strain between acute and chronic MI. However, when the strain measurements obtained in acute MI were compared, statistically significant differences were observed between sub-categories for both adjacent and infarcted segments. Higher strain values were obtained in adjacent segments which would subsequently be re-classified as remote, and lower strain values were obtained in segments which would be re-classified as infarcted. Infarcted segments which would subsequently be re-classified as adjacent had higher strain than those which remained infarcted. Strain measurements in adjacent and infarcted segments in acute MI may have prognostic value relating to the progression or recovery of contractile abnormalities in the chronic setting.

Segments with LGE were grouped according to the change in LGE_score and LGE%_score between acute and chronic MI (lower, unchanged, higher), and the changes in strain parameters between acute and chronic MI were compared for each group. The box plots for LGE%_score showed that the mean change in strain for all three groups was > 0 i.e. an increased value of strain in chronic compared to acute MI, which is consistent with the results of the previous comparison. The box plots also showed a tendency towards larger changes in strain values for segments with a lower score in chronic MI, i.e final infarct size smaller than initial size, and smaller changes in strain values for segments with a higher score in chronic MI, when compared to

segments in which the score was unchanged. Statistically significant differences were observed between changes in strain in segments with a lower score in chronic MI and those with a higher score for peak Ecc, strain rate and area/time. For LGE_score, there was a trend towards higher strain values in segments with a lower score in chronic MI compared to segments with an unchanged score, but there were an insufficient number of segments with a higher score to chronic MI to allow any interpretation to be made, and no statistically significant differences were observed between the groups.

A comparison of change in LGE% and change in strain showed that segments in which LGE decreased over time had a larger increase in strain, and conversely, those in which LGE increased had a lower increase in strain, for all strain parameters. The results were statistically significant, but the correlation coefficients were low. No statistically significant relationships were observed when the data was analysed on a whole slice basis.

While the acute and chronic data used in the comparisons were acquired using the same image acquisition protocol and the same criteria for selecting slice position, the slices are unlikely to be exactly co-located, and this is the main source of error in the analyses described above.

Strain in Remote and Healthy Myocardium

No statistically significant differences were found between strain in healthy myocardium and remote myocardium in chronic MI, or between remote myocardium in acute and chronic MI. In Section 2.2.2, it was mentioned that fibrosis can form in remote tissue as well as infarcted tissue following extensive MI. It is possible that DENSE is not sensitive enough to detect subtle changes in strain caused by remodelling of remote tissue, or the size of the injury in some of the patients included in the analysis may not have been sufficient to result in fibrosis in non-infarcted regions.

DENSE and Salvage

Relationships with MSI

An investigation into the relationships between DENSE strain parameters and MSI revealed statistically significant results for segment data, but with low to moderate correlation coefficients. The correlations obtained when analysing data on a whole slice basis were lower, and were not statistically significant.

Only data from injured segments was included in the MSI analysis. To allow all data to be taken into account, further analysis was performed using a score, MSI score, which included a category for non-injured segments. Moderate correlation coefficients were obtained for segment data, with similar results for peak Ecc, strain rate and area/time and lower correlation coefficients for area. The results of whole slice analysis were similar to those obtained for MSI, with low correlation coefficients which were not statistically significant.

The scatter plots of strain parameters and MSI show a wide range of values corresponding to MSI = 1. Segments with MSI = 1 exhibited T_2 hyperenhancement, i.e. oedema, in the acute setting, but had no evidence of infarction in the chronic setting. Non-infarcted segments which contain oedema are likely to be adjacent to infarcted segments, and since segments are not independent, their contractile function could be impaired.

The correlations between strain and MSI score were lower than those obtained with area at risk in acute MI for both segment and whole slice data. As mentioned previously, the remodelling process is complex, and the relationships between strain and salvage may not be informative.

DENSE and Cardiac Function

Relationships with LVEF and LVESV

An investigation into the relationships between strain parameters as measured by DENSE and LVEF revealed low to moderate correlations for all strain parameters, with lower correlation coefficients than those obtained in acute MI.

Similar results were obtained for LVESV, with low correlations for all strain parameters, and lower correlation coefficients than in acute MI.

Assessment of Longitudinal Changes

Statistically significant correlations between change in strain and change in cardiac function were observed for all strain parameters other than area. However, the correlation coefficients were low to moderate for LVEF, and low for LVESV.

8.6 Summary and Conclusions

The results of the investigations contained within this chapter showed that DENSE can be utilised in chronic MI, however the way in which strain data should be analysed in order to provide the most informative results differs from in acute MI.

The results obtained by separating segments into categories are similar to those obtained in acute MI. DENSE strain parameters can be used to differentiate between segments categorised as non-infarcted, <50% infarcted and >50% infarcted, particularly when the segments are scored using LGE%_score. It is also possible to differentiate between remote and infarcted segments, and between adjacent and infarcted segments, but unlike in acute MI, it is not possible to differentiate between remote and adjacent segments.

DENSE has high specificity for the detection of infarction in chronic MI, but lower sensitivity than in the acute setting. Detection rates increase as the percentage of LGE within the segment increases, but are lower than the corresponding detection rates in acute MI. The use of strain reference ranges for the detection of infarction may not be informative in chronic MI.

Strain correlates more closely with MSI score, which takes both non-injured and injured segments into account, than with MSI. However, the correlation coefficients in both cases are low to moderate, and the relationships between DENSE strain parameters and salvage may not be informative.

As in acute MI, strain appears to be more closely correlated with LVEF than LVESV. However, the correlation coefficients obtained in chronic MI are low to moderate, and

the relationships between DENSE strain parameters and cardiac function in chronic MI may not be informative.

The most informative results obtained using DENSE in chronic MI relate to longitudinal changes in contractile function over time. Statistically significant increases in strain were observed in both infarcted and adjacent segments. With segments sub-categorised according to change in proximity to infarction, statistically significant differences in strain measured in acute MI were observed for both adjacent and infarcted segments, which indicates that acute strain measurements may have prognostic value relating to the progression or recovery of contractile function in the chronic setting. For infarcted segments, statistically significant differences were observed between segments in which the final extent of LGE increased and those in which the final extent of LGE decreased.

There are statistically significant relationships between the change in strain and the change in LGE%, and between the change in strain and change in cardiac function, but in both cases, the correlation coefficients were low, and a wide spread of results were observed.

In acute MI, segment and whole slice data provided similar information on the relationships with, and detection of, infarction and injury. In chronic MI, whole slice data appears to be less informative than segment data, and the main reason to perform whole slice analysis would be to allow comparison with cardiac function. However, the correlations with chronic measures of cardiac function and changes in cardiac function were both low, and the benefit of performing this analysis is uncertain.

As in acute MI, peak Ecc, strain rate and area/time appear to be more informative strain parameters than area. It was thought that parameters which took account of how strain varied from the start of the cardiac cycle up to end-systole may provide additional information compared to measurements made at a single time point. However, the results of this study have provided no evidence of this, and since measurement of area and area/time require additional post-processing, it is suggested that future studies should focus on peak Ecc and strain rate.

Chapter 9

Summary and Future Directions

9.1 Summary of Main Findings

9.1.1 DENSE Image Acquisition and Analysis

The main findings from this study relating to DENSE image acquisition and analysis are illustrated in Figure 9-1.

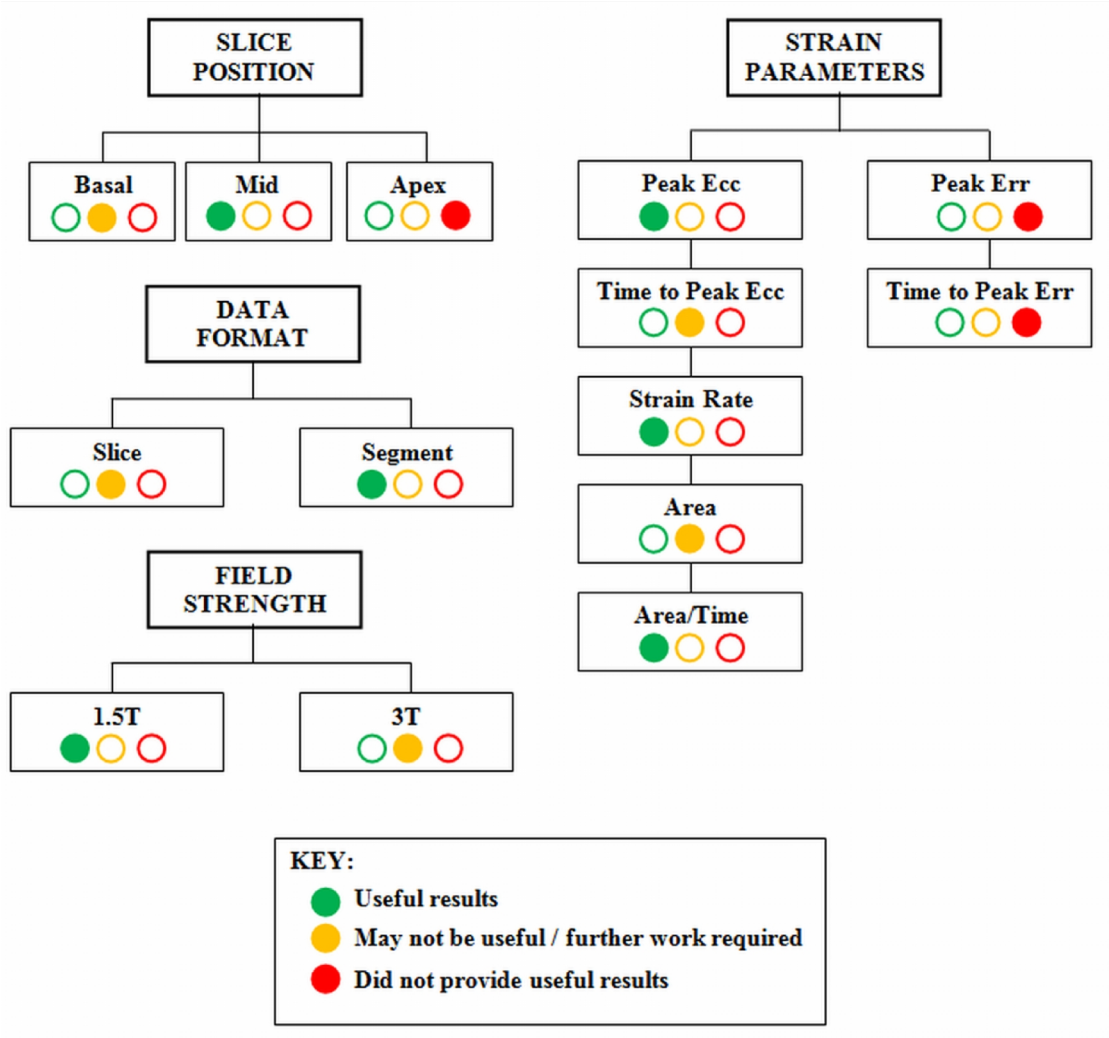

Figure 9-1: Illustration of main findings relating to DENSE image acquisition and analysis

The first steps in the investigation of DENSE image acquisition and analysis, prior to performing the evaluations illustrated in Figure 9-1, were to compare the strain measurements obtained using DENSE with measurements obtained using other techniques, and to assess the repeatability of strain values obtained using DENSE.

Strain measurements obtained using DENSE were found to be in reasonable agreement with measurements obtained using tagging in healthy subjects, and also with values reported in the literature.

The results obtained in Chapter 4 and Chapter 5 showed that high intra-operator, inter-operator and inter-scan repeatability were obtained for measurements of peak Ecc and time to peak Ecc, although the limits of agreement between scans for time to peak Ecc were wide and potentially clinically significant. Further investigation of repeatability according to the degree of hypokinesis showed statistically significant, and potentially clinically significant, differences in time to peak Ecc measured in severely hypokinetic segments compared to other segments, and hence it was recommended that measurements of time to peak Ecc which corresponded to measurements of peak Ecc < 5% should be excluded from further analysis. Three additional strain parameters (strain rate, area and area/time) were introduced in Chapter 6, and measurements of strain rate and area/time, which are related to time to peak Ecc, obtained from severely hypokinetic segments should also be excluded from further analysis.

The results for peak Err and time to peak Err were similar to those obtained for peak Ecc and time to peak Ecc, with the exception that statistically significant differences in inter-operator and inter-scan repeatability were observed for peak Err. During the healthy volunteer study described in Chapter 6, it became apparent that measurements of peak Err were unreliable, with only 21% of acquired radial strain datasets being suitable for analysis. This finding indicated that radial strain data acquired using the current implementation of DENSE should not be used in the assessment of contractile function.

For both the healthy volunteer and patient studies in Chapters 6 - 8, DENSE images were acquired from three short axis slices – basal, mid-ventricular and apical. The

analysis software (CIM_DENSE2D) is restricted to 6 segment analysis which is not appropriate for apical slices, and the position of the apical slices was often too close to the apex, which resulted in distorted strain curves. In this study, apical strain data obtained using DENSE was not found to be informative. Issues also occurred with the positioning of basal slices. Many slices were positioned too close to the LVOT, resulting in distorted strain curves, and overcompensation for this then led to "basal" slices being positioned in a mid-ventricular location. A sufficient number of basal images were acquired to allow comparison of basal and mid-ventricular strain in healthy subjects, but no further analysis of basal strain was performed. DENSE has the potential to provide information on basal strain, but particular care must be taken with regards to slice positioning.

Analysis of DENSE images can be performed on both whole slices and segments. In acute MI (Chapter 7), both slice and segment analysis provided information on the relationships with LGE and area at risk, and allowed detection of infarction with moderate to good sensitivity. Segment analysis produced slightly higher correlations and better sensitivity, and also provided additional information on the extent of infarction within segments and their proximity to infarction. Whole slice analysis provided information on the relationships between strain and cardiac function which was not obtainable from segment analysis. However, in chronic MI (Chapter 8), whole slice data appears to be less informative than segment data, and the main reason to perform whole slice analysis would be to allow comparison with cardiac function. The correlations between strain and both chronic measures of cardiac function and changes in cardiac function were low, and the benefit of performing this analysis is uncertain.

The majority of the DENSE strain data used within this thesis was acquired using a 1.5T MRI scanner, but as 3T scanners are becoming more common in both clinical and research settings, a comparison with strain data acquired at 3T was performed in Chapter 6 to facilitate future research projects and potential clinical applications involving DENSE. Higher strain values were obtained at 1.5T than 3T for all strain parameters, but although the differences were statistically significant, the magnitudes of the differences were small and are unlikely to be clinically significant. The 3T scanner has a 70cm bore, and it is more challenging to achieve good homogeneity

than with the 60cm bore 1.5T scanner. Further optimisation of the image acquisition protocol is recommended prior to any future studies involving DENSE at 3T.

Several circumferential and radial strain parameters were calculated from DENSE images and applied throughout this thesis. As mentioned previously, radial strain (Err) measurements were found to be unreliable, and were not considered from Chapter 6 onwards. Five parameters relating to circumferential strain (Ecc) were calculated – peak Ecc, time to peak Ecc, strain rate, area under Ecc curve (area) and average area under Ecc curve over time (area/time). Peak Ecc, time to peak Ecc and strain rate are inter-related, and performing analysis on all three of these parameters may be excessive. The rate at which strain increases to the peak value was considered to be more informative than the time taken to reach the peak, and so all analysis from Chapter 7 onwards was performed for peak Ecc, strain rate, area and area/time. For many of the investigations performed, similar results were obtained for peak Ecc, strain rate and area/time, with a slightly poorer performance for area. The results of the detection of infarction analysis in acute MI (Chapter 7) showed that peak Ecc has the highest sensitivity and is the only parameter which can distinguish between segments categorised as remote and adjacent, which implies that this may be the most informative strain parameter in MI. Information relating to the time taken to reach the peak strain value, e.g. strain rate, is also important, since a heart which contracts rapidly to a given peak Ecc value may be very different clinically from a heart which contracts slowly but achieves the same peak value. It was thought that parameters which took account of how strain varied from the start of the cardiac cycle up to end-systole may provide additional information compared to measurements made at a single time point, however the results of this study have shown no particular advantages to measuring area and area/time. Since measurements of area and area/time require additional post-processing, it is recommended that future studies relating to MI should focus on peak Ecc and strain rate.

DENSE images were successfully acquired and analysed from both healthy subjects and patients with myocardial infarction, which indicates that the technique is feasible in different clinical settings. One of the main challenges associated with acquiring DENSE images is the long breath hold, which can be up to 20 seconds. While the number of images considered to be non-diagnostic in this study was small (~4% in

both healthy volunteers and chronic MI patients), this is a potential obstacle to the inclusion of DENSE into routine clinical imaging. Developments of the DENSE pulse sequence are continuing, as described in Section 2.4.4.6, and implementation of a pulse sequence with a shorter breath hold or with navigator-gating would be desirable. It would also be beneficial to provide in-line processing for DENSE, as this would allow a preliminary assessment of the strain curves to be carried out while the patient was still in the scanner, and images which are potentially non-diagnostic could be re-acquired.

9.1.2 Performance of DENSE in Patients with Myocardial Infarction

The main findings from this study relating to the application and performance of DENSE in patients with myocardial infarction are illustrated in Figure 9-2.

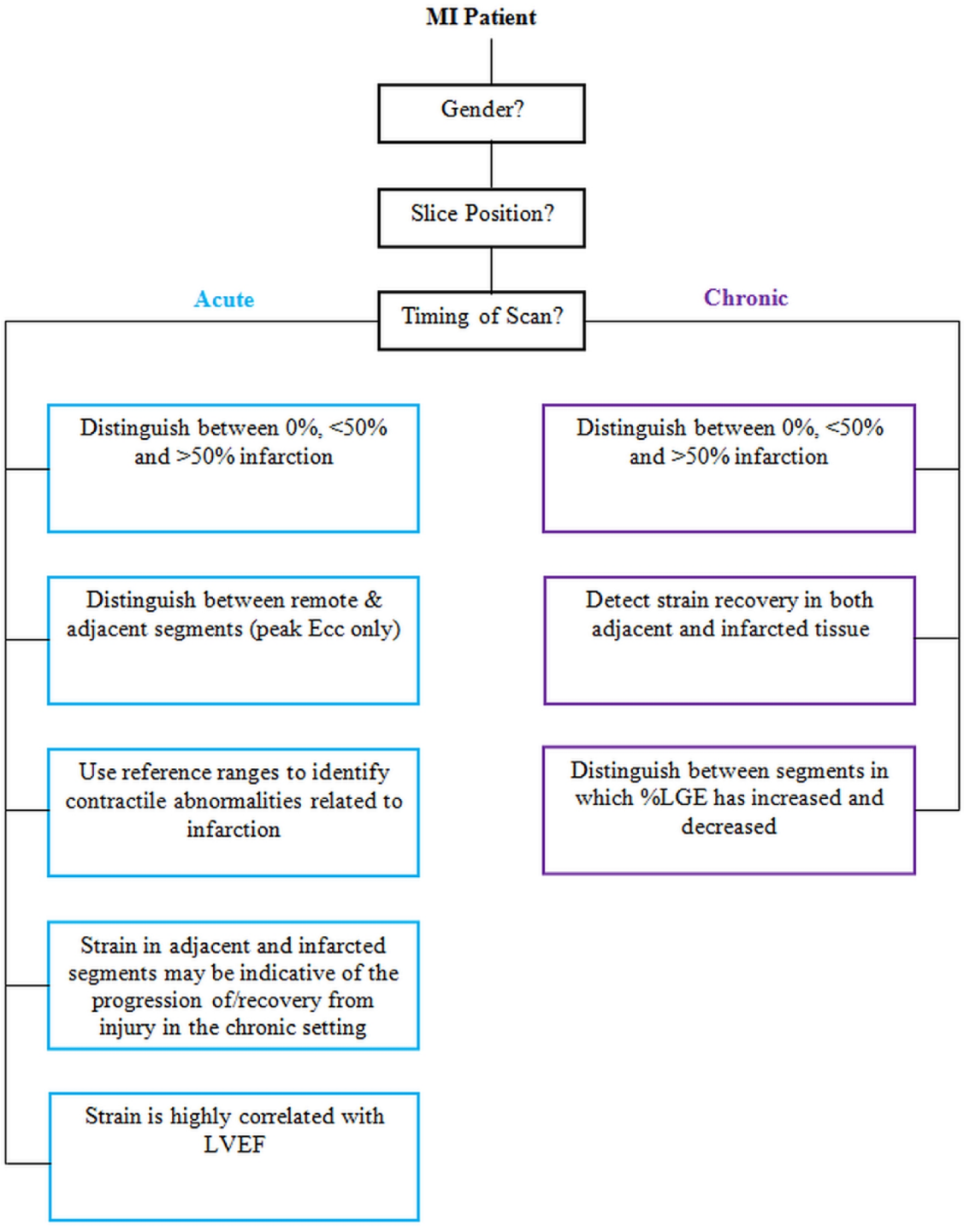

Figure 9-2: Illustration of the application and performance of DENSE in patients with myocardial infarction

The results of the healthy volunteer study in Chapter 6 indicated that there are three factors which must be taken into account to allow appropriate analysis of DENSE data acquired from MI patients: 1) patient gender (M/F), 2) slice position (basal/mid) and 3) timing of scan (acute/chronic).

Although the same DENSE strain parameters are obtained in both acute and chronic MI, the results obtained in Chapters 7 and 8 suggest that the way in which the data should be analysed in order to provide the most informative results depends on the timing of the scan.

In both acute and chronic MI, DENSE strain parameters can be used to distinguish between segments with 0%, <50% and >50% infarction. In this thesis, strain parameters from acute MI patients were compared to reference ranges established using data from healthy volunteers to assess whether infarction was present. It is possible that the data from this group of acute MI patients could be used to establish additional reference ranges, which could then be tested on data from another group of MI patients to investigate whether the extent of infarction can also be assessed.

In acute MI, four further potential applications of DENSE were identified:

- Peak Ecc can be used to distinguish between remote and adjacent segments. It is possible that the data from this group of acute MI patients could be used to establish additional reference ranges, which could then be tested on data from another group of MI patients to investigate whether the proximity to infarction can also be assessed.
- Reference ranges can be used to identify the presence of infarction with high specificity and moderate to high sensitivity.
- In segments which are classified as adjacent or remote, there are statistically significant differences in strain when the segments are sub-classified according to the subsequent classification in chronic MI. Strain measurements may provide prognostic information relating to the potential progression or recovery of contractile abnormalities. As for the detection of infarction, it is possible that the data from this group of acute MI patients could be used to establish additional reference ranges, which could then be tested on data from another

group of MI patients to investigate whether the potential progression of contractile abnormalities can be predicted.

- Peak Ecc is highly correlated with LVEF, and perhaps a scoring system could be constructed using peak Ecc to allow a preliminary assessment of cardiac function.

The first two applications may be of particular interest in patient groups where gadolinium contrast agents cannot be given e.g. patients with poor renal function. The remaining applications may also be of interest in this group, but could also be used in the wider MI population to assist with prediction of outcome and assessment of function.

In chronic MI, two further applications of DENSE were identified:

- Strain recovery can be detected in both adjacent and infarcted segments. Quantitative analysis allows improvements in contractile function to be identified which may be missed by conventional qualitative analysis of cine imaging.
- Strain measurements can be used to distinguish between segments in which LGE% has increased and those in which it has decreased.

Again, these applications have the potential to be of interest in both patient groups with poor renal function, and in the wider MI population.

In both acute and chronic MI, strain was found to be more closely related to the percentage of LGE within a segment than to the transmural extent of LGE. However, it is possible that neither score individually is fully representative of the injury caused by myocardial infarction, and it may be more informative to consider an additional score which takes into account both the size of the infarction and the transmural extent.

To conclude, the hypotheses established in Chapter 1 will be evaluated:

1. There is no difference in myocardial strain as measured by DENSE and myocardial strain as measured by other techniques. ***TRUE: Strain as measured by DENSE is in reasonable agreement with strain as measured by tagging, and with reported values in the literature.***
2. There is a strong relationship between DENSE strain parameters and the extent of myocardial infarction. ***TRUE: DENSE strain parameters have a high correlation with both the transmural extent of LGE and the percentage of LGE.***
3. DENSE strain parameters can be used to distinguish between varying extents of infarction. ***TRUE: DENSE strain parameters can be used to distinguish between 0%, <50% and >50% infarction in both acute and chronic MI when segments are scored according to the percentage of LGE.***
4. DENSE strain parameters can be used to distinguish between remote and infarcted tissue. ***TRUE: DENSE strain parameters can distinguish between remote and infarcted tissue, and between adjacent and infarcted tissue in both acute and chronic MI.***
5. DENSE strain parameters have high sensitivity and specificity for the detection of contractile abnormalities associated with myocardial infarction and injury. ***TRUE: DENSE strain parameters have moderate to high sensitivity and high specificity for the detection of contractile abnormalities associated with infarction and injury in acute MI, but lower sensitivity in chronic MI.***
6. Longitudinal measurements of strain with DENSE provide information relating to the changes in myocardial function over time following infarction. ***TRUE: Strain parameters allow detection of strain recovery in adjacent and infarcted segments, which may be missed by conventional qualitative assessments, and can distinguish between segments in which the percentage of LGE has increased and those in which it has decreased.***

9.2 Potential Future Studies

The first suggestion for a potential future study was mentioned during the discussion in Section 9.1. In this study, strain data from MI patients were compared to references ranges established using strain data from healthy volunteers to assess whether infarction was present. The data from MI patients could potentially be used to establish additional reference ranges, which could then allow further assessment of the extent of infarction i.e. <50% or >50%. This could be tested using strain data from a second group of MI patients.

The version of CIM_DENSE2D used in this study had the capability to analyse radial and circumferential strain from short axis images. An updated version of CIM_DENSE2D is currently being developed which will have the capability to analyse longitudinal strain from 4-chamber long axis images. Long axis DENSE images were acquired for all of the subjects who participated in the healthy volunteer study described in Chapter 6, and the investigations described in this thesis for the evaluation of circumferential strain could be repeated for longitudinal strain when the software becomes available.

DENSE has been shown to be informative in patients with ST-elevation myocardial infarction (STEMI), and the performance in other patient groups could now be evaluated. Patients with non-ST-elevation myocardial infarction (NSTEMI) often have smaller infarctions, and the ability of DENSE to identify more subtle contractile abnormalities could be investigated. There is also the potential to investigate changes in strain during pharmaceutical stress e.g. with adenosine, perhaps in healthy subjects and in patients with reversible ischaemia. However, the long breath hold associated with DENSE may not be feasible under stress conditions.

With the current implementation of DENSE, radial strain data was found to be unreliable, and the long breath hold is likely to be an obstacle for future research and clinical applications. Many of the further developments in DENSE described described in Section 2.4.4.6 were performed on Siemens MRI scanners, and opportunities for collaborations with the research groups carrying out this work should be investigated.

References

1. Gotte MJ, Van Rossum AC, Twisk JWR, Kuijer JPA, Marcus JT, Visser CA. Quantification of Regional Contractile Function After Infarction: Strain Analysis Superior to Wall Thickening Analysis in Discriminating Infarct From Remote Myocardium. J Am Coll Cardiol 2001; 37(3): 808 – 817
2. Peshock RM, Rokey R, Malloy GM, McNamee P, Buja LM, Parkey RW, Willerson JT. Assessment of Myocardial Systolic Wall Thickening Using Nuclear Magnetic Resonance Imaging. J Am Coll Cardiol 1989; 14: 653 – 659
3. Jolman ER, Buller VG, de Roos A, van der Geest RJ, Baur LH, van der Laarse A, Bruschke AV, Reiber JH, van der Wall EE. Detection and Quantification of Dysfunction Myocardium by Magnetic Resonance Imaging: A New Three-dimensional Method for Quantitative Wall-thickening Analysis. Circulation 1997; 95: 924 - 931
4. Axel L, Goncalves RC, Bloomgarden D. Regional Heart Wall Motion: Two-dimensional Analysis and Functional Imaging with MR Imaging. Radiology 1992; 183: 745 – 750
5. Kolipaka A, Chatzimavroudis GP, White RD, Lieber ML, Setser RM. Relationship Between the Extent of Non-viable Myocardium and Regional Left Ventricular Function in Chronic Ischemic Heart Disease. J Cardiovasc Magn Reson 2005; 7: 573 - 579
6. http://www.nhlbi.nih.gov/health/health-topics/topics/hhw/, cited 16/01/12
7. http://www.cvphysiology.com/Blood%20Flow/BF001.htm, cited 16/01/12
8. Martini FH. Fundamentals of Anatomy and Physiology, 7th Edition. San Francisco: Benjamin Cummings (Pearson Education Inc.); 2006
9. Iaizzo PA. Handbook of Cardiac Anatomy, Physiology, and Devices, 2nd Edition. New York: Springer Science+Business Media; 2009
10. Pfeffer MA. Left Ventricular Remodeling After Acute Myocardial Infarction. Annu Rev Med 1995; 46: 455 - 466
11. St. John Sutton MG, Sharpe N. Left Ventricular Remodeling After Myocardial Infarction: Pathophysiology and Therapy. Circulation 2000; 101: 2981 – 2988

12. Sun Y. Myocardial Repair/Remodelling Following Infarction: Roles of Local Factors. Cardiovascular Research 2009; 81: 482 – 490
13. Friedrich M. Myocardial Edema – A New Clinical Entity? Nat Rev Cardiol 2010; 7: 292 – 296
14. Abdel-Aty H, Sinonetti O, Friedrich MG. T2-Weighted Cardiovascular Magnetic Resonance Imaging. J Magn Reson Imaging 2007; 26: 452 - 459
15. Kleber AG. ST-Segment Elevation in the Electrocardiogram: A Sign of Myocardial Ischaemia. Cardiovascular Research 2000; 45: 111 – 118
16. Cerqueira MD, Weissnam NJ, Dilsizian V, et al. Standardized Myocardial Segmentation and Nomenclature for Tomographic Imaging of the Heart. Circulation 2002; 105: 539 – 542
17. Hundley WG, Bluemke D, Bogaert JG, Friedrich MG, Higgins CB, Lawson MA, McConnell MV, Raman SV, van Rossum AC, Flamm S, Kramer CM, Nagel E, Neubauer S. Society for Cardiovascular Magnetic Resonance Guidelines for Reporting Cardiovascular Magnetic Resonance Examinations. J Cardiovasc Magn Reson 2009; 11: 5
18. Chavhan GB, Babyn PS, Jankharia BG, Cheng HLM, Shroff MM. Steady-State MR Imaging Sequences: Physics, Classification and Clinical Applications. Radiographics 2008; 28: 1147 - 1160
19. Fuchs F, Laub G, Othomo K. TrueFISP – Technical Considerations and Cardiovascular Applications. Eur J Radiol 2003; 46: 28 – 32
20. Bluemke DA, Boxerman JL, Atalar E, McVeigh ER. Segmented K-Space Cine Breath-Hold Cardiovascular MR Imaging: Part 1. Principles and Technique. Am J Roentgenol 1997; 169: 395 - 400
21. Götte MJW, van Rossum AC, Twisk JWR, Kuijer JPA, Marcus, JT, Visser CA. Quantification of Regional Contractile Function After Infarction: Strain Analysis Superior to Wall Thickening Analysis in Discriminating Infarct From Remote Myocardium. J Am Coll Cardiol 2001; 37: 808 – 817
22. Nikitin NP, Loh PH, de Silva R, Witte KKA, Lukaschuk EI, Parker A, Farnsworth TA, Alamgir FM, Clark AL, Cleland JGF. Left Ventricular Morphology, Global and Longitudinal Function in Normal Older Individuals: A Cardiac Magnetic Resonance Study. Int J Cardiol 2006; 108: 76 - 83

23. Pflugfelder PW, Sechtem UP, White RD, Higgins CB. Quantification of Regional Myocardial Function by Rapid Cine MR Imaging. Am J Roentgenol 1988; 150: 523 – 529
24. Sechtem UP, Sommerhoff BA, Markiewicz W, White RD, Cheitlin MD, Higgins C. Regional Left Ventricular Wall Thickening by Magnetic Resonance Imaging: Evaluation in Normal Persons and Patients With Global and Regional Dysfunction. Am J Cardiol 1987; 59: 145 – 51
25. Lee VS. Cardiovascular MRI: Physical Principles to Practical Protocols. Philadelphia: Lippincott Williams & Wilkins; 2006
26. Edelman RR. Contrast-Enhanced MR Imaging of the Heart: Overview of the Literature. Radiology 2004; 232: 653 – 668
27. Kramer CM, Barkhaysen J, Flamm SD, Kim RJ, Nagel E. Standardized Cardiovascular Magnetic Resonance Imaging (CMR) Protocols, Society for Cardiovascular Magnetic Resonance: Board of Trustees Task Force on Standardized Protocols. J Cardiovasc Magn Reson 2008; 10: 35 - 45
28. Simonetti OP, Kim RJ, Fieno DS, Hillenbrand HB, Wu E, Bundy JM, Finn JP, Judd RM. An Improved MR Imaging Technique for the Visualization of Myocardial Infarction. Radiology 2001; 218: 215 – 223
29. Haase A, Frahm J, Matthaei D, Hanicke W, Merboldt KD. FLASH Imaging – Rapid NMR Imaging Using Low Flip-Angle Pulses. J Magn Reson 1986; 67: 258 – 266
30. Kim RJ, Fieno DS, Parrish TB, Harris K, Chen EL, Simonetti O, Bundy J, Finn JP, Klocke FJ, Judd RM. Relationship of MRI Delayed Contrast Enhancement to Irreversible Injury, Infarct Age and Contractile Function. Circulation 1999; 100: 1992 - 2002
31. Fieno DS, Kim RJ, Chen EL, Lomasney JW, Klocke FJ, Judd RM. Contrast-Enhanced Magnetic Resonance Imaging of Myocardium at Risk: Distinction Between Reversible and Irreversible Injury Through Infarct Healing. J Am Coll Cardiol 2000; 36: 1985 – 1991
32. Flett AS, Hasleton J, Cook C, Hausenloy D, Quarta G, Ariti C, Muthurangu V, Moon JC. Evaluation of Techniques for the Quantification of Myocardial Scar of Differing Etiology Using Cardiac Magnetic Resonance. JACC Cardiovasc Imaging 2011; 4: 150 – 156

33. Schaefer S, Malloy CR, Katz J, Parkey RW, Buja LM, Willerson JT, Peshock RM. Gadolinium-DTPA-Enhanced Nuclear Magnetic Resonance Imaging of Reperfused Myocardium: Identification of the Myocardial Bed at Risk. J Am Coll Cardiol 1988; 12: 1064 – 1072
34. Masui T, Saeed M, Wendland MF, Higgins CB. Occlusive and Reperfused Myocardial Infarcts: MR Imaging Differentiation with Nonionic Gd-DTPA-BMA. Radiology 1991; 181: 77 – 83
35. Kim RJ, Fieno DS, Parrish TB, Harris K, Chen EL, Simonetti O, Bundy J, Finn JP, Klocke FJ, Judd RM. Relationship of MRI Delayed Contrast Enhancement to Irreversible Injury, Infarct Age and Contractile Function. Circulation 1999; 100: 1992 - 2002
36. Kellman P, Aletras AH, Mancini C, McVeigh ER, Arai AE. T_2-Prepared SSFP Improves Diagnostic Confidence in Edema Imaging in Acute Myocardial Infarction Compared to Turbo Spin Echo. Magn Reson Med 2007; 57: 891 – 897
37. Giri S, Chung YC, Merchant A, Mihai G, Rajagopalan S, Raman SV, Simonetti OP. T_2 Quantification for Improved Detection of Myocardial Edema. J Cardiovasc Magn Reson 2009; 11: 56
38. Brittain JH, Hu BS, Wright GA, Meyer CH, Macovski A, Nishimura DG. Coronary Angiography with Magnetization-Prepared T_2 Contrast. Magn Reson Med 1995; 33: 689 - 696
39. Lonborg J, Vejlstrup N, Mathiasen AB, Thomsen C, Jensen JS, Engstrom T. Myocardial Area At Risk and Salvage Measured by T2-Weighted Cardiovascular Magnetic Resonance: Reproducibility and Comparison of Two T2-Weighted Protocols. J Cardiovasc Magn Reson 2011; 13:50
40. Berry C, Kellman P, Mancini C, Chen MY, Bandettini WP, Lowrey T, Hsu LY, Aletras AH, Arai AE. Magnetic Resonance Imaging Delineates the Ischemic Area-at-Risk and Myocardial Salvage in Patients with Acute Myocardial Infarction. Circ Cardiovasc Imaging 2010; 3: 527 – 535
41. Eitel I, Desch S, Fuernau G, Hilderbrand L, Gutberlet M, Schuler G, Thiele H. Prognostic Significance and Determinants of Myocardial Salvage Assessed by Cardiovascular Magnetic Resonance in Acute Myocardial Infarction. J Am Coll Cardiol 2010; 55: 2470 - 2479

42. Croisille P, Kim KW, Kim RJ. Controversies in Cardiovascular MR Imaging: T2-weighted Imaging Should Not Be Used to Delineate the Area at Risk in Ischemic Myocardial Injury. Radiology 2012; 256: 12 - 22
43. Garcia-Dorado D, Oliveras J, Gili J, Sanz E, Perez-Villa F, Barrabes J, Carreras MJ, Solares J, Soler-Soler J. Analysis of Myocardial Oedema by Magnetic Resonance Imaging Early After Coronary Artery Occlusion With or Without Reperfusion. Cardiovasc Res 1993; 27: 1462 - 1469
44. Aletras AH, Tilak GS, Natanzon A, Hsu LY, Gonzalez FM, Hoyt RF, Arai AE. Retrospective Determination of the Area at Risk for Reperfused Acute Myocardial Infarction with T2-Weighted Cardiac Magnetic Resonance IMaging: Histopathalogical and Displacement Encoding with Stimulated Echoes (DENSE) Functional Validations. Circulation 2006; 113: 1865 - 1870
45. Tilak GS, Hsu LY, Hoyt RF, Arai AE, Aletras AH. In Vivo T2-Weighted Magnetic Resonance Imaging Can Accurately Determine the Ischemic Area at Risk for 2-Day-Old Nonreperfused Myocardial Infarction. Invest Radiol 2008; 43: 7 - 15
46. Simpson RM, Keegan J, Firmin DN. MR Assessment of Regional Myocardial Mechanics. J Magn Reson Imaging 2013; 37: 576 - 599
47. Blessberger H, Binder T. Two Dimensional Speckle Tracking Echocardiography: Basic Principles. Heart 2010; 96: 716 – 722
48. Zerhouni EA, Parish DM, Rogers WJ, Yang A, Shapiro EP. Human Heart: Tagging with MR Imaging – A Method for Noninvasive Assessment of Myocardial Motion. Radiology 1988; 169: 59 – 63
49. Ibrahim ESH. Myocardial Tagging by Cardiovascular Magnetic Resonance: Evolution of Techniques – Pulse Sequences, Analysis Algorithms and Applications. J Cardiovasc Magn Reson 2011; 13: 36
50. Axel L, Dougherty L. MR Imaging of Motion with Spatial Modulation of Magnetization. Radiology 1989; 171: 841 – 845
51. Axel L, Dougherty L. Heart Wall Motion: Improved Method of Spatial Modulation of Magnetization for MR Imaging. Radiology 1989; 172: 349 - 350
52. Mosher TJ, Smith MB. A DANTE Tagging Sequence for the Evaluation of Translational Sample Motion. Magn Reson Med 1990; 15: 334 - 339

53. Morris GA, Freeman R. Selective Excitation in Fourier Transform Nuclear Magnetic Resonance. J Magn Reson 1978; 29: 433 – 362
54. McVeigh ER, Atalar E. Cardiac Tagging with Breath-Hold Cine MRI. Magn Reson Med 1992; 28: 318 - 327
55. Fischer SE, McKinnon GC, Maier SE, Boesiger P. Improved Myocardial Tagging Contrast. Magn Reson Med 1993; 30: 191 – 200
56. Arts T, Frits WP, Delhaas T, Milles JR, Rossi AC, Clarysse P. Mapping Displacement and Deformation of the Heart with Local Sine-Wave Modeling. IEEE Trans Med Imaging 2010; 29: 1114 - 1123
57. McVeigh ER, Zerhouni EA. Noninvasive Measurement of Transmural Gradients in Myocardial Strain with MR Imaging. Radiology 1991; 180: 677 – 683
58. Lima JAC, Jeremy R, Guier W, Bouton S, Zerhouni EA, McVeigh E, Buchalter MB, Weisfeldt ML, Shapiro EP, Weiss JL. Accurate Systolic Wall Thickening by Nuclear Magnetic Resonance Imaging with Tissue Tagging: Correlation with Sonomicrometers in Normal and Ischaemic Myocardium. J Am Coll Cardiol 1993; 21: 1741 – 1751
59. Yeon SB, Reichek N, Tallant BA, Lima JAC, Calhoun LP, Clark NR, Hoffman EA, Ho KKL, Axel L. Validation of In Vivo Myocardial Strain Measurement by Magnetic Resonance Tagging with Sonomicrometry. J Am Coll Cardiol 2001; 38: 555 – 561
60. Moore CC, McVeigh ER, Zerhouni EA. Quantitative Tagged Magnetic Resonance Imaging of the Normal Human Left Ventricle. Top Magn Reson Imaging 2000; 11: 359 – 371
61. Aletras AH, Ding S, Balaban RD, Wen H. DENSE: Displacement Encoding with Stimulated Echoes in Cardiac Functional MRI. J Magn Reson 1999; 137: 247 – 252
62. Osman NF, Sampath S, Atalar E, Prince JL. Imaging Longitudinal Cardiac Strain on Short-Axis Imaging Using Strain-Encoded MRI. Magn Reson Med 2001; 46(2): 324 - 334
63. Bryant DJ, Payne JA, Firmin DN, Longmore DB. Measurement of Flow with NMR Imaging Using a Gradient Pulse and Phase Difference Technique. J Comput Assist Tomogr 1984; 8: 588 – 593

64. Van Dijk P. Direct Cardiac NMR Imaging of Heart Wall and Blood Flow Velocity. J Comput Assist Tomogr 1984; 8: 429 – 436
65. Arai AE, Gaither CC, Epstein FH, Balaban R, Wolff SD. Myocardial Velocity Gradient Imaging by Phase Contrast MRI With Application to Regional Function in Myocardial Ischaemia. Magn Reson Med 1999; 42: 98 – 109
66. Pelc LR, Sayre J, Yun K, Castro LJ, Herfkens RJ, Miller DC, Pelc NJ. Evaluation of Myocardial Motion Tracking With Cine-Phase Contrast Magnetic Resonance Imaging. Invest Radiol 1994; 29:1038 – 1042
67. Burnstein D. Stimulated Echoes: Description, Applications, Practical Hints. Concepts Magn Reson 1996; 8: 269 – 278
68. McRobbie DW, Moore EA, Graves MJ, Prince MR. MRI – From Picture to Proton, Second Edition. Cambridge University Press, 2007
69. Sattin W, Mareci TH, Scott KN. Exploiting the Stimulated Echo in Nuclear Magnetic Resonance Imaging. I: Method. J Magn Reson 1985; 64: 177 - 182
70. Chenevert TL, Skovoroda AR, O'Donnell M, Emelianov SY. Elasticity Reconstructive Imaging by Means of Simulated Echo MRI. Magn Reson Med. 1998; 39: 482 – 490
71. Frahm J, Hanicke W, Bruhn H, Gyngell ML, Merboldt KD. High-Speed STEAM MRI of the Human Heart. Magn Reson Med 1991; 22: 133 - 142
72. Aletras AH, Balaban RS, Wen H. High-Resolution Strain Analysis of the Human Heart with Fast-DENSE. J Magn Reson 1999; 140: 41 – 57
73. Kim D, Gilson WD, Kramer CM, Epstein FH. Myocardial Tissue Tracking with Two-dimensional Cine Displacement-encoded Imaging: Development and Initial Validation. Radiology 2004; 230: 862 – 871
74. Gilson WD, Yang Z, French BA, Epstein FH. Complementary Displacement-Encoded MRI for Contrast-Enhanced Infarct Detection and Quantification of Myocardial Function in Mice. Magn Reson Med 2004; 51: 744 – 752
75. Zhong X, Spottiswoode BS, Cowart EA, Gilson WD, Epstein FH. Selective Suppression of Artifact-Generating Echoes in Cine DENSE Using Through-Plane Dephasing. Magn Reson Med 2006; 56: 1126 - 1131
76. Haacke EM, Brown RW, Thompson MR, Venkatesan R. Magnetic Resonance Imaging: Physical Principles and Sequence Design. John Wiley & Sons, Inc., 1999

77. Aletras AH, Arai AE. Meta-DENSE Complex Acquisition for Reduced Intravoxel Dephasing. J Magn Reson 2004; 169: 246 - 249
78. Wen H, Marsolo KA, Bennett EE, Kutten KS, Lewis RP, Lipps DB, Epstein ND, Plehn JF, Croisille P. Adaptive Postprocessing Techniques for Myocardial Tissue Tracking with Displacement-Encoded MR Imaging. Radiology 2008; 246: 229 - 240
79. Zhong X, Green J, Zuehlsdorff S. Siemens Applications Guide: CV_EPI_DENSE (WIP #611). August 2010
80. Young AA, Kirton RS, Cowan BR. Generalized Spatiotemporal Myocardial Strain Analysis for DENSE and SPAMM Imaging. Magn Reson Med 2012; 67: 1590 – 1599
81. Ghiglia DC, Romero LA. Robust Two-Dimensional Weighted and Unweighted Phase Unwrapping That Uses Fast Transforms and Iterative Methods. J Opt Soc Am A 1994; 11: 107 - 117
82. Witoszynskyj S, Rauscher A, Reichenbach JR, Barth M. Phase Unwrapping of MR Images using ΦUN – A Fast and Robust Region Growing Algorithm. Medical Image Analysis 2009; 13: 257 – 268
83. Wunsche BC, Lobb R. The Visualization of Myocardial Strain for the Improved Analysis of Cardiac Mechanics. Proceedings of the 2nd International Conference on Computer Graphics and Interactive Techniques 2004; pp 90 – 99. Available from ACM Digital Library: http://dl.acm.org/citation.cfm?id=988850 (accessed 03/10/13)
84. Kim D, Epstein FH, Gilson WD, Axel L. Increasing the Signal-to-Noise Ratio in DENSE MRI by Combining Displacement Echoes. Magn Reson Med 2004; 52: 188 - 192
85. Kar J, Knutsen AK, Cupps BP, Pasque MK. A Validation of Two-Dimensional In Vivo Regional Strain Computed from Displacement Encoding with Stimulated Echoes (DENSE), in Reference to Tagged Magnetic Resonance Imaging and Studies in Repeatability. Ann Biomed Eng 2013; DOI 10.1007/s10439-013-0931-2
86. Spottiswoode BS, Zhong X, Hess AT, Kramer CM, Meintjes EM, Mayosi BM, Epstein FH. Tracking Myocardial Motion From Cine DENSE Images

Using Spatiotemporal Phase Unwrapping and Temporal Fitting. IEEE Trans Med Imaging 2007; 26: 15 - 30

87. Miyaki H, Nagata M, Kitagawa K, Kato S, Takase S, Sigfridsson A, Ishida M, Dohi K, Ito M, Sakuma H. Quantitative Assessment of Myocardial Strain with Displacement Encoding with Stimulated Echoes MRI in Patients with Coronary Artery Disease. Int J Cardiovasc Imaging 2013; 29: 1779 - 1786
88. Gilson WD, Yang Z, French BA, Epstein FH. Measurement of Myocardial Mechanics in Mice Before and After Infarction using Multislice Displacement-Encoded MRI with 3D Motion Encoding. Am J Physiol Heart Circ Physiol 2004; 288: H1491 - H1497
89. Hess AT, Zhong X, Spottiswoode BS, Epstein FH, Meintjes EM. Myocardial 3D Strain Calculation by Combining Cine DENSE and Cine SENC Imaging. Magn Reson Med 2009; 62: 77 – 74
90. Spottiswoode BS, Zhong X, Lorenz CH, Mayosi BM, Meintjes EM, Epstein FH. 3D Myocardial Tissue Tracking With Slice Followed Cine DENSE MRI. J Magn Reson Imagaing 2008; 27: 1019 – 1027
91. Fischer SE, McKinnon GC, Scheidegger MB, Prins W, Meier D, Boesiger P. True Myocardial Motion Tracking. Magn Reson Med 1994; 31: 401 – 413
92. Zhong X, Spottiswoode BS, Meyer CH, Kramer CM, Epstein FH. Imaging Three-Dimensional Myocardial Mechanics Using Navigator-Gated Volumetric Spiral Cine DENSE MRI. Magn Reson Med 2010; 64: 1089 - 1097
93. Neizel M, Lossnitzer D, Korosoglou G, Schaufele T, Lewien A, Steen H, Katus HA, Osman NF, Giannitsis E. Strain-Encoded (SENC) Magnetic Resonance Imaging to Evaluate Regional Heterogeneity of Myocardial Strain in Healthy Volunteers: Comparison With Conventional Tagging. J Magn Reson Imaging 2009; 29: 99 – 105
94. Korosoglou G, Youssef AA, Bilchick KC, Ibrahim ES, Lardo AC, Lai S, Osman NF. Real-Time Fast Strain-Encoded Magnetic Resonance Imaging to Evaluate Regional Myocardial Function at 3.0 Tesla: Comparison to Conventional Tagging. J Magn Reson Imaging 2008; 27: 1012 – 1018
95. Harrild DM, Han Y, Geva T, Zhou J, Marcus E, Powell AJ. Comparison of Cardiac MRI Tissue Tracking and Myocardial Tagging for Assessment of Regional Ventricular Strain. Int J Cardiovasc Imaging 2012; 28: 2009 – 2018

96. Kramer CM, Reichek N, Ferrari VA, Theobald T, Dawson J, Axel L. Regional Heterogeneity of Function in Hypertrophic Cardiomyopathy. Circulation 1994 ; 90 : 186 – 194
97. Palmon LC, Reichek N, Yeon SB, Clark NR, Brownson D, Hoffman E, Axel L. Intramural Myocardial Shortening in Hypertensive Left Ventricular Hypertrophy with Normal Pump Function. Circulation 1994; 89: 122 – 131
98. Clark NR, Reichek N, Bergey P, Hoffman EA, Brownson D, Palmon L, Axel L. Circumferential Myocardial Shortening in the Normal Human Left Ventricle. Assessment by Magnetic Resonance Imaging Using Spatial Modulation of Magnetization. Circulation 1991; 84: 67 – 74
99. Kuijer JPA, Marcus JT, Gotte MJW, van Rossum AC, Heethaar RM. Three-Dimensional Myocardial Strains at End-Systole and During Diastole in the Left Ventricle of Normal Humans. J Cardiovasc Magn Reson 2002; 4(3): 341 – 351
100. Feng L, Donnino R, Babb J, Axel L, Kim D. Numerical and In Vivo Validation of Fast Cine DENSE MRI for Quantification of Regional Cardiac Function. Magn Reson Med 2009; 62(3): 682 - 690
101. Delfino JG, Fornwalt BK, Eisner RL, Leon AR, Oshinski JN. Determination of Transmural, Endocardial and Epicardial Radial Strain and Strain Rate From Phase Contrast MR Velocity Data. J Magn Reson Imaging 2008; 27: 522 - 528
102. Lawton JS, Cupps BP, Knutsen AK, Ma N, Brady BD, Reynolds LM Pasque MK. Magnetic Resonance Imaging Detects Significant Sex Differences in Human Myocardial Strain. Biomed Eng Online 2011; 10: 76
103. Augustine D, Lewandowski AJ, Lazdam M, Rai A, Francis J, Myerson S, Noble A, Becher H, Neubauer S, Petersen SE, Leeson P. Global and Regional Left Ventricular Myocardial Deformation Measures by Magnetic Resonance Feature Tracking in Healthy Volunteers: Comparison with Tagging and Relevance of Gender. J Cardiovasc Magn Reson 2013; 15: 8
104. Oxenham HC, Young AA, Cowan BR, Gentles TL, Occleshaw CJ, Fonseca CG, Doughty RN, Sharpe N. Age-Related Changes in Myocardial Relaxation Using Three-Dimensional Tagged Magnetic Resonance Imaging. J Cardivasc Magn Reson 2003; 5: 421 - 430

105. Inoue Y, Yang X, Nagao M, Higashino H, Hosokawa K, Kido T, Kurata A, Okayama H, Higaki J, Mochizuki T, Murase K. Peri-infarct Dysfunction in Post-Myocardial Infarction: Assessment of 3T Tagged and Late Enhancement MRI. Eur Radiol 2010; 20: 1139 - 1148

106. Neizel M, Lossnitzer D, Korosoglou G, Shaufele T, Peykarjou H, Steen H, Ocklenburg C, Giannitsis E, Katus HA, Osman NF. Strain-Encoded MRI for Evaluation of Left Ventricular Function and Transmurality in Acute Myocardial Infarction. Circ Cardiovasc Imaging 2009; 2: 116 – 122

107. O'Regan DP, Ariff B, Baksi AJ, Gordon F, Durighel G, Cook SA. Salvage Assessment with Cardiac MRI Following Acute Myocardial Infarction Underestimates Potential for Recovery of Systolic Strain. Eur Radiol 2013; 23: 1210 – 1217

108. Choi KM, Kim RJ, Gubernikoff G, Vargas JD, Parker M, Judd RM. Transmural Extent of Acute Myocardial Infarction Predicts Long-Term Improvement in Contractile Function. Circulation 2001; 104: 1101 – 1107

109. Ligabue G, Fiocchi F, Ferraresi S, Barbieri A, Romangnoli R, Torricelli P. How to Quantify Infarct Size on Delayed-enhancement MR Images: A Comparison between Visual and Quantitative Approach. Radiol Med 2007; 112: 959 – 968

110. Morse LR, Lazzari AA, Battaglino R, Stolzmann KL, Matthess KR, Gagnon DR, David SA, Garshick E. Dual Energy X-Ray Absoptiometry of the Distal Femur May Be More Reliable then the Proximal Tibia in Spinal Cord Injury. Arch Phys Med Rehabil 2009; 90: 827 - 831

111. Bland JM, Altman DG. Statistical Methods for Assessing Agreement Between Two Methods of Clinical Measurement. Lancet 1986; 1(8476): 307 – 310

112. Bland JM, Altman DG. Measuring Agreement in Method Comparison Studies. Stat Methods Med Res 1999; 8: 135 – 160

113. Alam M, Wardell J, Andersson E, Samad BA, Norlander R. Characteristics of Mitral and Tricuspid Annular Velocities Determined by Pulse Wave Doppler Tissue Imaging in Healthy Subjects. J Am Soc Echocardiogr 1999; 12: 618 – 628

114. Salmasi AM, Alimo A, Jepson E, Dancy M. Age-associated Change in Left Ventricular Diastolic Function are Related to Increasing Left Ventricular Mass. Am J Hypertens 2003; 16: 473 – 477

115. Munagala VK, Jacobsen SJ, Mahoney DW, Rodeheffer RJ, Bailey KR, Redfield MM. Association of Newer Diastolic Function Parameters with Age in Healthy Subjects: A Population-based Study. J Am Soc Echocardiogr 2003; 16: 1049 - 1056

116. Mor-Avi V, Spencer K, Gorcsan J, Demaria A, Kimball T, Monaghan M, Perez J, Sun JP, Weinart L, Bednarz J, Collins K, Edelman K, Kwan OL, Glascock B, Hancock J, Baumann C, Thomas J, Lang R. Normal Values of Regional Left Ventricular Endocardial Motion: Multicenter Color Kinesis Study. Am J Physiol Heart Circ Physiol 2000; 279: H2464 – H2476

117. Ruan Q, Nagueh SF. Effect of Age on Left Ventricular Systolic Function in Humans: A Studi of Systolic Isovolumetric Acceleration Rate. Exp Physiol 2005; 90: 527 - 534

Appendix A – Matlab Code

```
%*************************************************************************
%                         STRAIN_ANALYSIS
%*************************************************************************
%
% Purpose: read in output data from CIM_DENSE2D and calculate the
%          following parameters
%          - peak Ecc
%          - time to peak Ecc
%          - area under Ecc curve (up to ES)
%          - area/time (up to ES)
%          - area under Ecc curve (up to ED)
%          - area/time (up to ED)
%
% Functions Called: read_strain_data
%                   smooth_data
%                   calculate_strain_parameters
%
% Author: C. McComb / H. Gao
%
% Version: 1, June 2011
%          2, October 2013
%
%*************************************************************************

clear all; close all; clc;

fprintf(1,'%s\n','******************************');
fprintf(1,'%s\n','      STRAIN ANALYSIS         ');
fprintf(1,'%s\n\n','******************************');

% select input data file
[DataFile DataPath] = uigetfile('*.txt','Open Text File');
fileName = [DataPath DataFile];

fprintf(1,'%s\t%s\n','Input Filename:',fileName);

% analysis options
heading = str2mat('Strain Analysis');
lineno = [1 30];
prompt = {'No. of Frames','Perform Smoothing: 0 = No, 1 = Yes',…
 'Analysis: 0 - Ecc Only, 1 - Ecc + Err'};
defaults = {'30','0','1'};
answer = inputdlg(prompt,heading,lineno,defaults);
totalFrameNo = str2num(answer{1});
smoothFlag = str2num(answer{2});
analysisOption = str2num(answer{3});

if (smoothFlag == 1)
    heading = str2mat('Strain Analysis');
    lineno = [1 30];
    prompt = {'Window Size for Smoothing'};
    defaults = {'3'};
    answer = inputdlg(prompt,heading,lineno,defaults);
    windowSize = str2num(answer{1});
else
    windowSize = 1;
end

% read the strain from txt file
StrainData = read_strain_data(fileName, totalFrameNo);

% plot strain curves
h1 = figure(); hold on;

plot(StrainData.totalStrain.FrameTime,StrainData.totalStrain.CC,'k-', 'LineWidth', 2);
plot(StrainData.AntSept.FrameTime,StrainData.AntSept.CC, 'r-+');
plot(StrainData.Ant.FrameTime,StrainData.Ant.CC, 'r-*');
plot(StrainData.AntLat.FrameTime,StrainData.AntLat.CC, 'r-x');
plot(StrainData.InfLat.FrameTime,StrainData.InfLat.CC, '-.o');
plot(StrainData.Inf.FrameTime,StrainData.Inf.CC, '-.<');
plot(StrainData.InfSept.FrameTime,StrainData.InfSept.CC, '-.d');
title('Circumferential Strain');
xlabel('Time (ms)');
```

```
ylabel('Strain (%)');
legend('Total Strain', 'AntSept', 'Ant', 'AntLat', 'InfLat', 'Inf',
'InfSept','Location','SouthEast');

if (analysisOption == 1)
    h2 = figure(); hold on;
    plot(StrainData.totalStrain.FrameTime,StrainData.totalStrain.RR,…
        'k-', 'LineWidth', 2);
    plot(StrainData.AntSept.FrameTime,StrainData.AntSept.RR, 'r-+');
    plot(StrainData.Ant.FrameTime,StrainData.Ant.RR, 'r-*');
    plot(StrainData.AntLat.FrameTime,StrainData.AntLat.RR, 'r-x');
    plot(StrainData.InfLat.FrameTime,StrainData.InfLat.RR, '-.o');
    plot(StrainData.Inf.FrameTime,StrainData.Inf.RR, '-.<');
    plot(StrainData.InfSept.FrameTime,StrainData.InfSept.RR, '-.d');
    title('Radial Strain');
    xlabel('Time (ms)');
    ylabel('Strain (%)');
    legend('Total Strain', 'AntSept', 'Ant', 'AntLat', 'InfLat',…
         'Inf','InfSept','Location','NorthEast');
end

% smooth data
StrainDataSmooth = smooth_data(StrainData, totalFrameNo, windowSize);
StrainDataSmooth.EsFrame = StrainData.EsFrame;
StrainDataSmooth.ID = StrainData.ID;


% plot smoothed strain curves
if (smoothFlag == 1)
    h3 = figure(); hold on;

    plot(StrainDataSmooth.totalStrain.FrameTime,StrainDataSmooth.totalStrain.CC,…
        'k-', 'LineWidth', 2);
    plot(StrainDataSmooth.AntSept.FrameTime,StrainDataSmooth.AntSept.CC, 'r-+');
    plot(StrainDataSmooth.Ant.FrameTime,StrainDataSmooth.Ant.CC, 'r-*');
    plot(StrainDataSmooth.AntLat.FrameTime,StrainDataSmooth.AntLat.CC, 'r-x');
    plot(StrainDataSmooth.InfLat.FrameTime,StrainDataSmooth.InfLat.CC, '-.o');
    plot(StrainDataSmooth.Inf.FrameTime,StrainDataSmooth.Inf.CC, '-.<');
    plot(StrainDataSmooth.InfSept.FrameTime,StrainDataSmooth.InfSept.CC, '-.d');
    title('Circumferential Strain - Smoothed');
    xlabel('Time (ms)');
    ylabel('Strain (%)');
    legend('Total Strain', 'AntSept', 'Ant', 'AntLat', 'InfLat',…
         'Inf', 'InfSept','Location','SouthEast')

    if (analysisOption == 1)
        h4 = figure(); hold on;


        plot(StrainDataSmooth.totalStrain.FrameTime,StrainDataSmooth.totalStrain.RR,…
               'k-', 'LineWidth', 2);
        plot(StrainDataSmooth.AntSept.FrameTime,StrainDataSmooth.AntSept.RR, 'r-+');
        plot(StrainDataSmooth.Ant.FrameTime,StrainDataSmooth.Ant.RR, 'r-*');
        plot(StrainDataSmooth.AntLat.FrameTime,StrainDataSmooth.AntLat.RR, 'r-x');
        plot(StrainDataSmooth.InfLat.FrameTime,StrainDataSmooth.InfLat.RR, '-.o');
        plot(StrainDataSmooth.Inf.FrameTime,StrainDataSmooth.Inf.RR, '-.<');
        plot(StrainDataSmooth.InfSept.FrameTime,StrainDataSmooth.InfSept.RR, '-.d');
        title('Radial Strain - Smoothed');
        xlabel('Time (ms)');
        ylabel('Strain (%)');
        legend('Total Strain', 'AntSept', 'Ant', 'AntLat', 'InfLat', 'Inf',…
               'InfSept','Location','SouthEast');
    end
end

% calculate area under strain curve
[StrainArea, PeakValues] = calculate_strain_parameters(StrainDataSmooth, totalFrameNo,
analysisOption);

% write results to file
temp = strfind(DataFile,'.txt');
temp2 = DataFile(1,1:(temp-1));
temp3 = date;
DataFile2 = [temp2 '_results_' temp3 '.txt'];
filename2 = [DataPath DataFile2];

fprintf(1,'%s\t%s\n\n','Output Filename:',filename2);
```

```
fid2 = fopen(filename2,'w');
if (analysisOption == 1)
    fprintf(fid2,'%s\t%s\t%s\t%s\t%s\t%s\t%s\t%s\t%s\t%s\t%s\t%s\t%s\t%s\t%s\t%s\n',…
        'Segment','PeakEcc','TimePeakEcc','StrainRateEcc','AreaES',…
        'AreaTimeES','AreaED','AreaTimeED','PeakErr','TimePeakErr', …
        'StrainRateErr','AreaES','AreaTimeES','AreaED','AreaTimeED');
else
    fprintf(fid2,'%s\t%s\t%s\t%s\t%s\t%s\t%s\t%s\n','Segment','PeakEcc',…
        'TimePeakEcc','StrainRateEcc','AreaES','AreaTimeES','AreaED',…
        'AreaTimeED');
end

for segment = 1:7
    switch(segment)
        case 1
            title = 'Total';
            peakEcc = PeakValues.totalStrain.peakEcc;
            timePeakEcc = PeakValues.totalStrain.timePeakEcc;
            strainRateEcc = PeakValues.totalStrain.strainRateEcc;
            dataEccES = StrainArea.totalStrain.Ecc.ES;
            dataEccED = StrainArea.totalStrain.Ecc.ED;
            peakErr = PeakValues.totalStrain.peakErr;
            timePeakErr = PeakValues.totalStrain.timePeakErr;
            strainRateErr = PeakValues.totalStrain.strainRateErr;
            dataErrES = StrainArea.totalStrain.Err.ES;
            dataErrED = StrainArea.totalStrain.Err.ED;
        case 2
            title = 'AS';
            peakEcc = PeakValues.AntSept.peakEcc;
            timePeakEcc = PeakValues.AntSept.timePeakEcc;
            strainRateEcc = PeakValues.AntSept.strainRateEcc;
            dataEccES = StrainArea.AntSept.Ecc.ES;
            dataEccED = StrainArea.AntSept.Ecc.ED;
            peakErr = PeakValues.AntSept.peakErr;
            timePeakErr = PeakValues.AntSept.timePeakErr;
            strainRateErr = PeakValues.AntSept.strainRateErr;
            dataErrES = StrainArea.AntSept.Err.ES;
            dataErrED = StrainArea.AntSept.Err.ED;
        case 3
            title = 'A';
           peakEcc = PeakValues.Ant.peakEcc;
            timePeakEcc = PeakValues.Ant.timePeakEcc;
            strainRateEcc = PeakValues.Ant.strainRateEcc;
            dataEccES = StrainArea.Ant.Ecc.ES;
            dataEccED = StrainArea.Ant.Ecc.ED;
            peakErr = PeakValues.Ant.peakErr;
            timePeakErr = PeakValues.Ant.timePeakErr;
            strainRateErr = PeakValues.Ant.strainRateErr;
            dataErrES = StrainArea.Ant.Err.ES;
            dataErrED = StrainArea.Ant.Err.ED;
        case 4
            title = 'AL';
            peakEcc = PeakValues.AntLat.peakEcc;
            timePeakEcc = PeakValues.AntLat.timePeakEcc;
            strainRateEcc = PeakValues.AntLat.strainRateEcc;
            dataEccES = StrainArea.AntLat.Ecc.ES;
            dataEccED = StrainArea.AntLat.Ecc.ED;
            peakErr = PeakValues.AntLat.peakErr;
            timePeakErr = PeakValues.AntLat.timePeakErr;
            strainRateErr = PeakValues.AntLat.strainRateErr;
            dataErrES = StrainArea.AntLat.Err.ES;
            dataErrED = StrainArea.AntLat.Err.ED;
        case 5
            title = 'IL';
            peakEcc = PeakValues.InfLat.peakEcc;
            timePeakEcc = PeakValues.InfLat.timePeakEcc;
            strainRateEcc = PeakValues.InfLat.strainRateEcc;
            dataEccES = StrainArea.InfLat.Ecc.ES;
            dataEccED = StrainArea.InfLat.Ecc.ED;
            peakErr = PeakValues.InfLat.peakErr;
            timePeakErr = PeakValues.InfLat.timePeakErr;
            strainRateErr = PeakValues.InfLat.strainRateErr;
            dataErrES = StrainArea.InfLat.Err.ES;
            dataErrED = StrainArea.InfLat.Err.ED;
        case 6
            title = 'I';
```

```
            peakEcc = PeakValues.Inf.peakEcc;
            timePeakEcc = PeakValues.Inf.timePeakEcc;
            strainRateEcc = PeakValues.Inf.strainRateEcc;
            dataEccES = StrainArea.Inf.Ecc.ES;
            dataEccED = StrainArea.Inf.Ecc.ED;
            peakErr = PeakValues.Inf.peakErr;
            timePeakErr = PeakValues.Inf.timePeakErr;
            strainRateErr = PeakValues.Inf.strainRateErr;
            dataErrES = StrainArea.Inf.Err.ES;
            dataErrED = StrainArea.Inf.Err.ED;
        case 7
            title = 'IS';
            peakEcc = PeakValues.InfSept.peakEcc;
            timePeakEcc = PeakValues.InfSept.timePeakEcc;
            strainRateEcc = PeakValues.InfSept.strainRateEcc;
            dataEccES = StrainArea.InfSept.Ecc.ES;
            dataEccED = StrainArea.InfSept.Ecc.ED;
            peakErr = PeakValues.InfSept.peakErr;
            timePeakErr = PeakValues.InfSept.timePeakErr;
            strainRateErr = PeakValues.InfSept.strainRateErr;
            dataErrES = StrainArea.InfSept.Err.ES;
            dataErrED = StrainArea.InfSept.Err.ED;
    end

    fprintf(fid2,'%s\t',title);
    if (analysisOption == 1)

        fprintf(fid2,'%f\t%f\t%f\t%f\t%f\t%f\t%f\t%f\t%f\t%f\t%f\t%f\t%f\t%f\t%f\t%f\n',…
                peakEcc, timePeakEcc, strainRateEcc, dataEccES(1,1), dataEccES(1,2),…
                dataEccED(1,1), dataEccED(1,2), peakErr, timePeakErr, …
                strainRateErr, dataErrES(1,1), dataErrES(1,2), dataErrED(1,1),…
                dataErrED(1,2));
    else
         fprintf(fid2,'%f\t%f\t%f\t%f\t%f\t%f\t%f\n',peakEcc, timePeakEcc,…
                strainRateEcc, dataES(1,1), dataES(1,2), dataED(1,1), dataED(1,2));
    end

end
fclose(fid2);

fprintf(1,'%s\n\n','Analysis Completed');

%**************************************************************************
%               FUNCTION: READ_STRAIN_DATA
%**************************************************************************
%
% Purpose: read in strain data from text file and save in a structure
%               strainData.ID
%                 .ModelName
%                 .Series
%                 .Slice
%                 .EsFrame
%                 .totalStrain
%                 .AntSept
%                 .Ant
%                 .AntLat
%                 .InfLat
%                 .Inf
%                 .InfSept
%
% Functions Called: None
%
% Author: C. McComb / H. Gao
%
% Version: 1, June 2011
%
%**************************************************************************

function StrainData = read_strain_data(fileName, totalFrameNo)

% open text file
fid = fopen(fileName,'r');

% read patient name
tline = fgetl(fid);
strTemp = regexp(tline,':','split');
```

```
StrainData.ID = strtrim(strTemp{2});

% read model name
tline = fgetl(fid);
strTemp = regexp(tline,':','split');
StrainData.ModelName = strtrim(strTemp{2});

% read series
tline = fgetl(fid);
strTemp = regexp(tline,':','split');
StrainData.Series = strtrim(strTemp{2});

% read slice
tline = fgetl(fid);
strTemp = regexp(tline,':','split');
StrainData.Slice = strtrim(strTemp{2});

% read ES frame
tline = fgetl(fid);
strTemp = regexp(tline,':','split');
StrainData.EsFrame = str2double(strtrim(strTemp{2}));

% read the strain data into matrix - 7 series
fgetl(fid);
for strainSeriesToRead = 1 : 7
    fgetl(fid);         % strain name description - discard
    if strainSeriesToRead == 1
        fgetl(fid);     % extra line in total strain section
    end
    fgetl(fid);         % frame no
    % read in strain data
    FrameTime = zeros(totalFrameNo,1);
    CC = zeros(totalFrameNo,1);
    CR = zeros(totalFrameNo,1);
    RR = zeros(totalFrameNo,1);
    for frameNoIndex = 1 : totalFrameNo
        tline = fgetl(fid);
        strTemp = strrep(tline,'(', '');
        strTemp = strrep(strTemp,')', '');
        strainTemp = sscanf(strTemp, '%d%f%f%f%f');
        FrameTime(frameNoIndex) = strainTemp(2);    % time
        CC(frameNoIndex)=strainTemp(3);             % circumferential strain
        CR(frameNoIndex)=strainTemp(4);             % shear strain
        RR(frameNoIndex)=strainTemp(5);             % radial strain
    end
    switch strainSeriesToRead
        case 1
            totalStrain.FrameTime = FrameTime;
            totalStrain.CC = CC;
            totalStrain.CR = CR;
            totalStrain.RR = RR;
        case 2
            AntSept.FrameTime = FrameTime;
            AntSept.CC = CC;
            AntSept.CR = CR;
            AntSept.RR = RR;
       case 3
            Ant.FrameTime = FrameTime;
            Ant.CC = CC;
            Ant.CR = CR;
            Ant.RR = RR;
       case 4
            AntLat.FrameTime = FrameTime;
            AntLat.CC = CC;
            AntLat.CR = CR;
            AntLat.RR = RR;
       case 5
            InfLat.FrameTime = FrameTime;
            InfLat.CC = CC;
            InfLat.CR = CR;
            InfLat.RR = RR;
       case 6
            Inf.FrameTime = FrameTime;
            Inf.CC = CC;
            Inf.CR = CR;
            Inf.RR = RR;
        case 7
```

```
            InfSept.FrameTime = FrameTime;
            InfSept.CC = CC;
            InfSept.CR = CR;
            InfSept.RR = RR;
        otherwise
            disp('too many segments')
    end
    fgetl(fid);
    fgetl(fid);
end

StrainData.totalStrain = totalStrain;
StrainData.AntSept = AntSept;
StrainData.Ant = Ant;
StrainData.AntLat = AntLat;
StrainData.InfLat = InfLat;
StrainData.Inf = Inf;
StrainData.InfSept = InfSept;


fclose(fid);

%*************************************************************************
%                    FUNCTION: SMOOTH_DATA
%*************************************************************************
%
% Purpose: perform smoothing on data using a sliding window
%
% Functions Called: None
%
% Author: C. McComb
%
% Version: 1, October 2013
%
%*************************************************************************
function StrainDataSmooth = smooth_data(StrainData, totalFrameNo, windowSize)

% times are the same for all segments
for i = 1:totalFrameNo
    frameTime(i) = StrainData.totalStrain.FrameTime(i);
end

for region = 1:7

    switch region
        case 1
            dataCC = StrainData.totalStrain.CC;
            dataRR = StrainData.totalStrain.RR;
        case 2
            dataCC = StrainData.AntSept.CC;
            dataRR = StrainData.AntSept.RR;
        case 3
            dataCC = StrainData.Ant.CC;
            dataRR = StrainData.Ant.RR;
        case 4
            dataCC = StrainData.AntLat.CC;
            dataRR = StrainData.AntLat.RR;
        case 5
            dataCC = StrainData.InfLat.CC;
            dataRR = StrainData.InfLat.RR;
        case 6
            dataCC = StrainData.Inf.CC;
            dataRR = StrainData.Inf.RR;
        case 7
            dataCC = StrainData.InfSept.CC;
            dataRR = StrainData.InfSept.RR;
    end

    % define start and end positions for smoothing depending on window size
    % window size should be an odd number, with the pixel of interest in
    % the centre
    startPos = (windowSize + 1)/2;
    endPos = totalFrameNo - (windowSize - 1)/2;

    % perform smoothing
    for pos = 1:totalFrameNo
```

```
        if (pos < startPos || pos > endPos)
            dataSmoothCC(pos) = dataCC(pos);
            dataSmoothRR(pos) = dataRR(pos);
        else
            sumValuesCC = 0;
            sumValuesRR = 0;
            for counter = (pos - (windowSize-1)/2):(pos + (windowSize-1)/2)
                sumValuesCC = sumValuesCC + dataCC(counter);
                sumValuesRR = sumValuesRR + dataRR(counter);
            end

            % amoothed value is the average of the values within the window
            dataSmoothCC(pos) = sumValuesCC/windowSize;
            dataSmoothRR(pos) = sumValuesRR/windowSize;
        end
    end

    % copy smoothed data into structure
    switch region
        case 1
            StrainDataSmooth.totalStrain.CC = dataSmoothCC;
            StrainDataSmooth.totalStrain.RR = dataSmoothRR;
            StrainDataSmooth.totalStrain.FrameTime = frameTime;
        case 2
            StrainDataSmooth.AntSept.CC = dataSmoothCC;
            StrainDataSmooth.AntSept.RR = dataSmoothRR;
            StrainDataSmooth.AntSept.FrameTime = frameTime;
        case 3
            StrainDataSmooth.Ant.CC = dataSmoothCC;
            StrainDataSmooth.Ant.RR = dataSmoothRR;
            StrainDataSmooth.Ant.FrameTime = frameTime;
        case 4
            StrainDataSmooth.AntLat.CC = dataSmoothCC;
            StrainDataSmooth.AntLat.RR = dataSmoothRR;
            StrainDataSmooth.AntLat.FrameTime = frameTime;
        case 5
            StrainDataSmooth.InfLat.CC = dataSmoothCC;
            StrainDataSmooth.InfLat.RR = dataSmoothRR;
            StrainDataSmooth.InfLat.FrameTime = frameTime;
        case 6
            StrainDataSmooth.Inf.CC = dataSmoothCC;
            StrainDataSmooth.Inf.RR = dataSmoothRR;
            StrainDataSmooth.Inf.FrameTime = frameTime;
        case 7
            StrainDataSmooth.InfSept.CC = dataSmoothCC;
            StrainDataSmooth.InfSept.RR = dataSmoothRR;
            StrainDataSmooth.InfSept.FrameTime = frameTime;
    end

end

%**************************************************************************
%                   FUNCTION: CALCULATE_STRAIN_PARAMETERS
%**************************************************************************
%
% Purpose: Calculate the following strain parameters
%          - peak Ecc
%          - time to peak Ecc
%          - area under Ecc curve (up to ES)
%          - area/time (up to ES)
%          - area under Ecc curve (up to ED)
%          - area/time (up to ED)
%
% Function Called: calculate_area_under_curve
%
% Author: C. McComb / H. Gao
%
% Version: 1, June 2011
%          2, October 2013
%
%**************************************************************************

function [StrainArea, PeakValues] = calculate_strain_parameters(StrainDataSmooth,
totalFrameNo, analysisOption)

for segment = 1:7
    maxStrain = 0.0;
```

```
maxStrainTime = 0.0;
segmentIndex = 0;

switch segment
    case 1
        strainEcc = StrainDataSmooth.totalStrain.CC;
        strainErr = StrainDataSmooth.totalStrain.RR;
    case 2
        strainEcc = StrainDataSmooth.AntSept.CC;
        strainErr = StrainDataSmooth.AntSept.RR;
    case 3
        strainEcc = StrainDataSmooth.Ant.CC;
        strainErr = StrainDataSmooth.Ant.RR;
    case 4
        strainEcc = StrainDataSmooth.AntLat.CC;
        strainErr = StrainDataSmooth.AntLat.RR;
    case 5
        strainEcc = StrainDataSmooth.InfLat.CC;
        strainErr = StrainDataSmooth.InfLat.RR;
    case 6
        strainEcc = StrainDataSmooth.Inf.CC;
        strainErr = StrainDataSmooth.Inf.RR;
    case 7
        strainEcc = StrainDataSmooth.InfSept.CC;
        strainErr = StrainDataSmooth.InfSept.RR;
end

% calculate peak values
peakEcc = min(strainEcc);
peakErr = max(strainErr);

frameCounterEcc = 0;
frameCounterErr = 0;

% find corresponding times
for i=1:totalFrameNo
    if (strainEcc(1,i) == peakEcc)
        frameCounterEcc = i;
    end
    if (strainErr(1,i) == peakErr)
        frameCounterErr = i;
    end
end

timePeakEcc = StrainDataSmooth.totalStrain.FrameTime(1,frameCounterEcc);
timePeakErr = StrainDataSmooth.totalStrain.FrameTime(1,frameCounterErr);

strainRateEcc = (peakEcc/timePeakEcc)*1000;
strainRateErr = (peakErr/timePeakErr)*1000;

% copy data into structure
switch segment
    case 1
        PeakValues.totalStrain.peakEcc = peakEcc;
        PeakValues.totalStrain.timePeakEcc = timePeakEcc;
        PeakValues.totalStrain.peakFrameEcc = frameCounterEcc;
        PeakValues.totalStrain.strainRateEcc = strainRateEcc;
        PeakValues.totalStrain.peakErr = peakErr;
        PeakValues.totalStrain.timePeakErr = timePeakErr;
        PeakValues.totalStrain.peakFrameErr = frameCounterErr;
        PeakValues.totalStrain.strainRateErr = strainRateErr;
    case 2
        PeakValues.AntSept.peakEcc = peakEcc;
        PeakValues.AntSept.timePeakEcc = timePeakEcc;
        PeakValues.AntSept.peakFrameEcc = frameCounterEcc;
        PeakValues.AntSept.strainRateEcc = strainRateEcc;
        PeakValues.AntSept.peakErr = peakErr;
        PeakValues.AntSept.timePeakErr = timePeakErr;
        PeakValues.AntSept.peakFrameErr = frameCounterErr;
        PeakValues.AntSept.strainRateErr = strainRateErr;
    case 3
        PeakValues.Ant.peakEcc = peakEcc;
        PeakValues.Ant.timePeakEcc = timePeakEcc;
        PeakValues.Ant.peakFrameEcc = frameCounterEcc;
        PeakValues.Ant.strainRateEcc = strainRateEcc;
        PeakValues.Ant.peakErr = peakErr;
        PeakValues.Ant.timePeakErr = timePeakErr;
```

```
            PeakValues.Ant.peakFrameErr = frameCounterErr;
            PeakValues.Ant.strainRateErr = strainRateErr;
        case 4
            PeakValues.AntLat.peakEcc = peakEcc;
            PeakValues.AntLat.timePeakEcc = timePeakEcc;
            PeakValues.AntLat.peakFrameEcc = frameCounterEcc;
            PeakValues.AntLat.strainRateEcc = strainRateEcc;
            PeakValues.AntLat.peakErr = peakErr;
            PeakValues.AntLat.timePeakErr = timePeakErr;
            PeakValues.AntLat.peakFrameErr = frameCounterErr;
            PeakValues.AntLat.strainRateErr = strainRateErr;
        case 5
            PeakValues.InfLat.peakEcc = peakEcc;
            PeakValues.InfLat.timePeakEcc = timePeakEcc;
            PeakValues.InfLat.peakFrameEcc = frameCounterEcc;
            PeakValues.InfLat.strainRateEcc = strainRateEcc;
            PeakValues.InfLat.peakErr = peakErr;
            PeakValues.InfLat.timePeakErr = timePeakErr;
            PeakValues.InfLat.peakFrameErr = frameCounterErr;
            PeakValues.InfLat.strainRateErr = strainRateErr;
        case 6
            PeakValues.Inf.peakEcc = peakEcc;
            PeakValues.Inf.timePeakEcc = timePeakEcc;
            PeakValues.Inf.peakFrameEcc = frameCounterEcc;
            PeakValues.Inf.strainRateEcc = strainRateEcc;
            PeakValues.Inf.peakErr = peakErr;
            PeakValues.Inf.timePeakErr = timePeakErr;
            PeakValues.Inf.peakFrameErr = frameCounterErr;
            PeakValues.Inf.strainRateErr = strainRateErr;
        case 7
            PeakValues.InfSept.peakEcc = peakEcc;
            PeakValues.InfSept.timePeakEcc = timePeakEcc;
            PeakValues.InfSept.peakFrameEcc = frameCounterEcc;
            PeakValues.InfSept.strainRateEcc = strainRateEcc;
            PeakValues.InfSept.peakErr = peakErr;
            PeakValues.InfSept.timePeakErr = timePeakErr;
            PeakValues.InfSept.peakFrameErr = frameCounterErr;
            PeakValues.InfSept.strainRateErr = strainRateErr;
    end
end

EsFrame = StrainDataSmooth.EsFrame;
frameTime = StrainDataSmooth.totalStrain.FrameTime;

% calculate area under curve up to ES and ED
for i=1:2
    analysisFlag = i;

    % circumferential strain
    parameterFlag = 0;
    [totalStrainEcc, totalCC] = calculate_area_under_curve(frameTime,…
        StrainDataSmooth.totalStrain.CC,PeakValues.totalStrain.peakFrameEcc,…
        analysisFlag, parameterFlag);
    [AntSeptEcc, antSeptCC] = calculate_area_under_curve(frameTime,…
        StrainDataSmooth.AntSept.CC, PeakValues.AntSept.peakFrameEcc,…
        analysisFlag, parameterFlag);
    [AntEcc, antCC] = calculate_area_under_curve(frameTime,…
        StrainDataSmooth.Ant.CC, PeakValues.Ant.peakFrameEcc,…
        analysisFlag, parameterFlag);
    [AntLatEcc, antLatCC] = calculate_area_under_curve(frameTime,…
        StrainDataSmooth.AntLat.CC, PeakValues.AntLat.peakFrameEcc,…
        analysisFlag, parameterFlag);
    [InfLatEcc, infLatCC] = calculate_area_under_curve(frameTime,…
        StrainDataSmooth.InfLat.CC, PeakValues.InfLat.peakFrameEcc,…
        analysisFlag, parameterFlag);
    [InfEcc, infCC] = calculate_area_under_curve(frameTime,…
        StrainDataSmooth.Inf.CC, PeakValues.Inf.peakFrameEcc,…
        analysisFlag, parameterFlag);
    [InfSeptEcc, infSeptCC] = calculate_area_under_curve(frameTime,…
        StrainDataSmooth.InfSept.CC, PeakValues.InfSept.peakFrameEcc,…
        analysisFlag, parameterFlag);

    % radial strain
    parameterFlag = 1;
    [totalStrainErr, totalRR] = calculate_area_under_curve(frameTime,…
        StrainDataSmooth.totalStrain.RR, PeakValues.totalStrain.peakFrameErr,…
        analysisFlag, parameterFlag);
```

```
[AntSeptErr, antSeptRR] = calculate_area_under_curve(frameTime,…
    StrainDataSmooth.AntSept.RR, PeakValues.AntSept.peakFrameErr,…
    analysisFlag, parameterFlag);
[AntErr, antRR] = calculate_area_under_curve(frameTime,…
    StrainDataSmooth.Ant.RR, PeakValues.Ant.peakFrameErr,…
    analysisFlag, parameterFlag);
[AntLatErr, antLatRR] = calculate_area_under_curve(frameTime,…
    StrainDataSmooth.AntLat.RR, PeakValues.AntLat.peakFrameErr,…
    analysisFlag, parameterFlag);
[InfLatErr, infLatRR] = calculate_area_under_curve(frameTime,…
    StrainDataSmooth.InfLat.RR, PeakValues.InfLat.peakFrameErr,…
    analysisFlag, parameterFlag);
[InfErr, infRR] = calculate_area_under_curve(frameTime,…
    StrainDataSmooth.Inf.RR, PeakValues.Inf.peakFrameErr,…
    analysisFlag, parameterFlag);
[InfSeptErr, infSeptRR] = calculate_area_under_curve(frameTime,…
    StrainDataSmooth.InfSept.RR, PeakValues.InfSept.peakFrameErr,…
    analysisFlag, parameterFlag);

if (i == 1)
    StrainArea.totalStrain.Ecc.ES = totalStrainEcc;
    StrainArea.AntSept.Ecc.ES = AntSeptEcc;
    StrainArea.Ant.Ecc.ES = AntEcc;
    StrainArea.AntLat.Ecc.ES = AntLatEcc;
    StrainArea.InfLat.Ecc.ES = InfLatEcc;
    StrainArea.Inf.Ecc.ES = InfEcc;
    StrainArea.InfSept.Ecc.ES = InfSeptEcc;

    StrainArea.totalStrain.Err.ES = totalStrainErr;
    StrainArea.AntSept.Err.ES = AntSeptErr;
    StrainArea.Ant.Err.ES = AntErr;
    StrainArea.AntLat.Err.ES = AntLatErr;
    StrainArea.InfLat.Err.ES = InfLatErr;
    StrainArea.Inf.Err.ES = InfErr;
    StrainArea.InfSept.Err.ES = InfSeptErr;
else
    StrainArea.totalStrain.Ecc.ED = totalStrainEcc;
    StrainArea.AntSept.Ecc.ED = AntSeptEcc;
    StrainArea.Ant.Ecc.ED = AntEcc;
    StrainArea.AntLat.Ecc.ED = AntLatEcc;
    StrainArea.InfLat.Ecc.ED = InfLatEcc;
    StrainArea.Inf.Ecc.ED = InfEcc;
    StrainArea.InfSept.Ecc.ED = InfSeptEcc;

    StrainArea.totalStrain.Err.ED = totalStrainErr;
    StrainArea.AntSept.Err.ED = AntSeptErr;
    StrainArea.Ant.Err.ED = AntErr;
    StrainArea.AntLat.Err.ED = AntLatErr;
    StrainArea.InfLat.Err.ED = InfLatErr;
    StrainArea.Inf.Err.ED = InfErr;
    StrainArea.InfSept.Err.ED = InfSeptErr;

    h5 = figure(); hold on;

    plot(frameTime,totalCC,'k-', 'LineWidth', 2);
    plot(frameTime,antSeptCC, 'r-+');
    plot(frameTime,antCC, 'r-*');
    plot(frameTime,antLatCC, 'r-x');
    plot(frameTime,infLatCC, '-.o');
    plot(frameTime,infCC, '-.<');
    plot(frameTime,infSeptCC, '-.d');
    title('Circumferential strain - for analysis');
    xlabel('time (ms)');
    ylabel('strain (%)');
    legend('total strain', 'AntSept', 'Ant', 'AntLat', 'InfLat', 'Inf',…
            'InfSept', 'Location', 'SouthEast');

    if (analysisOption == 1)
        h6 = figure(); hold on;

        plot(frameTime,totalRR,'k-', 'LineWidth', 2);
        plot(frameTime,antSeptRR, 'r-+');
        plot(frameTime,antRR, 'r-*');
        plot(frameTime,antLatRR, 'r-x');
        plot(frameTime,infLatRR, '-.o');
        plot(frameTime,infRR, '-.<');
        plot(frameTime,infSeptRR, '-.d');
```

```
            title('Radial strain - for analysis');
            xlabel('time (ms)');
            ylabel('strain (%)');
            legend('total strain', 'AntSept', 'Ant', 'AntLat', 'InfLat', 'Inf',…
                'InfSept', 'Location', 'NorthEast');
        end
    end

end

%**************************************************************************
%               FUNCTION: CALCULATE_AREA_UNDER_CURVE
%**************************************************************************
%
% Purpose: calculate the area under the strain curve, and the average
%          area over time
%
% Functions Called: None
%
% Author: H. Gao
%
% Version: 1, June 2011
%
%**************************************************************************

function [ST, strainData] = calculate_area_under_curve(FrameTime, strainData,
peakFrame, analysisFlag, parameterFlag)

% when strain value > 0 from 0 to EsFrame for Ecc, or < 0 for Err, it will be set as 0
% ignore the end of the curve - stop analysing after 2*ES
finalFrame = 2*peakFrame;

if (analysisFlag == 1)
    stopFrame = peakFrame;
else
    stopFrame = size(FrameTime,2);
end

for i = 1:stopFrame
    if (parameterFlag == 0)
        if (strainData(i)>=0)
            strainData(i) = 0;
        end
    else
        if (strainData(i) <= 0)
            strainData(i) = 0;
        end
    end

    if (i > finalFrame)
        strainData(i) = 0;
    end
end

% calculate area under curve
% area is approximately estimated using a series of rectangles
% with height = midpoint of 2 adjacent measurements ((a+b)/2) and
% width = t2 - t1 = h

S= 0;
for i = 1 : stopFrame-1
    a= strainData(i);
    b= strainData(i+1);
    h = FrameTime(i+1) - FrameTime(i);
    S = S + (a+b)*h/2;
end

ST = [S S/(FrameTime(stopFrame) - FrameTime(1))];
```

Appendix B – Statistical Tests

The parametric (normal data) and non-parametric (non-normal data) tests used for data analysis in the investigations within this thesis are shown in Table A1.

Purpose	Parametric Test	Non-Parametric Test
Strength and direction of the linear relationship between two variables	Correlation (Pearson's coefficient)	Correlation (Pearson's coefficient)
Comparison of two independent groups	Two-sample t-test	Mann-Whitney test
Comparison of two dependent groups	Paired t-test	Wilcoxon signed ranks test
Comparison of *n* groups	One-way ANOVA with Tukey's post-hoc test	Kruskal-Wallis test, followed by individual Mann-Whitney tests with Bonferroni correction

Table A1: Statistical tests used for data analysis

The one-way ANOVA and Kruskal-Wallis tests identify whether there are statistically significant differences between the *n* groups, but do not specify where the differences lie. In addition, when comparing *n* groups it is necessary to apply a correction to the confidence level of the test to reduce the chances of obtaining false-positive results when multiple pairwise tests are performed on a single set of data.

A one-way ANOVA can be combined with a Tukey's post-hoc test. Tukey's test calculates a new critical significance level which takes into account the number of means being compared, and is based on a studentised range distribution rather than a t distribution [1]. The output of a one-way ANOVA with Tukey's post-hoc test shows whether there are any statistically significant differences between the groups, and then provides *p* values for each pairwise comparison.

Following a Kruskal-Wallis test, information about the differences between groups can be obtained through multiple pairwise Mann-Whitney tests, and in this situation a Bonferroni correction for the required confidence level can be used. The probability P of obtaining a significant result, i.e. the confidence level, from a single comparison is calculated using Equation A1, and the probability for n comparisons is calculated using Equation A2.

$$P = 1 - p \qquad \textbf{(Equation A1)}$$

$$P = 1 - \frac{p}{n} \qquad \textbf{(Equation A2)}$$

where p is the critical significance level. For example, a comparison of 4 groups at the level of $p = 0.05$ would result in a confidence level of 0.99, with a value of $p/n = 0.01$. The calculated confidence level is specified in the parameters for the Mann-Whitney test, and the results are significant at the level of p [2].

The confidence levels used for comparisons of n groups within this thesis are shown in Table A2. For the one-way ANOVA with Tukey's post-hoc tests, the values were calculated by Minitab, and the Bonferroni corrections for the Mann-Whitney tests were calculated using Equation A2. In all cases, the significance level was set at $p = 0.05$.

n	**Tukey**	**Bonferroni**
3	98.1	98.3
4	99.0	98.7
5	99.3	99.0
6	99.5	99.2

Table A2: Confidence levels (%) for multiple comparison tests

1. Tukey JW. Comparing Individual Means in the Analysis of Variance. Biometrics 1949; 5: 99 - 114
2. Bland JM, Altman DG. Multiple Significance Tests: The Bonferroni Method. BMJ 1995; 310: 170

Appendix C – Patient Information Sheet (Healthy Volunteers)

NHS National Waiting Times Centre

Department of Cardiology
Telephone: 0141 951 5180

NHS SCOTLAND

Version 1.1 February 2011

Information Sheet

Project title: Heart muscle strain in healthy adults revealed by MRI and echo.

You are being invited to take part in a clinical research study. Before you decide it is important for you to understand why the research is being done and what it will involve for you. Please take time to read the following carefully and discuss it with others if you wish. Please ask us if there is anything you are unclear about or if you would like more information. Take time to decide whether or not you wish to take part.

What does the title mean and what is the purpose of the study?

"MRI", or magnetic resonance imaging, can provide very clear pictures of the heart with either still or moving images. MRI can also provide insights into heart structure and function. The purpose of this study is to compare heart function revealed by the 1.5T and 3.0T MRI scanners and echocardiography (current standard of care) in order to provide images from adults without heart problems. This information will help us establish information in healthy subjects which will help us understand future findings in patients with heart problems.

Why have I been chosen?

You are well and do not have any known heart problems.

Do I have to take part?

No, it is up to you to decide whether or not to take part. If you do decide to take part you will be given this information sheet to keep and will be asked to sign a consent form. If you decide to take part you are still free to withdraw at any time and without giving a reason. A decision to withdraw at anytime, or a decision not to take part, will not affect the standard of care you might receive in the future.

What will happen to me if I take part?

The MRI scans last approximately one hour each. The scanner is basically tunnel shaped, like large "polo" mint, which is open at both ends. You slide into the centre of the "polo" and the scans are taken. Some people find it a little enclosing but you can come out at any time. The MRI scans and echocardiography would be done either in the morning or afternoon on the same day.

When you are in the scanner you will need to wear a pair of headphones. These are necessary because of the loud knocking noise that occurs when the pictures are

being taken. The headphones allow you to listen to music of your choice (you may bring your own CD) and allow us to communicate with you throughout the scan. Whilst in the scanner, you will be given an emergency buzzer and can very quickly be taken out should you feel uncomfortable. During the scan you will be asked to hold your breath at times to improve the quality of the pictures. We will compare your breathing in the scanner with your ability to breath into a portable tube called a spirometer that can be used to measure breathing.

The imaging information will be stored in a secure manner.

Is there any long term follow up: There is no follow up.

Women only: The effect of MRI scans on babies is unknown- for this reason, anyone who is pregnant or becomes pregnant during the study will be excluded. If you think you may be pregnant please inform the study doctor.

What are the risks?

The MRI scanner is very safe if you have no metal implants in your body. The MRI scan may reveal an abnormality in your body that you may not have been aware of. This is known as an incidental finding. In this case, the result you will be told about the finding if it is felt to be clinically significant (i.e. have implications for your health).

You may not be told about the result straight away since a report can take a few days to organise and it may need the opinion of another doctor. We may need to contact your GP and/or refer you to another doctor. Such findings might have implications for insurance policies you may have or wish to take out in the future.

Staff who are experienced in MRI will be present during MRI scan.

The amount of blood and urine taken does not place you at risk. Taking a blood sample may cause pain as the needle is put in, light-headedness at this time and bruising afterwards.

We would like to involve medical and/or physics students in our research team in order that they learn about and engage in research in imaging and heart disease.

What are the potential benefits of taking part?

You may not benefit directly from taking part in the study but the information that we get may help to improve treatment of patients in the future. You will be getting special scans of your heart which will provide additional information about your health and could even influence your future treatment.

What if something goes wrong?

If you are harmed by taking part in this research project, there are no special compensation arrangements. If you are harmed due to someone's negligence, then you have grounds for a legal action but you may have to pay for it. Regardless of this, if you wish to complain, or have any concerns about any aspect of the way you have been approached or treated during the course of this study, the normal NHS complaints mechanisms will be available to you.

Will my GP be informed?

If you agree we will inform your GP that you have agreed to take part in this study.

Will my taking part in this study be kept confidential?

All information that is collected about you during the course of the research will be kept strictly confidential. Aside from our contact with your GP, any information about you that leaves the hospital will have your name and address removed so that you cannot be recognised from it. Your personal information will be kept on file and stored in a secure place at the BHF Glasgow Cardiovascular Research Centre and in the Department of Cardiology. All examinations (including urine and blood results and gene data) will be labelled with a code and not with any personal details so that all analyses will be carried out anonymously. All information which is collected about you during the course or the research will be kept strictly confidential. Any information about you which leaves the hospital or the Clinical Investigation Unit will have your name and address removed so that you cannot be recognised from it.

What will happen to the results of the research study?

When the results become available they will be submitted to medical journals where they will be considered for publication. The final results will also be submitted to national and international medical conferences where they will be considered for publication. At the BHF Glasgow Cardiovascular Research Centre we will have events to inform the public about our ongoing research and about results from this and other studies.

You will not be identified in any report or publication.
If you would like a copy of the results, please ask your study doctor.

Who is organising and funding the research?

This study is organised by doctors from the Department of Cardiology, Golden Jubilee National Hospital, and scientists from the BHF Glasgow Cardiovascular Research Centre at Glasgow University. The study is funded by charities and researchers will not receive any payment for conducting this study.

Who has reviewed the study?

The West of Scotland Research Ethics Committee 1 has reviewed this study.

Who can I contact for further information?

Study doctor: Dr David Carrick
Department of Cardiology
Golden Jubilee National Hospital0141-951-5180

Supervisor: Dr Colin Berry

Thank you for taking the time to read this patient information sheet.

Appendix D – Patient Information Sheet (STEMI)

NHS National Waiting Times Centre

Version 1.2 September 2010

Patient Information Sheet

Project title: Detection and significance of heart injury in ST elevation MI

You are being asked to take part in a clinical research study. Before you decide it is important for you to understand why the research is being done and what it will involve for you. Please take time to read the following carefully and discuss it with others if you wish. Please ask us if there is anything you are unclear about or if you would like more information. Take time to decide whether or not you wish to take part.

What does the title mean and what is the purpose of the study?

Treatment of heart attack (myocardial infarction) has traditionally concentrated on opening the large heart arteries, whether by "clot busting" medication or balloons and stents (angioplasty). We now know that damage to the heart's tiny blood vessels also occurs during heart attack and this can contribute to longer-term heart damage. We plan to take measurements, which represent damage to the heart's small blood vessels during treatment for heart attack with angioplasty. We will then perform a special heart scan, an MRI scan, which would allow us to look at the blood supply to the heart, to look at the amount of damage to the heart as a whole and at the amount of damage to the small blood vessels. We would also like to obtain a blood and urine sample at the time of your admission to hospital and with each MRI scan in order to study some circulating cells and chemicals that may be involved in heart muscle and blood vessel repair. Our aim is to identify patients with significant damage to the hearts small blood vessels at the time of angioplasty therefore allowing us to identify future patients with treatment to minimise damage at the earliest opportunity.

Why have I been chosen?

You have had a heart attack and you require an angiography procedure to look at the arteries that supply the heart.

Do I have to take part?

No, it is up to you to decide whether or not to take part. If you do decide to take part you will be given this information sheet to keep and will be asked to sign a consent form. If you decide to take part you are still free to withdraw at any time and without giving a reason. A decision to withdraw at anytime, or a decision not to take part, will not affect the standard of care you receive.

What will happen to me if I take part?

During the angiography/angioplasty procedure we will make measurements that represent damage to the hearts small blood vessels. This involves injecting dye into the heart arteries under x-ray guidance allowing us to identify if any blockages are present. A tiny wire will be passed into the relevant heart artery allowing us to inflate balloons and deploy stents (like small scaffolds) over the blocked area. We will use a

pressure and temperature sensitive guidewire during the procedure. This wire is routinely used in our clinical practice. The measurements will take an additional 10 minutes during the procedure and do not pose any additional risk to you. While these measurements are being taken a drug called adenosine is used to increase the blood flow through the heart arteries.

You will have two heart MRI scans. One will occur within 48 hours after the angiography/angioplasty procedure and the other will be at around six months after your heart attack at a time that is convenient for you. If you agree, we would also like you to have three other MRI scans after the angiography procedure in order to study how heart injury changes. These 'extra' MRI scans would take place on the day you are admitted to hospital, on each of the first two days after admission and after discharge on day 5 - 7.

The MRI scans last approximately one hour each. The scanner is basically tunnel shaped, like large "polo" mint, which is open at both ends. You are slid into the centre of the "polo" on **a couch** and the scans are taken. Some people find it a little enclosing but you can come out at any time.

Before you go into the scanner, you will be invited to provide a urine sample. Following this, two small plastic tubes **or cannulas** (similar to that used when putting in a drip) will be inserted into the veins in your arms by a doctor. We would like to draw about 40 millilitres (about 3 tablespoonfuls) of blood from one of the plastic cannulas, and also ask you to provide a urine sample. We will examine new cells, such as progenitor cells, that may be involved in heart blood vessel injury/repair. We will also measure some of the circulating growth factors (small chemicals in the blood) which stimulate the release of these cells. We will count the number of these cells in each blood sample, and also prepare DNA and RNA from these cells to examine whether the genetic make-up has any connection with heart muscle and blood vessel repair (as assessed by MRI). Small blood and urine samples will be stored in a freezer to be analysed at a later stage, particularly when new markers of disease will have been developed by us or by other scientists. **Further approval will be required by the ethics committee for future studies with these samples.**

Following this, the cannula will permit us to inject gadolinium dye during your MRI scan.

Gadolinium is a clear fluid like water. It is used in MRI scanning because it accumulates in abnormal tissue and "lights up" that area so the scanner can detect it. It is useful in telling us which parts of the heart are abnormal, if any. After a short while the gadolinium fades away and is removed from your body (within a few hours). **There is a very small risk of kidney damage or allergy after gadolinium contrast administration.**

When you are in the scanner you will need to wear a pair of headphones. These are necessary because of the loud knocking noise that occurs when the pictures are being taken. The headphones allow you to listen to music of your choice (you may bring your own CD) and allow us to communicate with you throughout the scan. Whilst in the scanner, you will be given an emergency buzzer and can very quickly be taken out should you feel uncomfortable.

During the scan you will be asked to hold your breath at times to improve the quality of the pictures. During the 2nd MRI visit you may bring a CD of your own choice or you can ask a relative to bring one in.

Is there any long term follow up?

There is no direct follow up once you have had a repeat scan at 6 months. However, in the future, we would like to obtain information on your future well being from health records held by the National Health Service or Government (e.g. Registrar General). We would also like to obtain information on your drug therapy (medication). We can obtain this information through confidential electronic NHS and government records. This will not require us to contact you directly.

What are the risks?

There is no additional risk by taking these extra measurements during your angioplasty. The MRI scanner is very safe if you have not metal implants in your body.

The dye used during the cardiac MRI scans is called gadolinium. It is generally harmless and will be washed out of your system by your kidneys. Side effects include mild headache and nausea. Rarely (less than 1 % of the time) low blood pressure and light-headedness occurs. Very rarely (less than one in a thousand), patients are allergic to the contrast agent.

Senior doctors will be present during your angioplasty procedure and a senior doctor will be present during your cardiac MRI scans. The impact of any incidental finding will be followed up by referral to the appropriate specialist if not dealt with by cardiology staff.

The amount of blood and urine drawn does not place you at any risk.

We would like to involve medical and/or physics students in our research team in order that they learn about and engage in research in imaging and heart disease.

Women only: The effect of MRI scans on babies is unknown- for this reason, anyone who is pregnant or becomes pregnant during the study will be excluded. If you think you may be pregnant please inform the study doctor.

What are the potential benefits of taking part?

You are unlikely to benefit directly from taking part in the study but the information that we get may help to improve treatment of patients in the future. This will provide additional information about your health, which could influence your future treatment. While the blood and urine results may be useful for clinical research purposes, we do not anticipate these results to be useful for the treatment of your condition.

What if something goes wrong?

If you are harmed by taking part in this research project, there are no special compensation arrangements. If you are harmed due to someone's negligence, then you have grounds for a legal action but you may have to pay for it. Regardless of this, if you wish to complain, or have any concerns about any aspect of the way you have been approached or treated during the course of this study, the normal NHS complaints mechanisms will be available to you.

Will my GP be informed?

We will inform your GP that you have agreed to take part in this study.

Will my taking part in this study be kept confidential?

All information that is collected about you during the course of the research will be kept strictly confidential. Any information about you that leaves the hospital will have your name and address removed so that you cannot be recognised from it. Your personal information will be kept on file and stored in a secure place at the BHF Glasgow Cardiovascular Research Centre and in the Department of Cardiology. All examinations (including urine and blood results and gene data) will be labelled with a code and not with any personal details so that all analyses will be carried out anonymously. All information which is collected about you during the course or the research will be kept strictly confidential. Any information about you which leaves the hospital or the Clinical Investigation Unit will have your name and address removed so that you cannot be recognised from it.

What will happen to the results of the research study?

When the results become available they will be submitted to medical journals where they will be considered for publication. The final results will also be submitted to national and international medical conferences where they will be considered for publication. At the BHF Glasgow Cardiovascular Research Centre we will have events to inform the public about our ongoing research and about results from this and other studies.

You will not be identified in any report or publication.
If you would like a copy of the results, please ask your study doctor.

Who is organising and funding the research?

This study is organised by doctors from the Department of Cardiology, Golden Jubilee National Hospital, and scientists from the BHF Glasgow Cardiovascular Research Centre at Glasgow University. The study is funded by charities and researchers will not receive any payment for conducting this study.

Who has reviewed the study?

The West of Scotland Research Ethics Committee and the National Waiting Times Board has reviewed this study.

Who can I contact for further information?

Study doctors: Dr Alex Payne
Department of Cardiology
Golden Jubilee National Hospital0141-951-5875

Supervisor: Dr Colin Berry

Thank you for taking the time to read this patient information sheet.